Predictive Modeling of Sandstone Reservoir Distribution in the SW Scotian Basin

By

Justin Nagle

A Thesis Submitted to
Saint Mary's University, Halifax, Nova Scotia
In Partial Fulfillment of the Requirements for the
Degree of Masters of Science in Applied Science

May 2020, Halifax, Nova Scotia

Approved: Dr. Georgia Pe-Piper
Supervisor

Approved: Dr. David J.W. Piper
Geological Survey of Canada

Approved: Dr. Francky Saint-Ange
Beicip-Franlab

Approved: Dr. Emerson Marfisi
Beicip-Franlab

Approved: Dr. Cristian Suteanu
Professor

Date: May, 2020

Abstract

Predictive Modeling of Sandstone Reservoir Distribution in the SW Scotian Basin

By Justin Nagle

Forward stratigraphic modeling has been performed on the SW Scotian Basin in order to understand the geological evolution, sediment distribution, and deep-water clastic reservoir quality in the area. The SW Scotian Basin is hampered by complex salt tectonics, sparse seismic data, and its location on a transform jog. In all simulated models, sand is typically found on the shelf behind the carbonate reef front, and progrades into deep-water in the areas of the Shelburne Delta and canyon system near Mohawk B-93. Sensitivity analysis indicates that the main parameters controlling sand distribution in the basin are the geographic location of the sources, the water discharge volume of each source, and the diffusion coefficients for sand. Nevertheless, the best place to find deep-water clastic sediments is immediately down-dip of the Shelburne Delta, close to the shelf edge.

Date: May, 2020

Table of Contents

List of Figures

List of Tables

List of Appendices

Acknowledgements

This project was the result of a collaboration between Beicip-Franlab and Saint Mary's University, and would not have been possible without funding provided by the Nova Scotia Offshore Energy Research Association (OERA, Project No. 400-184) to GPP, a Natural Sciences and Engineering Research Council (NSERC) Discovery Grant to GPP, Beicip-Franlab, and Saint Mary's University.

I would like to thank my supervisors and committee members, specifically Georgia Pe-Piper and David J.W. Piper. They provided me guidance, mentorship, and support throughout the entire program. I am very thankful to them for teaching me to think critically, expanding my knowledge in geology, and for improving my technical writing skills.

I would also like to thank the support team at Beicip-Franlab, without them, I would still be having issues with the modeling process. Thank you to the Canada-Nova Scotia Offshore Petroleum Board (CNSOPB) particularly Mark Deptuck, and Adam MacDonald and Natasha Morrison of the Nova Scotia Department of Energy and Mines

Last but not least, I would like to thank my family, friends, and fellow graduate students, for keeping me motivated, pushing me to the next challenge, and for being there as support. Thank you.

Chapter 1: Introduction

The Scotian Basin is a large passive margin sedimentary basin located offshore eastern Canada, and extends from Georges Bank to the Grand Banks, and from the near shoreline of Nova Scotia into deep-water. The basin began development in late Triassic times with the breakup of Pangaea, due to the separation of the North American Plate from the African Plate (Jansa and Wade 1975, Wade and MacLean 1990). This created a series of half-grabens that trend northeast and a succession of depocenters which accumulated up to 15 km of carbonate, clastic, and evaporite rocks in Mesozoic-Cenozoic times (Wade and MacLean 1990). Salt tectonics influenced sediment distribution from the Middle Jurassic to the Late Cretaceous across the entire Scotian Basin, forming diapirs, walls, and allochthonous canopies due to sediment loading from prograding deltaic systems (Kendell 2012).

The depocenter of interest, the Shelburne sub-basin, accumulated up to 14 km of sediment, most of which was deposited in the Jurassic (Fig. 1.1) (Wade and MacLean 1990). The SW Scotian Basin is of important interest because exploration has been very limited in this part of the basin, with only four wells drilled within the study area (Fig. 1.1). In 2011, the Offshore Energy Technical Research (OETR) association conducted a study on the Scotian Basin and determined that the deep-water part of the Shelburne sub-basin is the most prospective for oil on the Scotian Margin. With the availability of this new information, as well as new reports by the Canada-Nova Scotia Offshore Petroleum Board (CNSOPB), the Nova Scotia Department of Energy and Mines, and academic researchers, exploration resumed in the SW Scotian Basin after 31 years. Although these new exploratory wells tested a variety of favourable hydrocarbon traps, no new discoveries of hydrocarbons were made. This puts a strong urge for large petroleum

companies to stop exploration in the SW Scotian Basin because rising costs and higher risks are associated with Nova Scotia compared to many other places in the world. This project aims at reducing the risk associated with exploration in the SW Scotian Basin by generating a predictive forward stratigraphic model of sediment dispersion for the mid-late Jurassic, the most prospective interval for hydrocarbons.

Modeling should be able to predict the distribution of sandy reservoir rocks that are located on the shelf, slope, and basin floor of the study area. Such a model has already been tested and successfully applied to other areas of the Scotian Basin (Hawie et al. 2019, Sangster et al. 2019), and elsewhere in the world (e.g. the Paris Basin (Granjeon and Joseph 1999), the Levant Basin (Hawie et al. 2017), and the Columbus Basin (Hawie et al. 2018)). Modeling would also give insight into the interaction between carbonate and clastic sedimentation processes, more specifically in the effect that a widespread reef would have on sediment transport into deep-water, and the effect of sea-level rise on deep-water sediment delivery. Finally, the model should be able to resolve uncertainties surrounding the formation of the Shelburne Delta and transport of its sediments to deep-water.

In order to generate a predictive stratigraphic model, the sediment supply to the SW Scotian Basin needs to be understood. This project will test the influence of different paleoriver systems from the literature, and their respective values of water discharge and sediment load. Three main sources of sediment supply have been identified for the SW Scotian Basin:

1. Southern Nova Scotia (Dutuc et al. 2017)
2. Maine (Chavez et al. 2019)

3. New Brunswick through the Bay of Fundy (Chavez et al. 2019)

The first two sources of sediment supply can be reasonably constrained because the petrology and provenance has been well documented for the COST G-2 well (Chavez et al. 2019) and the Mohawk B-93 well (Dutuc et al. 2017). The third source of sediment supply is not well constrained. There is no well control on sediments entering the SW Scotian Basin from the Bay of Fundy. The petrology and provenance of sediments derived from New Brunswick is sampled in the fluvial Chaswood Formation at Vinegar Hill (Piper et al. 2007).

In general, modeling is used for testing geological concepts and hypotheses. Modeling can give insight into the distribution of sediments from various sources constrained by a variety of input parameters (Hawie et al. 2019, Sangster et al. 2019). Modeling is also used in order to reconstruct past geological architectures (e.g. Granjeon 2014, Kolodka et al. 2016, Hawie et al. 2018), as well as to predict the distribution of sedimentary facies (e.g. Granjeon et al. 2017). It can be used to predict the formation of different carbonate environments (e.g. (Seard et al. 2013, Montaggioni et al. 2015, Leroux et al. 2017, Liechoscki de Paula Faria et al. 2017, Busson et al. 2019), and the effect of sea-level variation on sediment delivery (Harris et al. 2016, 2018). Once a model is calibrated with the available geological data, multiple simulations of the uncertain domain are performed in order to find out which parameters are the most sensitive to change (Gervais et al. 2018, Hawie et al. 2019, Sangster et al. 2019). This provides a statistical assessment of the predictivity of the model. All together, this makes modeling an extremely effective tool in understanding and testing a wide range of geological uncertainties and hypotheses.

Modeling of sediment distribution in the SW Scotian Basin has been done using DionisosFlow™ software. It is used to simulate sediment supply from the three sources, and to test the transport of sand into deep-water. This project builds on the previous work that has been done in the Scotian Basin (e.g. Wade and MacLean 1990, Kidston et al. 2005, OETR 2011, Weston et al. 2012, Pe-Piper and Piper 2012a, Deptuck et al. 2015, NSDoE 2015), in addition to available provenance data (e.g. Pe-Piper and MacKay 2006, Piper et al. 2007, Reynolds et al. 2009, 2012, Tsikouras et al. 2011, Li et al. 2012, Zhang et al. 2014, Dutuc et al. 2017, Chavez et al. 2018, 2019). Stratigraphic thickness from seismic controlled by well intersections and sediment facies interpreted from well logs have been used to calibrate the reference case model. The reference case model uses the relationships between river catchment area, relief, climate, and sediment supply, which provide a quantitative sand budget and relative predictions on the distribution of sand from the various sources, as well as information on the following geological uncertainties and hypotheses:

1. How was sediment dispersed from the Shelburne Delta? Were progradational packages present in the Jurassic, and if so, was sand transported into deep-water?
2. Did the initial bathymetric depth in the early Jurassic have a large effect on sediment accumulation in the basin?

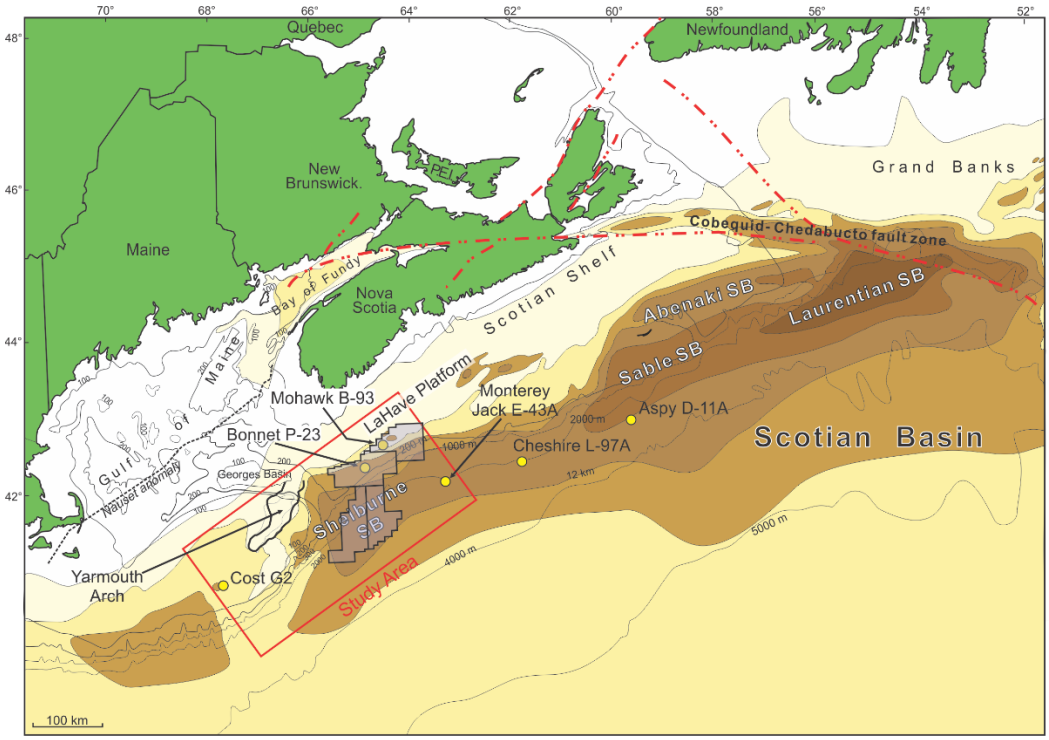

Figure 1.1: Map of the Scotian Basin showing the four subbasins from southeast to northwest: Shelburne, Sable, Abenaki, and Laurentian. The southern purple exploration license blocks belong to Statoil (now Equinor Canada Ltd.) and the northern purple exploration blocks are unclaimed. The study area for the model is outlined in red, with yellow dots corresponding to recent exploration wells, and wells of interest. Modified from Wade and MacLean (1990), and Williams and Grant (1998). Exploration licence locations from Deptuck et al. (2015).

1.1 Thesis Organization

This thesis has been organized around two journal articles, which are presented as Chapters 4 and 5. Chapter 4 introduces the reference case model, sensitivity analysis, and bathymetric changes with respect to the geological data present in the Shelburne sub-basin. Chapter 5 presents a variety of models with hypothetically less amounts of geological data compared to the reference case model introduced in Chapter 4; allowing for sediment distribution from the Shelburne Delta to be understood. The geological setting and methods are located in Chapters 2 and 3, and are also discussed in the each of the journal articles.

Chapter 2: Geological Setting

2.1 Regional Geology

2.1.1 Georges Bank Basin

The Georges Bank Basin began to develop in the Late Triassic – Early Jurassic with the breakup of Pangaea, and the separation of the Africa and Eurasia plates from the North American Plate (Jansa and Wade 1975, Wade and MacLean 1990, Poppe and Poag 1993). This created complex faulting and half-grabens which influenced sediment pathways and deposition in the basin. The basin is located on the continental shelf beneath the present day central and southwestern part of Georges Bank, and is bounded to the northeast by the Yarmouth Arch (Fig. 1.1) and the southwest by the Long Island Platform (Wade and MacLean 1990, Poppe and Poag 1993). Eight exploration wells and two Continental Offshore Stratigraphic Test (COST) wells were drilled between the 1970's and 1980's.

During the Early and Middle Jurassic, the basin subsided rapidly allowing accumulation of up to 4 km of clastic, carbonate, and evaporite rocks thinning towards the Yarmouth Arch (Wade and MacLean 1990). There is no evidence that sediment crossed the Arch into the Shelburne sub-basin. By the Late Middle Jurassic, seismic data indicates that the Arch had subsided so that sediments were able to bypass Georges Bank Basin, and deposit in the Shelburne sub-basin (Wade and MacLean 1990). This, along with reduced subsidence rates, slowed down sedimentation in Georges Bank Basin, allowing for only 4-5 km of sediment to accumulate from the Late Jurassic to the Cenozoic (Wade and MacLean 1990).

2.1.2 Shelburne sub-basin

Towards the southeast of the Georges Bank Basin lies the Shelburne sub-basin, which is located within the Scotian Basin. The Shelburne sub-basin occupies the area from Yarmouth Arch to approximately the Shebenacadie H-100 well. In this study, only the southwestern part of the sub-basin will be investigated (Fig. 1.1). This sub-basin shares a similar evolution history as the central Scotian Basin, and has been an active depocentre for sediment accumulation since the Early Jurassic post-rift unconformity. Most of the deposition that has occurred on the shelf happened in the Jurassic (Wade and MacLean 1990), with sediment thickness in deep-water governed by the sediment supply. It is estimated that oceanic crust began to form at 177 Ma from recent interpretations on constant spreading rates between the East Coast Magnetic Anomaly (ECMA) and the Blake Spur Magnetic Anomaly (BSMA) with mantle exhumation starting at 190 Ma (Sibuet et al. 2012). Salt movement began in the Middle Jurassic (Kidston et al. 2002), and affected sediment pathways and distribution in deep-water. Salt is commonly found as diapirs, pillows, and canopies, which are typically caused by sediment loading from prograding deltaic systems such as the Shelburne Delta (Kidston et al. 2002, Deptuck et al. 2015). However, Deptuck (2011) argued that the salt tectonics east of the Yarmouth Transform were driven by gravity gliding due to margin tilting, not sediment loading. Between the salt diapirs in the basin, minibasins formed and trapped sediments, creating complex sediment pathways. Further out in the basin, a large salt canopy developed in the Jurassic known as the Shelburne Canopy, with most of its expulsion in the mid-late Jurassic (Deptuck et al. 2015).

2.1.3 Yarmouth Arch

The Yarmouth Arch is a large south-southwest trending faulted basement horst block that separates the Georges Bank Basin from the Shelburne sub-basin (Wade and MacLean 1990, Deptuck et al. 2015). It extends for at least 150 km seaward of the LaHave Platform (Fig. 1.1), varies between 12-38 km in width, and is interpreted to be generally flat lying, meaning that the arch remained relatively flat while the basins around it subsided (Wade and MacLean 1990, Deptuck et al. 2015). It is thought that the Yarmouth Arch is composed of Meguma Terrane metasediments, but Deptuck et al. (2015) cautions that the Arch has not been sampled. In seismics, volcanic mounds are present along the Arch, probably related to the CAMP volcanism ~200 Ma (Deptuck et al. 2015). These volcanogenic features may be related to the breakup of Pangaea, however, unless the Yarmouth Arch is sampled, we cannot know for certain.

2.1.4 Yarmouth Transform

Towards the east of the Yarmouth Arch lies the Yarmouth Transform Fault Zone. The Yarmouth Transform is a large strike-slip fault zone that trends NW-SE and with more than 60 km of dextral offset (Deptuck et al. 2015).

2.1.5 Shelburne Delta

The Shelburne Delta occurs within the Shelburne sub-basin. This large deltaic system was able to persist from the Middle Jurassic to the Late Cretaceous, and survived many transgression and regression cycles, effectively transporting a large amount of sediment into deep-water (Deptuck et al. 2015). The clearest progradation of this delta occurred above the J-150 seismic marker (outside of our modeled time span) (Deptuck et al. 2015), however, it does not mean that progradation did not occur earlier. It has been

proposed that the Sable River, which supplied sediment to the Sable Delta in the Central Scotian Basin, was intermittently diverted along the Cobequid-Chedabucto Fault System, through the Bay of Fundy, towards the Shelburne sub-basin in the Early Cretaceous (Piper et al. 2011, Bowman et al. 2012, Zhang et al. 2014). However, alternative proposals for the source of the river feeding the delta exist in the literature. Dutuc et al. (2017) proposed that rivers depositing the Chaswood Formation at Vinegar Hill, New Brunswick, could have flowed through the lowlands of the Fundy Basin, towards the Shelburne sub-basin, forming this smaller deltaic system. Chavez et al. (2018, 2019) concluded that the river system suppling the Shelburne Delta would have been relatively small since there is no recorded influence of the Sable River affecting provenance or zircon geochronology at the COST G-2 well although a minor contribution cannot be excluded. Blowick et al. (submitted) show the presence of rare Grenville feldspars in the Middle and Upper Jurassic at Mohawk B-93. Thus, a small Canadian Shield contribution to the Shelburne Delta is likely in the Jurassic.

2.2 Stratigraphy

Sediment deposition in the Scotian Basin started in the Late Triassic – Early Jurassic, with the initial filling of the half-grabens created from the rifting of Pangaea, with the red clastics of the Eurydice Formation and coeval evaporites of the Argo Formation (Wade and MacLean 1990). The presence of red beds and evaporites suggest a hot and arid climate at this time (Jansa and Wade 1975).

The Eurydice and Argo formations are unconformably overlain by the dolomitic rocks of the Iroquois Formation. In places, where clastic input drowns out carbonate production, the Mohican Formation dominated (Fig. 2.1) (Wade and MacLean 1990). It

has been proposed that through the Middle Jurassic, the Iroquois Formation accumulated on the outer shelf passing landward into the Mohican Formation clastic rocks and seaward into basinal shales (Pe-Piper and Piper 2012a). The depositional setting for the Iroquois Formation is a typical sabkha type environment (Weston et al. 2012).

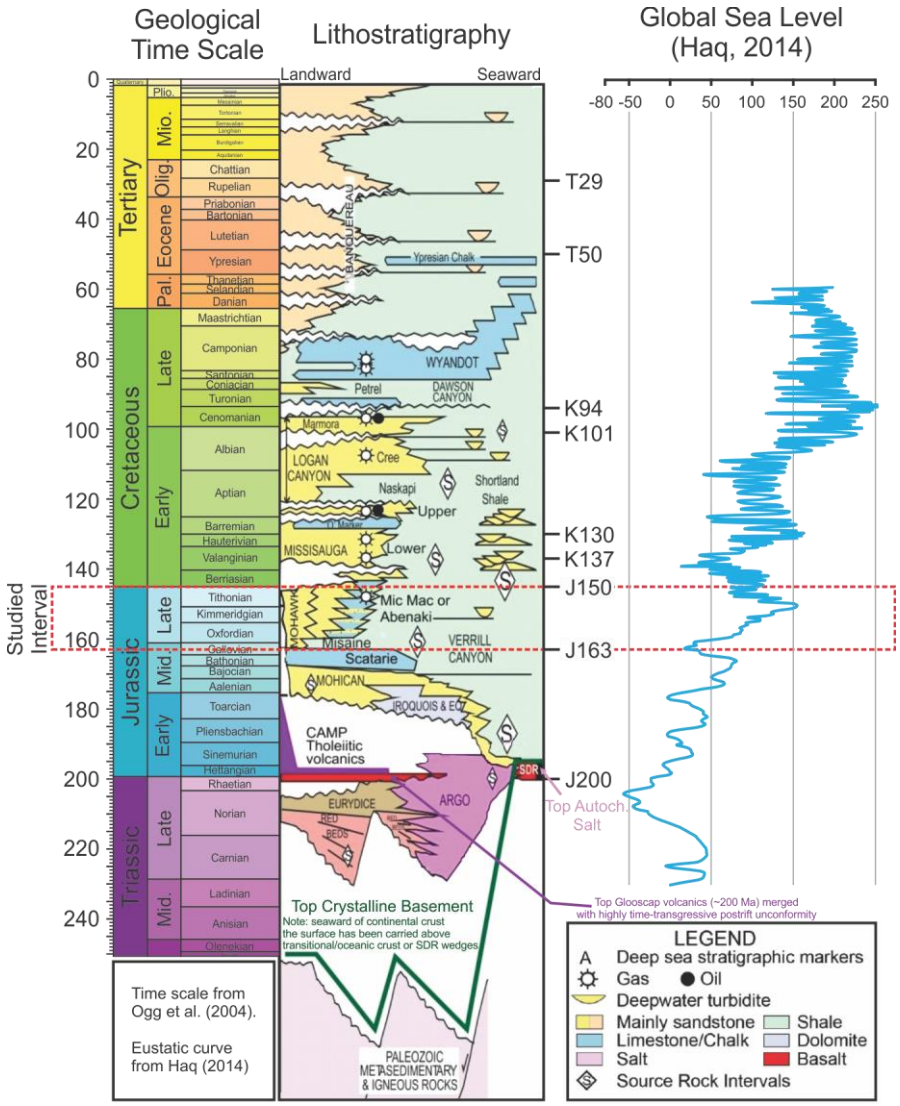

Figure 2.1: Stratigraphic column of the SW Scotian Basin. The red rectangle represents the studied interval for the model. Modified from Deptuck et al. (2015) and OETR (2011).

During the Bajocian to Bathonian, there was a depositional change from normal marine conditions of the Mohican Formation and the sabkha facies environment of the Iroquois Formation, to widespread carbonate deposition corresponding to the Abenaki

Formation (Weston et al. 2012). The Abenaki Formation is an extensive limestone-dominated formation that extends from the Scotian Margin up to the Grand Banks, and is generally a narrow carbonate platform that has been influenced by siliciclastic deposition on its landward side (Wade and MacLean 1990, Wierzbicki et al. 2006). This formation developed over 40 million years and is subdivided into four members, from oldest to youngest: the Scatarie Member, the Misaine Member, the Baccaro Member, and the Artimon Member (Fig. 2.2) (Wade and MacLean 1990, Kidston et al. 2005). The Scatarie Member is the most persistent, extending across most of the shelf during this time. It consists mainly of oolitic limestone (Wade and MacLean 1990). The Misaine member corresponds to a time of fluctuating sea level, which led to the deposition of a transgressive shale package (Wade and MacLean 1990, Kidston et al. 2005, Weston et al. 2012). Another hypothesis for the deposition of this shale package is the Callovian carbonate crisis. This regional carbonate crisis stunted production along the shelf and has been related to a Late Callovian – Early Oxfordian cooling phase. It is predicted that sea level and temperatures drastically decreased at this time based on recent oxygen-isotope data (Tremolada et al. 2006, Jadoul 2018). This regional cooling event could have been caused by a short lived ice age at the mid-late Jurassic transition (Dromart et al. 2003).

Following the deposition of the Misaine Member, the Baccaro Member flourished as ocean waters returned to warmer temperatures. This is the thickest member of the Abenaki Formation, and consists of mainly oolitic limestones and complex reef facies (Kidston et al. 2005). It extends along the whole Scotian Margin, however, it is limited to a narrow section at the edge of the Jurassic hinge line, between 15-25 km wide (Wade and MacLean 1990, Kidston et al. 2005). The Baccaro Member is subdivided into five,

third order stratigraphic sequence units approximately 100-300 metres thick (Abenaki 2-6 Fig. 2.2) (Kidston et al. 2005). The Artimon Member is the youngest member of the Abenaki Formation, and is Early Cretaceous in age (Wade and MacLean 1990, Kidston et al. 2005). It consists of stromatoporoid mounds and thrombolitic sponges composed of argillaceous limestone (Wade and MacLean 1990, Kidston et al. 2005). According to Kidson et al. (2005), these sponge mounds were deposited on top of the drowned platform during a sea level rise in the Berriasian, possibly in water depths between 100-200 metres.

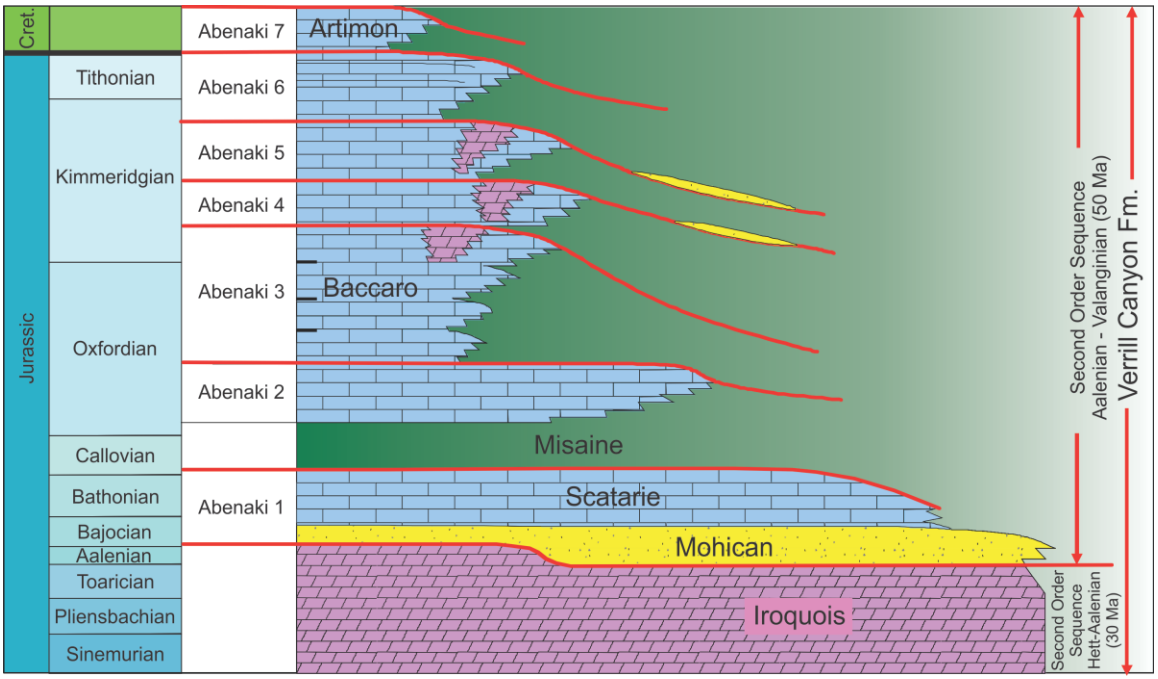

Figure 2.2: Sequence stratigraphy of the Abenaki Formation. Modified from Kidston et al. (2005).

The Abenaki Formation grades distally and interfingers with the Verrill Canyon Formation shales (Figs. 2.1, 2.2) (Weston et al. 2012). However, closer to shore, the lateral equivalent to the Baccaro Member of the Abenaki Formation is the clastic Mohawk and Mic Mac formations (Fig. 2.1).

The Mic Mac Formation is the lateral equivalent of the Baccaro Member in the eastern and central Scotian Basin and consists of sandstone, shale, and carbonate deposited in a clinoform-like fashion (Wade and MacLean 1990). The topset of the clinoform consists of carbonate-sandstone, the foreset consists of sandstone-shale, and the bottomset consists of shale-sandstone (Wade and MacLean 1990). Landward, the lateral equivalent to the Mic Mac Formation is the Mohawk Formation. It is considered to represent the more continental facies of the Mic Mac Formation, and consists of coarser-grained feldspathic sandstone and siltstone, interbedded with green and red shales, and minor amounts of carbonate (Wade and MacLean 1990), deposited in a shallow marine environment during the Callovian – Kimmeridgian.

During the Late Jurassic to Early Cretaceous, the Scotian Basin changed from being dominated by carbonate precipitation to clastic sedimentation, due to the uplift of the Labrador Rift and the delivery of clastic sediments by the Sable River to the central Scotian Basin. Also at this time, the Avalon Uplift along the Newfoundland margin and the Grand Banks occurred, when the North Atlantic Ocean started to open between the Iberian and North American plates (Wade and MacLean 1990). This caused significant uplift and erosion, resulting in the Avalon Unconformity (Jansa and Wade 1975). The effects of this uplift are less prominent in the Scotian Basin (Pe-Piper and Piper 2012a), and diminish closer to Georges Bank.

2.3 Paleoriver Systems

Paleoriver systems are very important to be defined in order to understand where sediments were being transported from, and how they flowed into the Scotian Basin. These ancient river systems help to define where certain types of sediments were coming

from and help to act as an input when modeling (see section 3.1). Paleoriver names and locations have changed through the years within the literature (e.g., Ancestral St. Lawrence River → Sable River); however, they have become more refined with each additional provenance study. Typically, a river drainage area is first defined by observing the provenance of different types of detrital mineral grains at a stratigraphic level in a well. This then allows researchers to estimate where the sediment was sourced from by looking at rock type distributions (e.g. Fig. 2.3) onshore. Below is a short description of the different river systems that fed sediment into the Scotian Basin.

During the Late Triassic, small local rivers derived from the Meguma Terrane are thought to have fed sediments into the Fundy Basin and Orpheus Graben through the Minas Fault Zone, while the rest of the Scotian Basin and parts of the Orpheus Graben experienced evaporite deposition (Li et al. 2012, Piper et al. 2013). Only the Fundy Basin recorded Early Jurassic clastic sediments, while the rest of the Scotian Basin and Orpheus Graben experienced a hiatus at this time. This lack of sedimentation is thought to be caused by rift shoulder uplift of the Meguma Terrane (Li et al. 2012, Dutuc et al. 2017). This would have effectively diverted river systems towards the Fundy Basin instead of the Scotian Basin. By the Middle Jurassic, sedimentation was restored to the Scotian Basin through peneplanation and rift shoulder subsidence of the Meguma Terrane (Li et al. 2012, Dutuc et al. 2017). Provenance data from Li et al. (2012) indicates that local Meguma Terrane rivers were operating for most of the Middle Jurassic, principally depositing the Mohican Formation offshore Nova Scotia. Rare polycyclic minerals found in this formation may indicate a more distal source, such as the inboard Appalachian terranes. In the Middle and Upper Jurassic, rare garnets characteristic of metamafic rocks

(Dutuc et al. 2017) and Grenville feldspars (Blowick et al. submitted) at Mohawk B-93 suggest a river draining the Grenville Province discharged into the Shelburne Delta.

The principal river system that supplied the central Scotian Basin with sediments was the Sable River, which built the Sable Delta (Jansa and Wade 1975). This river system, originally interpreted as a paleo-St. Lawrence River, drained both Labrador and the Appalachians (Tsikouras et al. 2011, Pe-Piper and Piper 2012a, Zhang et al. 2014). The Sable River system became active in the Late Jurassic (mid-Kimmeridgian) as it started to drain the uplifted area around the Labrador Rift in Labrador, as well as areas within the Appalachians (Zhang et al. 2014). It then flowed into the Central Scotian Basin (Fig. 2.3) and built large deltaic systems that deposited kilometres of clastic material known as the Missisauga and Logan Canyon Formations.

Another major Cretaceous river system that was thought to operate in the Cretaceous is known as the Banquereau River (Pe-Piper and Piper 2012b). This river also drained the Labrador Rift area, however, provenance studies indicate the main source of detrital minerals was from western and central Newfoundland (Zhang et al. 2014). This river would have deposited its sediments in the eastern part of the Scotian Basin. Some wells in the Scotian Basin also record sediments from the nearby Meguma Terrane. The Meguma Terrane was a local source feeding sediments directly into the central and western Scotian Basin through small river systems (Fig. 2.3) (Dutuc et al. 2017). The sediment load of such local rivers consisted, of detritus from metamorphosed sandstones and shales, as well as the Devonian granites.

Although paleoriver systems have been defined for the central and eastern Scotian Basin, the SW Scotian Basin lacks many in-depth studies due to the limited number of

wells. This makes it hard to better define river drainage areas, especially because the strike of the Appalachian orogen parallels the Scotian Basin (Pe-Piper et al. 2008, Chavez et al. 2019). Sediment supply to the COST G-2 and Mohawk B-93 wells have been reasonably constrained by provenance studies Chavez et al. (2019) and Dutuc et al. (2017), respectively. The sediment supply to the COST G-2 well changed through the Late Jurassic to the Early Cretaceous. During the Oxfordian, the river system drained the areas of coastal Maine, and by the uppermost Jurassic, the river catchment area enlarged to include more of Maine, and possibly parts of New Hampshire and New Brunswick (Chavez et al. 2019). By the Early Cretaceous, the river system changed drastically, perhaps as a response to climate change, with more moisture being conveyed further inland. The minerals assemblage that was present in the Jurassic was significantly reduced in the Lower Cretaceous by increased amounts of ilmenite, staurolite, and zircon (Chavez et al. 2019). The river catchment area expanded in this way to include most of Maine and New Brunswick, as well as some parts of New Hampshire. A similar study by Dutuc et al. (2017) concluded that the majority of sediments for the Mohawk B-93 well were sourced from the Meguma Terrane, with minor amounts coming from more distal sources. The paucity of detrital chromite makes a Sable River source unlikely; there may have been a different river draining New Brunswick and the adjacent areas of Grenville in Quebec.

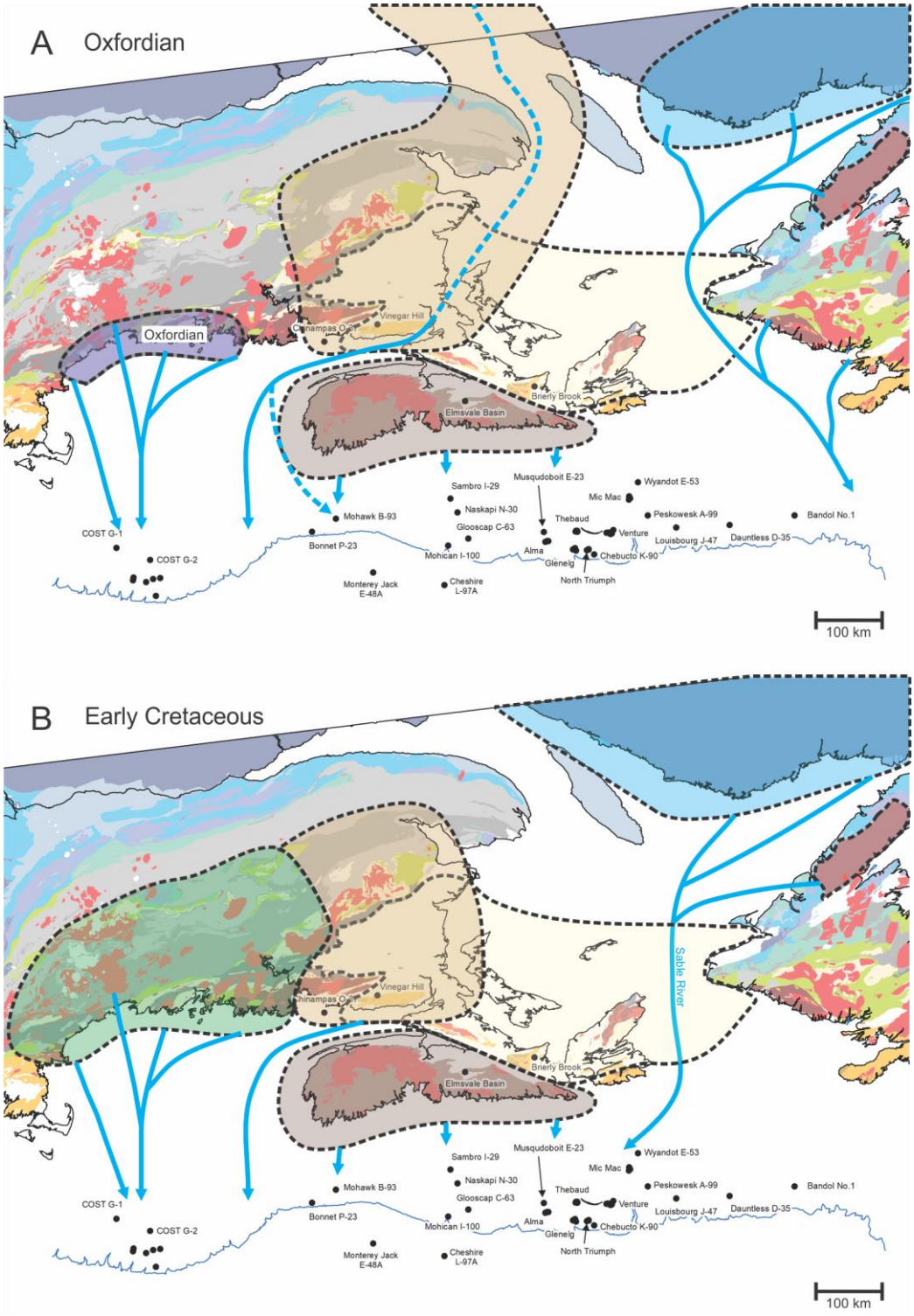

Figure 2.3: Map of eastern Canada showing the possible drainage areas of river systems for (A) the Oxfordian and (B) the Early Cretaceous from the literature (e.g. Tsikouras et al. 2011, Li et al. 2012, Zhang et al. 2014, Dutuc et al. 2017, Chavez et al. 2019) that would have transported sediments into the Scotian Basin. Base map modified from Waldron et al. (2018).

Chapter 3: Methodology

Stratigraphic modeling of the SW Scotian Basin was the objective of this thesis and it was done using DionisosFlow™, a diffusion based, deterministic 4D forward stratigraphic modeling software, which simulates basin infill on geological time scales (Granjeon 2014). The models in this study are calibrated against stratigraphic thickness from seismic horizons and interpreted sediment facies from well logs. Sensitivity analysis is then performed on the calibrated models using CougarFlow™, a statistical analysis software which uses response surface methodology (RSM) to evaluate the most influential uncertain parameters (Agrawal et al. 2015, Hawie et al. 2015, 2019). The goal of this modeling process is to reproduce large-scale and long-term geological trends of sediment distribution in the basin.

3.1 DionisosFlow™

The DionisosFlow™ software was developed in the late 1990's, and is able to simulate basin infill on a scale of tens to hundreds of kilometers, over a period of tens of thousands of years to hundreds of millions of years (Granjeon and Joseph 1999, Granjeon 2014, Granjeon et al. 2017). It works by calculating the relationship between accommodation space, sediment supply, and sediment transport for each time step of the model (Kolodka et al. 2016, Granjeon et al. 2017, Hawie et al. 2017).

Accommodation space is defined as the amount of available space for sediment accumulation and is governed by eustatic sea level variations as well as tectonic processes, such as: subsidence and uplift, compaction, and salt diapirism. Sediment supply refers to the amount of terrigenous sediment input and in situ carbonate production (Kolodka et al. 2016). Carbonate production considers the different producers

of biogenic carbonate, constrained by their respective environmental properties (wave energy, bathymetry, fluvial discharge, and water column turbidity). Transport of the sediments is simulated using diffusion equations.

There are two different diffusion equations that can model sediment transport in DionisosFlow^{TM}. Both equations combine empirical water- and gravity-driven diffusion processes as either (1) linear slope-driven diffusion (transport proportional to slope), known as hill-slope creep; or (2) non-linear slope- and water-driven diffusion (water discharge driven transport) (Hawie et al. 2017). This study utilized non-linear slope- and water-driven diffusion, described by the following equation:

$$Q_s = -(K_s/\vec{\nabla}h \ + \ K_w Q_w^m S^n)$$

where Q_s is the sediment flux (km^3/Ma), K_s and K_w are the diffusion coefficients for hill slope creeping and water discharge driven transport, (km^2/ka) respectively, h is the elevation (m), Q_w is water discharge (m^3/s), S is the gradient of the slope in the basin, and m and n are constants between 1 and 2 (Tucker and Slingerland 1994).

In order to reproduce natural systems, the diffusion coefficients obey a set of rules that govern the model: e.g., terrigenous mud is more diffusive than sand, which is more diffusive than carbonate reefs. This means that the grain size of mud is more easily transported than the grain size of sand, and that when a reef starts to grow, it will tend to stay in place and build upwards, rather than being completely transported into deep-water.

In order to account for different types of sediment flow within natural systems, DionisosFlow^{TM} uses the following two processes: (1) Low energy long term (LELT) processes, which represents continual fluvial input into the basin, carbonate production,

and hemipelagic sedimentation. (2) High energy short term (HEST) processes, which represents high energy sediment delivery into the basin, caused by storms and fluvial flooding, as well as turbidites. Although this last type of sediment flow is short-lived, it may be responsible for transporting most sediment into the basin, especially into deep-water environments.

3.2 CougarFlow™

Following the manual calibration of the reference case model, CougarFlow™ software was used to test sensitivity within the defined DionisosFlow™ parameters, by running numerous DionisosFlow™ models with varying uncertain parameters. This study employs Latin Hypercube experimental design in order to define a set of simulations which allows for uniform sampling of the entire uncertain domain (Agrawal et al. 2015, Hawie et al. 2015). The user defines the number of simulations to run, however with increasing uncertain parameters, a higher number of simulations will be required in order to accurately define the response surface, which is a mathematical regression model.

Response Surface Methodology (RSM) is the process of exploring the relationship between the uncertain parameters used in the experimental design and one or more responses (Hawie et al. 2015). In the case of this study, the responses are the calibration indicators (section 3.3) and areas of interest in the model (e.g. the Shelburne Delta). The goal of RSM is to approximate the output results through a second-degree polynomial function or by kriging (Hawie et al. 2015, 2019), which allows for a qualitative and quantitative analysis of the uncertain parameters on the response surface. To test the accuracy of the response surface, a small number of confirmation runs are ran, against the surface, in order to determine the predictivity of the surface. Once this is

completed, a Monte-Carlo analysis is performed on the response surface, in which a probabilistic distribution of uncertain parameters is applied to the response surface, and the results are recorded. This allows for the response to be estimated without running additional simulations.

3.3 Model Calibration Strategy

One model was calibrated for the studied time span (163-150 Ma), representing the deposition of the Misaine member, and the Abenaki, Mic Mac, and Mohawk formations. The bounding surfaces (top and bottom) of the model are represented by seismic horizons modified from the 2015 Shelburne sub-basin Play Fairway Analysis, the J163 (top Callovian) and J150 (top Tithonian) horizons, both of which are maximum flooding surfaces (MFS). From these surfaces, a regional thickness map is determined for the study area. This thickness map accounts for the vertical salt movement that occurred during this time; however, this movement is averaged through the modeled time span, when in reality salt movement may have occurred at different rates and at different times during this period. In areas of the thickness map that contained negative or zero values, they were assumed to be salt, and were given low thickness values extrapolated from neighbouring cells. Sediments are modeled with zero porosity; therefore, sediment compaction is not considered, and thus sediment supply in the model may be overestimated. The size of the model is 400 km x 225 km, with a cell size of 5 km x 5 km, and time steps consisting of 0.1 Ma.

The model was calibrated by altering sediment supply and water discharge for each source, as well as carbonate production, carbonate environmental conditions, diffusion coefficients, and subsidence. The calibration goal of the study was to obtain a

minimum 80 % regional thickness and well lithofacies match. This was verified by comparing the simulated thickness to the regional thickness map, seismic lines within the study area, as well as running a variety of scripts, referred to as calibration indicators.

Sediments in reference wells have been grouped into lithofacies (e.g. reef, limestone, sandstone, shale, marl, etc.), based on well cuttings information as well as petrophysical analysis. In order to assign lithofacies in DionisosFlow™, a range of sediment proportions are required; therefore, the limiting proportions of simulated lithofacies have been chosen to match the observed lithofacies in wells, instead of using composite rock or facies classifications. This approach is only qualitative, because it does not consider the proportion of each grain size available in a traditional lithofacies classification scheme. Since the interpreted lithofacies are at a much higher resolution than the simulated lithofacies, it was necessary to upscale the well logs in some of the reference wells. This was accomplished by averaging the lithofacies in time steps, in order to match the cell size and time steps of the simulation.

In order to determine how well the simulated lithofacies match the actual lithofacies in wells, a calibration indicator script was used. This indicator takes into account the similarity of each facies and its thickness. For example, a 100 % match would occur if the model simulated 10 m of sandstone at a reference well, and the actual reference well reported 10 m of sandstone; whereas an 85 % match would occur if the model simulated 7 m of sandstone and 3 m of shale. This is due to the limitation associated with the cell size of the model, therefore, simulating shale when the well reports sandstone yields a 50 % calibration instead of 0 %. In order to report the global facies calibration indicator, the well facies calibration indicator at each well were added

together and divided by the total number of reference case wells. This global facies calibration indicator is important because it provides an overview on the scale of the entire study area as how well the facies are calibrated.

To measure the well thickness calibration, another script was used that calculated the difference between the actual well thickness and the absolute value of the actual well thickness minus the simulated thickness divided by the actual well thickness. The value of this indicator can be increased by varying the subsidence amount around the individual well, in order to increase or decrease accommodation space, allowing for a higher well thickness calibration.

3.4 Modeling Limitations and Assumptions

It is important to understand some of the limitations and assumptions associated with DionisosFlow™. For instance, subsidence in the model is considered to be uniform and constant through time, but in reality, differential subsidence most likely occurred. In order to develop a calibrated model, reef production was limited to the J150 shelf edge, instead of the entirety of the J163 bathymetric map. A negative source was used in the model in order to allow for an open-box approach, allowing sediment to leave the modeled area, like in a natural environment. Within DionisosFlow™, it is difficult to reproduce small-scale features due to the limitation of the cell size (Kolodka et al. 2016) and the assumptions inherent in a diffusion-based model. It also uses a grid for the model space, and can create unnatural results near the boundary of the model as well as unnatural facies distribution.

Chapter 4: Forward stratigraphic modeling to test rift and early drift deep-water clastic reservoirs at a transform jog; Shelburne sub-basin, SE Canadian margin

Submitted paper to AAPG Bulletin

4.1 Introduction

Transforms developed during continental rifting create early tectonic depocentres and focus drainage from the continent. In extensional basins they allow for accommodation between individual fault and basin segments during half-graben development (Gawthorpe and Hurst 1993). Maximum displacement occurs near the middle of the fault segment, and dissipates towards the end of the fault plane, such that the hanging wall tends to increase and the footwall tends to decrease towards a transfer zone (Gawthorpe and Hurst 1993). These tectonically induced slopes exert a fundamental control on geomorphology and facies distribution in basin stratigraphy (Leeder and Gawthorpe 1987).

One such area is the Shelburne sub-basin, which developed around the Yarmouth Transform and is located offshore eastern Canada (Fig. 4.1). The deep-water part of the Shelburne sub-basin is considered to be the most prospective place to find oil on the passive Scotian Basin (OETR 2011, NSDoE 2015). However, the Shelburne sub-basin is an under-explored sedimentary basin, as only four wells have been drilled in the study area (Fig. 4.1), with only one located in deep water. Seismic interpretation in this part of the basin is hampered by severe salt tectonics and complex relationships between carbonate and clastic sediments. The Shelburne sub-basin is of specific interest because of the potential for deep-water clastic reservoirs and source rocks. The main risks associated with exploration in this area are the distribution, size, and reservoir quality of

deep-water sands. One way to reduce these risks is to develop a forward stratigraphic model of sediment dispersion for the lesser-known Mid–Late Jurassic successions.

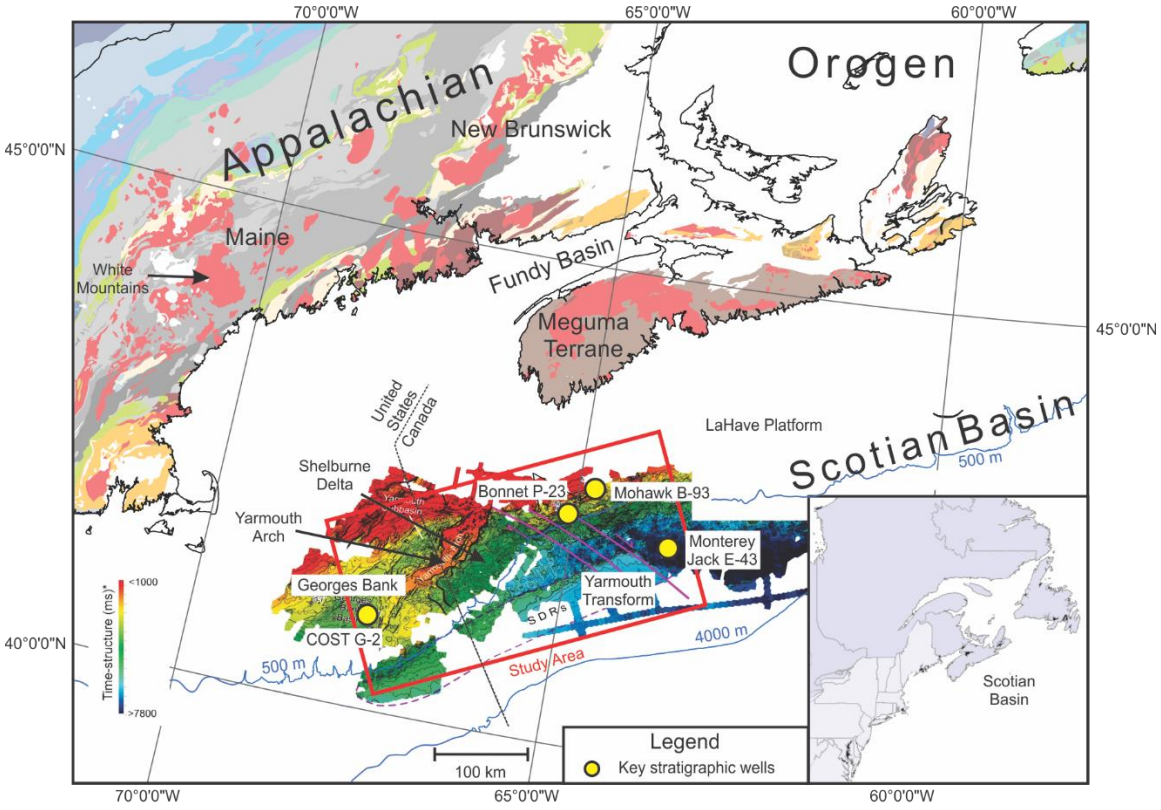

Figure 4.1: Map of the Scotian Basin and its hinterland showing time-structure maps of the Shelburne sub-basin from Deptuck et al. (2015). Terrestrial geology map modified from Waldron et al. (2019). Study area outlined in red.

In general, forward stratigraphic modeling is used to test a variety of geological concepts and hypotheses. It can give insight into the distribution of sediments from various sources constrained by a variety of input parameters (Hawie et al. 2019, Sangster et al. 2019). Modeling can also be used to reconstruct past geological architectures (e.g. Granjeon 2014, Kolodka et al. 2016, Hawie et al. 2018), predict the distribution of sedimentary facies (e.g. Granjeon et al. 2017) and carbonate environments (e.g. (Seard et al. 2013, Montaggioni et al. 2015, Leroux et al. 2017, Liechoscki de Paula Faria et al. 2017, Busson et al. 2019), as well as the effect of sea-level variation on sediment delivery

(Harris et al. 2016, 2018). All together, this makes modeling an effective tool in understanding and testing a wide range of geological uncertainties and hypotheses.

The goal of this study is to better understand geological evolution, sediment distribution, and deep-water clastic reservoir quality in the Shelburne sub-basin through development of a forward stratigraphic model. Statistical evaluation of the uncertainty in key model parameters will refine the model through sensitivity analysis. The model will test hypotheses about the geological evolution of the Shelburne sub-basin in the Middle–Late Jurassic, including the role of the Yarmouth Transform, and the ability of the Shelburne Delta to deliver clastic sediments into deep-water.

4.2 Geological Setting

The Shelburne sub-basin, located in the Scotian Basin offshore eastern Canada, began to develop in the Mid–Late Triassic, with the rifting of Pangaea as the Africa Plate separated from the North American Plate (Jansa and Wade 1975, Wade and MacLean 1990). By 177 Ma, oceanic crust began to form (Sibuet et al. 2012). The Yarmouth Transform is a large strike-slip fault zone that developed during rifting (Fig. 4.1). It trends NW-SE and offsets the East Coast Magnetic Anomaly (ECMA) and the shelf hinge-line, by more than 60 km (~37 mi) of dextral movement (Deptuck et al. 2015). Seaward dipping reflectors (SDRs) off Georges Bank appear to terminate at the transform, and cannot be traced into the central Scotian Basin. The other prominent basement feature in the study area is the Yarmouth Arch, which is a large south-southwest trending faulted and segmented basement horst block that separated Georges Bank Basin from the Shelburne sub-basin in the Early to Middle Jurassic (Wade and

MacLean 1990, Deptuck et al. 2015). It extends for at least 150 km (~93 mi) seaward of the LaHave Platform, and varies between 12-38 km (7-23 mi) in width (Fig. 4.1).

Sediment fill in the Shelburne sub-basin began with the continental clastics of the Eurydice Formation and the coeval evaporites of the Argo Formation in the Late Triassic – Early Jurassic. The CAMP magmatic event is represented by basalt flows in the Fundy Basin and at the Glooscap C-83 well (Pe-Piper and Piper 1999). Middle Jurassic sediments consist of the marine clastics of the Mohican Formation that pass seaward into the dolomitic rocks of the Iroquois Formation, and basinward into shales (Pe-Piper and Piper 2012a). The J163 seismic marker corresponds to the Callovian maximum flooding surface (MFS) (Figs. 4.2-4.4), which was a time of rising sea level that led to reef drowning (Kidston et al. 2005, Weston et al. 2012). The base of the Monterey Jack E-43 well intersected the J163 marker beneath the present continental slope. Cuttings samples contain shallow water limestone. OERA (2020) considered that this limestone indicated a shallow water carbonate ramp similar to the Lower–Middle Jurassic in the conjugate Moroccan High Atlas (Pierre et al. 2010).

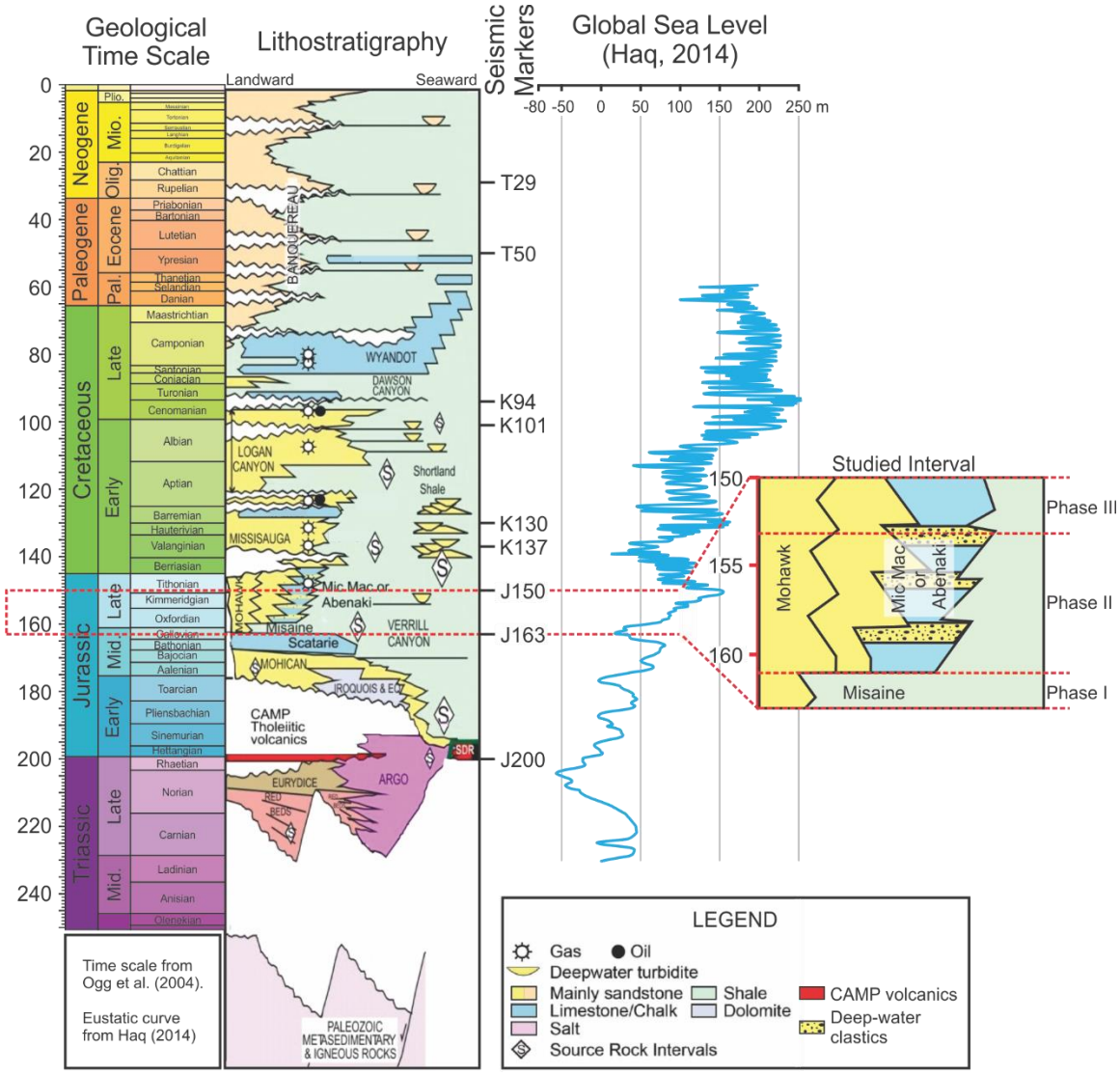

Figure 4.2: Stratigraphic column of the SW Scotian Basin. The red rectangle represents the studied time interval for the model. Modified from OETR (2011) and Deptuck et al. (2015). Phase I = carbonate drowning, Phase II = clastic sedimentation, Phase III = carbonate re-establishment.

Upper Jurassic sediments on the shelf consist of the limestone-dominated carbonate platform of the Abenaki Formation, with a carbonate reef front. Landward are coastal clastics of the Mohawk Formation and seaward are un-named marlstones and claystones (Figs. 4.3, 4.4). The J150 seismic marker corresponds to the Tithonian MFS (Fig. 4.2), when sea levels significantly rose, and carbonate was deposited in a deeper

water transgressive bank margin setting (Kidston et al. 2005). In the eastern Shelburne sub-basin, the Upper Jurassic aggrading carbonate bank experienced a small amount of clastic sediment bypass (Moscardelli et al. 2019), from prograding shelf-edge deltas. However most clastic sediments at that time accumulated landward of the carbonate platform, and sediment pathways in deep-water followed topographic lows (Moscardelli et al. 2019). Farther west, on SE Georges Bank, the large Shelburne Delta developed (Fig. 4.1). It persisted from the Mid-Jurassic to the Late Cretaceous, and survived multiple transgression and regression cycles, transporting clastic sediment into deep-water (Deptuck et al. 2015). The study area was located at ~27° latitude at the time of the J163 marker (Leinfelder et al. 2002), and the vegetation cover was tropical xerophytic scrubland, based on climate modeling (Sellwood and Valdes 2008).

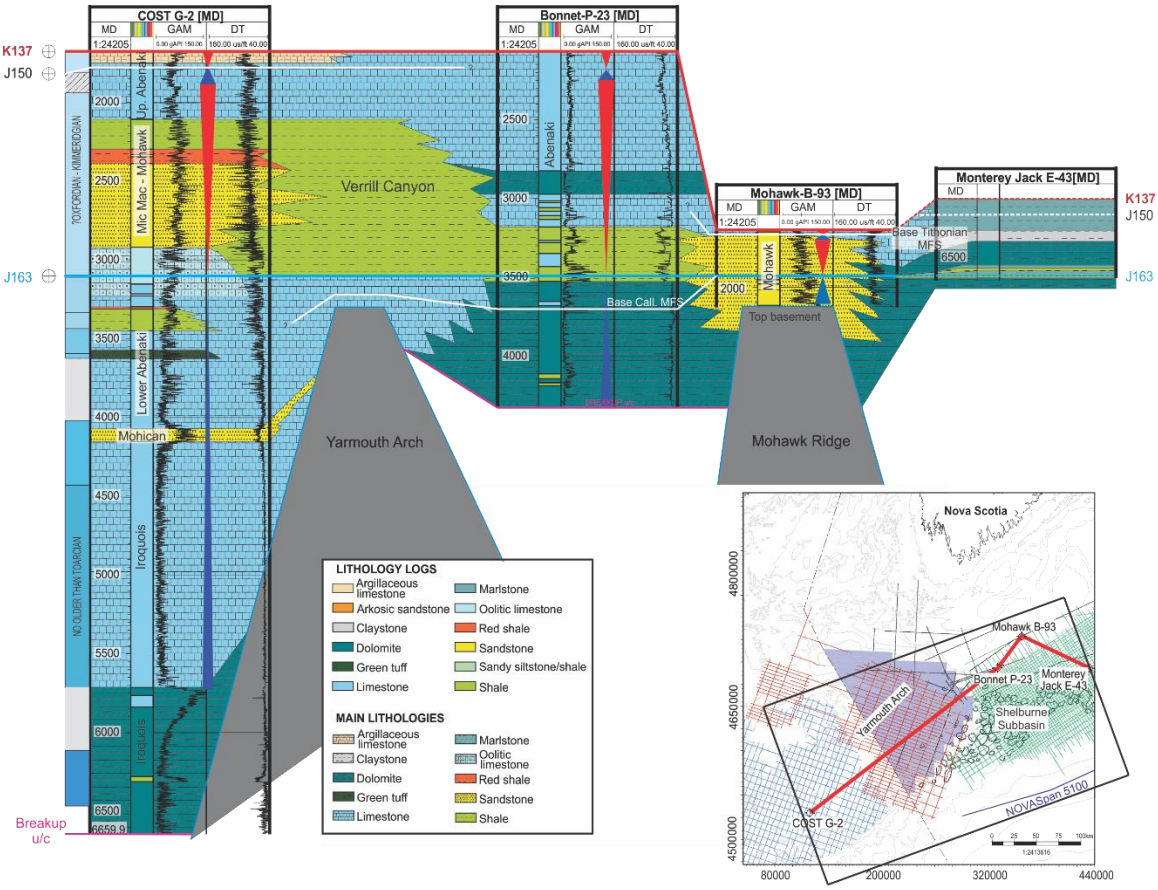

Figure 4.3: Well correlation diagram for the studied wells of interest from the breakup unconformity to the K137 seismic marker. Flattened on the J163 seismic marker.

Salt movement in the basin began in the Middle Jurassic (Kidston et al. 2002), and affected sediment pathways and distribution in deep-water. Salt is commonly found as diapirs, pillows, and large salt rollers, which are typically caused by sediment loading due to prograding deltaic systems such as the Shelburne Delta (Kidston et al. 2002, Deptuck et al. 2015). Shimeld (2004) classified different styles of salt tectonics in the Scotian Basin. Subprovince I is located immediately down-dip of Georges Bank and consists of autochthonous salt diapirs. Subprovince II coincides with the Scotian Shelf east of Bonnet-P-23, and consists of salt walls that roughly parallel the Abenaki carbonate bank (Ings and Shimeld 2006). Structural Style C of Albertz et al. (2010) consists of salt diapirs and walls with intervening minibasins.

Hinterland geology consists of the Neoproterozoic–Paleozoic Appalachian orogen (van Staal and Barr 2012) with overlying Carboniferous and Triassic basins, and further towards the stable cratonic interior, the Mesoproterozoic crystalline basement rocks of the Grenville Province (Fig. 4.5).

Paleoriver systems and river drainage areas have been defined for the Scotian Basin based on provenance studies. The principal river system that supplied the central Scotian Basin with sediment was the Sable River, which built the Sable Delta (Jansa and Wade 1975), and drained the area of the Labrador rift and the Appalachians from the Late Jurassic to the mid-Cretaceous (Pe-Piper and Piper 2012a). The Meguma Terrane supplied sediment to the central and western Scotian Basin in the Middle Jurassic (Li et al. 2012), continuing through the Late Jurassic and Early Cretaceous in the western Scotian Basin through small local river systems (Fig. 4.5) (Dutuc et al. 2017).

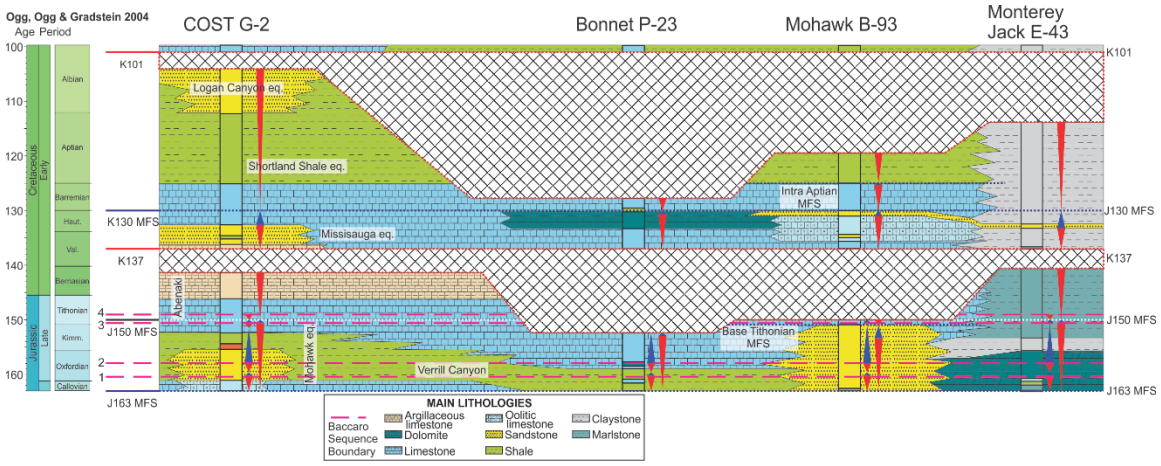

Figure 4.4: Chronostratigraphic correlation of the studied wells from the breakup unconformity to the K101 seismic marker. Modified from NSDoE (2015).

In the study area, detrital petrology of the Mohawk B-93 well (Fig. 4.1) indicates a predominant Meguma Terrane source through the Jurassic and Cretaceous, implying supply from small river systems draining southern Nova Scotia (Fig. 4.5) (Dutuc et al. 2017). However, minor chemically distinct garnets and Pb isotopes in feldspars suggest a minor contribution from the Canadian Shield (Fig. 4.5A) (Blowick et al., submitted), presumably via a river flowing through the Fundy Basin and possibly represented by the Vinegar Hill deposit in southern New Brunswick (Piper et al. 2007). On Georges Bank, sediment supply to the COST G-2 well changed throughout the Late Jurassic to Early Cretaceous, partly as a response to tectonics or climate change (Chavez et al. 2019). During the Oxfordian, sediment supply was from coastal Maine, but by the uppermost Jurassic, the river drained more inbound Appalachian terranes (Fig. 4.5A). By the Early Cretaceous, the drainage area enlarged to include most of Maine, New Brunswick, and parts of New Hampshire (Fig. 4.5B) (Chavez et al. 2019).

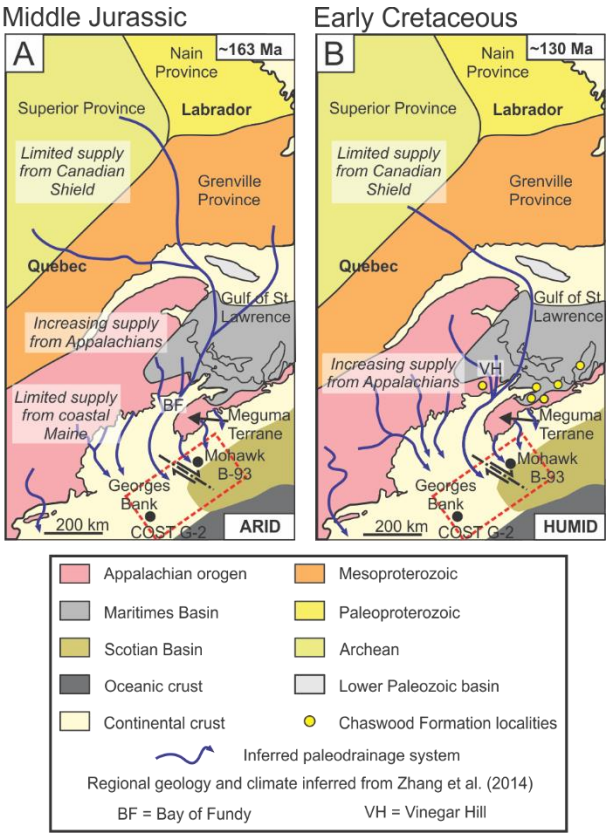

Figure 4.5: Map of eastern Canada showing the possible drainage areas of river systems for (A) Middle Jurassic and (B) Early Cretaceous from the literature (e.g. Tsikouras et al. 2011, Li et al. 2012, Zhang et al. 2014, Dutuc et al. 2017, Chavez et al. 2019, Blowick et al. submitted) that would have transported sediments into the Scotian Basin.

4.3 Modeling Procedures

In order to simulate sediment distribution in the Mid–Late Jurassic, DionisosFlow™ was used to create high-resolution forward stratigraphic models. These models are calibrated against stratigraphic thickness from seismic horizons and interpreted sediment facies from well logs. Sensitivity analysis is then performed on the calibrated models using CougarFlow™, a statistical analysis software, which uses response surface methodology (RSM) to evaluate the most influential uncertain parameters (Agrawal et al. 2015, Hawie et al. 2015, 2019). The goal of this modeling process is to reproduce large-scale and long-term geological trends of sediment distribution in the basin.

4.3.1 DionisosFlow™

DionisosFlow™ is a diffusion-based modeling software that was developed in the late 1990's, and is able to simulate basin infill on a scale of tens to hundreds of kilometers, over a period of tens of thousands of years to hundreds of millions of years (Granjeon and Joseph 1999, Granjeon 2014, Granjeon et al. 2017). It works by calculating the relationship between accommodation, sediment supply, and sediment transport for each time step of the model (Kolodka et al. 2016, Granjeon et al. 2017, Hawie et al. 2017). The sediment entry points for fluvial supply of sediment are user-defined in terms of geographic location, sediment yield and grain size proportions through time.

Accommodation is defined as the amount of available space for sediment accumulation, and is governed by eustatic sea level variations as well as processes such as tectonic subsidence and uplift, compaction, and salt diapirism. Sediment supply refers to the amount of terrigenous sediment input plus in situ carbonate production (Kolodka et al. 2016). Carbonate production considers the different producers of biogenic carbonate, constrained by their respective environmental properties (wave energy, bathymetry, fluvial discharge, and water column turbidity). Transport of the sediments is simulated using a diffusion equation applied to the different sediment grain sizes (e.g. clay, sand, eroded carbonates) considered in the model.

This study utilized non-linear slope- and water-driven diffusion that combines empirical water- and gravity-driven diffusion processes (water discharge driven transport) (Hawie et al. 2017). The following equation describes sediment transport in the model:

$$Q_s = -(K_s/\vec{\nabla}h \; + \; K_w Q_w^m S^n)$$

where Q_s is the sediment flux (km^3/Ma), K_s and K_w are the diffusion coefficients (km^2/ka) for hill slope creeping and water discharge driven transport, respectively, h is the elevation (m), Q_w is water discharge (m^3/s), S is the gradient of the slope in the basin, and m and n are constants between 1 and 2 (Tucker and Slingerland 1994). The diffusion coefficients vary according to sediment grain size e.g., terrigenous mud is more diffusive than sand.

In order to account for different types of sediment flow within natural systems, DionisosFlow™ uses two processes. (1) Low energy long term (LELT) processes, which represent continual and long-term sediment transport into the basin. (2) High energy short term (HEST) processes, which represent high energy sediment delivery into the basin, caused by storms and fluvial flooding, resulting in turbidity currents. Although HEST processes are short-lived, they may be responsible for transporting most sediment into the basin, especially into deep-water environments.

4.3.2 CougarFlow™

Following the manual calibration of the reference case model, CougarFlow™ software was used to test sensitivity within the defined DionisosFlow™ parameters. This software works by running multiple DionisosFlow™ models with varying uncertain parameters. This study employs Latin Hypercube experimental design in order to define a set of simulations which allows for uniform sampling of the entire uncertain domain (Agrawal et al. 2015, Hawie et al. 2015). With increasingly uncertain parameters, a higher number of simulations will be required in order to accurately define the response surface, which is a mathematical regression model.

Response Surface Methodology (RSM) is the process of exploring the relationship between the uncertain parameters used in the experimental design and one or more responses (Hawie et al. 2015). In the case of this study, the responses are the calibration indicators (section 4.3.3) and areas of interest in the model (e.g. the Shelburne Delta or facies extent of basin floor fans). The goal of RSM is to approximate the output results through a second-degree polynomial function or by kriging interpolation (Hawie et al. 2015, 2019), which allows for a qualitative and quantitative analysis of the uncertain parameters on the response surface. To test the accuracy of the response surface, a small number of confirmation runs are run against the surface, in order to determine the predictivity of the surface. Once this is completed, a Monte-Carlo analysis is performed on the response surface, in which a probabilistic distribution of uncertain parameters is applied to the response surface, and the results are recorded. This allows a probabilistic display of results and the possibility to get predictions on the behaviour of the sedimentary system without running additional simulations.

4.3.3 Model Calibration Strategy

One model was calibrated for the studied time span (163-150 Ma), representing the deposition of the Abenaki, and Mohawk formations. The bounding surfaces of the model are represented by the J163 (top Callovian) and J150 (top Tithonian) seismic horizons (NSDoE 2015), both of which are maximum flooding surfaces (MFS). A regional thickness map from these surfaces accounts for any vertical salt movement. This movement is assumed to be uniform and averaged through the modeled time span. Areas of the thickness map with negative or zero values, were assumed to be salt, and were given low thickness values extrapolated from neighbouring cells. Sediments are modeled

with zero porosity, and therefore sediment compaction is not considered, so that sediment flux in the model needs to be corrected for this effect in comparison to modern rivers. The size of the model is 400 x 225 km (248 mi x 140 mi), with a cell size of 5 km x 5 km (3.1 mi x 3.1 mi), and time steps are of 0.1 Ma.

The model was calibrated by altering sediment supply and water discharge from each of several river input points, as well as altering carbonate production, carbonate environmental conditions, diffusion coefficients, and subsidence. The calibration goal of the study was to obtain a minimum 80 % match to regional thickness and well lithofacies. This was verified by comparing the simulated thickness to the regional thickness map and to selected seismic lines within the study area, and comparison with lithofacies and thickness in wells using calibration indicators (see Appendix 4, Supplementary Table S4).

Sediments in reference wells have been grouped into lithofacies (e.g. reef, limestone, sandstone, shale, marl, etc.), based on well cuttings and petrophysical logs. In order to assign lithofacies in DionisosFlow^{TM}, allowable ranges of sediment proportions are required, and are chosen to match the observed lithofacies in well (Appendix 4, Supplementary Table S1). This approach is only qualitative, because it does not consider the proportion of each grain size available in a traditional lithofacies classification scheme (Sangster et al. 2019). Since the observed lithofacies are at a much higher resolution than the simulated lithofacies, it was necessary to upscale the well logs in some reference wells, by averaging the lithofacies through time, to match the cell size and time steps of the simulation.

Simulated lithofacies were compared with actual lithofacies using a calibration indicator script that takes into account the similarity of each facies and its thickness. The global facies calibration indicator is the average of the well facies calibration indicator at each reference well and provides an overview on the scale of the entire study area as to how well the facies are calibrated.

To measure the well thickness calibration, another script was used that calculated the proportional difference between the simulated thickness and the actual well thickness. The value of this indicator can be increased by varying the rate of subsidence around the individual well, in order to increase or decrease accommodation, allowing for a higher well thickness calibration.

4.3.4 Modeling Limitations and Assumptions

It is important to understand limitations and assumptions associated with the forward stratigraphic modeling process. For instance, subsidence in the model is considered to be uniform and constant through a user defined period of time, but in reality, differential subsidence most likely occurred. In order to develop a calibrated model, reef production was limited to the J150 shelf edge, instead of the entire carbonate ramp defined for the J163 marker. A negative source was used in the model in order to allow for an open-box approach, allowing sediment to leave the modeled area, as in a natural environment. As DionisosFlow™ reproduces sedimentation and erosion on a scale of thousands of years or more, it is not possible to reproduce individual small-scale sedimentary features due to the limitation of the cell size (Kolodka et al. 2016) and the assumptions inherent in a diffusion-based model. This limitation represents a valid compromise between small-scale models, which are able to provide detailed and almost

instantaneous sedimentation results that are impossible to extrapolate to thousands or millions of years (Seybold et al. 2007), whereas medium- to large-scale models consider only the long-term behaviour of sedimentary systems (Granjeon and Joseph 1999).

4.4 DionisosFlow™ Parameters

In order for DionisosFlow™ to produce geologically accurate reference case models, information about the sea floor bathymetry, eustasy, sediment supply (water discharge, sediment load, and grain size), carbonate production, and regional thickness of stratigraphic units are necessary to provide geological constraints to the model.

4.4.1 Eustasy

The eustatic curve from Haq (2014) was used in order to simulate transgressive and regressive events within the model. The sediment proportion for each input point was normalized to the eustatic curve to induce a climatic control on the proportion of fine to coarse clastic supply, allowing more sands coming to the basin during regressive episodes, and less during transgressions.

4.4.2 Carbonate Production

Carbonate production for the model has been interpreted from modern analogs in the Great Barrier Reef, with values of production ranging from 1000-8000 m/Ma (3280-26,246 ft/Ma) (Davies and Hopjey 1983), except where clastic sedimentation rates are greater than 250 m/Ma (~820 ft/Ma), causing a noticeable decrease in carbonate production due to turbidity (Woolfe and Larcombe 1999). Two separate sediment classes in the model account for carbonate production: (1) reef sediments and ooids, which follow a traditional T-factory growth curve (Schlager 2005), and have a grain size of 1 mm (0.04 in). (2) Fine-grained carbonate sediments (micrite, marl, etc.), which follow a

M-factory growth curve (Schlager 2005), and have a grain size of 0.04 mm (0.00157 in). The reliability of Holocene reef analogs to ancient reef environments is unknown, as the extent of reefs was at least 10° greater in latitude than today (Leinfelder et al. 2002), and the climate was warm and arid (Sellwood and Valdes 2008).

4.4.3 Sediment Supply

Recent provenance studies were used in order to define different river systems providing the input points to the modeled area for the Mid–Late Jurassic. The three main river systems are as follows:

1. Small local rivers derived from the Meguma Terrane, which were the principal source of sediment to the Mohawk B-93 well (Dutuc et al. 2017).
2. A large river draining coastal Maine in the Oxfordian, that expanded in the Late Jurassic to drain parts of New Brunswick, New Hampshire, and the majority of Maine (Chavez et al. 2019).
3. A large river draining parts of New Brunswick, and possibly further back to the Canadian Shield (Dutuc et al., 2017; Blowick et al., submitted) that flowed through the Bay of Fundy. This river system was responsible for building the Shelburne Delta and supplied small amounts of sediment to the Mohawk B-93 well.

Sediment supply from these three river systems have been estimated from modern river systems (Milliman and Syvitski 1992) on the basis of the size of the catchment area, and amount of uplift that had occurred during the modeled time span (Appendix 4, Supplementary Table S2) (Fig. 4.6). Two grain sizes are modeled from these river

systems: sand with a grain size of 0.2 mm (~0.008 in), and terrigenous mud with a grain size of 0.02 mm (~0.0008 in).

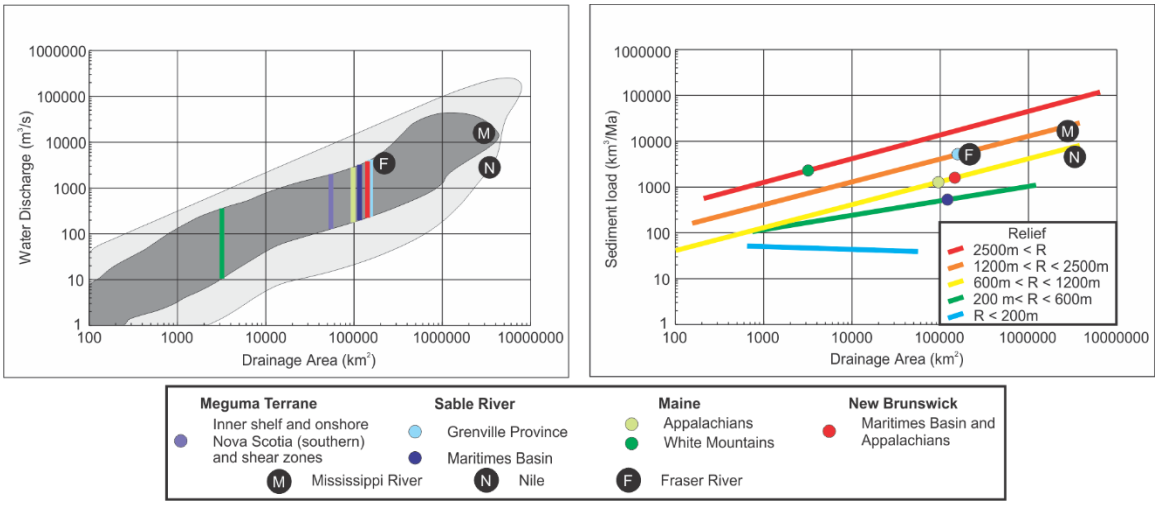

Figure 4.6: Location of ancient river systems and representative values of area and uplift plotted on modern river systems defined by Milliman and Syvitski (1992) in order to estimate the values of water discharge and sediment load of the ancient river systems.

The Meguma Terrane river catchment area is relatively small, since it is bounded by the Fundy Basin. A 130 km x 150 km (~80 mi x ~93 mi) catchment area is assumed. For the Maine river catchment area, apatite fission track analysis indicates that the White Mountains had approximately 3 km (~2 mi) of uplift (Doherty and Lyons 1980, Amidon et al. 2016), and coastal Maine had approximately 0.5 km (0.31 mi) of uplift in the Jurassic (Doherty and Lyons 1980). Naeser and Brookins (1975) indicated that central and coastal Maine experienced 12.5 km of uplift between the Permian and the Jurassic based on apatite and sphene fission track analysis; however, Doherty and Lyons (1980) cautions that this large amount of uplift may be unrealistic based on the high apatite annealing temperature that was used. Therefore, we assume that the rest of the river catchment area in Maine had a maximum of 1.3 km (~0.8 mi) of uplift in the modeled time span. For the larger Bay of Fundy river catchment area, an estimate of 1 km (0.62

mi) of uplift was used based on analogues from the Appalachians (Naeser and Brookins 1975, Doherty and Lyons 1980, Matmon et al. 2003).

4.4.4 Bathymetry

In order to begin the modeling process, DionisosFlow™ requires an initial paleobathymetry surface representing the geometry of the basin. The initial bathymetry at the J163 marker (Fig. 4.7A) was adopted from the Shelburne Subbasin Postmortem Analysis (OERA 2020), because the only well in deep-water, Monterey Jack E-43, had a consensus evaluation of a shallow carbonate ramp environment. Water depths on the shelf were estimated from reference wells for both the initial and final bathymetries. The bathymetry at the J150 marker was also included to put constraints on the accommodation space at the final age of the model. This bathymetry map (Fig. 4.7B) used seismic interpretation (OETR 2011), basement morphology, water depths of modern analogues, and thermal models of rifted margins, for basinal water depths. The water depth in the basin was interpreted to ~1400 m (~4600 ft).

Due to the uncertainty in the available bathymetric data, two other models were made to test the variance from the reference case model. Model B assumes that a shelf edge reef was present at J163 and supplied reworked shallow-water limestone to Monterey Jack E-43. The water depth in the basin was set at approximately 1000 m (3280 ft) (Fig. 4.7C). The final bathymetry is unchanged from the reference case model (Fig. 4.7D). Model C assumes that the bathymetry for the J163 and J150 was much deeper (Figs. 4.7E, F), based on calculated subsidence rates of oceanic crust (Sclater and Parsons 1977) since initial spreading at 177 Ma estimated from constant spreading rates between the East Coast Magnetic Anomaly (ECMA) and the Blake Spur Magnetic Anomaly

(BSMA), with mantle exhumation starting at 190 Ma (Sibuet et al. 2012). In Model C the J163 and J150 basin water depths reach ~1500 m (~4900 ft) and ~2100 m (~6900 ft), respectively.

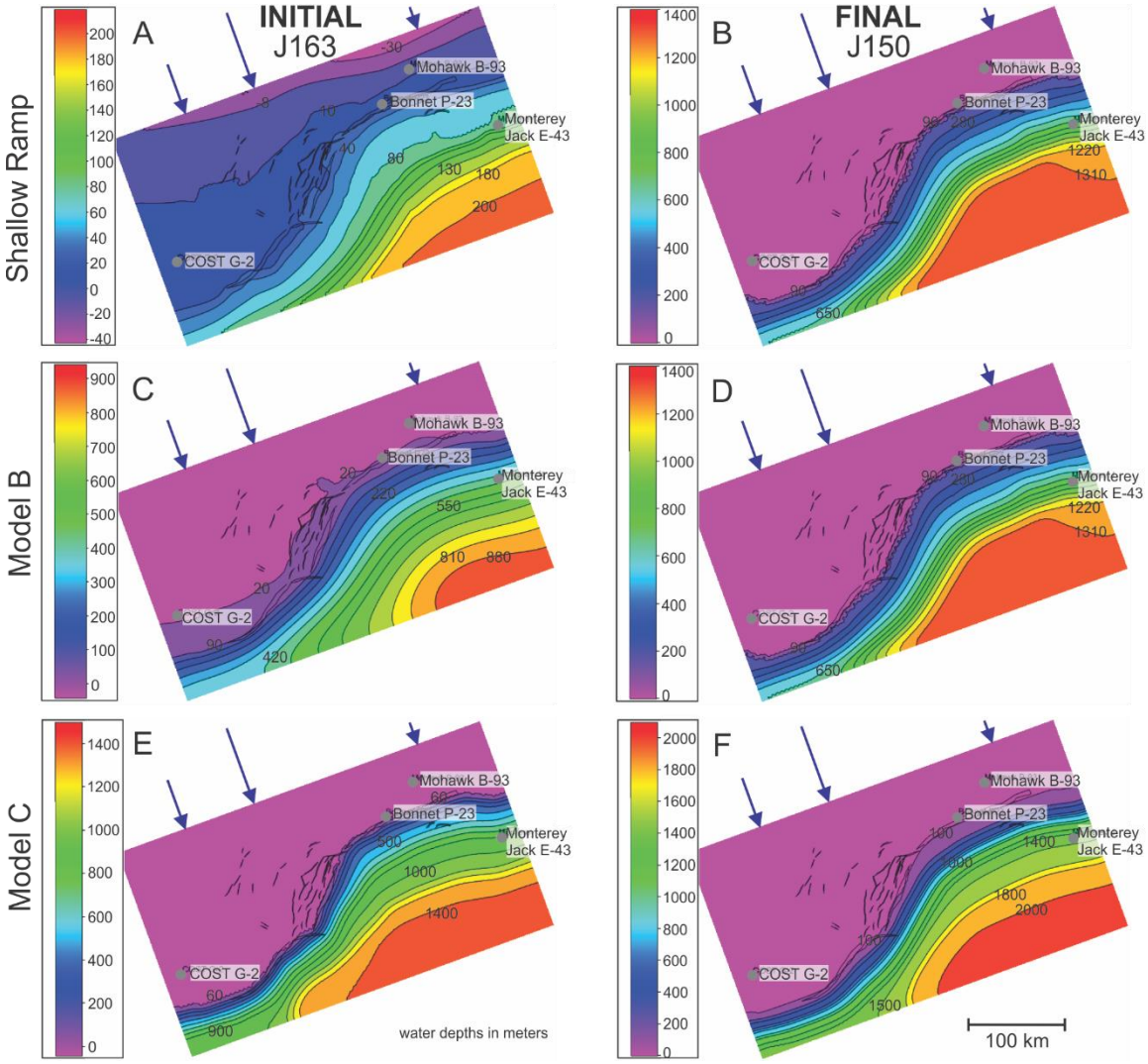

Figure 4.7: The initial (J163) and final (J150) paleobathymetries defined for the three bathymetric models. Blue arrows indicate river inputs (A) Reference case (ramp). (B) Model B (persistent reef). (C) Model C (deep basin). Black lines indicate faults cutting J150.

4.4.5 Diffusion Coefficients

Low energy long term (LELT) diffusion coefficients are estimated for each sediment grain size in the model using the non-linear sediment transport equation (section 4.3.1). Following the first initial run of the model, each diffusion coefficient is modified by the same proportion in order to respect regional seismic interpretation and geological architecture. High energy short term (HEST) diffusion coefficients are based on Sangster et al. (2019), who used climate modeling from Haywood et al. (2004) for the Early Cretaceous of the North Atlantic region. However, the Jurassic climate was more arid and likely highly seasonal (Sellwood and Valdes 2008) and so high energy events were set to double the Early Cretaceous frequency of Sangster et al (2019), and brought in double the water discharge values and delivered 40% more sediment compared to LELT times.

4.5 CougarFlow™ Parameters

Sensitivity analysis was performed using CougarFlow™ in order to test the distribution of sand compared to the uncertain parameters. Fifteen uncertain parameters were chosen from the available geological data (Supplementary Table S3).

Since the model is well calibrated for regional thickness, only the value for water discharge, the location of the source, and the sediment proportions of different grain sizes in the sediment were varied for each interpreted river system. Water discharge is varied -20 % to +50 % in order to account for uncertainty in river catchment areas, degree of uplift, and Middle Jurassic climate. Increasing water discharge causes clastic sediments to prograde further into the basin. The positions of the input points were each varied ±30 km (18.6 mi) along strike, given the uncertainties in their interpreted location. The

sediment proportion of each source was varied ±20 % in order to account for uncertainty in normalizing to the eustasy curve.

The initial bathymetric map was varied +32 % to account for geological uncertainties, particularly regarding the water depth at the base of the Monterey Jack well. Carbonate production was varied ±20 % to account for differences in carbonate production with respect to clastic sediment supply.

To test the extremes of sediment transport, the diffusion coefficients for sand in a continental and marine environment were varied by an order of magnitude. Increasing the diffusion coefficients results in sand being transported further seaward in the model. Climate influences total water and sediment discharge and the frequency of floods, as modeled by HEST events. Water discharge during HEST events was allowed to vary between 1.6 and 10 times LELT water discharge values.

4.6 Results

4.6.1 Reference Case Model

Simulation results for the reference case model are divided into three main temporal phases: (1) carbonate drowning, (2) clastic sedimentation, and (3) return to a carbonate environment. Values of sediment supply for each temporal phase of sedimentation, along with carbonate and hemipelagic sedimentation rates can be found in Appendix 4, Supplementary Tables S5 and S6, respectively. The results for each phase are described in reference to their paleogeographic location (shelf, slope, and basin floor), extent of each sediment class, and overall thickness. After the initial reference case model is described, the results for the different bathymetric models B and C are presented.

4.6.1.1 Carbonate Drowning Phase

From 163–161 Ma, clastic sediments with ~6–52 % sand are mostly deposited landward of the paleo shelf edge (Fig. 4.8A). Reef sediments decrease in extent from 163–161 Ma, and occupy the area between the shelf edge and marine clastic deposits. The slope and basin floor consist of hemipelagic mud and carbonate mud, with less than 1 % of sand. A small amount of clastic sediment with higher amounts of sand progrades into deep-water seaward of Georges Bank and the canyon system near Mohawk B-93 (Fig. 4.8A), which may be the result of the small regression at this time (Figs. 4.2, 4.3).

4.6.1.2 Clastic Sedimentation Phase

The interval from 161–153.1 Ma represents a large pulse of clastic sediment delivery to the shelf, slope, and basin floor. Reef sediments become limited to patches along the shelf edge. A large amount of sand is transported to the shelf edge (Fig. 4.8B) from the Bay of Fundy source, building the Shelburne Delta. Sediments crossing the delta front are delivered to the slope and basin floor. Away from clastic inputs, basin floor and slope sediments consist of hemipelagic mud and carbonate mud. Sand content during this phase is 10–45 % on the shelf, 5–40 % on the slope in the areas of Georges Bank and the large canyon system near Mohawk B-93, and less than 1 % in the deep basin (Fig. 4.8B). This phase is dominated by a sea level rise, indicating that erosion in the hinterlands and delivery of sediment to the Shelburne Delta overprinted this transgression.

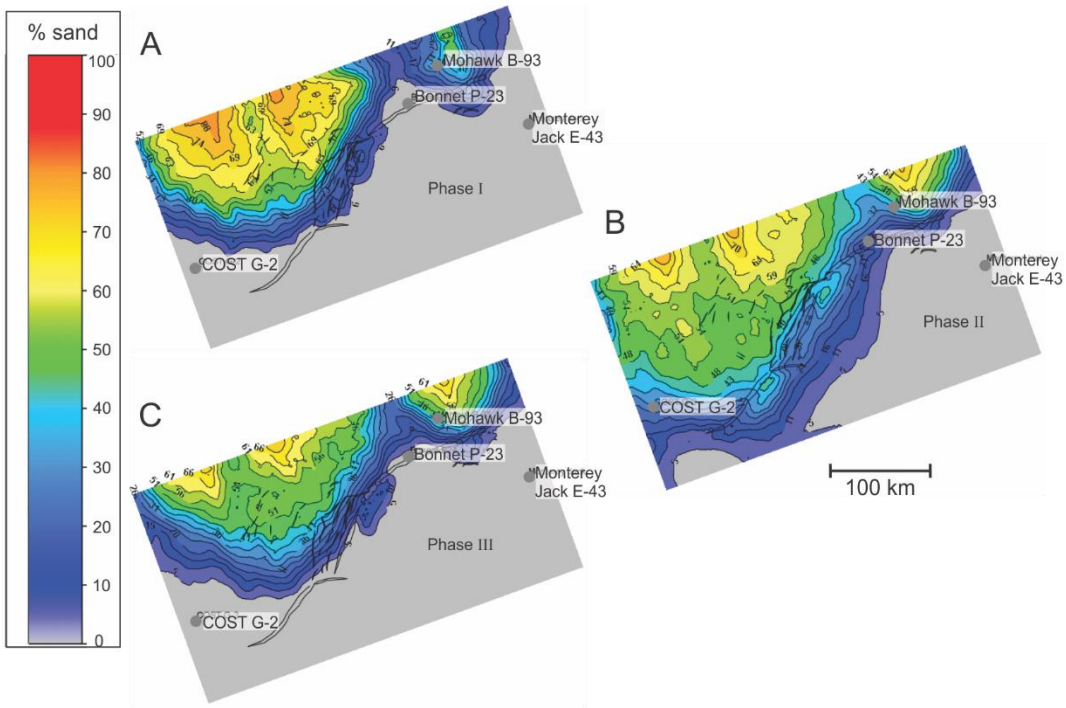

Figure 4.8: Sand distribution for the three phases of sedimentation in the reference case model. (A) Carbonate drowning phase I (163–161 Ma). (B) Clastic sedimentation phase II (161–153.1 Ma). (C) Carbonate re-establishment phase III (153.1–150 Ma). Black lines indicate faults cutting J150.

4.6.1.3 Carbonate Re-establishment Phase

From 153.1–150 Ma, there is a decrease in sediment supply from the Maine and Bay of Fundy river systems. This phase is marked by a return to a carbonate-dominated environment. Reef sediments extend all along the shelf, and coarse clastic sediments are largely restricted to the shelf. Near the shelf edge, in the vicinity of the Shelburne Delta and the canyon system near Mohawk B-93, a small amount of clastic sediment progrades into the basin (Fig. 4.8C). Fine-grained carbonate mud occurs in the back-reef, possibly forming lagoonal deposits. The slope and basin floor consist of hemipelagic mud and carbonate mud at this time. Although there is a marked decrease in sediment supply, sand is still transported deep into the basin. The average sand content on the shelf is up to 45

%, the slope in prograding clastic areas contain 5–15 %, and the deep basin contains less than 1 % (Fig. 4.8C).

4.6.2 Full Modeled Sequence

The simulated time span from 163–150 Ma was calibrated to match geological data (well logs and facies), regional thickness, and geological architecture interpretations from seismic records (Appendix 4, Supplementary Table S4). The model matches reference well facies and thickness with an overall calibration of 76 % and 99 %, respectively. A lower facies calibration percent is inevitable given the simplification of the lithofacies in some of the reference wells in order to match the 5 km x 5 km (3.1 mi x 3.1 mi) cell size and 0.1 Ma time step in the model. Overall regional thickness calibration is 98 %, with areas of low calibration along the slope and at the deep-water edge of the model (Fig. 4.9A).

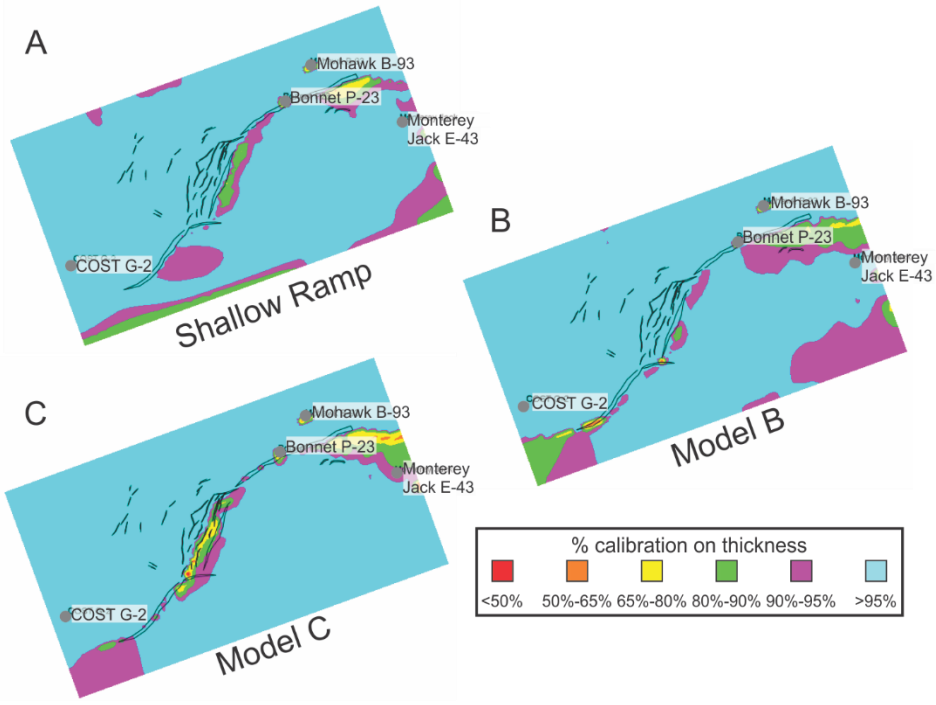

Figure 4.9: Thickness calibration percent for the three bathymetric models. Percent maps are calculated by simulated 100*thickness/actual thickness. (A) Reference case (ramp).

(B) Model B (persistent reef). (C) Model C (deep basin). Black lines are faults cutting J150.

The maximum thickness of sand is ~1400 m (~4600 ft), in faulted areas near the shelf edge and a salt withdrawal minibasin. Deep-water clastics seaward of the Shelburne Delta form a basin floor fan up to 700 m (~2300 ft) thick with up to 33 % sand. Small tongues of sandy clastic sediment are also present in the deep basin, suggesting that clastics, crossing the Shelburne Delta, are accumulating outside of the study area.

4.6.3 CougarFlow Analysis of the Reference Case Model

Sensitivity analysis of 350 simulations indicate that the location of the sources, the diffusion coefficients for sand, and the initial bathymetry are the most sensitive parameters controlling facies calibration. The basin floor fan (Fig. 4.10B) is highly predictive at 90 %, with the diffusion coefficients for sand, the water discharge value for the Bay of Fundy source, and the location of the Maine source affecting overall thickness. The least variance of sand distribution occurs immediately down-dip of the Shelburne Delta, just past the shelf edge (Fig. 4.10C).

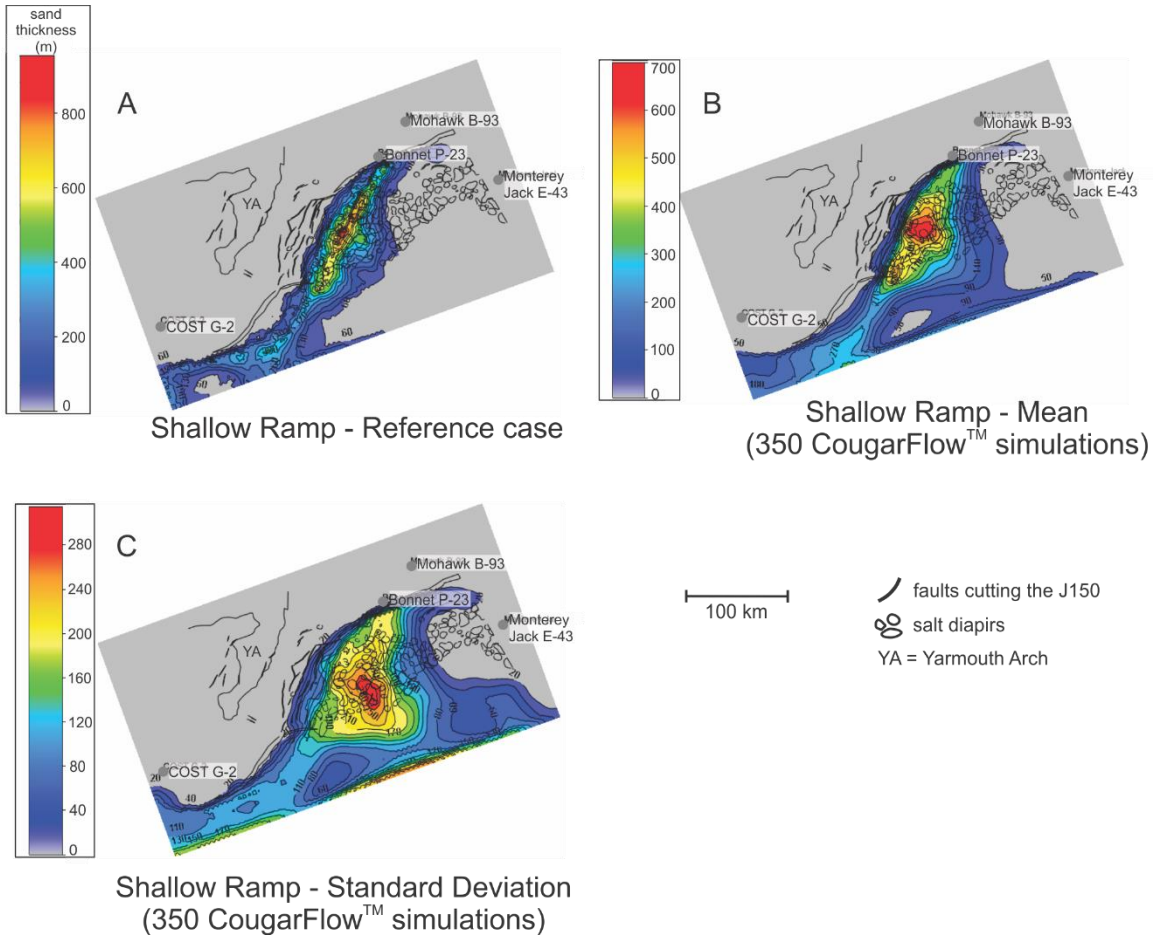

Figure 4.10: Thickness maps of the basin floor fans (BFF) facies for the reference case model and CougarFlow™ results. (A) Reference case model. (B) Mean facies thickness from 350 simulations. (C) Standard deviation of the 350 simulations from (B).

The average sand proportion of the 350 simulations ranges from ~10–45 % on the shelf, 9–43% on the slope (down-dip of the Shelburne Delta), to less than 3 % in the deep basin. The sand content on the shelf near Mohawk B-93, seaward of the Meguma river input point, has the most variance from 9–20.5 % (Fig. 4.11A2). Seaward of the Bay of Fundy and Maine river input points, higher variance of 10–17 % occurs near the input point, but closer to the shelf edge, there is much less variance in sand content. Sand content has a variance of 5–12 %, along the slope, not just in the area of the Shelburne Delta. This suggests that the Bay of Fundy and Maine sources fed sediments into deep-

water all along Georges Bank, although most of the sand is located in the area of the Shelburne Delta. The high clastic content and slope architecture off southwestern Georges Bank is an artifact of edge effects created by the model. The rest of the basin has low variance in sand content.

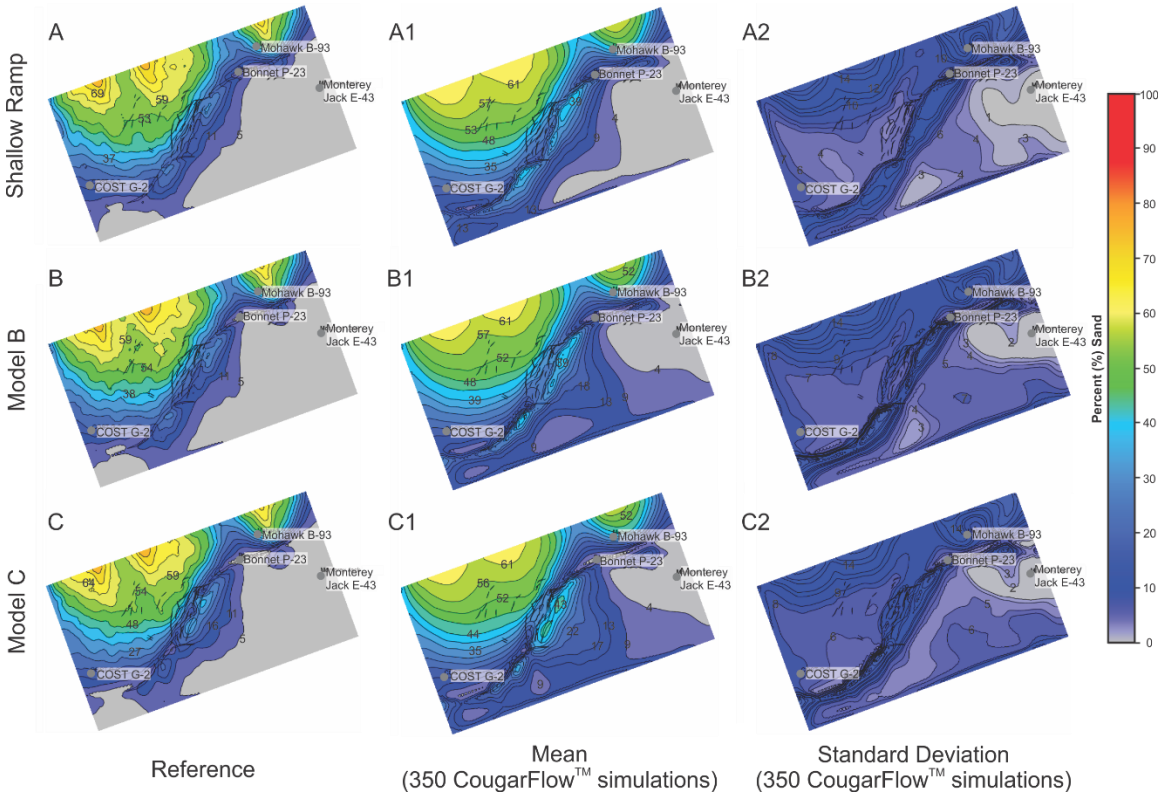

Figure 4.11: Sand distribution maps for each bathymetric model and their respective CougarFlow™ model. (A, A1, A2) Reference case (ramp). (B, B1, B2) Model B (persistent reef). (C, C1, C2) Model C (deep basin). Black lines indicate faults cutting J150.

Further sensitivity analysis was performed on carbonate sediments because they make up a major component of the sedimentary system. CougarFlow™ results from the 350 simulations indicate that the distribution of carbonate sediments on the shelf is very stable throughout the uncertainty testing. A reef consistently forms along the shelf edge, except in the area of the Shelburne Delta. Closer to shore, the proportion of carbonate sediments diminishes to less than 20 %, as clastic sediments enter the marine

environment. The main parameters controlling the location of the carbonate sediments on the shelf are the eustatic variations, the location of the river inputs, the initial bathymetry, and the diffusion coefficients for sand. Carbonate sediments show little variance on Georges Bank, however, they show up to 35 % variance east of Bonnet P-23. This suggests that the Meguma river source may have been an important supply that was able to reduce the growth of carbonate sediments.

4.6.4 Variation in Sediment Distribution with Different Paleobathymetries

The two additional calibrated models, B and C, test the uncertainty in the paleobathymetry using the same sediment supply values, diffusion coefficients, carbonate production, and eustasy curve as the reference case model (A). The models differ with respect to subsidence and hemipelagic sedimentation rates, slope, water depth, and sediment distribution in the basin. Calibration indicators for these models are found in Appendix 4, Supplementary Table S4.

Model B, with a shallow basin and shelf edge reef at J163, has a very similar distribution of sediment on the shelf as the reference case model, but the slope contains a higher sand content and thickness (Fig. 4.11B) and sand also extends further into the basin, likely due to the increased regional gradient. A thicker basin floor fan developed close to the base of slope, immediately down-dip of the Shelburne Delta. Model C with a deeper basin, also has a similar sediment distribution as the reference case model. Sand content and thickness are greater in deep water than in the reference case model and model B down-dip of the Shelburne Delta (Fig. 4.11C).

4.6.5 Seismic Evidence for Deep-water Sand Facies

Seismic analysis on the study area, particularly in deep-water, was performed in order to better understand sediment pathways around Georges Bank, in the vicinity of the Shelburne Delta. It shows multiple pinch-out, onlap, toplap, and channels features (Fig. 4.12). However, interpretation is difficult due to complicated salt tectonics, and the sparsity of data coverage. Nevertheless, a large, approximately 2.5 km (~1.5 mi) channel was found, with well developed levee crests (Fig. 4.12B), corresponding to Phase 2 of clastic sedimentation in the model, demonstrating the presence of clastic sediments in deep-water.

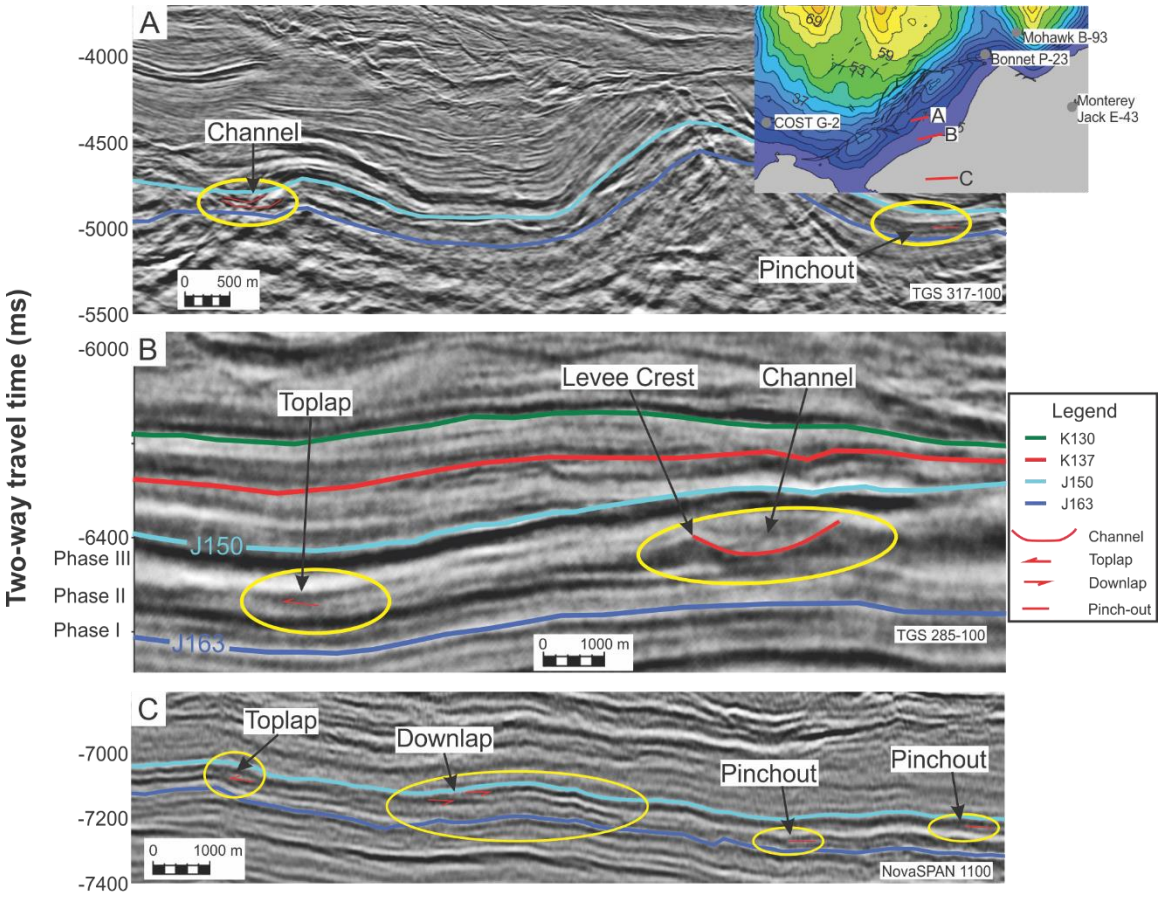

Figure 4.12: Representative seismic interpretations seaward of the Shelburne Delta. (A) Pinch-outs and channels. (B) Toplap and channel levee systems. (C) Toplap, downlap, and pinch-outs.

4.7 Discussion

4.7.1 Model Performance in Predicting Geological Features

4.7.1.1 Data Used for Calibration

All models show relatively low facies calibration (67–75 %) for the Mohawk B-93 and COST G-2 wells compared to similar modeling studies (Sangster et al. 2019). This is most likely due to averaging the lithofacies in order to match the cell size of the model. Closely spaced wells in the Central Scotian Basin show rapid lateral changes in facies (Cummings et al. 2006, Gould et al. 2012) that Sangster et al. (2019) showed could not be captured by a 5 km (3.1 mi) grid. Although the cell size of the models may be too large to capture these lateral variations in facies, the model was able to simulate the COST G-2 well sequences accurately when compared to the well log of Amato and Simonis (1980) (see Appendix 4, supplementary appendix S7). This suggests that the time step of 0.1 Ma is appropriate for the model because this fine-scale alternation of facies over time was captured.

The reference case model appears plausible because it matches our understanding of the regional geology. It also reproduces sedimentary sequences and alternating packages of carbonate and clastic sediments. It respects the lithofacies interpretation at wells, the regional thickness map and shelf edge interpretations from seismic data. However, even if a model seems plausible and matches observed data, it is just one possible scenario among several other possible combinations. The information in a single model will never be enough to conclude without reasonable doubt if the model is correct. On top of this, the interactions between carbonate and clastic sediment are difficult to accurately predict in numerical models due to the level of complexity of vertical and

lateral facies transitions in mixed sediment systems. When comparing the reference case model to regional seismic lines (e.g. NovaSPAN 1100, OETR (2011)), it is clear that most of the shelf consists of the Abenaki Formation carbonate platform, while deep-water contains probable calciturbidite deposits. In order to get the Abenaki Formation to grow in the reference case model, the use of ponderation maps were required because the initial carbonate ramp bathymetry caused the reef to prograde into deep-water, pushing the shelf edge significantly basinward. Multiple reef constraints (e.g. turbidity, wave energy, drift energy, water discharge, distance to shore, and composition of the seafloor) were used to help limit the extent of the reef, however, none were able to control the location of the reef precisely. These parameters either continued to allow the reef to grow in places where it is not developed, or completely killed production. Therefore, it was necessary to limit the extent to which the reef could grow to the J150 shelf edge. This was not required in Models B and C, however, there was little reef progradation past the J150 shelf edge in Model B, suggesting that an initial deeper bathymetry is capable of stabilizing the shelf edge. This implies that the interpretation of a carbonate ramp setting for the J163 seismic marker may be incorrect. Alternatively, it is more likely a modeling scaling effect that might be corrected by reducing the cell size in order for the reef constraint parameters to control the extent of the reef. This reflects the very fine-scale control that is necessary for mixed carbonate and clastic systems (Kolodka et al. 2016).

Although deciphering seismic facies for carbonate on the shelf is relatively straightforward, it is difficult to track the extent of calciturbidites into deep-water. The reference case model suggests that carbonate sediments extended into deep-water approximately 15 km (~9.3 mi) from the shelf edge. This narrow progradation of

carbonate sediments may not accurately represent the extent of calciturbidites deposits in the basin, furthermore, the model may not have used the appropriate diffusion coefficients in order to develop extensive calciturbidite deposits. Seismic interpretation by Kidston et al. (2005) indicates that foreslope deposits (bypass sands, reef talus, debris flows) occurred up to 13 km (~8 mi) from the shelf edge. This agrees with the reference case model.

4.7.1.2 Data not Used for Calibration

Although upper slope seismic lines were used in the interpretation of the three sedimentation phases, the model was not strictly calibrated to produce the Shelburne Delta. Instead, the model was built to respect the geometry of the margin, regional thickness, and well log and facies interpretation. The Shelburne Delta is a long-lived deltaic system that has been defined from well developed clinoforms in seismic of Cretaceous age (above the J150 seismic marker) (Deptuck et al. 2015), which was used as evidence for significant input from the Bay of Fundy river system (Chavez et al. 2019). Due to the lack of persistent marginal reef, as shown by seismics, the Shelburne Delta is thought to have been active for the Middle–Late Jurassic, and delivered clastic sediment into deep-water.

The presence of a channel-levee system (Fig. 4.12B) suggests that sand was delivered past the slope into the basin, possibly past the edge of the model. This idea of sediment bypass on the slope is reaffirmed by Moscardelli et al. (2019), who used time-thickness maps of the Middle–Upper Jurassic and Top Jurassic J150, to show that sediment pathways in the outboard region followed topographic lows defined by

underlying structures. This suggests that our model east of Bonnet P-23 should have experienced sediment bypass on the slope in the Upper Jurassic.

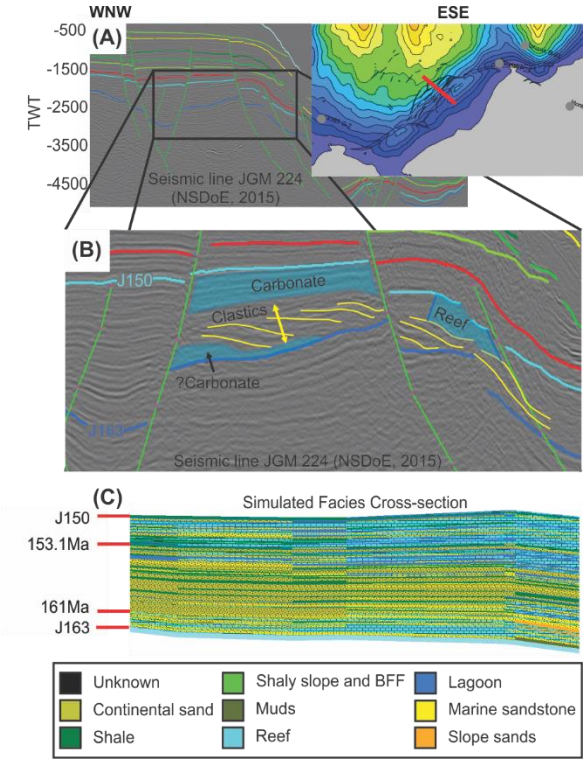

Figure 4.13: (A) Representative seismic line and (B) interpretation from NSDoE (2015) compared to (C) the reference case model. This seismic line crosses outer Georges Bank and shows the progradation of the Shelburne Delta.

Comparing the reference case model to the interpreted seismics only allows for the gross sediment trends to be realized (Figs. 4.13, 4.14), because the cell size of the model is larger than the seismic features. The Shelburne Delta commonly delivered sand to the shelf edge through the Bay of Fundy input points during all three phases of sedimentation, although supply was greatest in phase 2. Once at the delta front, sand was transported through gravity flows through channel levee systems with sand bypassing the upper slope and depositing sand on the lower slope where sand spreads out as basin floor fans. Transported sand extends to the southern limit of the model, suggesting that a small proportion of sand could be found deeper in the basin, past the edge of the model. When comparing to the two alternative bathymetry models (B and C) (Figs. 4.11 B, C), a larger proportion of sand occurs on the slope and in deep water due to the increased gradient.

The CougarFlow^{TM} analyses for each model indicate that sand can be found in deep-water, even for very small values of water discharge, sand diffusion coefficients, and climate sensitivity (HEST values). Although the diffusion coefficients and water discharge directly correlate to the distance that sand is transported, initial bathymetry is the most important parameter in controlling overall geological architecture and sand distribution in the basin. According to the analysis, the best place to find sand in all three models appears to be immediately down-dip of the Shelburne Delta, just past the shelf edge (Fig. 4.11).

Although the reference case model is well calibrated for the regional thickness map, and facies distribution on the shelf, it does not fully capture the complexity of the salt movement that occurred in the basin. Controls on salt timing are poorly defined for this part of the Scotian Basin, and only the simplistic net movements of salt are able to be captured by the model. Furthermore, the models do not discriminate between whether the shallow water biota at the base of Monterey Jack E-43 represent in-situ deposition on a carbonate ramp or resedimented material from a reef front.

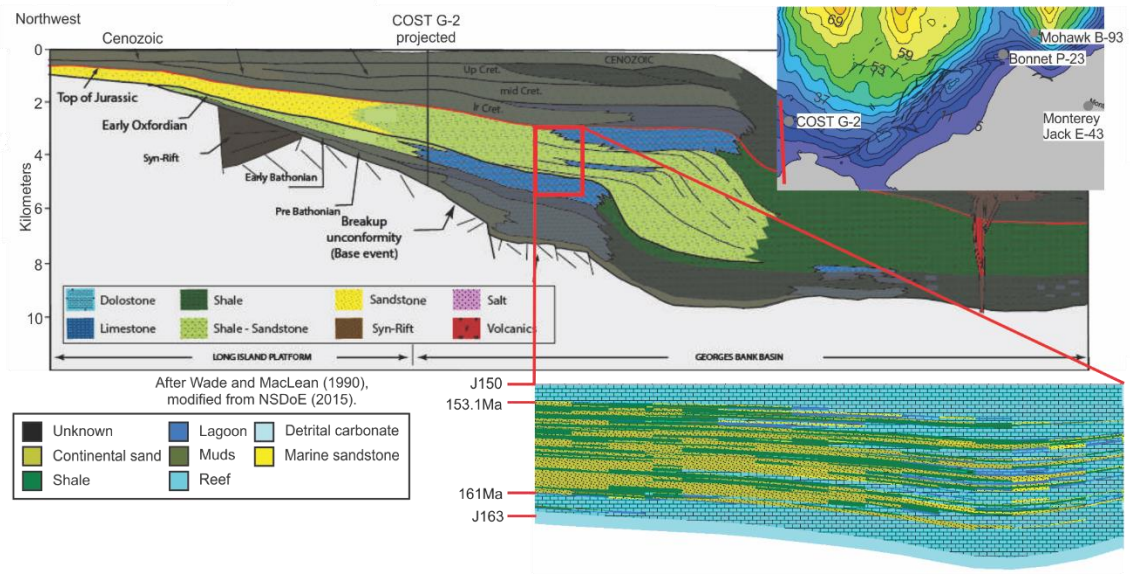

Figure 4.14: Representative seismic interpretation at western edge of study area from Wade and MacLean (1990) compared to the reference case model.

4.7.2 Transform Margins – Shelburne sub-basin

Rifted continental margins are typically divided into three main types: extension, transform, and oblique (Nemčok et al. 2016). Transform margins result from strike-slip motion along a transform fault, first within a continental domain, then between continental-oceanic domain, and passively with oceanic accretion along the axis of the transform margin (Fig. 4.15) (Mercier de Lépinay et al. 2016). Each end of the transform margin is connected to a divergent segment, with oceanic accretion starting in the inner corner (concave towards the ocean) of the transform. Transform margins are different from extensional margins because they are not normally associated with major uplift related to the thermal effects of rifting. Some uplift still occurs, through heating by newly accreted oceanic crust, progressive change in initial strike-slip regime to transpression, or flow of lower crustal material. This uplift exerts a profound effect on sediment transport through creation of bathymetric features, steeper slopes, and marginal ridges.

In the Shelburne sub-basin, the Yarmouth Transform separate shallow basement with seaward dipping reflectors (SDRs) (likely synchronous with the CAMP regional magmatic event at ~200 Ma) from deeper basement to the east. The Yarmouth Transform clearly offsets the East Coast Magnetic Anomaly (ECMA), which can be restored with 60 km of dextral rotation (Deptuck et al. 2015). Oceanic crust began to form at 177 Ma (Sibuet et al. 2012) in this area, as the basin entered the drift stage.

Transforms, extending onto land, focus drainage towards the transform as the elevation of the hanging wall increases and the footwall decreases (Fig. 4.15B) (Gawthorpe and Hurst 1993). This is evident within the recorded provenance of the

reference case wells. Mohawk B-93 records drainage as far away as the Canadian Shield (Blowick et al., submitted), whereas COST G-2 records local drainage in the Oxfordian, which expanded by the Kimmeridgian–Tithonian (Chavez et al. 2019).

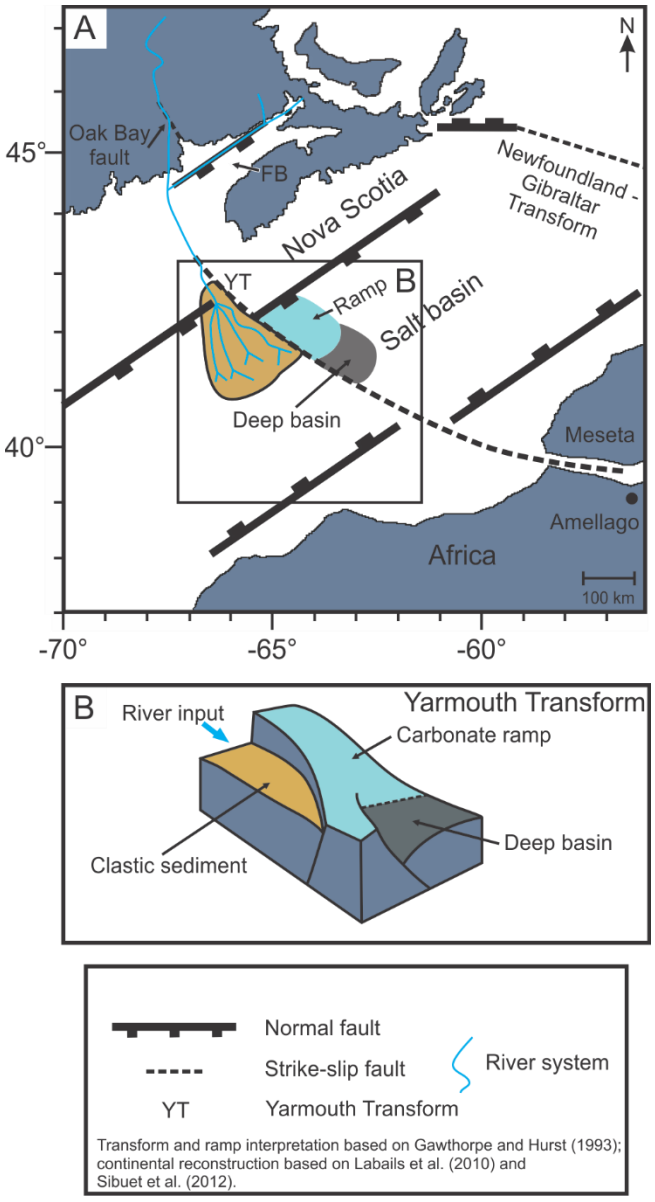

Figure 4.15: (A) Ramp and (B) cartoon block diagram showing the evolution of transform faults and river drainage in the Shelburne sub-basin. Reconstruction from the onset of oceanic spreading (177 Ma, Sibuet et al. 2012) with Middle Jurassic Shelburne Delta and carbonate ramp superimposed. Concepts and reconstruction based on Gawthorpe and Hurst (1993), Labails et al. (2010), and Sibuet et al. (2012).

Transforms may also favour development of large drainage basins. The Yarmouth Transform probably linked to the Oak Bay fault (Barosh 1992) along an old late Paleozoic lineament (Pe-Piper et al. 2010). It guided the course of the river that supplied

sediments to the Shelburne Delta (Fig. 4.15B). This fundamental control on drainage patterns by the transform zones is an important characteristic of rifted margins.

However, transform zones also allow for prediction of bathymetry, as well as basin stratigraphy and facies distribution (Leeder and Gawthorpe 1987). The Shelburne sub-basin is a wide margin in the classification of Davison (1997), having a broad zone of thinned crust (Sibuet et al. 2012), and well-developed salt deposits. Closing of the Atlantic Ocean (Sibuet et al. 2012) shows that the Yarmouth Transform is conjugate with the major tectonic boundary in Morocco between the main Africa Plate in the Atlas and the Meseta block (Fig. 15A) (Burkhard et al. 2006). The Yarmouth Transform is parallel to the Newfoundland-Gibraltar Transform that bounded the Jurassic Atlantic Ocean to the north. Rift phase deformation on the Yarmouth Transform resulted in relative uplift on the outer shelf and slope east of the transform on the Nova Scotian side of the opening ocean (Fig. 4.15B), resulting in uplift and delayed onset of Jurassic sedimentation at Mohawk B-93 and Bonnet P-23 (Figs. 4.1, 4.3) and carbonate ramp conditions beneath the slope, as sampled at the base of Monterey Jack E-43. This area may be similar to Esh el Mellaha located in the Gulf of Suez, in which a carbonate ramp developed within the transfer zone, while carbonate platforms developed on interbasin transfer zones (Gawthorpe and Hurst 1993). The carbonate ramp probably resembled the coeval Amellago ramp in the central High Atlas of Morocco (Pierre et al. 2010). At the same time, the Yarmouth Transform focussed drainage of the hinterland to a narrow zone, the Shelburne Delta, which persisted over more than 60 million years of geological time. To either side of this narrow clastic zone, Middle–Late Jurassic and much of the Early Cretaceous sedimentation was dominated by carbonates in the Georges Bank Basin and

on the LaHave platform. Our reference case model provides evidence that the observed turbidite channel and onlap features (Fig. 4.12) are quite consistent with relatively shallow water depths in the turbidite basin and the ramp carbonates at Monterey Jack E-43.

4.7.3 Application to Atlantic-type Passive Margins

Passive margin basins located off southeastern Brazil and Western Africa that have experienced mixed carbonate and clastic sedimentation in addition to salt movement, are prime targets of this modeling application. One such basin, the Pelotas Basin, located off southeastern Brazil and northern Uruguay, is also located on an important transform jog created by the Rio Grande Fracture Zone (Stica et al. 2014). This basin is under-explored, with the petroleum system not yet proven. Shelfal deposits in the basin consist of Albian-age carbonates of the Porto Belo Formation and fluvial-deltaic rocks of the Tramandaí Formation (Conti et al. 2017), which represents a shallow, mixed sedimentation environment. Deep-water environments consist of shales and mud-rich carbonate rocks belonging to the Atlântida Formation (Contreras et al. 2010). By the early Coniacian, seismic interpretation suggests sediment bypass on the shelf, and turbidite transport into deep-water (Contreras et al. 2010, Conti et al. 2017). Although salt is not as defined in this basin as other well explored Brazilian basins (e.g. Campos, Santos), the application of our modeling framework could give insight into the distribution of sand in deep-water as well as potential clastic reservoirs.

4.8 Conclusions

(1) Modeling of frontier basins is possible with information only on sparse wells and seismic data on thickness and major lithofacies. General geological trends and

facies distribution can be deduced through careful examination of the input parameters as well as sensitivity analysis.

(2) Transform margin development in the Shelburne sub-basin had an important effect on sediment distribution. Carbonate ramp environments were created within the transfer zone, and carbonate platforms were created outside of it. Topographic lows created by the transform zone focussed river supply in a narrow zone that persisted for 60 Ma, forming the Shelburne Delta.

(3) The model successfully predicts base of slope basin floor fans down-dip of the Shelburne Delta, as confirmed by very limited seismic data.

Chapter 5: Pitfalls Associated with Stratigraphic Modeling in Frontier Basins: A Case Study of the Shelburne sub-basin, Offshore Eastern Canada

Submitted paper to Basin Research

5.1 Introduction

Frontier basins, especially in deep water, have the least amount of geological information available. They tend to have very few exploratory wells drilled, and seismic imaging may be poor. Challenging tectonic regimes or complex salt movement, and the expense of drilling, all make frontier basins less attractive. Exploration in these under-explored areas requires an understanding of the entire sedimentary system as well as the petroleum potential. However, this information is usually difficult to obtain through the limited number of available wells. One way to aid in the prediction of the sedimentary processes and give insight into the distribution of facies, petroleum potential, and sediment distribution, is modeling the stratigraphic evolution of the basin. New technologies in numerical modeling allow the researcher to mimic the interaction of sedimentary and tectonic processes to generate 4D representations of basin architecture and facies distribution. These models are fully based on user's comprehension of the basin, so their pertinence is directly linked to modeling hypothesis and consequent set up parameters.

One such frontier basin, located off eastern Canada, is the Shelburne sub-basin (Fig. 5.1A). This basin is considered under-explored, with recent reports indicating that its deep-water part is the most prospective place to find oil anywhere offshore Nova Scotia (OETR 2011). Only four exploration wells have been drilled in the study area (Fig. 5.1A), with one located in deep-water. These wells cover a distance over 400 km in

length along the continental margin. Complicated tectonics and salt movement cause difficulty with seismic interpretation of the area, and uncertainty with the interactions between carbonate and clastic sediments in deep-water. The Shelburne sub-basin is of specific interest because of the possibility for deep-water clastic reservoirs in Mid–Late Jurassic successions, with the main risks in deep-water being the distribution, size, and reservoir quality of sands.

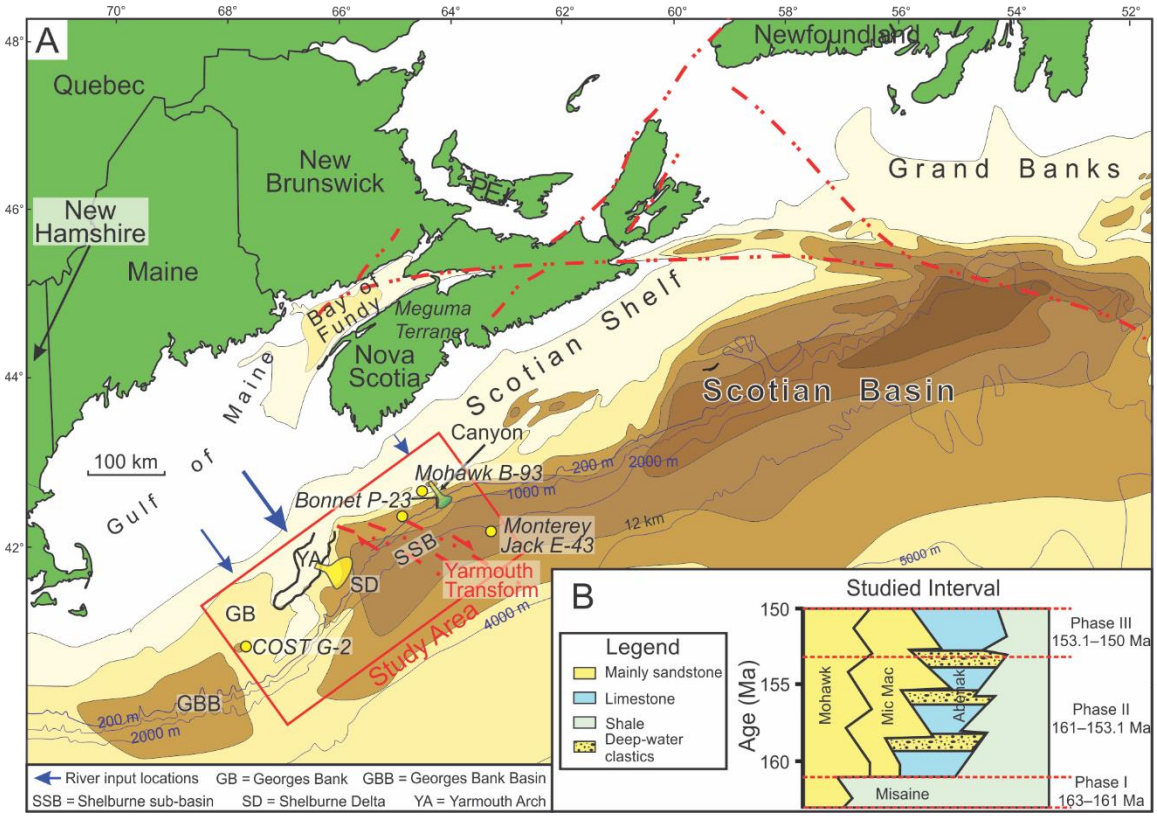

Figure 5.1: A: Regional map of the study area modified from Wade and MacLean (1990) and Williams and Grant (1998). River input locations are defined by blue arrows for the reference case model of Nagle et al. (submitted). B: Stratigraphic time scale of the modeled time interval, showing the three phases of sedimentation discussed in text.

The purpose of this paper is to explore how different results obtained through forward stratigraphic modeling depend on the amount of available geological data. This study uses hypothetically different amounts of the available geological data and compares the results to a reference case model reported by Nagle et al. (submitted). This will help

to refine modeling procedures and to identify which model parameters are the most important to be defined in frontier basins.

5.2 Geological Setting

The Shelburne sub-basin is located in the Scotian Basin offshore eastern Canada and is a large passive margin sedimentary basin. Evolution of the basin started in Middle–Late Triassic as rifting began to break apart Pangaea, with the separation of the African Plate from the North American Plate (Jansa and Wade 1975, Wade and MacLean 1990). Basement features such as the Yarmouth Transform and Yarmouth Arch formed at this time (Fig. 5.1A). The Yarmouth Transform is a large strike-slip fault zone that trends NE-SW, and provided more than 60 km of dextral offset (Deptuck et al. 2015). The Yarmouth Arch is a large faulted and segmented basement horst block that trends SW and separated the Shelburne sub-basin from the Georges Bank Basin in the Early–Middle Jurassic (Wade & MacLean, 1990; Deptuck et al., 2015).

Sediment fill in the basin began in the Late Triassic–Early Jurassic with the continental clastics of the Eurydice Formation and the coeval evaporites of the Argo Formation (Wade and MacLean 1990). Middle Jurassic sediments consist of the dolomitic rocks of the Iroquois Formation on the shelf, and pass landward into the marine clastics of the Mohican Formation. Late Jurassic sediments consist of the continental and marine clastics of the Mohawk and Mic Mac formations, respectively, with the shelf consisting of the limestone-dominant carbonate platform and reef front of the Abenaki Formation (Fig. 5.1B). This extensive carbonate platform did experience sediment bypass in the eastern part of the Shelburne sub-basin, as small shelf edge deltas fed clastic sediment into deep-water (Moscardelli et al. 2019). Towards the west of the Shelburne

sub-basin, on Georges Bank, a large deltaic system developed, known as the Shelburne Delta. It was active from the Middle Jurassic to the Late Cretaceous, survived multiple sea level rises, and transported a large amount of clastic sediment into deep-water (Deptuck et al. 2015). Salt movement in the basin began in the Middle Jurassic (Kidston et al. 2002), and affected sediment distribution and pathway development in deep-water. Salt is commonly found as diapirs, pillows, and large salt rollers, which are typically formed by sediment loading from deltaic systems (Kidston et al., 2002; Deptuck et al., 2015).

A summary of the ancient river systems for the Shelburne sub-basin has been presented by Nagle et al. (submitted) for the Middle–Late Jurassic. Three main river systems were active in the study area at this time: (1) Small local rivers draining the southwestern Meguma Terrane, supplied clastic sediment to the Mohawk B-93 well (Dutuc et al. 2017). (2) A larger river system supplied sediment to the COST G-2 well, draining the areas of coastal Maine in the Oxfordian, and expanding by the Late Jurassic to include the majority of Maine, and parts of New Brunswick and New Hampshire (Chavez et al. 2019). (3) A large river system supplying sediment to the Shelburne Delta via the present Bay of Fundy, draining the areas of New Brunswick, and possibly further back into the Grenville Province of the Canadian Shield (Dutuc et al. 2017; Blowick, Pe-Piper, Piper, Zhang, & Tyrrell, submitted).

The area encompassing the Shelburne sub-basin and the eastern part of Georges Bank basin has been modeled from J163 (Callovian) to J150 (Tithonian) by Nagle et al. (submitted). The model is controlled by the wells COST G-2, Bonnet P-23, Mohawk B-93, and Monterey Jack E-43. Three phases of sedimentation were recognized for the

modeled interval: (1) Carbonate drowning (163–161 Ma), (2) Clastic sedimentation (161–153.1 Ma), and (3) Re-establishment of a carbonate-dominant environment (153.1–150 Ma).

5.3 Methodology

5.3.1 DionisosFlow™

In this study, simulation of sediment dispersion is performed with DionisosFlow™, a 4D diffusion-based deterministic multilithology forward stratigraphic modeling software. DionisosFlow™ is able to simulate basin infill on the scale of tens to hundreds of kilometers, over a period of tens of thousands of years to hundreds of millions of years (Granjeon and Joseph 1999, Granjeon 2014). It reproduces the net product of sediment supply, transport, and accommodation, with respect to tectonic subsidence and uplift, compaction, salt diapirism, and eustatic sea level variations for each time step of the model (Hawie et al. 2017). The aim of DionisosFlow™ is to simulate the average geometry and facies of the sedimentary unit at basin scales (Granjeon and Joseph 1999). Transport of sediments in the model is simulated using diffusion equations.

DionisosFlow™ combines empirical water- and gravity-driven diffusion processes as either (1) linear slope-driven diffusion (transport proportional to slope), and (2) non-linear water and slope-driven diffusion (water discharge driven transport) (Hawie et al. 2017). This study utilizes the following non-linear diffusion equation:

$$Q_s = -(K_s/\vec{\nabla}h \; + \; K_w Q_w^m S^n)$$

Where: Q_s: sediment flux (km^3/Ma)
K_s: diffusion coefficient for hill slope creeping (km^2/ka)
h: elevation (m)
K_w: diffusion coefficient water discharge driven transport (km^2/ka)

Q_w: water discharge (m^3/s)
S: gradient of the slope in the basin
m and n: represent constants between 1 and 2 (Tucker and Slingerland 1994).

The diffusion coefficients vary according to each sediment grain size, such that mud is more diffusive than sand, and reef sediments are resistant to transport. Turbidity currents simulated under the non-linear diffusion equation are assumed to be mainly river fed (Hawie et al. 2019).

In order to better reproduce natural systems, DionisosFlow™ accounts for two types of sediment inflow. (1) Low energy long term (LELT) processes, which represent carbonate production, dispersion of sediment by waves and tidal currents, fluvial input, and hemipelagic sedimentation. (2) High energy short term (HEST) processes, which represent high energy delivery of sediment into the basin through storms and fluvial flooding and transport by turbidity currents. Even though HEST events are short-lived, they may be responsible for transporting most sediment into the basin.

5.3.2 Model Calibration

All models presented in this study use the reference case model of Nagle et al. (submitted) as a base, and a similar calibration process. Individual models are calibrated to match geological data (well logs and facies), interpreted position of the paleo-shelf edge, and seismic horizon picks, with the main goal of comparing the difference between the newly simulated model and the reference case model.

5.4 Changed Model Parameters

All models used in this study changed a key parameter or set of parameters compared to the reference case model of Nagle et al. (submitted), as follows:

5.4.1 Wrong Seismic Pick

This model deals with the possibility that the wrong seismic pick was used in the reference case model for the J150 seismic horizon at the top of the modeled interval. An alternative pick, which on average decreased the thickness of the modeled interval by ~65 %, was used instead (NSDoE 2015). This decrease in thickness requires a reduction in sediment supply, hemipelagic sedimentation rates, and subsidence. All other parameters remained the same as in the reference case model.

5.4.2 No Information on Input Sources

The goal of this model is to observe what happens if river systems are unconstrained. Three sources are assumed to supply the study area with ~50 % sand and ~50 % mud. If less than three sources are used, then the model becomes poorly calibrated on Georges Bank. This model differs from the reference case model because the sand content from the sources were not normalized to the eustatic curve, and relatively constant values of sediment load and water discharge were used to create the variety of stratigraphic units in the reference wells (see Appendix 5, supplementary appendix 1). All other parameters remained the same as the reference case model.

5.4.3 No Information from the COST G-2 Well

This model investigates what would happen if the most informative well (the COST G-2 well on Georges Bank) had not been drilled. Only two river systems are required to simulate sedimentation in the basin because there is no information on facies on Georges Bank. The average sediment load and water discharge of the Bay of Fundy river system were increased by ~5 % and ~0.7 %, respectively, in order to respect the

seismic thickness calibration on Georges Bank. All other parameters remained the same as the reference case model.

5.4.4 Different Bathymetry

Nagle et al. (submitted) described two additional models to test the uncertainty with the initial paleobathymetry with maximum water depths in the basin ranging from ~1000 m to 1500 m. In order to maintain calibration, hemipelagic sedimentation and subsidence rates had to be altered compared to the reference case model in which maximum water depth for the initial paleobathymetry was ~220 m. All other parameters remained the same as the reference case model.

5.4.5 Carbonate Extent

Four additional models were tested in order to understand how reef sediments are distributed in DionisosFlow^{TM}, two for the reference case model with a shallow carbonate ramp, and one for each of the models with deeper initial bathymetry discussed above. DionisosFlow^{TM} accounts for transport of reef sediments by two main processes: erosion, and transformation rate. Erosion can be controlled simply by increasing the erosion rate for reef sediments, while transformation rate indicates the amount of reworking. To test the erosion parameter, all sediments were set to the same erosion rate of 100 m/Ma, except for reef sediments, which were set to 1000 m/Ma and 5000 m/Ma. All other parameters remained the same as the reference case model. To test the transformation rate parameter, only the value for reef sediments was increased.

5.5 Results

The following models are described in terms of three phases of sedimentation distinguished in the reference case model (Fig. 5.1B) and are compared to that model.

The results are described based on their geographic location (shelf, slope, and basin floor; Fig. 5.2A), thickness of sediments, location of the basin-floor-fan facies class, and overall thickness of the sequence. This section is presented with a focus on where sand occurs in the basin (sections 5.1-5.4) and the extent of detrital (reworked) carbonate facies (section 5.5). A workflow outlining the modeling process can be found in Appendix 5, supplementary appendix 2.

5.5.1. Wrong seismic pick (reduced sediment thickness)

Using a different seismic pick from the reference case model means that total sediment thickness is reduced by ~65 %. Therefore, it requires a drastic decrease in sediment supply and carbonate production rates. For the first phase of sedimentation from 163–161 Ma, sand is commonly found on the shelf, behind the shelf edge reef, in similar abundance as the reference case model (Fig. 5.2B). Towards the outer edge of Georges Bank, up to 10 % carbonate mud is found, compared to 7% in the reference model. In the vicinity of the Shelburne Delta and the canyon system near Mohawk B-93, slope sediments contain up to 7 % and 32 % sand in the reduced sediment thickness and reference case model, respectively. Away from clastic inputs, the slope and basin floor are similar to the reference case model, consisting of carbonate mud and hemipelagic terrigenous mud, with less than 1 % sand. From 161–153.1 Ma, there is a large pulse of sediment supply into the basin and sand content on the shelf is ~5 % higher than the reference case model, whereas it is similar on the slope and basin floor (Fig. 5.2B1). In the west, this sediment pulse limited reef sediments to patches along the shelf edge near the Shelburne Delta. The reef is also well established east of Georges Bank, unlike in the reference case model. Small patches of carbonate mud occur on the outer Georges Bank

shelf, whereas there is a larger extent in the reference case model. A higher proportion of sand and wider sediment pathways are located on the slope, down-dip of the Shelburne Delta (Fig. 5.2B1), in comparison to the reference case model (Fig. 5.2A1). From 153.1–150 Ma, sediment supply is reduced from the input sources, similarly to the reference case model. Proportions of sand on the shelf are similar between both models, however, 30 % more sand is found on the slope, down-dip of the Shelburne Delta (Fig. 5.2B2). A large proportion of sand occurs at the southwest edge of the model, which is not present in the reference case model, and is likely an edge effect of the model.

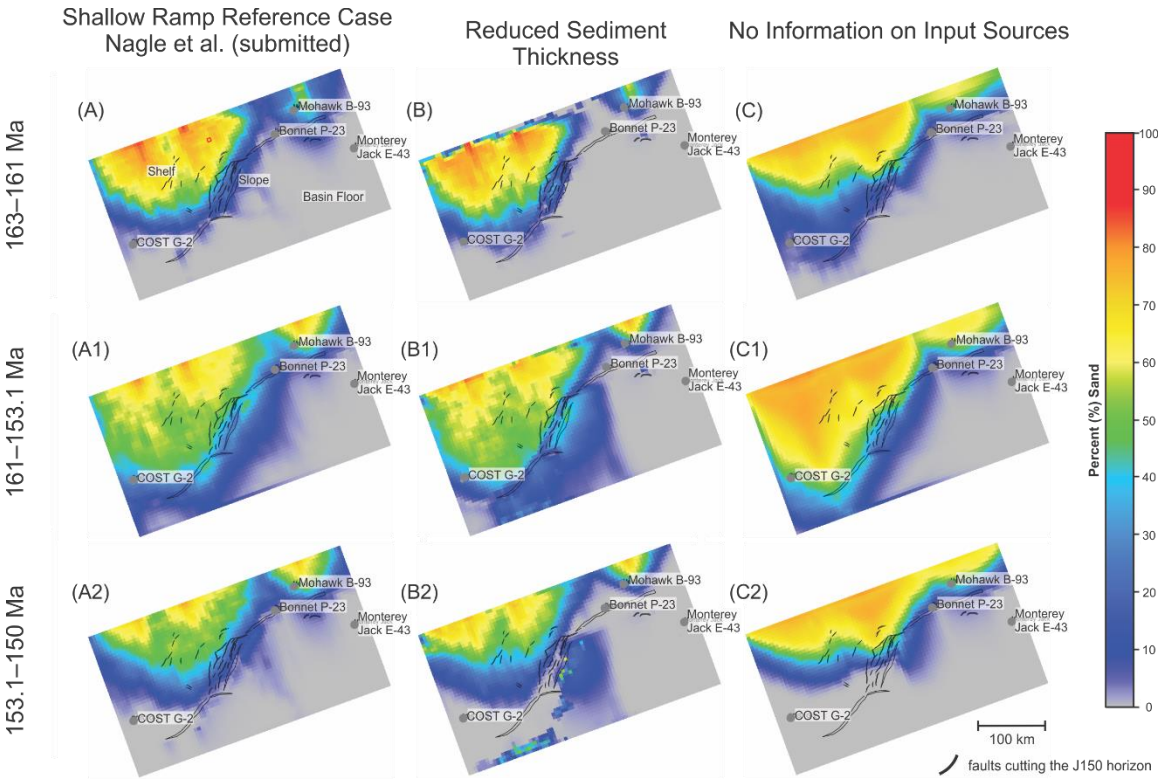

Figure 5.2: Average sand proportion maps for the three stages of sedimentation for the reference case model, the reduced sediment thickness model, and the no information on sources model.

The reduced sediment thickness model shows a large difference in calibration compared to the reference case model. Overall facies calibration is ~74 %, compared to 76 %, and regional thickness calibration is very low, at 81 % compared to 98 % (Table

1). This low calibration is mostly due to areas in deep-water, down-dip of the Shelburne Delta and the eastern part of the model, where Monterey Jack E-43 is located (Fig. 5.3B), and the chosen seismic pick particularly underestimates sediment thickness. The comparison of overall sand sedimentation indicates that both models show similar sedimentation on the shelf, but differ in deep-water (Fig. 5.4B). The maximum thickness of sand reaches ~1150 m in faulted areas along the shelf edge and a salt withdrawal minibasin, compared to ~1400 m in the reference case model. Basin floor fans build up to 880 m thick on the slope and basin floor immediately down-dip of the Shelburne Delta, compared to ~950 m in the reference case model (Fig. 5.5B).

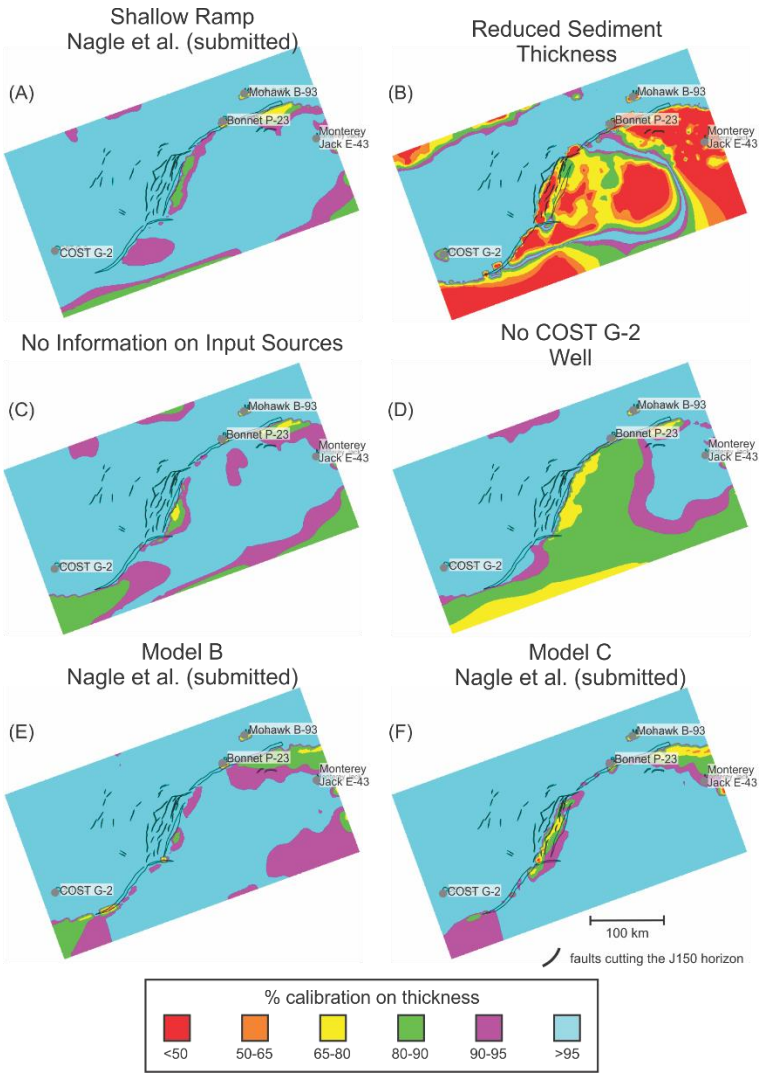

Figure 5.3: Calibration percent maps for the entire modeled time span from 163–150 Ma.

Table 5.1: Calibration Indicator Percent for the various models

Calibrated Models	COST G-2		Bonnet P-23		Mohawk B-93		Monterey Jack E-43A		Total Well Thickness	Total Facies	Total Well (thickness + facies)	Thickness Map
	Thickness	Facies	Thickness	Facies	Thickness	Facies	Thickness	Facies				
Reference case model from Nagle et al. (submitted)	99.34	67.26	99.02	82.18	95.22	74.88	99.4	87.47	98.87	76.23	87.55	97.67
Wrong Seismic Pick	95.93	62.24	89.96	88.24	88.86	51.51	28.24	87.59	85.05	74.71	79.88	81.84
No Information on Input Sources	99.38	74.89	99.22	88.24	96.37	77.02	99.83	87.47	99.12	81.88	90.5	96.86
No COST G-2 Reference Well	N/A	N/A	99.21	87.35	95.77	75.18	98.9	87.47	N/A	N/A	N/A	92.95
Model B from Nagle et al. (submitted)	99.37	70	99.84	88.24	96.16	75.48	99.3	87.46	99.28	79.8	89.54	97.78
Model C from Nagle et al. (submitted)	99.39	68.6	99.28	88.24	96.22	75.24	89.66	87.41	97.94	79.21	88.58	98

5.5.2. No information on input sources

If no information is provided on the position at which river sources enter the basin, then the only calibration controls on the model become the wells, regional thickness map, and seismic interpretation. In order to obtain a proper thickness calibration in this model, three river systems are required, like in the reference case model. If less than three river systems are used, it becomes difficult to obtain the proper thickness in the model, leading to improper sediment type in the wells. For the first phase of sedimentation from 163–161 Ma, sand is mostly limited to the shelf behind the shelf edge reef, containing a similar proportion of sand as the reference case model (Fig. 5.2C). A small amount of sand, between 5–43 % occurs down-dip of the Shelburne Delta, and the canyon near Mohawk B-93, which is ~11 % higher than the reference case model. The rest of the basin is similar to the reference case model, consisting of carbonate mud and hemipelagic terrigenous mud with less than 1 % sand. From 161–153.1 Ma, the shelf consists mostly of sand, ranging from 48–59 %, which is ~7 % higher than the reference case model (Fig. 5.2C1). Reef sediments are limited to patches along the shelf edge, and sandy clastic sediments accumulate along the slope and basin floor, ranging from 5–45 %, similar to the reference case model. However, a higher proportion of sand progrades further into the basin in the reference case model (Fig. 5.2A1). Mud is abundant along the slope suggesting that the Shelburne Delta and other Georges Bank river systems were delivering a large amount of muddy sediment during the clastic phase of sedimentation, compared to the reference case model. A large proportion of sand appears to accumulate off Georges Bank in the southwest of the model, which is not as pronounced in the reference case model (Fig. 5.2C1). Small clastic channels extend towards the edge of the

model in this region and are most likely created by edge effects in the model. The rest of the slope and basin floor consists of hemipelagic terrigenous mud and carbonate mud similar to the reference case model. From 153.1–150 Ma, sedimentation is similar to the reference case model, with a decrease in sediment supply, causing sand to accumulate on the shelf, as carbonate sediments re-establish along the outer shelf and shelf edge. Sand ranges up to 45 % on the shelf, which is similar to the reference case model. In areas of prograding systems, on the slope and basin floor, sand varies from 3–35 %, which is ~20 % greater than the reference case model (Fig. 5.2C2).

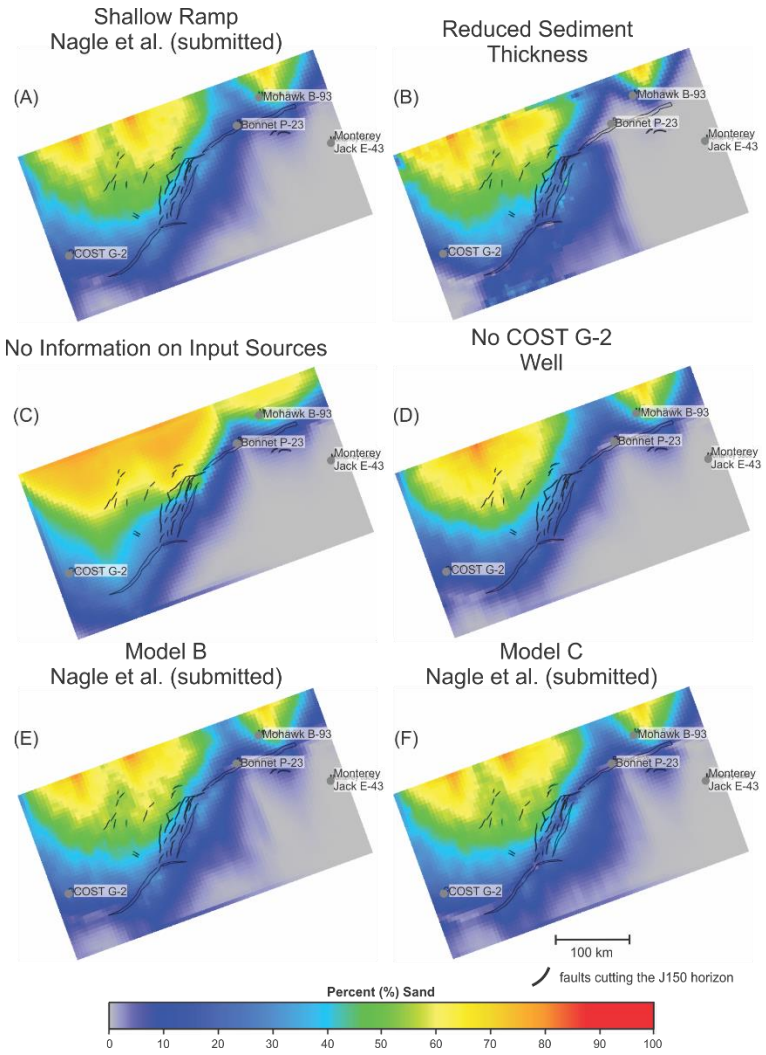

Figure 5.4: Average sand proportion maps for the entire modeled time span from 163–150 Ma.

The model with no information on river sources matches regional thickness and well facies very well, similarly to the reference case model. Regional thickness calibration is 96 %, compared to 98 %, and overall facies calibration is 81 %, compared to 76 % (Table 1). Areas of low calibration are very similar to the reference case model, occurring along the slope and deep-water edge of the model (Fig. 5.3C). In this model, a higher proportion of sand occurred on the shelf, slope, and basin floor, although, sand is transported further into the basin in the reference case model (Fig. 5.4C). Sand content in the model with no information on sources appears to be much more uniformly distributed compared to the reference case model. This is due to using relatively constant sediment supply and percentage of sand for the river systems (see Appendix 5, supplementary appendix 1 for values). The maximum thickness of sand is ~1900 m in faulted areas near the shelf edge and a salt withdrawal minibasin, compared to ~1400 m in the reference case model. Deep-water clastic sediments down-dip of the Shelburne Delta form a basin floor fan complex up to 1400 m thick, compared to ~950 m in the reference case model (Fig. 5.5C).

5.5.3. No COST G-2 Well

Without the well on Georges Bank, the model only has to respect regional thickness, the three other wells, estimated sediment supply, and seismic interpretations. Only two river systems are required to calibrate the study area. For the first phase of sedimentation from 163–161 Ma, sand is limited on the shelf, ranging from 8–45 % (Fig. 5.6B), which is similar to the reference case model. However, the majority of the shelf on Georges Bank consists of carbonate sediments and a shelf edge reef, in contrast to widespread clastic sediment in the reference case model (Fig. 5.6A). Sand does not

prograde into deep-water from the Shelburne Delta at this time, compared to the reference case model, although the two models are similar for the canyon system near Mohawk B-93 (Figs. 5.6 A, B). The rest of the slope and basin floor away from clastic inputs consist of hemipelagic mud and carbonate mud, similar to the reference case model. From 161–153.1 Ma, there is a large increase in sediment supply, as reef sediments become limited to the shelf edge, and in the area of the Shelburne Delta, reef sediments are significantly drowned by clastic inputs, similar to the reference case model (Fig. 5.6B1). Sand on the shelf ranges from 25–56 %, which is similar to the reference case model. In areas of prograding systems such as the Shelburne Delta and the canyon system near Mohawk B-93, clastic sediments with 3.5–30 % sand are found, which is ~15 % higher than the reference case model (Fig. 5.6B1). Small sediment pathways extending from the clastic slope deposits appear to deliver sediment to the edge of the model (Fig. 5.6B1), however the extent of clastic sediment is greater in the reference case model (Fig. 5.6A1). From 153.1–150 Ma, there is a decrease in sediment supply, and carbonate sediments re-establish on the outer shelf and shelf edge (Fig. 5.6B2), similar to the reference case model. Sand content during this phase is 4–41% on the shelf, which is ~4 % lower than the reference case model. However, sand barely accumulates in the basin down-dip of the Shelburne Delta (Fig. 5.6B2), compared to the reference case model (Fig. 5.6A2).

The model with no COST G-2 well is highly calibrated, like the reference case model. The average facies calibration from the three reference wells is ~83 %, compared to 76 % in the reference case model, and the regional thickness calibration is 92 %, compared to 98 % (Table 1). This lower regional thickness calibration is due to the lack

of thickness along the slope and basin floor down-dip of the Shelburne Delta (Fig. 5.3D). The overall comparison of sand content between the two models is very similar, except that a higher proportion of sand is found further in the basin for the reference case model (Fig. 5.4D). The maximum thickness of sand is up to 1100 m in faulted areas along the shelf edge and a salt withdrawal minibasin, compared to ~1400 m in the reference case model. Deep-water clastic sediments derived from the Shelburne Delta, form a basin floor fan complex that is up to 1140 m thick, compared to ~950 m in the reference case model (Fig. 5.5D).

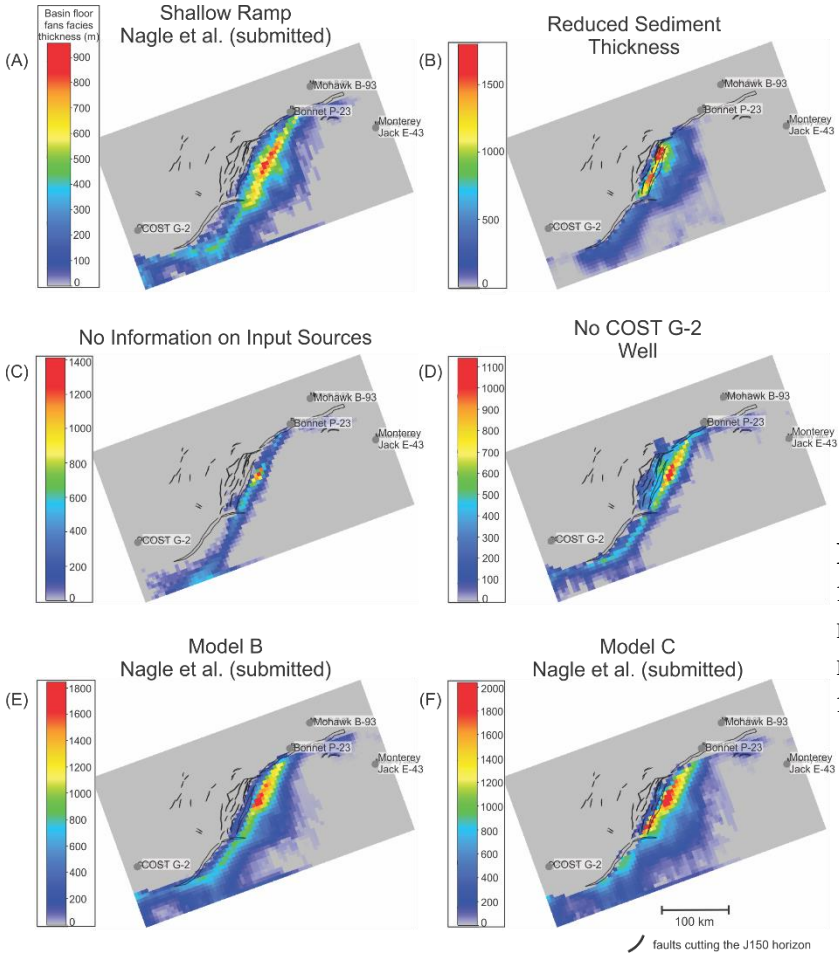

Figure 5.5: Basin-floor-fan thickness maps for the entire modeled time span from 163–150 Ma.

5.5.4. Different Initial Bathymetry

Two models with deeper initial bathymetry at J163, from Nagle et al. (submitted), were used to show differences in deep-water sedimentation due to the presence of a shelf edge reef at J163. Both models show a high facies and regional thickness calibration (Figs. 5.3E, 5.3F) (Table 1). Sand has a very similar distribution as the reference case model (Figs. 5.4E, 5.4F, 5.7) although, a higher proportion of sand is located on the slope and basin floor, likely due to the increased gradients and water depths. A thicker basin floor fan complex developed closer to the slope, immediately down-dip of the Shelburne Delta, in both deeper bathymetry models, which is closer to the shelf edge than in the reference case model (Figs. 5.5E, 5.5F). Small clastic channels appear to extend to the edge of the model (Figs. 5.5E, 5.5F, 5.7B, 5.7C), similar to the reference case model.

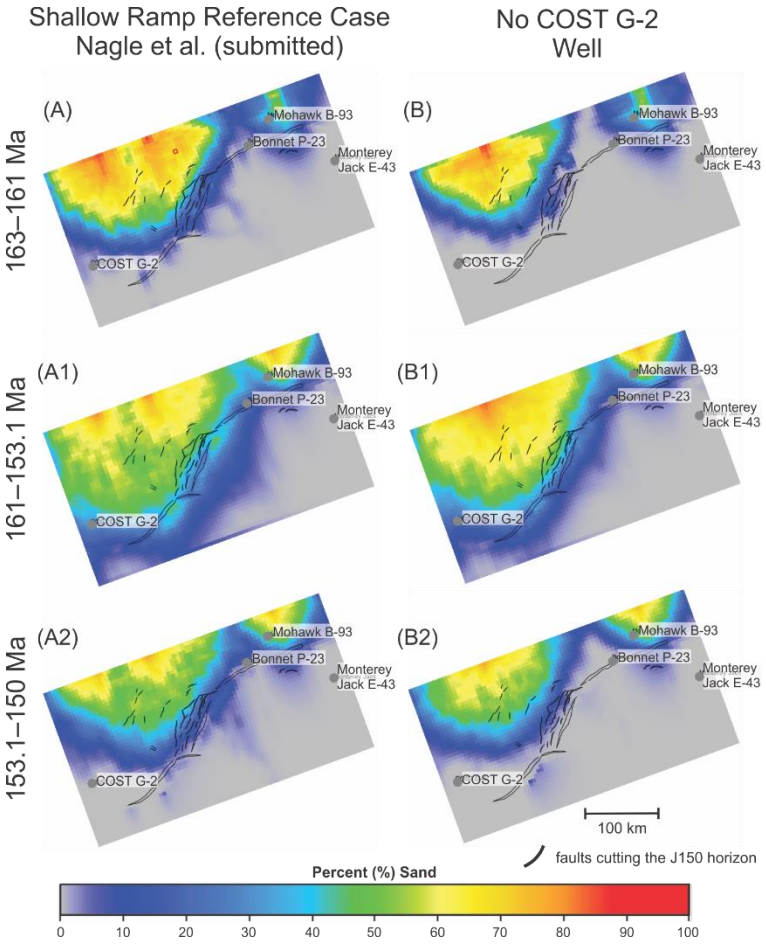

Figure 5.6: Average sand proportion maps for the three stages of sedimentation for the reference case model, and the no COST G-2 well model.

5.5.5. Carbonate Extent (erosion vs transformation rate)

In order to understand which parameter controls the extent of carbonate sediments beyond the shelf edge, four additional models were created. The first model, Carbonate Extent A, compares the erosion rate of carbonate reefs to the reference case model. There is little difference in the extent of the detrital carbonate facies when 10x the erosion rate is used for reefs, compared to the reference case model (Figs. 5.8B, 5.8B1, 5.8B2). When the erosion rate of reef sediments is increased to 50x greater than the reference case model, the shelf edge progrades into the basin (Fig. 5.9B, 5.9B1, 5.9B2). If any other diffusion coefficients are changed for the reef sediment class, compared to the reference

case model, such as increasing the transport due to waves, then the shelf edge also progrades into the basin.

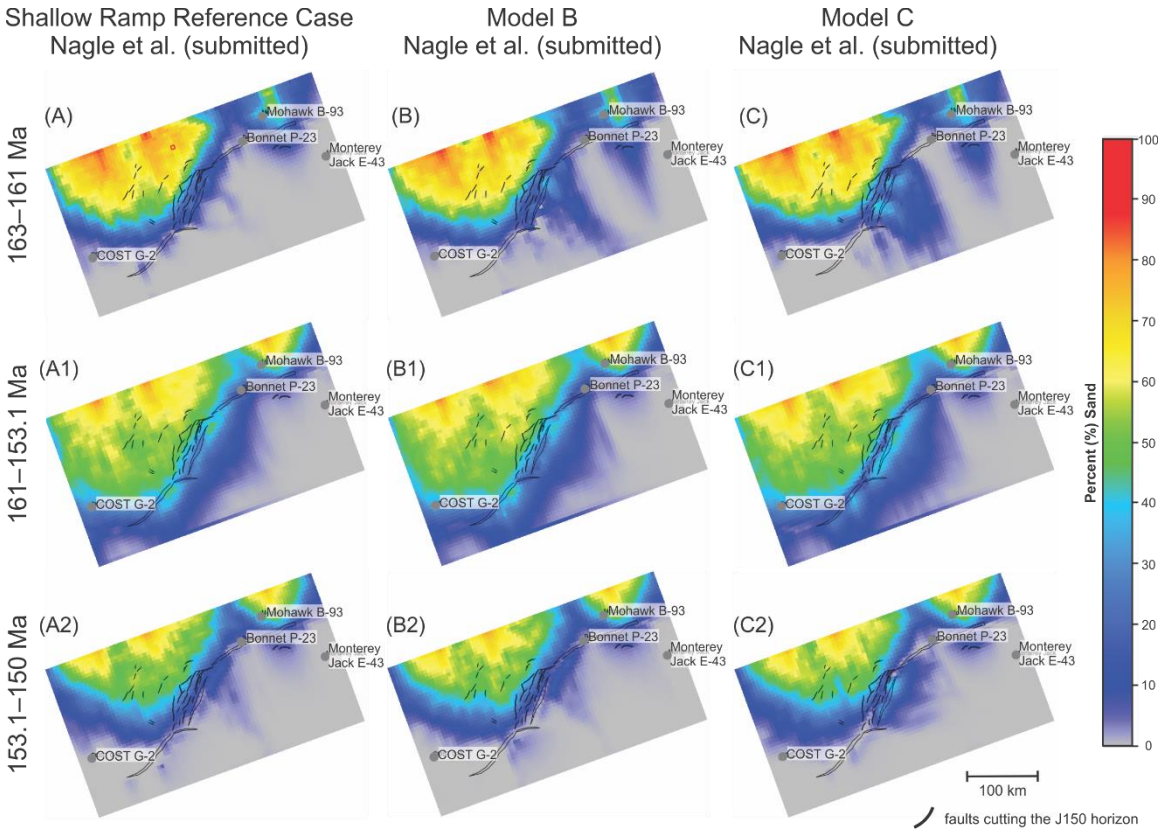

Figure 5.7: Average sand proportion maps for the three stages of sedimentation for the reference case model, and the deeper bathymetry models B and C from Nagle et al. (submitted).

To test the effect of the transportation rate parameter on carbonate transport, the model Carbonate Extent B was created and compared to the reference case model. Only a slight increase in the extent of the detrital carbonate facies in deep-water was noted (Figs. 5.8C, 5.8C1, 5.8C2) compared to the reference case model (Fig. 5.8A, 5.8A1, 5.8A2).

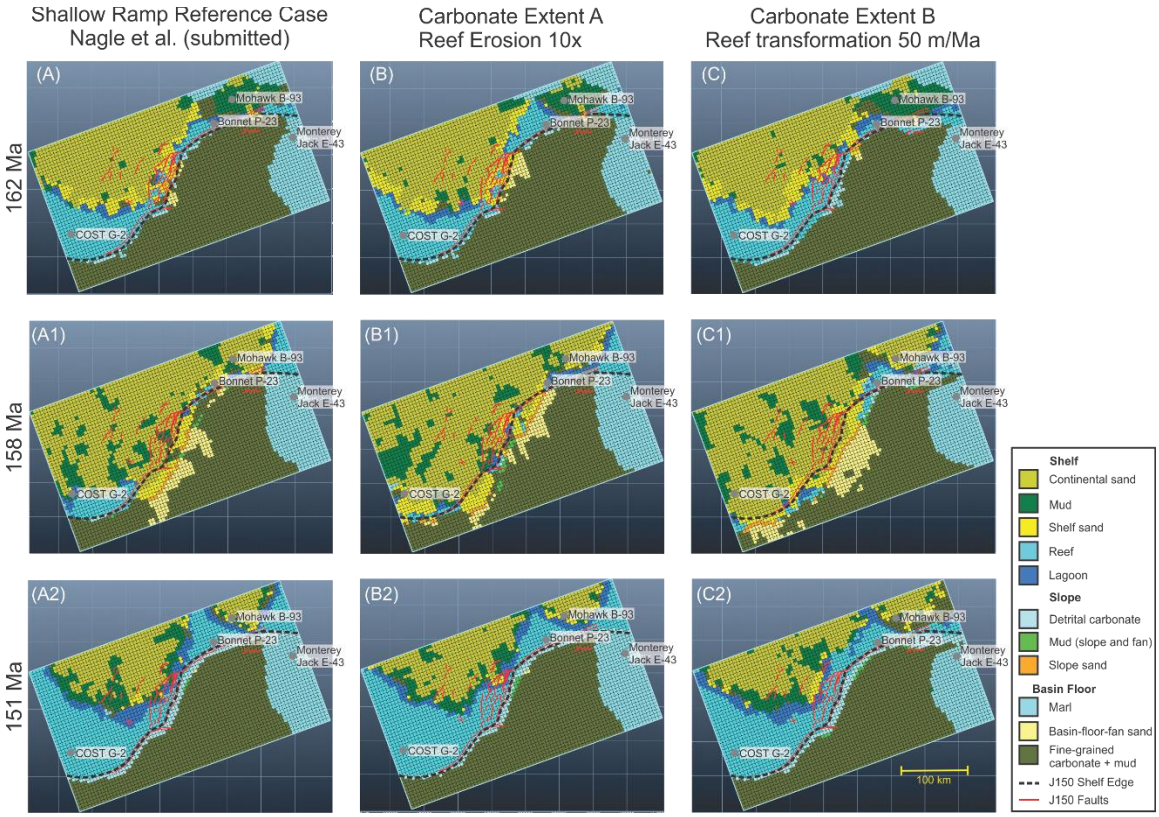

Figure 5.8: Reef extent comparison of the reference case model and Carbonate Extent models A and B. Dashed line represents the limit of the J150 shelf edge.

To test whether the initial bathymetry was influencing the extent of the detrital carbonate facies in the basin, the transformation rate as well as the diffusion coefficient for gravity-driven transport of reef sediment was tested for each deeper bathymetric model of Nagle et al. (submitted). These models, Carbonate Extent C and D (Figs. 5.10, 5.11), had an initial water depth in the basin at J163 of ~1000 m and ~1500 m, respectively. With increasing values of the transformation rate and the diffusion coefficient for gravity-driven transport, the extent of detrital carbonate in the basin was significantly increased. Not unexpectedly, the reworked reef sediments are more easily transported by gravitational processes into the basin with a deeper initial paleobathymetry and the resulting higher seafloor gradient.

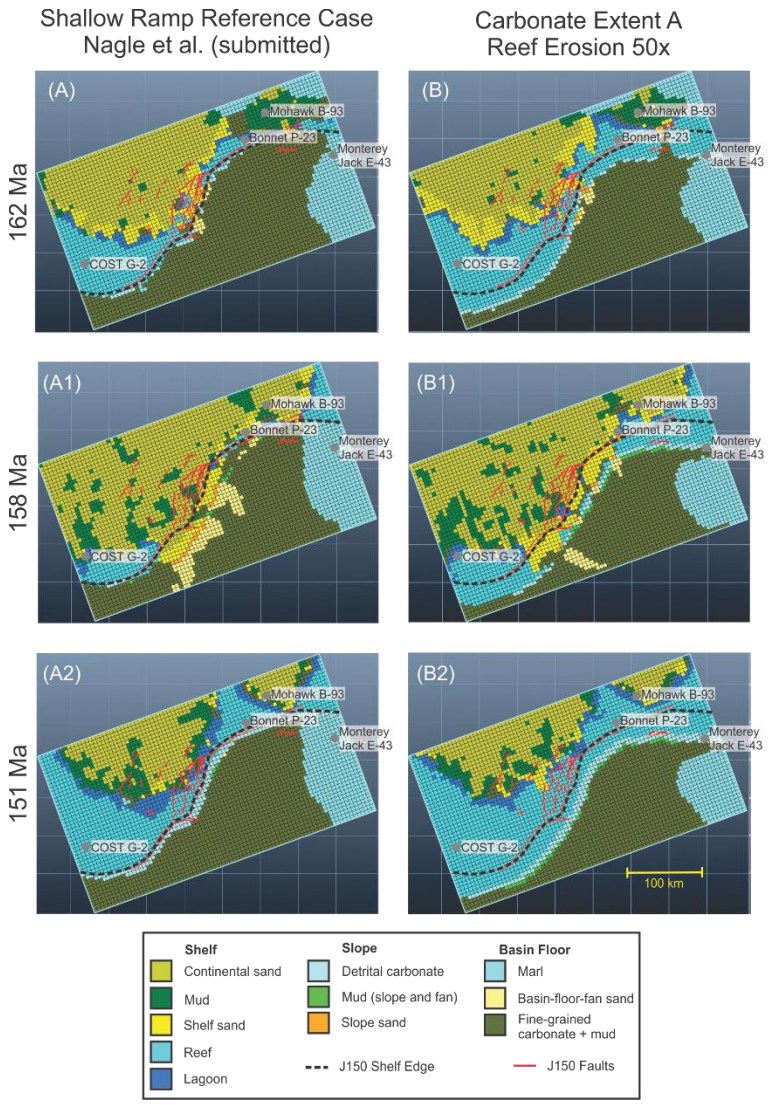

Figure 5.9: Reef extent comparison of the reference case model and Carbonate Extent A model. When erosion and/or diffusion coefficients are increased too high, progradation of the shelf edge occurs. Dashed line represents the limit of the J150 shelf edge.

5.6 Discussion

5.6.1 Application of modeling approach to frontier basins

When using the modeling approach of Nagle et al. (submitted) for the reference case model, there is a good match between simulated facies and regional thickness as well as the seismic interpretation. However, this does not mean it is the only plausible simulation, given the limited amount of geological information available. When less geological information is used than what the reference case model was built on, it becomes apparent that some geological information is more important than others.

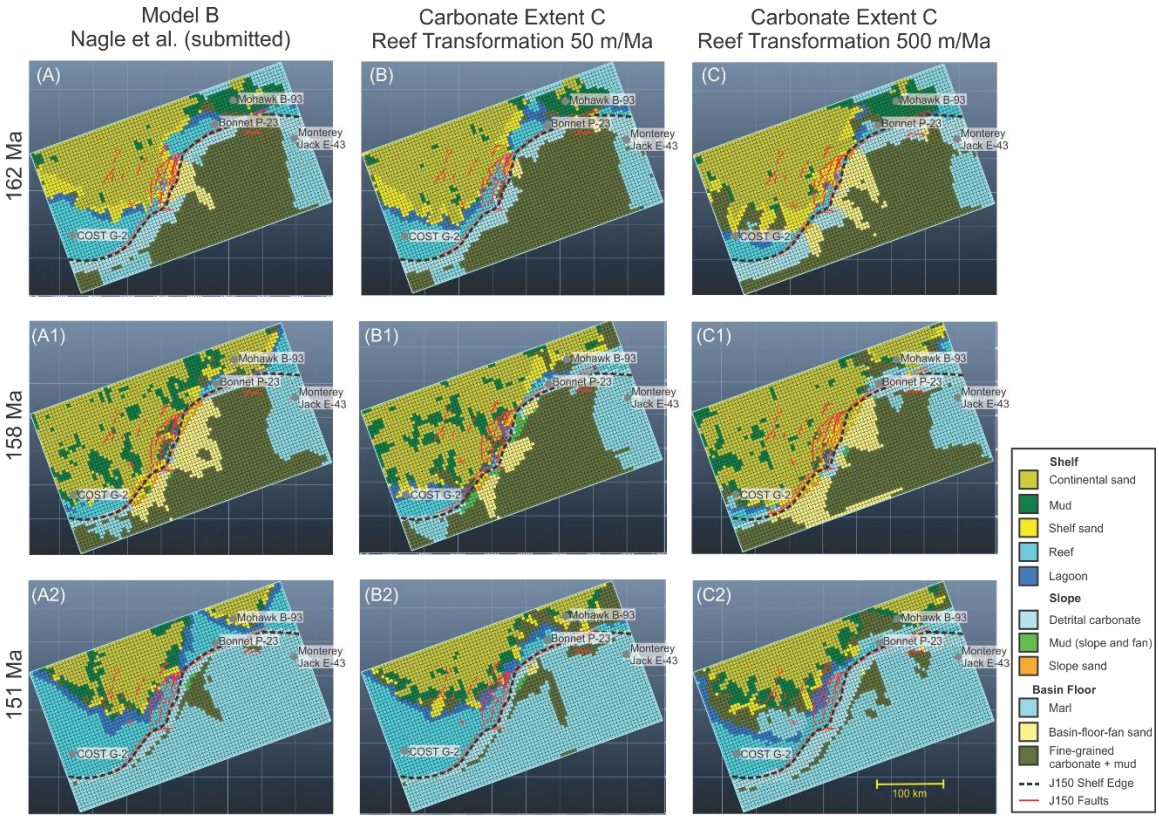

Figure 5.10: Reef extent comparison of Model B (Nagle et al., submitted) and Carbonate Extent C. For reef transformation = 500 m/Ma, the gravity diffusion coefficient for reef in a marine environment was also increased by an order of magnitude. Dashed line represents the limit of the J150 shelf edge.

The single most important geological information is the seismic surfaces of the study area. These surfaces define the regional thickness map for the model, which is used to calculate the subsidence or uplift rate applied during the simulation. It is also important for modelers to understand the seismic interpretation of the study area, including an understanding of the different stratigraphic geometries and interpreted seismic facies which provide first order information on the evolution of a frontier basin.

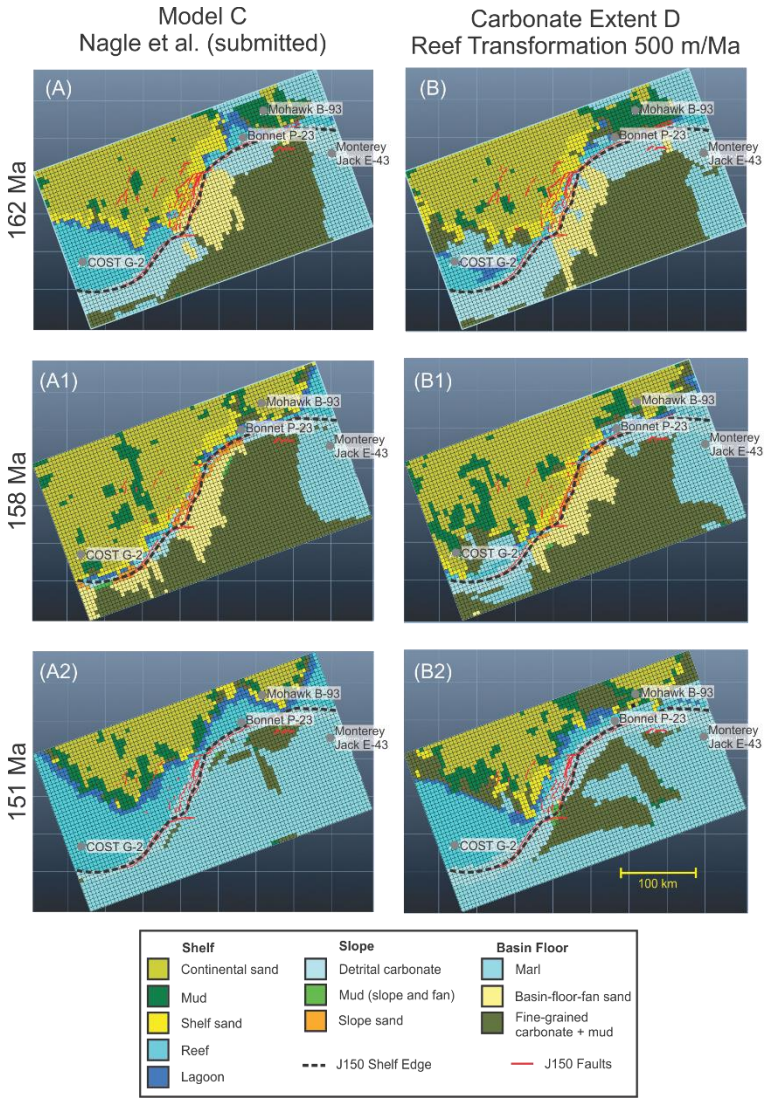

Figure 5.11: Reef extent comparison of Model C (Nagle et al., submitted) and Carbonate Extent D. For reef transformation = 500 m/Ma, the gravity diffusion coefficient for reef in a marine environment was also increased by an order of magnitude. Dashed line represents the limit of the J150 shelf edge.

The paleobathymetry for each seismic surface is important, because it controls the overall morphology of the model and the extent of different biogenic carbonate producers. As in the case of the Shelburne sub-basin, paleobathymetry may be the most influential unknown in the model. Basin-scale paleobathymetry depends on tectonic context and eustasy interaction, and thus several possible end members may need to be tested. In the Shelburne sub-basin the limited number of wells and regional seismic dip lines give insight into water depths on the shelf, and less precise information about the slope.

Although paleoriver systems and their respective sediment supply were defined for the reference case model, they do not appear to be of critical importance in modeling. Sand has a very similar distribution on the shelf between the alternative models (Fig. 5.4). If the regional thickness and extent of facies are relatively known, then the number of river systems and their respective sediment supply will come out during the calibration process. If simulated thickness is insufficient on the shelf, compared to the regional thickness map, and seismic interpretation indicates the presence of clastic sediment, then either the river system requires a higher sediment load and/or water discharge, or another river system is required to supply sediment to that area of the model.

Nevertheless, defining paleoriver systems and their respective sediment supply is valuable in the later stages of stratigraphic modeling. This can allow for realistic sediment proportions for each defined river system, detailed values of sediment load and water discharge, and a higher resolution for the defined facies. River systems with different petrographic types in their sediment load may ultimately influence reservoir quality (Sangster et al. submitted). Recent models (e.g. Harris et al. 2018, Hawie et al. 2019, Sangster et al. 2019) have successfully defined river systems for their study area, and created well calibrated high-resolution models. However, most stratigraphic models assume that a river system supplied a constant sediment load and water discharge for the modeled time interval. Although not always geologically accurate, this assumption is necessary if the detailed climate history of the hinterlands is unknown. Some models (e.g. Hu et al. 2019) define river systems by using the average sediment thickness of the simulated time span. This is useful for estimating the value of sediment load for the river

system, however; it raises questions about water discharge values and may cause overestimation of sediment load if carbonate or evaporite sediments are present.

The challenges with calibrating stratigraphic models in frontier basins become further complicated in mixed carbonate and clastic sediment systems. This is because clastic sediment not only dilutes carbonate sediment but also suppresses carbonate production. Therefore, fine-scale control between both sediment types is required in order for carbonate sediment to grow. This could necessitate the use of brute force for the calibration process because there are many parameters that are closely related to the growth or demise of carbonate sediments, and may require work-arounds in order to obtain the proper distribution and thickness of carbonate sediments in the model (Nagle et al., submitted).

5.6.2 Difficulty in running a constrained model verses an unconstrained model

When comparing a geologically constrained reference case model (Nagle et al., submitted) with an unconstrained model, such as above, a few key differences stand out. Firstly, the constrained model is more difficult to calibrate than the unconstrained model because the constrained model needs to match a larger amount of diverse data. The unconstrained model has looser calibration criteria, which is most appropriate for proof of concept scenarios that are intended to provide an overall representation of geometries and facies distribution expected in the basin. Secondly, unrealistic sediment distribution may occur in the less constrained model. This could be because of improper sediment supply, diffusion coefficients, or wrong input source locations. However, sediment distribution errors could also occur in the reference case model by placing too much significance on some geological constraints, which may not be representative at the scale

of the model. Previous modeling work on the central Scotian Basin by Sangster et al. (2019) indicates that larger cell sizes with time steps greater than 0.25 Ma are not able to capture the lateral variability in sands recorded by (Gould et al. 2012). In the present study, the variability of facies is well captured in the Mohawk B-93 well because a smaller time step of 0.1 Ma is used compared to Sangster et al. (2019) study. This allows for the fine-scale alternation of facies to occur in the model, although the lateral extent of each facies class may be under or over estimated due to the limitation of the 5 km x 5 km cell size.

All the models are relatively similar to each other on the shelf (Fig. 5.4) and begin to differ in deep-water. Nevertheless, each model shows some amount of sand prograding from the Shelburne Delta into deep-water. The main difference between each model is the amount of sand in deep-water and the extent of clastic sediment in the basin. Therefore, a longer calibration time is associated with the geologically constrained reference case model, unlike the unconstrained models, all of which show sand in deep-water.

Geologically constrained models require longer computational times compared to unconstrained models. A common procedure in stratigraphic modeling implies working at a coarse scale until suitable results are obtained in terms of simulated thickness and sediment distribution, and then to switch to more refined models that need higher computation time. This technique allows results to be obtained in minutes for the coarse models to a few hours for the more refined version. However, computation time is not only related to the number of cells in the model but also to the number of processes activated during the simulation and their respective setting values. Unconstrained models

will typically have the tendency to be simpler with fewer processes activated and less constraints on the choice of setting values, which is not always the case for geologically constrained models. Even if the current technology allows for the model to run with a cluster of processors, drastically reducing the computation time, the modeler will need to pay special attention to the choice of the activated processes during the simulation and the setting of overall parameters values.

5.6.3 Can a set of parameters be predefined to start a stratigraphic model in a frontier basin?

In modeling a frontier basin, where available data are limited, it would be useful to start with a pre-set group of parameters: carbonate growth curves, average sediment proportions of modern river systems, and the use of wide river-mouth input point(s). We also suggest using a set of diffusion coefficients that have been defined from previous modeling studies. In DionisosFlow™, these are available in newer versions of the software. Although such pre-defined parameters may make the model easier to start, as well as aid in the iterative calibration process, it is important to understand the limitations of doing so and compare the simulation results to the calibration criteria and seismic interpretation.

Pre-defining different carbonate producers based on each carbonate growth factory is useful; however, it is not possible to accurately define environmental conditions and respective production rates in most frontier basins. This complex relationship between different types of carbonate producers is difficult to estimate, because taxa and environmental conditions were significantly different in the geological past compared to the Holocene (Leinfelder et al. 2002). Thus, the limitations with using

pre-defined carbonate parameters may make the model harder to calibrate, as well as create unrealistic boundaries between the different carbonate producers and/or clastic sediments. Therefore, it is more important for stratigraphic modelers to have an understanding of the seismic interpretation of the study area rather than of the different carbonate parameters.

Pre-defining sediment proportion for the different river sources appears to be beneficial. For instance, consider a river system providing 30 % sand and 70 % mud to the study area. This supplies the model with a realistic proportion of sediment, which can aid the calibration process; however, this proportion may not always be appropriate. Using sediment proportions of modern river systems is dependant on the study location, as some may require different proportions than what was initially estimated (e.g. Hu et al., 2019). This could be due to underestimated sediment load or water discharge values, as well as improper diffusion coefficients, which lead to lower thickness and facies calibration in the model.

By using wide river-mouth input points, some of the above limitations can be addressed, allowing for a lower amount of knowledge of ancient river systems. When the river-mouth input points are wide (> 20 km), it helps to account for variations that would occur over geological time spans. This method is useful for a first calibration of the model. However, if more information is known about the river systems in the study area, the application of wide river-mouth input points could cause difficulties with calibration, and possibly erroneous sediment distribution around river-mouth input points.

Using pre-determined diffusion coefficients from DionisosFlow^{TM} is extremely useful when first starting out a model. It allows users to experiment and get familiar with

how other parameters influence sedimentation in the basin. Nevertheless, problems can arise when different transportation laws are required (transport proportional to slope vs water discharge driven transport), or the geological architecture is incorrect. Diffusion coefficients are responsible for creating the general trends in sediment distribution, for instance, a higher diffusion coefficient is given to muddy sediment over sandy sediment, in this way mud is transported further in the basin than sand. Many stratigraphic modelers (e.g. Williams et al. 2011, Gvirtzman et al. 2014, Harris et al. 2018) test the influence of different diffusion coefficient values on the extent of sediment distribution. Thus, improper diffusion coefficients can cause inaccurate values of sediment supply, unrealistic sediment distribution on the shelf, slope, and basin floor, as well as issues with calibrating the model.

In summary, diffusion-based stratigraphic modeling has been successfully applied to the Shelburne sub-basin. All of the unconstrained models show some amount of sand prograding from the Shelburne Delta into deep-water, similar to the reference case model. Many parameters in the reference case model have been geologically constrained, compared to the unconstrained models. However, there is not a substantial difference in sand distribution between the different models, suggesting that some geological parameters are more important than others. The most important parameters to define in frontier basins, such as the Shelburne sub-basin, are the seismic surfaces, and the paleobathymetry. The least important parameter is the paleoriver systems and the sediment supply values for each river, although, they become more important to define when investigating reservoir quality and high-resolution facies distribution. Therefore, in frontier basins, the following parameters should be predefined before starting the

modeling process: seismic surfaces, paleobathymetry, carbonate growth curves, sediment proportion of the river system(s), wide river-mouth input point(s), and the predefined diffusion coefficients in DionisosFlow^{TM}. The use of these predefined parameters will aid in the calibration process and lead to an improved geologically accurate model.

5.7 Summary and Conclusions

(1) Unconstrained models serve a useful purpose in modeling frontier basins. By using a coarser grid and simulating fewer geological processes, significantly less computation time is required compared to geologically constrained models. In the Shelburne sub-basin, all unconstrained models show some amount of sand prograding from the Shelburne Delta into the deep-water area. Therefore, the geologically constrained reference case model may not be significantly different in sediment distribution compared to the alternative unconstrained models. This is explained by the fact that the unconstrained models keep the same conceptual principles as the reference case model, e.g. the interaction between a deltaic source, a carbonate platform, and an initial shelf to basin bathymetry. This is clear evidence for how useful unconstrained models can be, to give a first overview of the probable architecture of the basin.

(2) As in many other frontier basins, the initial paleobathymetry is not well constrained in the Shelburne sub-basin. The modeling process offers a way to evaluate the impact of results of applying a given paleobathymetry, but making the correct choice is a matter of geological judgement. This is a general pitfall of forward stratigraphic modeling, because the initial bathymetry is a critical parameter on which the simulation is constructed. Choosing a suitable initial paleobathymetry implies the necessary compilation and analysis of the available geological data, and therefore, first building

a conceptual model about the facts and hypotheses of the basin before any simulation is performed.

(3) Fine-scale control between carbonate and clastic sediments is not always possible in frontier basins. In the model, carbonate production is influenced by the diffusion of clastic sediment. This pitfall develops because there is not enough information on the different biogenic carbonate producers in the study area, and a limited number of sediment size classes are used in the model. A reasonable increase of the number of sediment classes coupled with a decrease in cell size of the model may lead to more realistic results, however, computation time will significantly increase as well as the difficulty in obtaining calibration.

(4) The most important parameters to define in a new frontier basin are paleobathymetry and sediment thickness from seismic interpretation. The paleoriver system is less significant, but in this study the model would not calibrate unless three input points were chosen, as demonstrated independently from detrital petrology studies. Calibrating the model to sediment thickness and well lithofacies is generally achieved by modifying simulated sediment supply. Deltaic systems are by definition highly diffusive systems, and when coupled with an efficient reworking by waves and tidal currents, can produce a high dispersion of sediments along the shelf making it difficult to identify the precise position of the source.

Chapter 6: Discussion

This chapter discusses the broader issues around forward stratigraphic modeling. It also evaluates the large-scale tectonic evolution of the Shelburne sub-basin. Finally, it assesses the possibility of deep-water sand deposits down-dip of the Shelburne Delta.

6.1: Application of modeling to frontier basins

6.1.1: Ability to reproduce geological features and predict new ones

Diffusion-based models are good at simulating sediment distribution on medium to large scales and over geological time spans. However, in frontier basins where data is limited, modeling parameters such as spatial ponderation maps may have to be used in order to obtain geologically sensible results. Spatial ponderation maps offer a way to control the location of carbonate or hemipelagic sediments by either reducing their growth or defining areas where they are not allowed to grow (see Appendix 2). Diffusion-based models cannot be refined indefinitely trying to match every little calibration detail. Some geological processes are stochastic (e.g. delta distributary switching, precise position of estuarine channel sands versus tidal flat muds) and occur over short time spans and short distances, and therefore are not well represented by diffusion-based models. The complex interaction of deep-water turbidity currents with gradient and channel forms can be represented on a broad scale by diffusion-based modeling, but such modeling will not be able to predict individual sand body geometry or heterogeneities within the sand body.

All simulated models for the Shelburne sub-basin show a high calibration with respect to the overall sequence thickness and facies distribution, matching the simulation goal of at least 80 %. Calibration is also generally very high with respect to thickness and

facies variation in wells, however, facies calibration is lower in the COST G-2 and Mohawk B-93 wells. This could be due to the large cell size used in the models (5km x 5km), which is not able to capture the fine-scale lateral variation in facies (Sangster et al. 2019), or an issue with some model parameters such as environmental carbonate constraints, initial paleobathymetry, or diffusion coefficients.

The reference case model is a credible representation of the regional geology based on the limited amount of geological information available. It reproduces the shelf edge reef, the variation of facies on the shelf, and it matches regional seismic interpretations of thickness. The reference case model was not strictly calibrated to reproduce seismic facies such as the Shelburne Delta, calciturbidites, and deep-water sands. Nevertheless, the presence of deep-water sediment has been confirmed through limited seismic analysis (Fig. 4.12), and work by Kidston et al. (2005) and Deptuck et al. (2015).

Further testing of the predicted geological features was done through statistical sensitivity analysis. The most sensitive parameters that influence the distribution of sand in deep-water are the diffusion coefficients for sand, the water discharge value of the Bay of Fundy source, and the location of the Maine river source. These results indicate that even for very small values of these parameters, some amount of sand will always prograde into deep-water from the Shelburne Delta. Additionally, simulation results from the two deeper bathymetric models indicate that sand is still transferred into deep-water, even with a persistent reef front and increased continental slope and basinal water depths.

6.1.2: Application of provenance model

The river supply to the study area is unusually well known from provenance studies. Provenance studies for the COST G-2 well (Chavez et al. 2019) suggest that river catchment areas were changing throughout the Middle–Late Jurassic. (1) The river system supplying sediment to the COST G-2 well was limited to coastal Maine in the Oxfordian, expanding by the uppermost Jurassic to include more inboard Appalachian terranes (Fig. 2.3) (Chavez et al. 2019). This change in sediment supply to the COST G-2 well was documented by a distinct increase in detrital minerals such as tourmaline and ilmenite (Chavez et al. 2019). (2) Farther east in the study area, Mohawk B-93 did not experience a change in sediment supply, suggesting that the river catchment area remained rather consistent throughout the modeled time span in the southern Meguma terrane (Fig. 2.3) (Dutuc et al. 2017). (3) The river system draining the Bay of Fundy and inboard Appalachian terranes, is the least geologically constrained in the study area. It was responsible for building the Shelburne Delta, and suppling minor sediment from the Canadian Shield to the Mohawk B-93 well (Fig. 2.3) (Blowick et al. submitted).

The high degree of both regional thickness and facies calibration in the reference case model suggests that the river catchment areas proposed by the various provenance studies in the literature are correct for the study area. Nevertheless, several unconstrained models were made to test this assumption. If no information is known about the river systems for the study area, the unconstrained model still calibrates relatively well. Sand is still distributed on the shelf and progrades from the Shelburne Delta into deep-water; although it is more uniform in distribution compared to the constrained models (Figs. 5.2, 5.6, 5.7). This does not appear to be a pitfall of the provenance approach to frontier

basins, rather it relates to the limited amount of geological data available. As more geological information becomes available, or additional wells are drilled, the provenance model approach may lead to a better calibrated model. Defining river catchment areas and relative sediment supply is also important because the petrology of the sediment load may influence reservoir quality and distribution (Sangster et al. submitted).

6.1.3: The influence of climate on sediment budget calculations and deep-water sand delivery

Although the influence of climate on sediment supply and deep-water sediment delivery is relatively unknown for the Middle–Late Jurassic in the Shelburne sub-basin, the effect of climatic variations were tested using sensitivity analysis. At the time of the J163 seismic marker, the study area was located at ~27° latitude (Leinfelder et al. 2002), and climatic modeling suggests that the vegetation cover was tropical xerophytic scrubland (Sellwood and Valdes 2008). For the reference case model, high-energy events and variations in precipitation were modeled using the HEST parameters. The HEST diffusion coefficients were based on Sangster et al. (2019), who used climate modeling from Haywood et al. (2004) for the Early Cretaceous of the North Atlantic region. However, the Middle–Late Jurassic climate was more arid and likely highly seasonal (Sellwood and Valdes 2008) compared to the Early Cretaceous. In this way, HEST events were set to double the frequency of the Early Cretaceous, brought in double the water discharge, and delivered 40 % more sediment compared to LELT times.

Sensitivity analysis on the reference case model indicates that even for reduced river discharge volumes, HEST/LELT ratio, sand proportion, and sand diffusion coefficients, sand is still able to prograde from the Shelburne Delta into deep-water. The

main controls, indicated by sensitivity analysis on deep-water sediment delivery, are the location of the Maine river source, the diffusion coefficients for sand, and the amount of water discharge from the Bay of Fundy source. This demonstrates, that if there was higher aridity in the Jurassic than what was initially thought, that was not a significant control on deep-water sediment delivery from the Shelburne Delta. The implication that some amount of sand will make it into deep-water indicates that other modeling parameters may be more important to define than climatic variables, since diffusion-based models cannot refine the thickness and area of individual sand bodies and their respective heterogeneities with only frontier basin data.

6.2: Sand distribution: similarities and differences between all models

Sand is consistently found on the shelf in all simulated models, and progrades into deep-water from the Shelburne Delta and a large canyon system near Mohawk B-93. However, not all of the sand distribution is the same throughout the entire modeled time span for each simulated model. For instance, sand does not prograde into the basin from 163-161Ma in the unconstrained model with no information on the COST G-2 well. Sand has a very similar pattern of distribution on the shelf (Figs. 5.2, 5.6, 5.7) for all models except for the unconstrained model with no information on the input sources. Finally, sand progrades farthest into the basin as water depths increase (Fig. 5.7) (Models B and C), indicating that increased slope and water depths not unexpectedly lead to greater amounts of sand farther away from the Shelburne Delta. Sensitivity analysis on the reference case model and Models B and C also support further sand transported into the basin, as water discharge volume and sand diffusion coefficients are increased.

The distribution of sand predicted from modeling is consistent with regional seismic interpretations and our understanding of the sedimentary system. Analysis of all models, including sensitivity analysis, indicate that the best place to find sand in deep-water is immediately down-dip of the Shelburne Delta, close to the shelf edge.

6.3: Limitations associated with forward stratigraphic modeling

It is important to understand the assumptions associated with forward stratigraphic modeling in order to properly interpret simulation results. For the reference case model, assumptions were made on the geological system due to lack of available data. This included using uniform and constant rates of subsidence for the modeled time span, when in reality, differential subsidence most likely occurred. In order to stabilize the shelf edge reef on the shallow ramp bathymetry for the J163 seismic marker, spatial ponderation maps were used to limit the growth of carbonate sediments in the basin. A negative source was also used at the edge of the modeled area in the deep basin in order to allow for an open-box approach, allowing sediment to leave the modeled area. All of these assumptions could negatively influence the simulation results and therefore, it is important to understand their effect on sedimentation. Constant subsidence creates a uniform rate of accommodation space, affecting rates of sedimentation, possibly reducing sedimentation from high-energy events, or limiting the effect of sea level variations. Limiting carbonate growth to the J150 shelf edge may be the reason why reef sediments are not seen further in the deep basin, as well as why shallow water carbonate sediments could not be simulated at the base of Monterey Jack E-43. Furthermore, using an open-box approach to sedimentation may cause over-estimation of sediment supply, however, this is unlikely since using an open-box approach mirrors a natural system.

Nevertheless, the limitations associated with forward stratigraphic modeling are also important to understand. The goal of DionisosFlow™ is to simulate the average geometry and facies at basin scales and geological time spans (Granjeon and Joseph 1999). Therefore, it is not possible to reproduce small-scale sedimentary features, such as heterogeneities in reservoir distribution, due to the limitation of the cell size (Kolodka et al. 2016), and the assumptions inherent in a diffusion based model.

6.4: Predefining model parameters to aid in frontier basin stratigraphic modeling

Predefining model parameters for frontier basins appears to be beneficial for areas that have not been previously modeled. The following parameters should be predefined before modeling commences: seismic surfaces, paleobathymetry, carbonate growth curves, average sediment proportions of modern river systems, and the use of wide river-mouth sediment entry point(s). Diffusion coefficients defined in reference DionisosFlow™ models should also be used. Nevertheless, if these predefined model parameters are used, it is important to understand their limitations and how they may influence overall sedimentation.

Properly defining seismic surfaces is the most important challenge when using forward stratigraphic modeling software. They define the regional thickness map for the model, and ultimately control the overall thickness of the sediments. If there is an error in the thickness map, it could cause erroneous amounts of sedimentation, improper location of sediment entry points, and difficulty in calibration. The next most important parameter to define is the paleobathymetry, because it controls the overall basin geometry as well as the extent of different biogenic carbonate producers. Improper paleobathymetry could result in difficultly in calibration, incorrect location of the shelf edge, slope, or basin

floor. Using published carbonate growth curves for each of the different carbonate factories in the model is important in order to define each producer present. Properly defining these carbonate growth curves (e.g. Schlager, 2005) allows the model to respect modern geological conditions. However, it is not always possible to accurately define carbonate environmental parameters outside of recent geological time because growth conditions were different from what present Holocene examples indicate (Leinfelder et al. 2002).

Using average sediment proportions from modern river systems will allow for the simulated model to respect natural systems, however, caution must be used if the study area is located close to shore or far offshore. This will influence the proportions of the different petrographic types of the sediment load. Improper values of sediment proportions could cause difficulty in calibration and incorrect distribution of facies. Some of the limitations of the above parameters can be solved using wide river-mouth sediment entry point(s). Using a wide river-mouth allows for the sediment supply to be varied over an area, similar to natural systems. This will help if the sediment entry point(s) cannot be identified in seismic interpretation, or if there is little information known about ancient river systems. Although using wide river-mouth sediment entry point(s) may aid in the calibration process, they can also create erroneous sedimentation around the sediment entry point.

Finally, using predefined diffusion coefficients is important because it can aid in the calibration process of the model. Diffusion coefficients are responsible for creating general trends in sediment distribution, such that a higher value is given to muddy sediment over sandy sediment, in this way mud is transported further into the basin than

sand. Nevertheless, problems can arise if incorrect diffusion coefficients are used. They can cause issues in sedimentation, leading to inaccurate values of sediment supply, incorrect distribution of facies, inaccurate basin geometry, and extreme difficulty in calibration.

6.5: The role of transform margins and their effect on sediment delivery into the Shelburne sub-basin

Transforms, developed during continental rifting, are important features that focus drainage from the continent. According to Gawthorpe and Hurst (1993), transforms can direct drainage due to the elevation difference between the hanging wall and footwall of the transform. In the Shelburne sub-basin, the Yarmouth Transform separates shallow basement with seaward dipping reflectors (SDRs) from deeper basement to the east, and offsets the East Coast Magnetic Anomaly (ECMA) by approximately 60 km of dextral movement (Deptuck et al. 2015). It was an important feature during early basin development, which extended onto land, and helped focus drainage from the hinterlands to the area of the Shelburne Delta. This can be seen in the reference wells, where COST G-2 recorded a change in provenance from the Oxfordian to the Kimmeridgian-Tithonian (Chavez et al. 2019), as well as in Mohawk B-93 which recorded provenance influence as far away as the Canadian Shield (Blowick et al. submitted). A carbonate ramp environment developed within the Yarmouth Transform, as supported by evidence at Monterey Jack, and carbonate platforms developed on either side of it, except in the area of the Shelburne Delta.

Comparing the south-western Shelburne sub-basin (this study) to the north-eastern Shelburne sub-basin (Moscardelli et al. 2019) allows for a few details on

sedimentation patterns to stand out. Firstly, the north-eastern part of the Shelburne sub-basin is not located near the Yarmouth Transform. This allowed for the north-eastern part of the basin to develop oolitic shoals, which trapped clastic sediments on the shelf until the Early Cretaceous. After which, sediment bypass and erosion on the outer slope occurred (Moscardelli et al. 2019). In comparison, the south-western part of the basin developed a carbonate ramp setting in the transform zone, as indicated by Monterey Jack E-43, and carbonate platforms on either side of it. The transform also extended onto land and focused drainage from the hinterlands to the Shelburne Delta. Secondly, both areas show similar sedimentation patterns on the slope. Little clastic sediment occurs on the upper slope due to sediment bypass, however, levee channel systems and turbidite successions develop on the lower part of the slope. Finally, both areas show that sediment pathways in the basin tend to follow topographic lows, and that the almost-immediate deactivation of the carbonate factory is not always applicable due to deep-water clastic sedimentation (Moscardelli et al. 2019). Carbonate sediments are found in both areas of the sub-basin, however, they become significantly drowned-out in areas of prograding systems such as the Shelburne Delta, and small deltaic systems prograding from the LaHave Platform.

The Sable sub-basin is not located on a transform fault, however, it shares some similarities in sedimentation with the Shelburne sub-basin. Transforms extending onto land between Cape Breton and Newfoundland (Li et al. 2012), helped to focus drainage of the Sable River to the Sable sub-basin. This is similar to the Shelburne sub-basin, where the transform extended onto land, and focused drainage from the hinterlands to the area of the Shelburne Delta.

6.6: Reduced exploration risk in the Shelburne sub-basin

The Shelburne sub-basin is considered an under-explored passive margin sedimentary basin. Little is known on the distribution of clastic sediments and the possibility of deep-water clastic sandstone reservoirs. Nevertheless, recent reports by the Offshore Energy Technical Research association (OETR 2011) indicate that the deep-water part of the Shelburne sub-basin is the most prospective place to find oil in the entire Scotian Basin. This prediction was based on the potential for Triassic or Early Jurassic source rocks that are not overmature, unlike in the Sable sub-basin to the east. However, the Shelburne sub-basin is complicated by complex, tectonic regimes, salt diapirism, and interactions between carbonate and clastic sedimentation.

Forward stratigraphic modeling results of the Shelburne sub-basin indicate that a shallow ramp bathymetry was possible for the J163 seismic marker. Furthermore, the reference case model was able to demonstrate the presence of deep-water clastic sediments, confirming the analysis of limited seismic data in the area. Sensitivity analysis on the reference case model indicates that the best place to find deep-water clastic sediments in the Shelburne sub-basin is immediately down-dip of the Shelburne Delta, close to the shelf edge. Additional simulations were performed in order to understand the sedimentary system and if the presence of deep-water sands were still indicated. Modifying the paleobathymetry to represent a persistent reef front and deep basin environment, still allowed for clastic sediments to prograde from the Shelburne Delta into deep-water. Unconstraining the reference case model further, yielded similar results. This indicates that the presence of deep-water clastic sediments down-dip of the Shelburne Delta is likely. However, further work should be performed in understanding the complex

salt tectonics as well as the influence of climate on sediment delivery. Additionally, reducing the cell size of the reference case model, may lead to insights on the distribution of clastic sediments down-dip of the Shelburne Delta, a refinement of facies, and may resolve some of the limitations and assumptions that were made on the model.

6.7: Review of Objectives

The first objective of this study was to simulate sediment distribution from the Shelburne Delta for the Callovian–Tithonian. This was accomplished using DionisosFlow^{TM} stratigraphic modeling software. For the modeled time interval, clastic sediment was seen prograding from the Shelburne Delta into deep-water in the reference case model. This confirmed the hypothesis that sediment was able to prograde from the Shelburne Delta at this time, however, it was only one possible scenario among several possibilities. Therefore, further simulations were performed to better understand sediment distribution from the Shelburne Delta with respect to initial paleobathymetry regime, information on sources, reference wells, seismic picks, and carbonate extent, in addition to sensitivity analysis. All modeling results indicate that sand prograded from the Shelburne Delta into deep-water during the modeled time span, further confirming the original hypothesis.

The final objective was to test if the initial paleobathymetry had a large influence on sediment accumulation in the basin. A shallow ramp bathymetry for the J163 seismic marker was much harder to calibrate compared to the persistent reef (Model B) and deep-basin (Model C) models. Shelfal deposits remained the same between each model, however, sand was able to prograde much farther from the Shelburne Delta into deep-water in the deeper bathymetric models. This is most likely due to the increased water

depths and slope, allowing sand to increase in velocity, bypass the shelf edge, and spread out as toe of slope basin floor fans. Some ways to test if the initial bathymetry is correct or not, is to reduce the cell size in the model, add additional sediment classes and carbonate producers, and refine the salt diapir movement. Performing these additional steps may allow for the proper bathymetry to come out. If one of the bathymetric models cannot be calibrated with the additional parameters, then possibly it is not geologically correct.

Chapter 7: Conclusions

1. The reference case simulation shows high calibration with respect to the regional thickness map as well as facies distribution. This suggests that the provenance pathways from the literature are appropriate, however, they may cause over-estimation of sediment supply due to the few reference wells that define them. This model matches our current understanding of the sedimentary system as well as confirms the presence of sand down-dip of the Shelburne Delta.
2. Sensitivity analysis on all possible paleobathymetric models shows that clastic sediments from the Shelburne Delta prograded into deep-water. The best place to find sand in deep-water is immediately down-dip of the Shelburne Delta, close to the shelf edge. This area is defined by high sand thickness and shows the least variance. The main parameters controlling the distribution of sand in deep-water are the location of the Maine river source, the water discharge volume from the Bay of Fundy source, and the diffusion coefficients for sand.
3. The Yarmouth Transform played a key role in sediment routing during the early stages of basin development in the Shelburne sub-basin. A carbonate ramp environment developed within the transform zone as indicated by Monterey Jack E-43, and carbonate platforms developed on either side of it. This led to routing of the drainage systems, mainly from the transform extending onto land, and focused them to the narrow area of the Shelburne Delta.
4. Modeling of frontier basins is possible even with limited information from sparse wells, seismic analysis, and lithofacies interpretation. As a first order task, it is important to first make a conceptual model of the basin, before any simulation is

performed. This will create an understanding of the general geological trends and facies distribution, as well as the uncertainty in different input parameters. Accurate seismic surfaces and initial bathymetry are important. Sensitivity analysis is critical because it can show how multiple models can match the calibration criteria, leading to a better understanding of the sedimentary system, and a better calibrated final model.

5. Modeling the interaction between carbonate and clastic sediments is not always possible in frontier basins. The behaviour of different biogenic carbonate producers and the impact of clastic supply remain poorly constrained. Decreasing the cell size and reasonably increasing in the number of sediment classes may allow for more realistic results, however, this will significantly increase the computation time as well as difficulty in obtaining calibration.
6. The presence of possible sandstone reservoirs down-dip of the Shelburne Delta as indicated by modeling, increase the sub-basin's prospectivity. If there is a likely source in the Triassic or Early Jurassic, that is not overmature, then it is likely that the clastic sediment delivered into the basin from the Shelburne Delta could be a potential reservoir. Add in stratigraphic traps from the modeled turbidite successions, structural traps from salt movement, and the petroleum system becomes more viable.

Chapter 8. References

Agrawal, D., Dwivedi, S., Barrois, A., Koeck, C., El-Wazir, Z., Al-Madani, N., and Aillud, G. 2015. Impact of Environmental Parameters on Forward Stratigraphic Modelling from Uncertainty Analysis; Lower Cretaceous, Abu Dhabi. *In* SPE Reservoir Characterisation and Simulation Conference and Exhibition. Society of Petroleum Engineers. doi:10.2118/175683-MS.

Albertz, M., Beaumont, C., Shimeld, J.W., Ings, S.J., and Gradmann, S. 2010. An investigation of salt tectonic structural styles in the Scotian Basin, offshore Atlantic Canada: 1. Comparison of observations with geometrically simple numerical models. Tectonics, **29**: 1–29. doi:10.1029/2009TC002539.

Amato, R. V, and Simonis, E.K. 1980. Geologic and Operational Summary, Cost no. G-2 well, Georges Bank area, North Atlantic OCS. U.S. Geological Survey Open-File Report 80-269.

Amidon, W.H., Roden-Tice, M., Anderson, A.J., McKeon, R.E., and Shuster, D.L. 2016. Late Cretaceous unroofing of the White Mountains, New Hampshire, USA: An episode of passive margin rejuvenation? Geology, **44**: 415–418. doi:10.1130/G37429.1.

Barosh, P.J. 1992. North-west trending basement fracture zones in the eastern United States and their role in controlling neotectonic movement and earthquakes. *In* Basement Tectonics 7. *Edited by* R. Mason. Springer. pp. 409–423.

Blowick, A., Pe-Piper, G., Piper, D.J.W., Zhang, Y., and Tyrrell, S. (submitted). First-

cycle sand supply and the evolution of the eastern Canadian continental margin: insights from Pb isotopes in the Mesozoic Scotian Basin. GSA Bulletin,.

Bowman, S.J., Pe-Piper, G., Piper, D.J.W., Fensome, R.A., and King, E.L. 2012. Early Cretaceous volcanism in the Scotian Basin. Canadian Journal of Earth Sciences, **49**: 1523–1539. doi:10.1139/e2012-063.

Burkhard, M., Caritg, S., Helg, U., Robert-Charrue, C., and Soulaimani, A. 2006. Tectonics of the Anti-Atlas of Morocco. Comptes Rendus Geoscience, **338**: 11–24. doi:10.1016/j.crte.2005.11.012.

Busson, J., Joseph, P., Mulder, T., Teles, V., Borgomano, J., Granjeon, D., Betzler, C., Poli, E., and Wunsch, M. 2019. High-resolution stratigraphic forward modeling of a Quaternary carbonate margin: Controls and dynamic of the progradation. Sedimentary Geology, **379**: 77–96. Elsevier B.V. doi:10.1016/j.sedgeo.2018.11.004.

Chavez, I., Pe-Piper, G., Piper, D.J.W., and MacRae, R.A. 2019. Late Mesozoic sediment provenance on Georges Bank: Enlargement of river drainages to the Atlantic Ocean in the Late Jurassic–Early Cretaceous. AAPG Bulletin, **103**: 1321–1350. doi:10.1306/10261817348.

Chavez, I., Piper, D.J.W., and Pe-Piper, G. 2018. Correlation of the Aptian Naskapi Member of the Scotian Basin and its regional implications. Canadian Journal of Earth Sciences, **55**: 514–535. doi:10.1139/cjes-2017-0205.

Conti, B., Perinotto, J.A. de J., Veroslavsky, G., Castillo, M.G., de Santa Ana, H., Soto, M., and Morales, E. 2017. Speculative petroleum systems of the southern Pelotas

Basin, offshore Uruguay. Marine and Petroleum Geology, **83**: 1–25. Elsevier Ltd. doi:10.1016/j.marpetgeo.2017.02.022.

Contreras, J., Zühlke, R., Bowman, S., and Bechstädt, T. 2010. Seismic stratigraphy and subsidence analysis of the southern Brazilian margin (Campos, Santos and Pelotas basins). Marine and Petroleum Geology, **27**: 1952–1980. Elsevier Ltd. doi:10.1016/j.marpetgeo.2010.06.007.

Cummings, D.I., Arnott, R.W.C., and Hart, B.S. 2006. Sedimentology and stratigraphy of a thick, areally extensive fluvial-marine transition, Missisauga Formation, offshore Nova Scotia, and its correlation with shelf margin and slope strata. Bulletin of Canadian Petroleum Geology, **54**: 152–174.

Davies, P.J., and Hopjey, D. 1983. Growth facies and growth rates of Holocene reefs in the Great Barrier Reef. Journal of Australian Geology and Geophysics, **8**: 237–251.

Davison, I. 1997. Wide and narrow margins of the Brazilian South Atlantic. Journal of the Geological Society, **154**: 471–476. doi:10.1144/gsjgs.154.3.0471.

Deptuck, M.E. 2011. Proximal to distal postrit structural provinces of the western Scotian Margin, offshore Eastern Canada: Geological context and parcel prospectivity for Call for Bids NS11-1.

Deptuck, M.E., Brown, D.E., and Altheim, B. 2015. Call for Bids NS15-1 – Exploration history, geologic setting, and exploration potential : Western and Central regions. CNSOPB Geoscience Open File Report, 2015-001MF, 49 p.

Doherty, J.T., and Lyons, J.B. 1980. Mesozoic erosion rates in northern New England. Geological Society of America Bulletin, **91**: 16. doi:10.1130/0016-7606(1980)91<16:MERINN>2.0.CO;2.

Dromart, G., Garcia, J.-P., Picard, S., Atrops, F., Lécuyer, C., and Sheppard, S.M.F. 2003. Ice age at the Middle–Late Jurassic transition? Earth and Planetary Science Letters, **213**: 205–220. Elsevier. doi:10.1016/S0012-821X(03)00287-5.

Dutuc, D.-C., Pe-Piper, G., and Piper, D.J.W. 2017. The provenance of Jurassic and Lower Cretaceous clastic sediments offshore southwestern Nova Scotia. Canadian Journal of Earth Sciences, **54**: 33–51. doi:10.1139/cjes-2016-0109.

Gawthorpe, R.L., and Hurst, J.M. 1993. Transfer zones in extensional basins: their structural style and influence on drainage development and stratigraphy. Journal of the Geological Society, **150**: 1137–1152. doi:10.1144/gsjgs.150.6.1137.

Gervais, V., Ducros, M., and Granjeon, D. 2018. Probability maps of reservoir presence and sensitivity analysis in stratigraphic forward modeling. AAPG Bulletin, **102**: 613–628. doi:10.1306/0913171611517242.

Gould, K.M., Piper, D.J.W., and Pe-Piper, G. 2012. Lateral variation in sandstone lithofacies from conventional core, Scotian Basin: implications for reservoir quality and connectivity. Canadian Journal of Earth Sciences, **49**: 1478–1503. doi:10.1139/e2012-064.

Granjeon, D. 2014. 3D forward modelling of the impact of sediment transport and base level cycles on continental margins and incised valleys. *In* From Depositional

Systems to Sedimentary Successions on the Norwegian Continental Margin. *Edited by* A.W. Martinius, R. Ravnas, J.A. Howell, R.J. Steel, and J.P. Wonham. John Wiley & Sons, Ltd, Chichester, UK. pp. 453–472. doi:10.1002/9781118920435.ch16.

Granjeon, D., and Joseph, P. 1999. Concepts and Applications of A 3-D Multiple Lithology, Diffusive Model in Stratigraphic Modeling. *In* Numerical Experiments in Stratigraphy Recent Advances in Stratigraphic and Sedimentologic Computer Simulations. SEPM Society for Sedimentary Geology. pp. 197–210. doi:10.2110/pec.99.62.0197.

Granjeon, D., Pellan, C., and Barbier, M. 2017. Assessment of facies distribution in carbonate fields using stratigraphic forward, diagenetic and seismic modelling. *In* 22nd World Petroleum Congress.

Gvirtzman, Z., Csato, I., and Granjeon, D. 2014. Constraining sediment transport to deep marine basins through submarine channels: The Levant margin in the Late Cenozoic. Marine Geology, **347**: 12–26. Elsevier. doi:10.1016/J.MARGEO.2013.10.010.

Haq, B.U. 2014. Cretaceous eustasy revisited. Global and Planetary Change, **113**: 44–58. Elsevier B.V. doi:10.1016/j.gloplacha.2013.12.007.

Harris, A.D., Baumgardner, S.E., Sun, T., and Granjeon, D. 2018. A Poor Relationship Between Sea Level and Deep-Water Sand Delivery. Sedimentary Geology, **370**: 42–51. Elsevier B.V. doi:10.1016/j.sedgeo.2018.04.002.

Harris, A.D., Covault, J.A., Madof, A.S., Sun, T., Sylvester, Z., and Granjeon, D. 2016. Three-Dimensional Numerical Modeling of Eustatic Control On Continental-Margin Sand Distribution. Journal of Sedimentary Research, **86**: 1434–1443. doi:10.2110/jsr.2016.85.

Hawie, N., Barrois, A., Marfisi, E., Murat, B., Hall, J., El-Wazir, Z., Al-Madani, N., and Aillud, G. 2015. Forward Stratigraphic Modelling, Deterministic Approach to Improve Carbonate Heterogeneity Prediction; Lower Cretaceous, Abu Dhabi. *In* Abu Dhabi International Petroleum Exhibition and Conference. Society of Petroleum Engineers. doi:10.2118/177519-MS.

Hawie, N., Covault, J.A., Dunlap, D., and Sylvester, Z. 2018. Slope-fan depositional architecture from high-resolution forward stratigraphic models. Marine and Petroleum Geology, **91**: 576–585. doi:10.1016/j.marpetgeo.2017.12.033.

Hawie, N., Deschamps, R., Granjeon, D., Nader, F.H., Gorini, C., Müller, C., Montadert, L., and Baudin, F. 2017. Multi-scale constraints of sediment source to sink systems in frontier basins: a forward stratigraphic modelling case study of the Levant region. Basin Research, **29**: 418–445. doi:10.1111/bre.12156.

Hawie, N., Marfisi, E., Saint-Ange, F., and MacDonald, A.W.A. 2019. Statistical analysis of forward stratigraphic models in complex salt provinces: The central Scotian Basin case study. AAPG Bulletin, **103**: 433–467. doi:10.1306/07031817054.

Haywood, A.M., Valdes, P.J., and Markwick, P.J. 2004. Cretaceous (Wealden) climates: a modelling perspective. Cretaceous Research, **25**: 303–311.

doi:10.1016/j.cretres.2004.01.005.

Hu, Y., Ma, Y., Guo, B., Gao, Z., and He, W. 2019. Application of stratigraphic-sedimentological forward modeling of sedimentary processes to predict high-quality reservoirs within tight sandstone. Marine and Petroleum Geology, **101**: 540–555. doi:10.1016/j.marpetgeo.2018.11.027.

Ings, S.J., and Shimeld, J.W. 2006. A new conceptual model for the structural evolution of a regional salt detachment on the northeast Scotian margin, offshore eastern Canada. AAPG Bulletin, **90**: 1407–1423. doi:10.1306/04050605159.

Jadoul, F. 2018. Stratigraphic-paleogeographic evolution of Eastern Sardinia Jurassic passive margin carbonates : synthesis and future developments. **10**: 147–154. doi:10.3304/JMES.2018.006.

Jansa, L.F., and Wade, J.A. 1975. Paleogeography and sedimentation in the Mesozoic and Cenozoic, southeastern Canada. *In* Canada's continental margins and off-shore petroleum exploration. *Edited by* C.J. Yorath, E.R. Parker, and D.J. Glass. Canadian Society of Petroleum Geologists, Calgary. pp. 79–102.

Kendell, K.L. 2012. Variations in salt expulsion style within the Sable Canopy Complex, central Scotian margin. Canadian Journal of Earth Sciences, **49**: 1504–1522. doi:10.1139/e2012-069.

Kidston, A.G., Brown, D.E., Altheim, B., and Smith, B.M. 2002. Hydrocarbon potential of the deep-water Scotian Slope. Canada-Nova Scotia Offshore Petroleum Board.

Kidston, A.G., Brown, D.E., Smith, B.M., and Altheim, B. 2005. The Upper Jurassic Abenaki Formation Offshore Nova Scotia : A Seismic and Geologic Perspective. Canada-Nova Scotia Offshore Petroleum Board.

Kolodka, C., Vennin, E., Bourillot, R., Granjeon, D., and Desaubliaux, G. 2016. Stratigraphic modelling of platform architecture and carbonate production: a Messinian case study (Sorbas Basin, SE Spain). Basin Research, **28**: 658–684. doi:10.1111/bre.12125.

Labails, C., Olivet, J.-L., Aslanian, D., and Roest, W.R. 2010. An alternative early opening scenario for the Central Atlantic Ocean. Earth and Planetary Science Letters, **297**: 355–368. Elsevier B.V. doi:10.1016/j.epsl.2010.06.024.

Leeder, M.R., and Gawthorpe, R.L. 1987. Sedimentary models for extensional tilt-block/half-graben basins. Geological Society, London, Special Publications, **28**: 139–152. doi:10.1144/GSL.SP.1987.028.01.11.

Leinfelder, R.R., Schmid, D.U., Nose, M., and Werner, W. 2002. Jurassic reef patterns—The expression of a changing globe. *In* Phanerozoic Reef Patterns. SEPM. pp. 465–520. doi:10.2110/pec.02.72.0465.

Leroux, E., Granjeon, D., and Counts, J. 2017. Cenozoic evolution of the Glorieuses isolated carbonate platform (Eparses Islands, SW Indian Ocean) reconstructed by numerical stratigraphic modeling preliminary results (abstract). *In* International Meeting of Sedimentology, Toulouse, 10-12 October 2017.

Li, G., Pe-Piper, G., and Piper, D.J.W. 2012. The provenance of Middle Jurassic

sandstones in the Scotian Basin: petrographic evidence of passive margin tectonics. Canadian Journal of Earth Sciences, **49**: 1463–1477. doi:10.1139/e2012-061.

Liechoscki de Paula Faria, D., Tadeu dos Reis, A., and Gomes de Souza, O. 2017. Three-dimensional stratigraphic-sedimentological forward modeling of an Aptian carbonate reservoir deposited during the sag stage in the Santos basin, Brazil. Marine and Petroleum Geology, **88**: 676–695. doi:10.1016/j.marpetgeo.2017.09.013.

Matmon, A., Bierman, P.R., Larsen, J., Southworth, S., Pavich, M., and Caffee, M. 2003. Temporally and spatially uniform rates of erosion in the southern Appalachian Great Smoky Mountains. Geology, **31**: 155. doi:10.1130/0091-7613(2003)031<0155:TASURO>2.0.CO;2.

Mercier de Lépinay, M., Loncke, L., Basile, C., Roest, W.R., Patriat, M., Maillard, A., and De Clarens, P. 2016. Transform continental margins – Part 2: A worldwide review. Tectonophysics, **693**: 96–115. Elsevier B.V. doi:10.1016/j.tecto.2016.05.038.

Milliman, J.D., and Syvitski, J.P.M. 1992. Geomorphic / Tectonic Control of Sediment Discharge to the Ocean : The Importance of Small Mountainous Rivers. Journal of Geology, **100**: 525–544.

Montaggioni, L.F., Borgomano, J., Fournier, F., and Granjeon, D. 2015. Quaternary atoll development: New insights from the two-dimensional stratigraphic forward modelling of Mururoa Island (Central Pacific Ocean). Sedimentology, **62**: 466–500. doi:10.1111/sed.12175.

Moscardelli, L., Ochoa, J., Lunt, I., and Zahm, L. 2019. Mixed siliciclastic–carbonate systems and their impact for the development of deep-water turbidites in continental margins: A case study from the Late Jurassic to Early Cretaceous Shelburne subbasin in offshore Nova Scotia. AAPG Bulletin, **103**: 2487–2520. doi:10.1306/02151917318.

Naeser, C.W., and Brookins, D.G. 1975. Comparison of fission-track, K-Ar, and Rb-Sr radiometric age determinations from some granite plutons in Maine. Journal of Research of the U.S. Geological Survey, **3**: 229–231.

Nagle, J., Piper, D.J.W., Marfisi, E., Pe-Piper, G., and Saint-Ange, F. (submitted). Forward stratigraphic modeling to test Jurassic deep-water reservoirs at a transform jog: Shelburne sub-basin, SE Canadian margin. AAPG Bulletin,.

Nemčok, M., Rybár, S., Sinha, S.T., Hermeston, S.A., and Ledvényiová, L. 2016. Transform margins: development, controls and petroleum systems – an introduction. *In* Transform Margins: Development, Controls and Petroleum Systems. *Edited by* M. Nemčok, S. Rybár, S.T. Sinha, S.A. Hermeston, and L. Ledvényiová. Geological Society of London, Special Publications, 431. pp. 1–38. doi:10.1144/SP431.15.

NSDoE. 2015. Play Fairway Analysis - South West Nova Scotia Expansion Atlas. Available from https://energy.novascotia.ca/oil-and-gas/offshore/play-fairway-analysis/analysis/shelburne-basin.

OERA. 2020. Shelburne subbasin postmortem analysis. Review of Cheshire L-97 and Monterey Jack E-43. Comparison with OETR 2011 Play Fairway Analysis.

Available from https://oera.ca/research/shelburne-sub-basin-play-fairway-analysis-update.

OETR. 2011. Play Fairway Analysis Atlas - Offshore Nova Scotia. Nova Scotia Department of Energy Report 88-11-0004-01, 349p.

Pe-Piper, G., Kamo, S.L., and McCall, C. 2010. The German Bank pluton, offshore SW Nova Scotia: Age, petrology, and regional significance for Alleghanian plutonism. Geological Society of America Bulletin, **122**: 690–700. doi:10.1130/B30031.1.

Pe-Piper, G., and MacKay, R.M. 2006. Provenance of Lower Cretaceous sandstones onshore and offshore Nova Scotia from electron microprobe geochronology and chemical variation of detrital monazite. Bulletin of Canadian Petroleum Geology, **54**: 366–379. doi:10.2113/gscpgbull.54.4.366.

Pe-Piper, G., and Piper, D.J.W. 1999. Were Jurassic tholeiitic lavas originally widespread in southeastern Canada?: a test of the broad terrane hypothesis. Canadian Journal of Earth Sciences, **36**: 1509–1516. doi:10.1139/e99-059.

Pe-Piper, G., Triantafyllidis, S., and Piper, D.J.W. 2008. Geochemical Identification of Clastic Sediment Provenance from Known Sources of Similar Geology: The Cretaceous Scotian Basin, Canada. Journal of Sedimentary Research, **78**: 595–607. doi:10.2110/jsr.2008.067.

Pe-Piper, G., and Piper, D.J.W. 2012a. The Impact of Early Cretaceous Deformation on Deposition in the Passive-Margin Scotian Basin, Offshore Eastern Canada. *In* Tectonics of Sedimentary Basins. John Wiley & Sons, Ltd, Chichester, UK. pp.

270–287. doi:10.1002/9781444347166.ch13.

Pe-Piper, G., and Piper, D.J.W. 2012b. Chapter 13: Application of Mineral Provenance Studies to Petroleum Exploration: Case Study of the Scotian Basin. *In* Quantitative Mineralogy and Microanalysis of Sediments and Sedimentary Rocks. *Edited by* P. Sylvester. Mineralogical Association of Canada. pp. 249–264.

Pierre, A., Durlet, C., Razin, P., and Chellai, E.H. 2010. Spatial and temporal distribution of ooids along a Jurassic carbonate ramp: Amellago outcrop transect, High-Atlas, Morocco. Geological Society, London, Special Publications, **329**: 65–88. doi:10.1144/SP329.4.

Piper, D.J.W., Bowman, S.J., Pe-Piper, G., and MacRae, R.A. 2011. The ups and downs of Guysborough County - the mid Cretaceous Naskapi Member in the Scotian Basin: eustacy or tectonics? Atlantic Geology, **47**: 37–38.

Piper, D.J.W., Pe-Piper, G., Hundert, T., and Venugopal, D.V. 2007. The Lower Cretaceous Chaswood Formation in southern New Brunswick; provenance and tectonics. Canadian Journal of Earth Sciences, **44**: 665–677. doi:10.1139/E06-134.

Piper, D.J.W., Pe-Piper, G., and Zhang, Y. 2013. Rift tectonics of the eastern Canadian continental margin : insights from detrital petrology and provenance. *In* GeoConvention 2013: Integration. pp. 1–7.

Poppe, L.J., and Poag, C.W. 1993. Mesozoic stratigraphy and paleoenvironments of the Georges Bank Basin: A correlation of exploratory and cost wells. Marine Geology, **113**: 147–162. doi:10.1016/0025-3227(93)90015-N.

Reynolds, P.H., Pe-Piper, G., Piper, D.J.W., Dehler, S., Deptuck, M., and Karim, A. 2012. Detrital muscovite geochronology and the Cretaceous tectonics of the inner Scotian Shelf, southeastern Canada. Canadian Journal of Earth Sciences, **49**: 1558–1566. doi:10.1139/e2012-062.

Reynolds, P.H., Pe-Piper, G., Piper, D.J.W., and Grist, A.M. 2009. Single-grain detrital-muscovite ages from Lower Cretaceous sandstones, Scotian basin, and their implications for provenance. Bulletin of Canadian Petroleum Geology, **57**: 63–80. doi:10.2113/gscpgbull.57.1.63.

Sangster, C., Pe-Piper, G., Piper, D.J.W., and Saint-Ange, F. (submitted). Predictive modelling of reservoir quality associated with the dissolution of K-feldspar during diagenesis: Lower Cretaceous, central Scotian Basin. AAPG Bulletin,.

Sangster, C., Piper, D.J.W., Hawie, N., Pe-Piper, G., and Saint-Ange, F. 2019. Forward stratigraphic modelling of sediment pathways and depocentres in salt-influenced passive-margin basins: Lower Cretaceous, central Scotian Basin. Basin Research, **31**: 728–753. doi:10.1111/bre.12342.

Schlager, W. 2005. Carbonate Sedimentology and Sequence Stratigraphy. *In* Carbonate Sedimentology and Sequence Stratigraphy. *Edited By*W. Schlager. SEPM (Society for Sedimentary Geology). doi:10.2110/csp.05.08.

Sclater, J.G., and Parsons, B. 1977. An analysis of the variation of ocean floor bathymetry and heat flow with age. Journal of Geophysical Research, **82**.

Seard, C., Borgomano, J., Granjeon, D., and Camoin, G. 2013. Impact of environmental

parameters on coral reef development and drowning: Forward modelling of the last deglacial reefs from Tahiti (French Polynesia; IODP Expedition #310). Sedimentology, **60**: n/a-n/a. doi:10.1111/sed.12030.

Sellwood, B.W., and Valdes, P.J. 2008. Jurassic climates. Proceedings of the Geologists' Association, **119**: 5–17. Geological Society of London. doi:10.1016/S0016-7878(59)80068-7.

Seybold, H., Andrade, J.S., and Herrmann, H.J. 2007. Modeling river delta formation. Proceedings of the National Academy of Sciences, **104**: 16804–16809. doi:10.1073/pnas.0705265104.

Shimeld, J. 2004. A Comparison of Salt Tectonic Subprovinces Beneath the Scotian Slope and Laurentian Fan. *In* Salt Sediment Interactions and Hydrocarbon Prospectivity: Concepts, Applications, and Case Studies for the 21st Century: 24th Annual GCSSPEM Foundation Bob F. Perkins Research Conference, Housten, Texas, December 5-8. *Edited by* P.J. Post, D.L. Olsen, K.T. Lyons, S.L. Palmes, P.F. Harrison, and N.C. Rosen. pp. 502–532. doi:10.5724/gcs.04.24.0502.

Sibuet, J.-C., Rouzo, S., and Srivastava, S. 2012. Plate tectonic reconstructions and paleogeographic maps of the central and North Atlantic oceans. Canadian Journal of Earth Sciences, **49**: 1395–1415. doi:10.1139/e2012-071.

van Staal, C.R., and Barr, S.M. 2012. Lithospheric architecture and tectonic evolution of the Canadian Appalachians and associated Atlantic margin. Tectonic Styles in Canada: the LITHOPROBE Perspective, **Special Pa**: 41–95.

Stica, J.M., Zalán, P.V., and Ferrari, A.L. 2014. The evolution of rifting on the volcanic margin of the Pelotas Basin and the contextualization of the Paraná–Etendeka LIP in the separation of Gondwana in the South Atlantic. Marine and Petroleum Geology, **50**: 1–21. Elsevier Ltd. doi:10.1016/j.marpetgeo.2013.10.015.

Tremolada, F., Erba, E., van de Schootbrugge, B., and Mattioli, E. 2006. Calcareous nannofossil changes during the late Callovian–early Oxfordian cooling phase. Marine Micropaleontology, **59**: 197–209. Elsevier. doi:10.1016/J.MARMICRO.2006.02.007.

Tsikouras, B., Pe-Piper, G., Piper, D.J.W., and Schaffer, M. 2011. Varietal heavy mineral analysis of sediment provenance, Lower Cretaceous Scotian Basin, eastern Canada. Sedimentary Geology, **237**: 150–165. Elsevier B.V. doi:10.1016/j.sedgeo.2011.02.011.

Tucker, G.E., and Slingerland, R.L. 1994. Erosional dynamics, flexural isostasy, and long-lived escarpments: A numerical modeling study. Journal of Geophysical Research: Solid Earth, **99**: 12229–12243. doi:10.1029/94JB00320.

Wade, J.A., and MacLean, B.C. 1990. The Geology of the Southeastern Margin of Canada, Chapter 5. *In* Geology of the Continental Margin of Eastern Canada. *Edited by* M.J. Keen and G.L. Williams. Geological Survey of Canada. pp. 169–238.

Waldron, J.W.F., Schofield, D.I., and Murphy, J.B. 2019. Diachronous Paleozoic accretion of peri-Gondwanan terranes at the Laurentian margin. Geological Society, London, Special Publications, **470**: 289–310. doi:10.1144/SP470.11.

Weston, J.F., MacRae, R.A., Ascoli, P., Cooper, M.K.E., Fensome, R.A., Shaw, D., and Williams, G.L. 2012. A revised biostratigraphic and well-log sequence-stratigraphic framework for the Scotian Margin, offshore eastern Canada. Canadian Journal of Earth Sciences, **49**: 1417–1462. doi:10.1139/e2012-070.

Wierzbicki, R., Dravis, J.J., Al-Aasm, I., and Harland, N. 2006. Burial dolomitization and dissolution of Upper Jurassic Abenaki platform carbonates, Deep Panuke reservoir, Nova Scotia, Canada. AAPG Bulletin, **90**: 1843–1861. doi:10.1306/03200605074.

Williams, H., and Grant, A.C. 1998. Tectonic assemblages, Atlantic Region, Canada. 1:3 000 000 map. Geological Survey of Canada, Open File 3657.

Williams, H.D., Burgess, P.M., Wright, V.P., Della Porta, G., and Granjeon, D. 2011. Investigating Carbonate Platform Types: Multiple Controls and a Continuum of Geometries. Journal of Sedimentary Research, **81**: 18–37. doi:10.2110/jsr.2011.6.

Woolfe, K.J., and Larcombe, P. 1999. Terrigenous sedimentation and coral reef growth: a conceptual framework. Marine Geology, **155**: 331–345. doi:10.1016/S0025-3227(98)00131-5.

Zhang, Y., Pe-Piper, G., and Piper, D.J.W. 2014. Sediment geochemistry as a provenance indicator: Unravelling the cryptic signatures of polycyclic sources, climate change, tectonism and volcanism. Sedimentology, **61**: 383–410. doi:10.1111/sed.12066.

Appendix 1:
Bathymetry Comparisons

Calibrated Models	COST G-2		Bonnet P-23		Mohawk B-93		Monterey Jack E-43		Total Well Thickness	Total Facies	Total Well (thickness + facies)	Thickness Map
	Thickness	Facies	Thickness	Facies	Thickness	Facies	Thickness	Facies				
Shallow Ramp (Reference case)	99.34	67.26	99.02	82.18	95.22	74.88	99.4	87.47	98.87	76.23	87.55	97.67
Model B	99.37	70	99.84	88.24	96.16	75.48	99.3	87.46	99.28	79.8	89.54	97.78
Model C	99.39	68.6	99.28	88.24	96.22	75.24	89.66	87.41	97.94	79.21	88.58	98

Table 1.1: Calibration indicators of the three models.

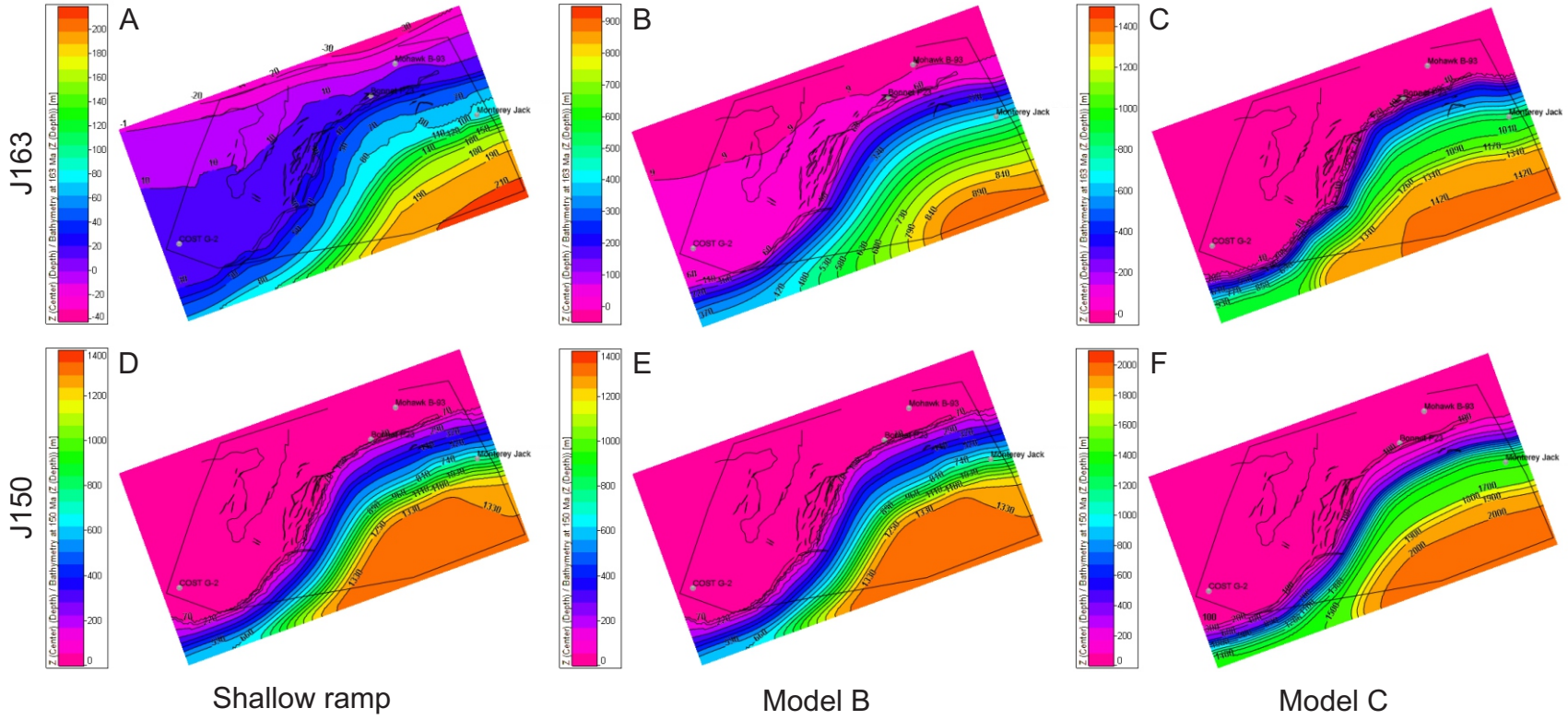

Figure 1.1: Different bathmetric profiles for the three calibrated models.
A,D: The J163 is a shallow carbonate ramp environment. Maximum water depths are 219m. By the J150, there is an establishment of a reef environment. Maximum water depths are 1402m.
B,E: Model B. Slightly deeper shelf and basin bathymetry compared to A. J163 consists of an established reef environment. Maximum water depths are 942m. J150 bathymetry is the same model 1.
C,F: Model C. Shelf and basin floor water depths are significantly deeper than the other two models. Maximum water depths are 1500m. J150 also has a deeper shelf and basin floor, maximum water depths are 2100m.

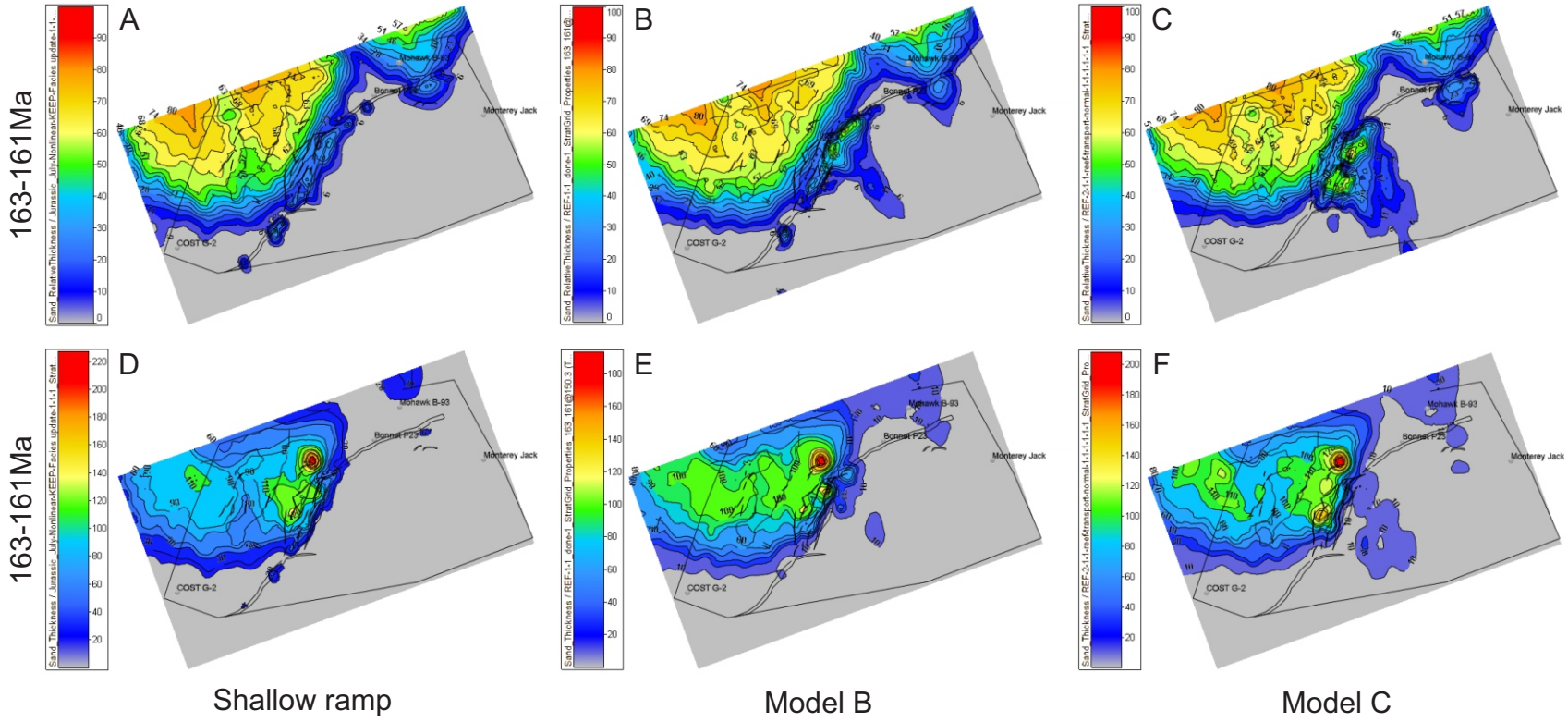

Figure 1.2: Comparison of the first sequence (163-161Ma) in the three models.
A,B,C: Shows the elemental thickness weighted average of sand.
D,E,F: Shows the thickness of sand in meters.

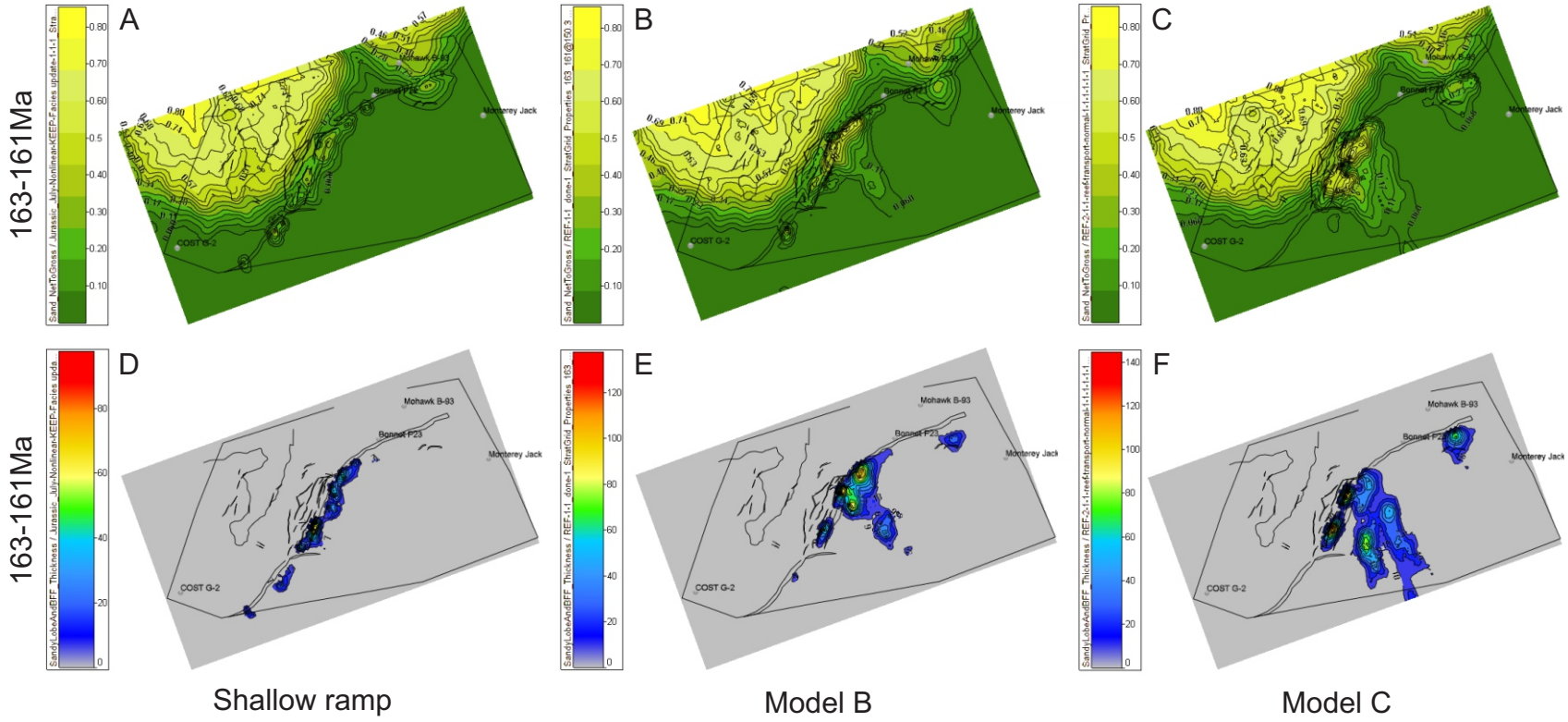

Figure 1.3: Comparison of the first sequence (163-161Ma) in the three models.
A,B,C: Shows the net-gross ratio of sand.
D,E,F: Shows the basin floor fan facies thickness meters.

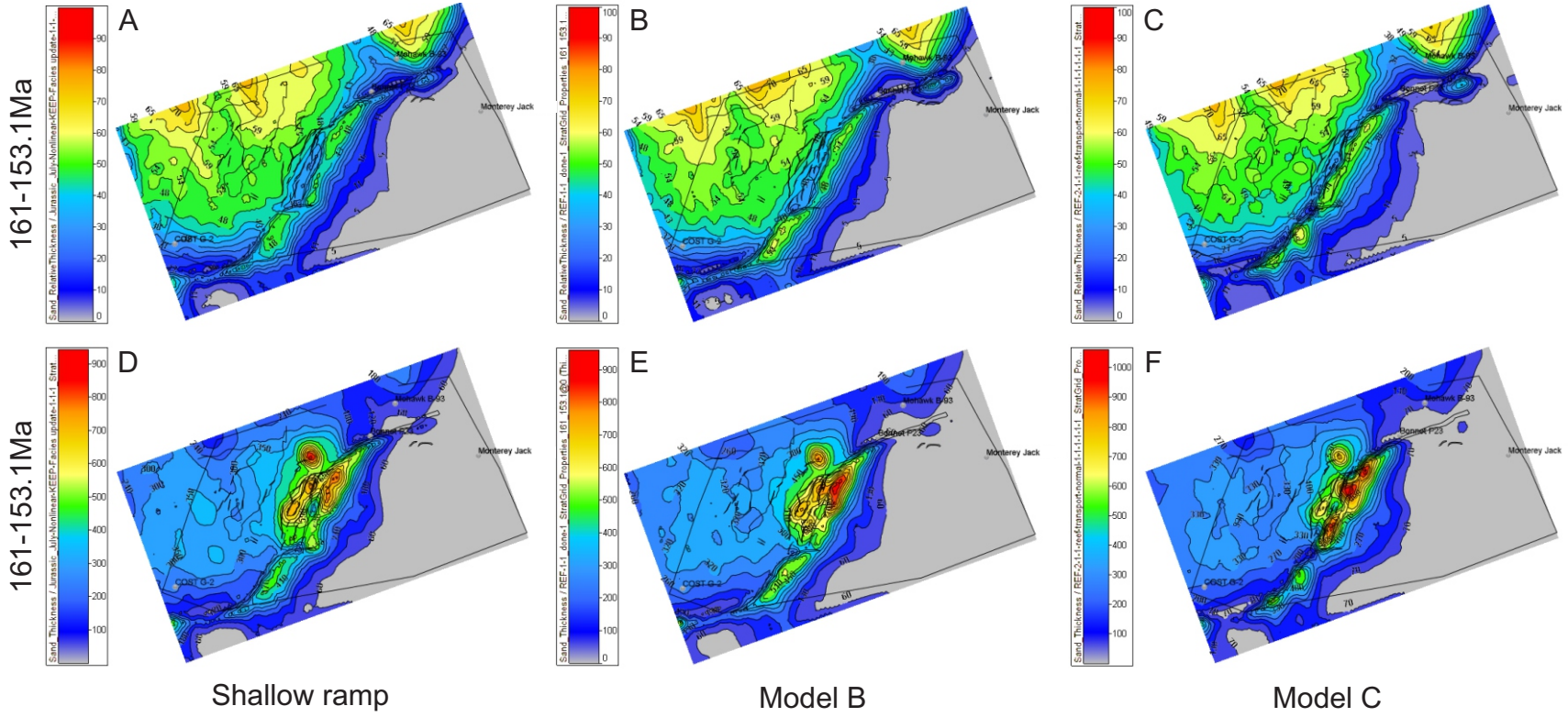

Figure 1.4: Comparison of the second sequence (161-153.1Ma) in the three models.
A,B,C: Shows the elemental thickness weighted average of sand.
D,E,F: Shows the thickness of sand in meters.

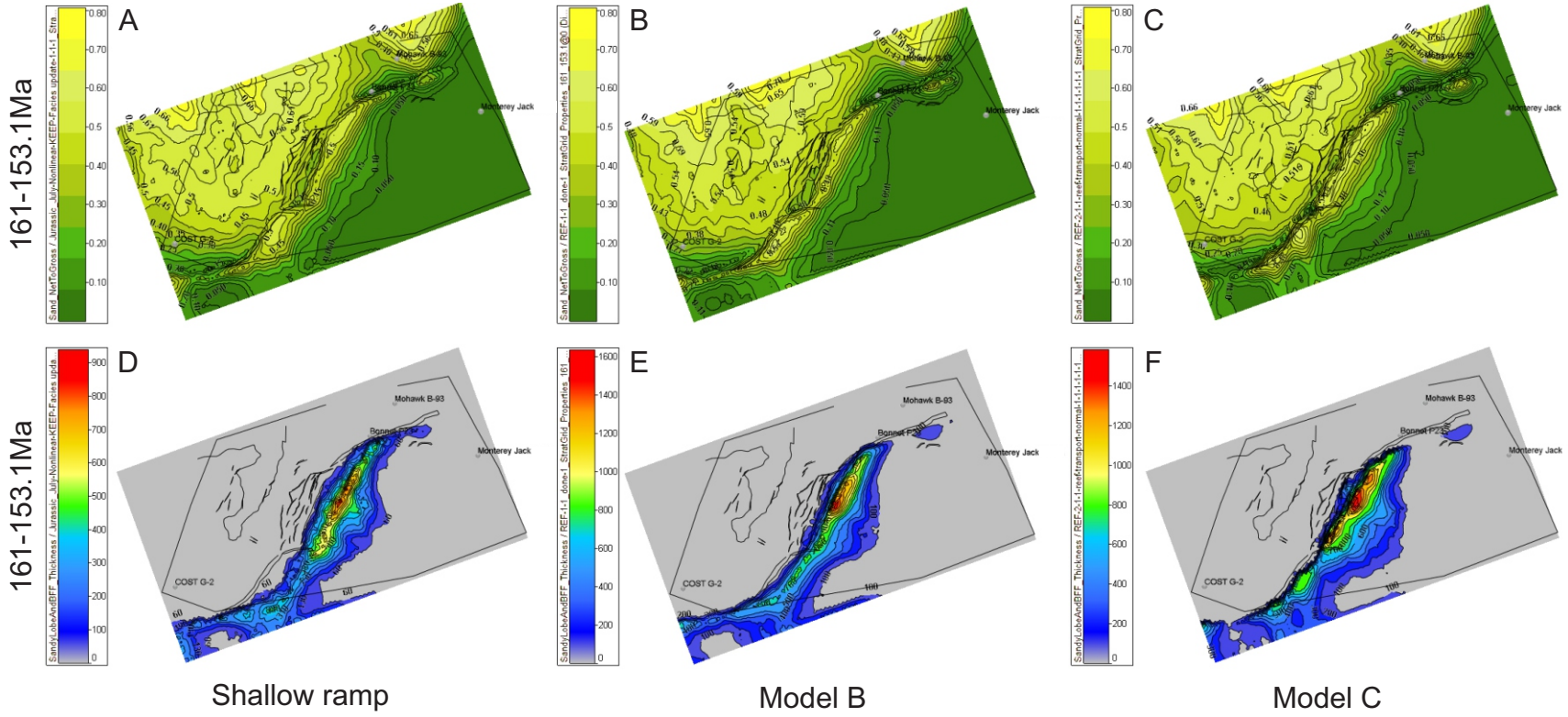

Figure 1.5: Comparison of the second sequence (161-153.1Ma) in the three models.
A,B,C: Shows the net-gross ratio of sand.
D,E,F: Shows the basin floor fan facies thickness meters.

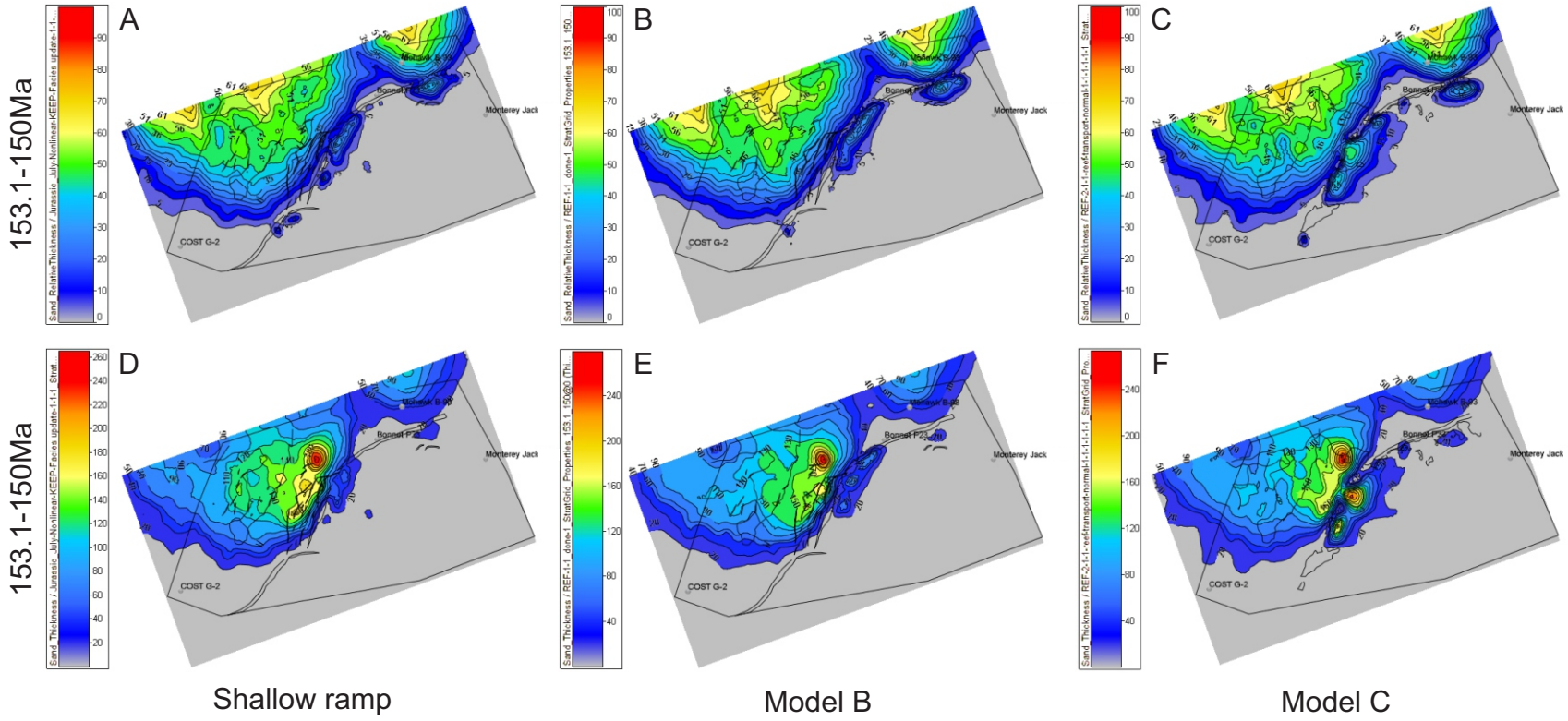

Figure 1.6: Comparison of the third sequence (153.1-150Ma) in the three models.
A,B,C: Shows the elemental thickness weighted average of sand.
D,E,F: Shows the thickness of sand in meters.

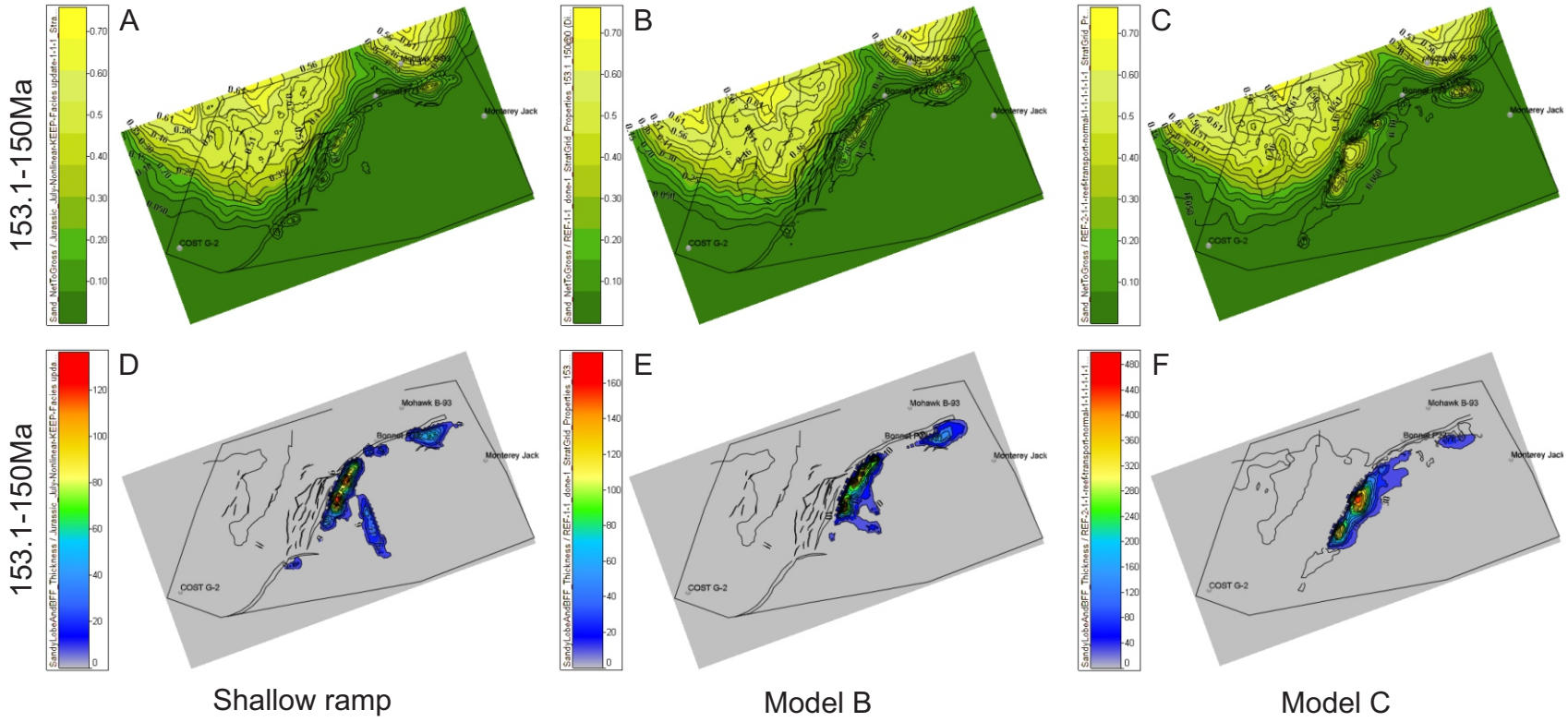

Figure 1.7: Comparison of the third sequence (153.1-150Ma) in the three models.
A,B,C: Shows the net-gross ratio of sand.
D,E,F: Shows the basin floor fan facies thickness meters.

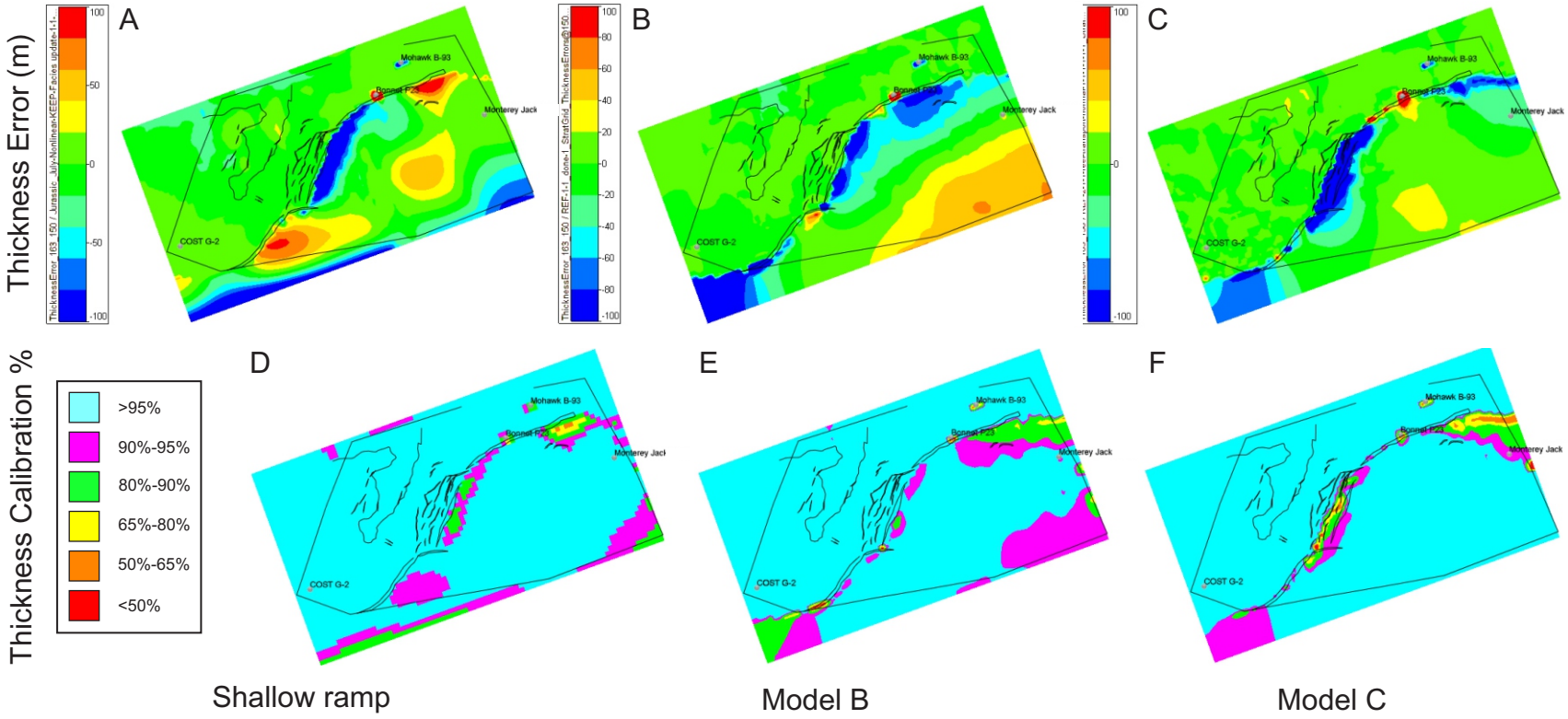

Figure 1.8: Comparison of the thickness error (m) and the thickness calibration % in the three models.
A,B,C: Shows the thickness error (m). Note images are scaled to ±100m; therefore error may be greater than the maximum and minimum values shown.
D,E,F: Shows the thickness calibration %. Models have a very high calibration (>95%), except in some areas along the shelf edge, after the shelf break basinward of the Shelburne Delta, and where the negative source is located.

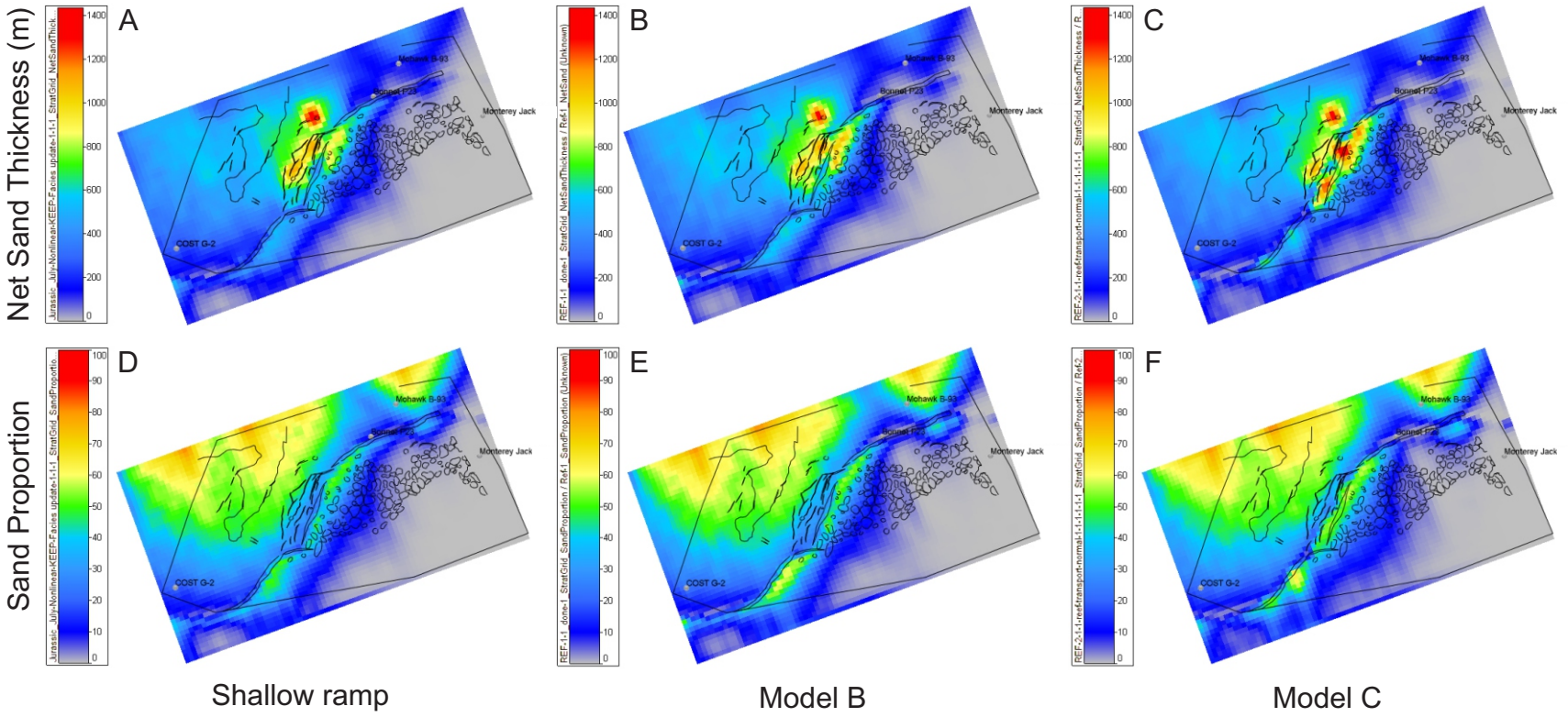

Figure 1.9: Comparison of the extracted maps from 163-150Ma from the three models.
A,B,C: Net sand thickness (m) maps. All maps are to the same colour scale.
D,E,F: Sand proportion maps. All maps are to the same colour scale.

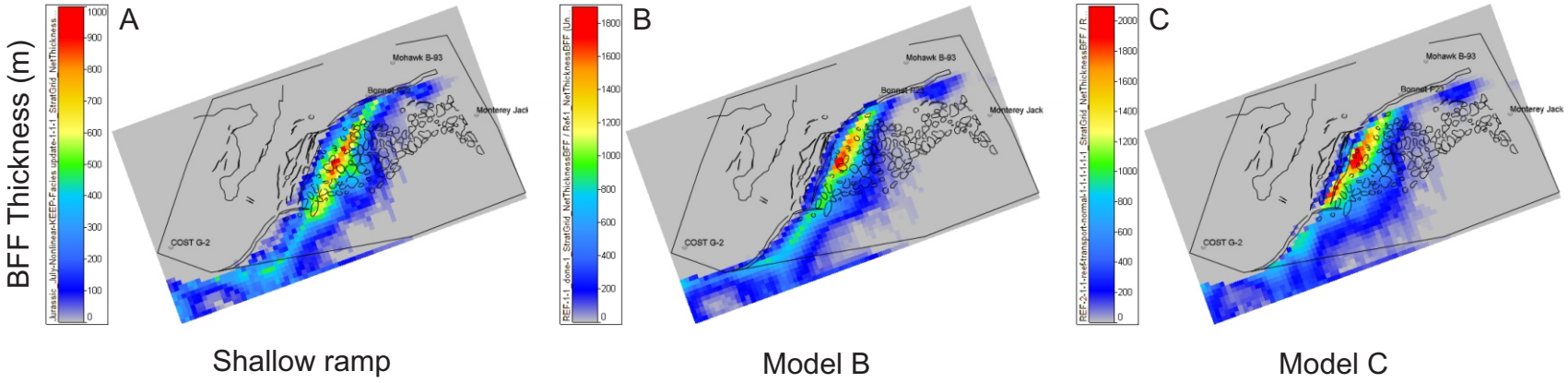

Figure 1.10: Comparison of the basin floor fan facies (BFF) class from 163-150Ma for the three models.
A,B,C: Shows the net basin floor fan thickness (m). Sand accumulates in thicker packages closer to the shelf edge with increasing water depths.

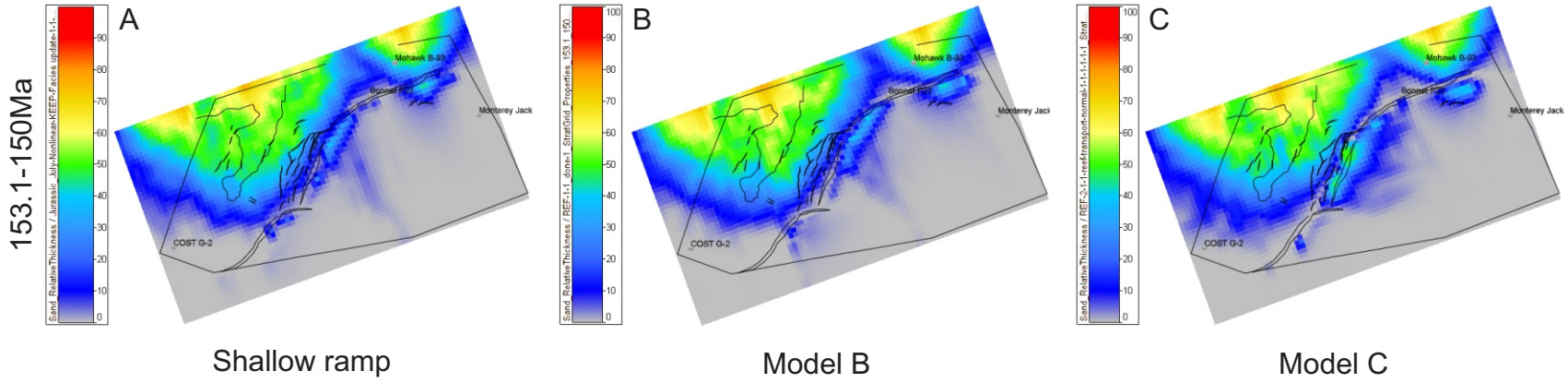

Figure 1.11: Comparison of the element thickness weighted average 153.1-150Ma for the three models. **A,B,C:** Shows the relative thickness of sand. More sand makes it into the basin as bathymetry increases.

Appendix 2:

Parameters for shallow ramp reference case model

This supplementary appendix contains all of the parameters used in the Shallow Ramp reference case model. The values are in relative order with respect to DionisosFlow™.

Domain Definition

Bounding Box

Xo (m): 130000

Yo (m): 4445000

Azimuth (°): -20

X length (m): 400000

Y length (m): 225000

Mesh Attributes Section

NX: 80

NY: 45

DX (m): 5000

DY (m): 5000

Sediment Classes & Properties

Carbo_Mud

Grain size: 0.04 mm

Solid density: 2700 kg/m^3

Reef

Grain size: 1 mm

Solid density: 2700 kg/m^3

Sand

Grain size: 0.2 mm

Solid density: 2675 kg/m^3

Shale

Grain size: 0.02 mm

Solid density: 2645 kg/m^3

Structural Evolution

Time Definition

Start Age = 163 Ma

End Age = 150 Ma

Calculation Mode

Forward Subsidence

Subsidence maps are calculated from the bathymetry maps and thickness maps within DionisosFlow™.

Substratum = 100 m of Carbo_Mud

Eustasy

The eustatic curve from Haq (2014) was used for the model (see Figure 2 in main body of paper).

Sediment Supply

Boundary Calculation Mode

Set to LINEAR Interpolation between Ages

Total Boundary Supply Parameters and Hydric Balance Properties

Rain Fall and Evaporation was set to 0 mm/year for the whole model time span.

Computation

Sediment Supply (km^3/Ma): 155

Fluvial Discharge (m^3/s): 100

Concentration (kg/m^3): 0.098

Source Information:

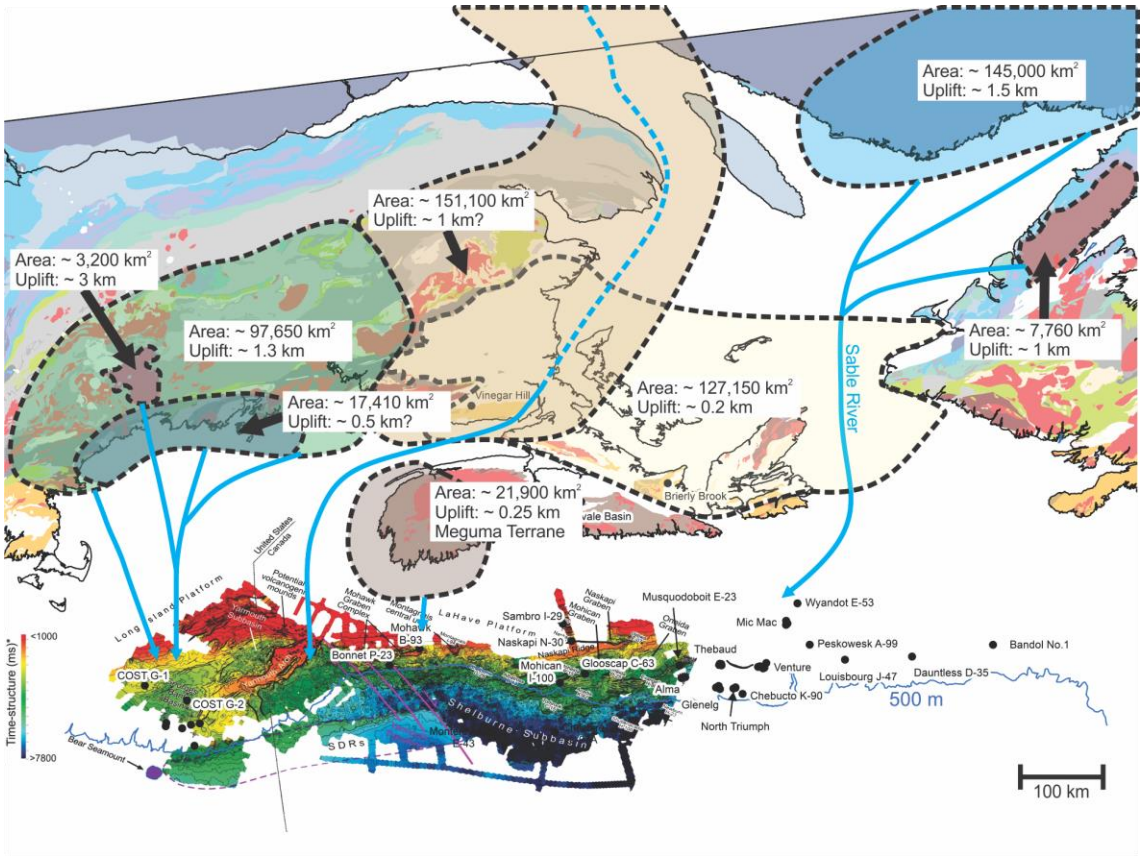

Source River	Source Area	Area (km²)	Uplift (km)	Water Discharge (m³/s)			Sediment Load (km³/Ma)
				Max	Min	Avg.	
Bay of Fundy Area	Appalachians + Maritimes Basin	151100	1?	3900	225	2062.5	1070
Maine	Appalachians	97650	1.3	2872	183	1527.5	1353
	Coastal Maine	17410	0.5?	1127	65	596	284
	White Mountians	3200	3	361	11	186	2348
Meguma Terrane	Shear Zones	50	0.4	6	1	3.5	
	Inner Shelf and Onshore Nova Scotia	55150	0.25	2000	145	1072.5	417

Source		Location																								
	Age (Ma)	Relative Side	Position	Width (m)	Average	163	162	161.5	161.4	161.3	161	160	159	158	157.8	157	156.5	156	155	154	153.3	153.1	153	152	151	150
Maine	Supply (km^3/Ma)	North	80000	8000	279.37	900	700	1100	1100	1400	2400	3100	2300	2600	2300	2600	2300	2300	2500	2300	2350	1800	1000	350	350	150
	Fluvial Discharge (m^3/s)				598.65	1300	1300	2000	1600	1900	3300	4400	4400	4800	4800	5300	4400	4400	3500	3000	3100	2500	1500	400	400	400
	Carbo_Mud (%)				0	0	0	0	0	0	0	0	0	0	0	0	0	0	0	0	0	0	0	0	0	0
	Reef (%)				0	0	0	0	0	0	0	0	0	0	0	0	0	0	0	0	0	0	0	0	0	0
	Sand (%)				44.76	56.8	58.89	58	58.54	58.48	57.78	55.17	51.2	49.8	49.7	49.52	49.38	49.24	40	40	45.67	45.44	45.32	44.57	41.19	40.17
	Shale (%)				55.24	43.2	41.11	42	41.46	41.52	42.22	44.83	48.8	50.2	50.3	50.48	50.62	50.76	60	60	54.33	54.56	54.68	55.43	58.81	59.83
Bay of Fundy	Supply (km^3/Ma)	North	150000	5000	1974.86	500	1500	1000	950	800	1500	3500	2500	2500	2000	2000	1600	1700	800	500	1250	1400	1500	1500	1800	2000
	Fluvial Discharge (m^3/s)				2778.53	1500	2500	2000	1900	2000	3000	4000	3000	3500	2950	2500	2300	2500	2100	1500	2000	2400	2500	2500	2000	2800
	Carbo_Mud (%)				0	0	0	0	0	0	0	0	0	0	0	0	0	0	0	0	0	0	0	0	0	0
	Reef (%)				0	0	0	0	0	0	0	0	0	0	0	0	0	0	0	0	0	0	0	0	0	0
	Sand (%)				40.84	56.8	58.89	58	58.54	58.48	57.78	55.17	51.2	49.8	49.7	49.52	49.38	49.24	48.89	46.48	45.67	45.44	45.32	44.57	41.19	40.17
	Shale (%)				59.16	43.2	41.11	42	41.46	41.52	42.22	44.83	48.8	50.2	50.3	50.48	50.62	50.76	51.11	53.52	54.33	54.56	54.68	55.43	58.81	59.83
Meguma	Supply (km^3/Ma)	North	330000	15000	339.03	50	200	250	200	200	250	250	200	200	50	100	150	150	200	300	300	260	250	200	300	350
	Fluvial Discharge (m^3/s)				540.03	200	400	400	250	500	300	500	400	500	300	550	300	200	400	400	475	490	500	600	500	550
	Carbo_Mud (%)				0	0	0	0	0	0	0	0	0	0	0	0	0	0	0	0	0	0	0	0	0	0
	Reef (%)				0	0	0	0	0	0	0	0	0	0	0	0	0	0	0	0	0	0	0	0	0	0
	Sand (%)				40.4	30	20	30	35	40	57.78	55.17	51.2	49.8	40	40	40	45	48.89	46.48	45.67	45.44	45.32	44.57	41.19	40.17
	Shale (%)				59.6	70	80	70	65	60	42.22	44.83	48.8	50.2	60	60	60	55	51.11	53.52	54.33	54.56	54.68	55.43	58.81	59.83
Suction	Supply (km^3/Ma)	South	110000	600000	-350	-350	-350	-350	-350	-350	-350	-350	-350	-350	-350	-350	-350	-350	-350	-350	-350	-350	-350	-350	-350	-350
	Fluvial Discharge (m^3/s)				-350	-350	-350	-350	-350	-350	-350	-350	-350	-350	-350	-350	-350	-350	-350	-350	-350	-350	-350	-350	-350	-350
	Carbo_Mud (%)				0	0	0	0	0	0	0	0	0	0	0	0	0	0	0	0	0	0	0	0	0	0
	Reef (%)				0	0	0	0	0	0	0	0	0	0	0	0	0	0	0	0	0	0	0	0	0	0
	Sand (%)				50	50	50	50	50	50	50	50	50	50	50	50	50	50	50	50	50	50	50	50	50	50
	Shale (%)				50	50	50	50	50	50	50	50	50	50	50	50	50	50	50	50	50	50	50	50	50	50

Carbonate Production

Carbonate Production vs. Time

LINEAR interpolation between ages

Age (Ma)	Carbo_Mud (m/Ma)	Reef (m/Ma)	Sand (m/Ma)	Shale (m/Ma)
0	18	180	0	10
150	40	250	0	45
160	35	250	0	35
160.9	45	250	0	10
161.3	40	250	0	10
161.5	35	250	0	10
161.7	30	250	0	10
162	10	250	0	10
162.5	10	250	0	10
163	0	0	0	10

Carbonate Production vs. Water Depth

Water Depth (m)	Carbo_Mud (m/Ma)	Reef (m/Ma)	Sand (m/Ma)	Shale (m/Ma)
0	1	0	0	1
1	1	0	0	1
5	1	0	0	1
6	1	1	0	1
10	1	1	0	1
15	1	0.95	0	1
20	1	0.85	0	1
25	1	0.75	0	1
30	1	0.65	0	1
35	1	0.5	0	1
40	1	0.38	0	1
45	1	0.25	0	1
50	1	0.15	0	1
75	1	0.02	0	1
100	1	0	0	1
125	1	0	0	1
150	1	0	0	1
175	1	0	0	1
200	1	0	0	1

Spatial Ponderation maps

Were used to control the location that Carbo_Mud, Reef, and shale were allowed to grow.

Reef

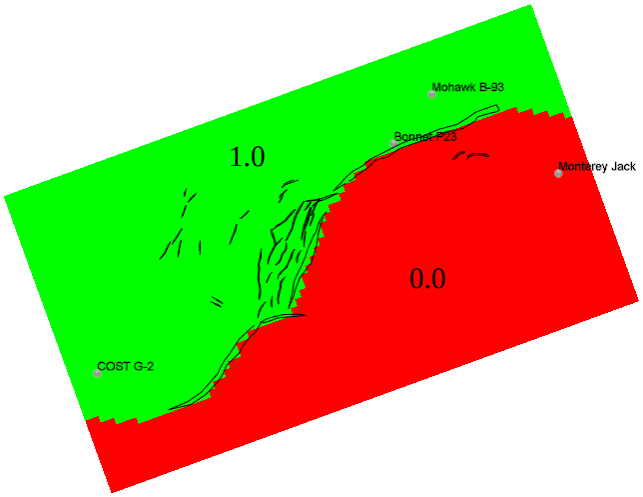

Carbonate Mud

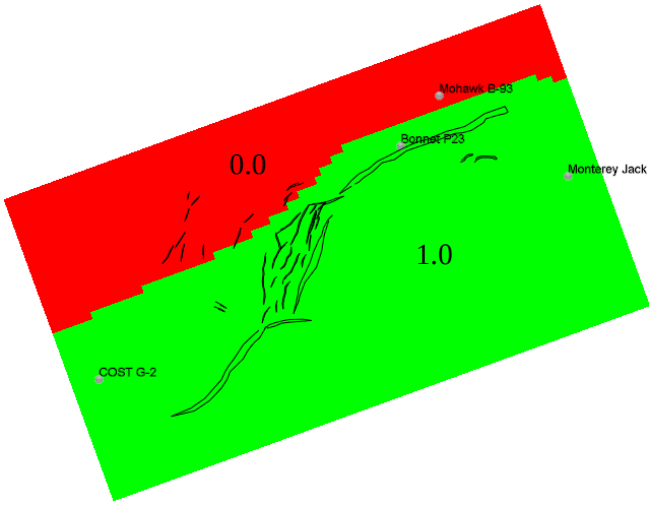

Hemipelagic Shale

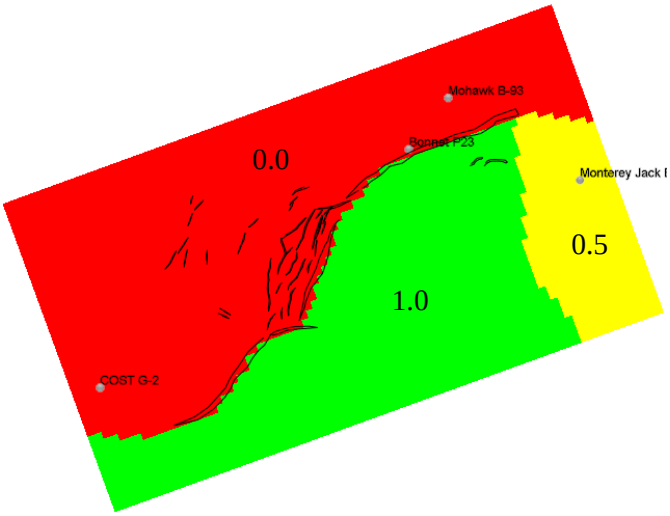

Environmental Constraints

Sediment	Constraint Type	Min Constraint	Max Constraint
Carbo_Mud	Wave Energy (kW/m)	Min	15
Reef	Wave Energy (kW/m)	15	Max

Boundaries Tolerance

	Carbo_Mud	Reef	Sand	Shale
Tolerance (%)	10.0	10.0	0.0	0.0

Transport Processes

Diffusion Transport Law = Non-Linear Diffusive Transport Law
(Qs=S*Kslope+S^ns*Q^nq*Kwater)

Channelized Force = 0.8

Transport Model

HEST parameters definition:

HEST/LELT Water Discharge Ratio (/) = 2

Relative Duration of the HEST Period (month) = 6

Proportion of Sediment Inflow coming during HEST times (%) = 40

Slope Failure Model

No Slope Failure

Erosion Model

Uniform Weathering Rate

Maximum Sediment Weathering Rate (m/Ma) = 100

Maximum Substratum Weathering Rate (m/Ma) = 1

Transport Parameters for each Sediment

Gravity-Driven Diffusion Coefficient: Kgravity	**Carbo_Mud**	**Reef**	**Sand**	**Shale**
Continental (km^2/kyr)	0.1000	0.0010	0.1000	0.1000
Marine (km^2/kyr)	0.1000	0.0010	0.1000	0.1000
Water-Driven Diffusion Coefficient: Kwater				
Continental (km^2/kyr)	500.0000	200.0000	200.0000	1000.0000
Marine (km^2/kyr)	2.5000	0.0010	0.5000	2.5000
Wave Diffusion Coefficient: Kwave				
Kwave (km^2/kyr)	2.5000	0.0100	0.5000	2.5000
High-Energy Short-Term Transport: Khest				
Continental (km^2/kyr)	500.0000	200.0000	200.0000	1000.0000
Marine (km^2/kyr)	2.5000	0.0010	0.5000	2.5000

Waves Impact

Wave Energy Type

Wave Energy decreases from Sea Level to Wave Base (1D)

Wave Parameters

Wave Base (m) = 20

Wave Propagation Azimuth (°) = 0

Frequency in a Year (%) = 100

Simulation Parameters

Start Options

Starting Age of GeoModel

Run Options

Use a specific bathymetry map: Bathymetry at 163 Ma

Age at Initial Bathymetry: 163 Ma

Perform a simulation until Age: 150 Ma

Time Step: 0.1 Ma

Number of Time Steps: 130

Save Options

At all calculator time steps

Present Day Burial

Compute using Geogrid Data

Output Properties

Geometry and Stratigraphy

Age

Stratigraphy

Environmental Properties

Bathymetry

Slope

Sediment Properties

Sediment Proportion

Sedimentation Rate

Hydrodynamism Properties

HEST (Ratio)

HESTflow

Water

Wave Energy

Appendix 3: Shallow ramp reference case model sediment distribution, facies, and sedimentation rate maps

Sediment distribution maps

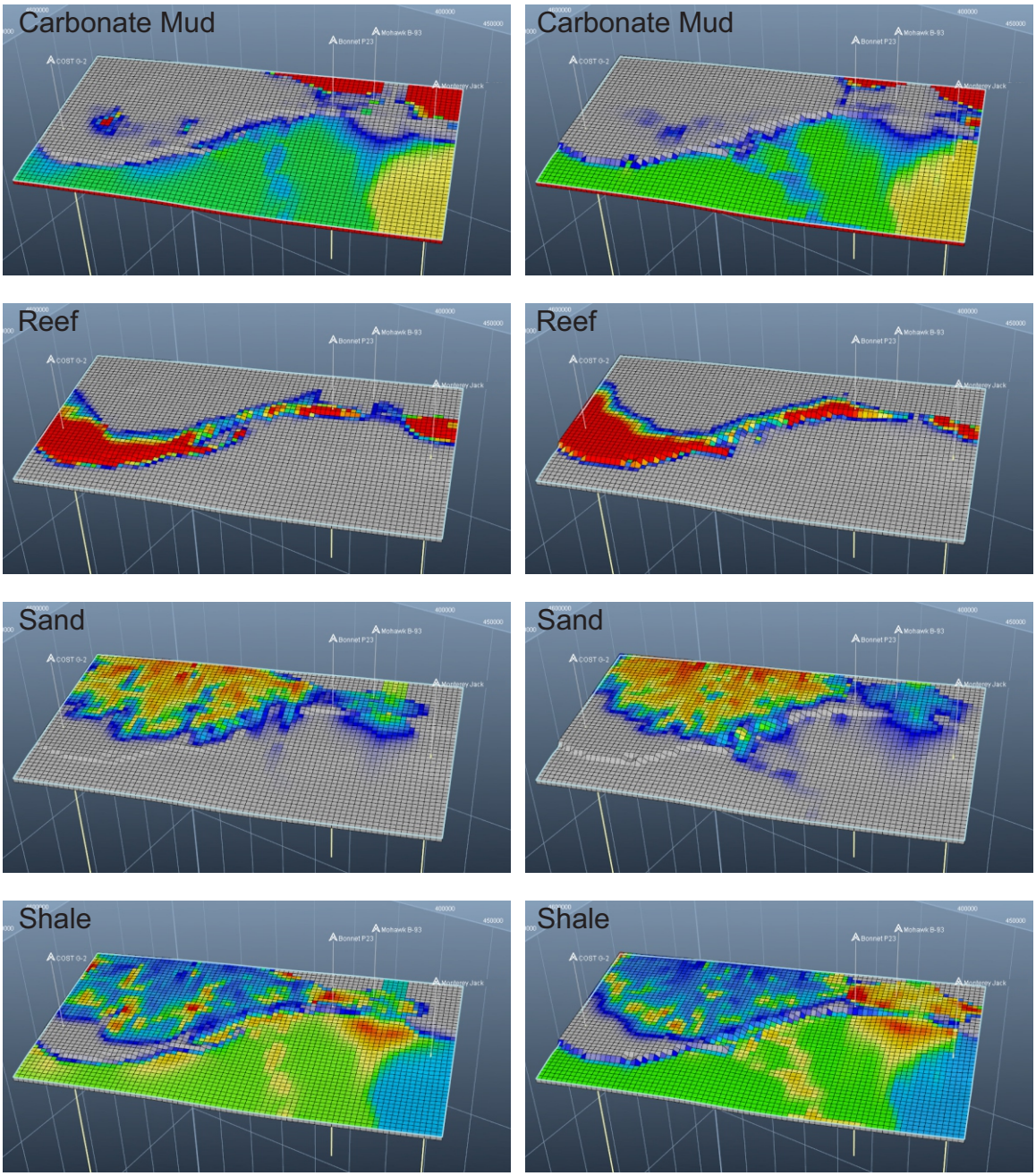

Figure 3.1: Sediment distribution maps. Vertical Exaggeration = 40x.

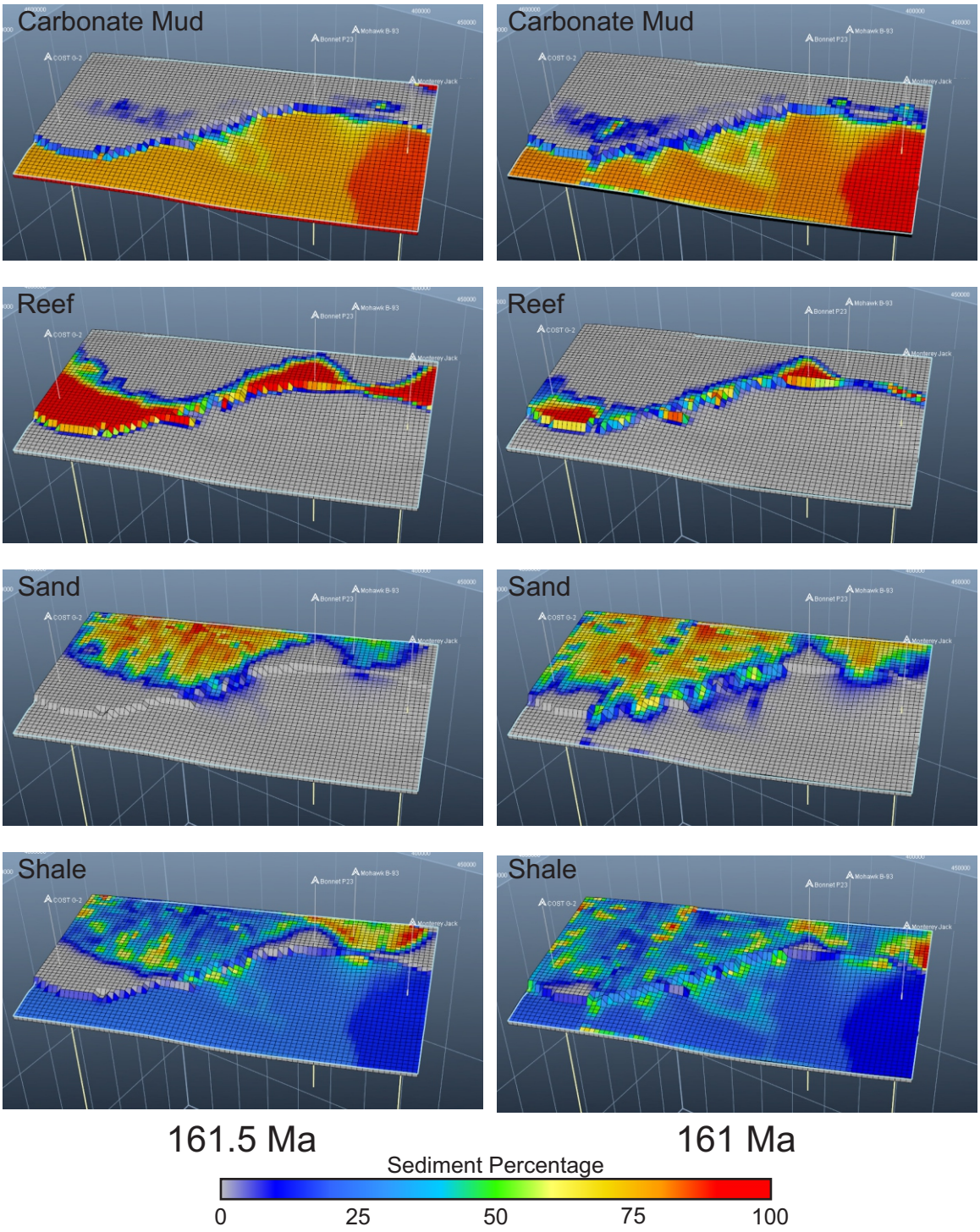

Figure 3.2: Sediment distribution maps. Vertical Exaggeration = 40x.

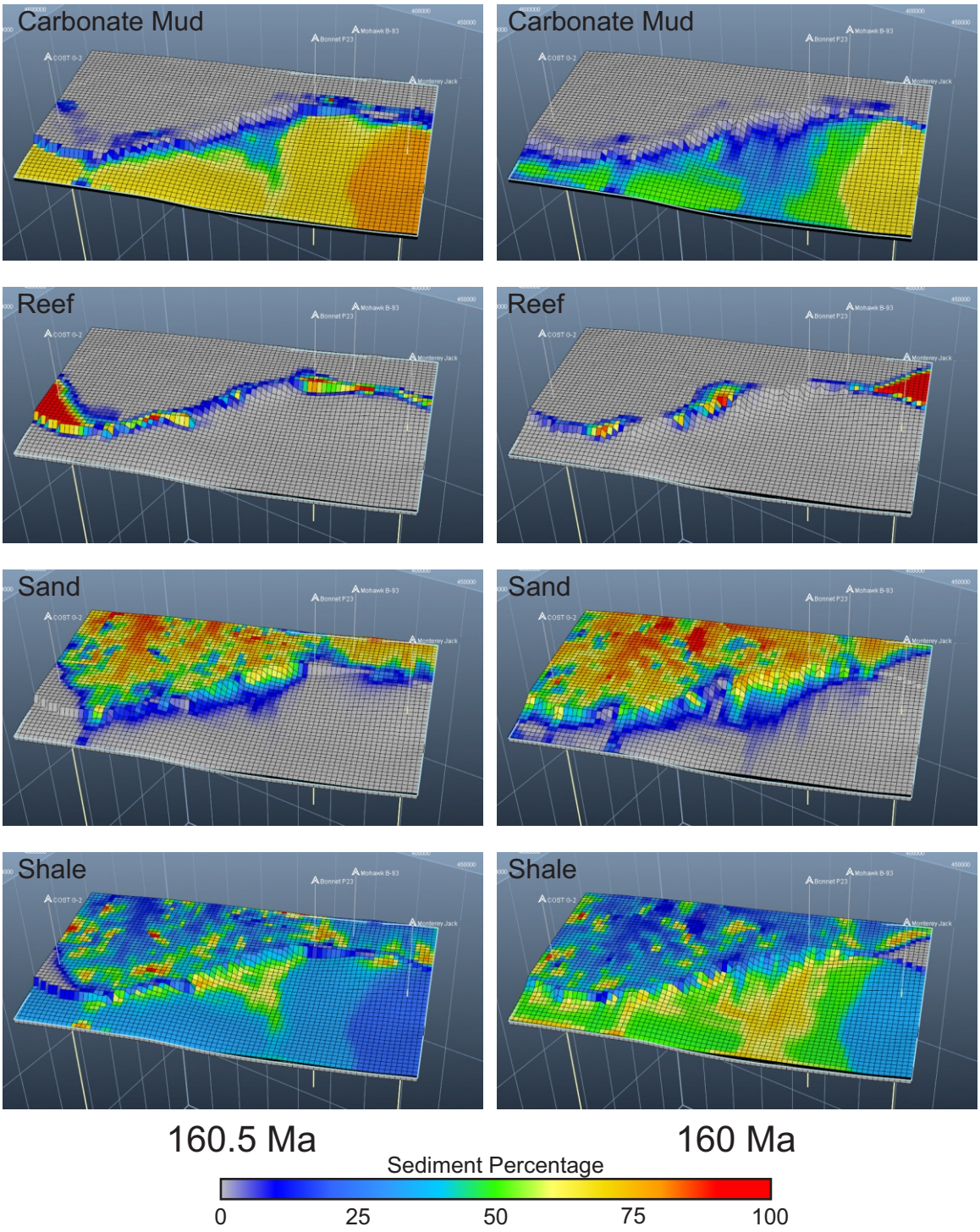

Figure 3.3: Sediment distribution maps. Vertical Exaggeration = 40x.

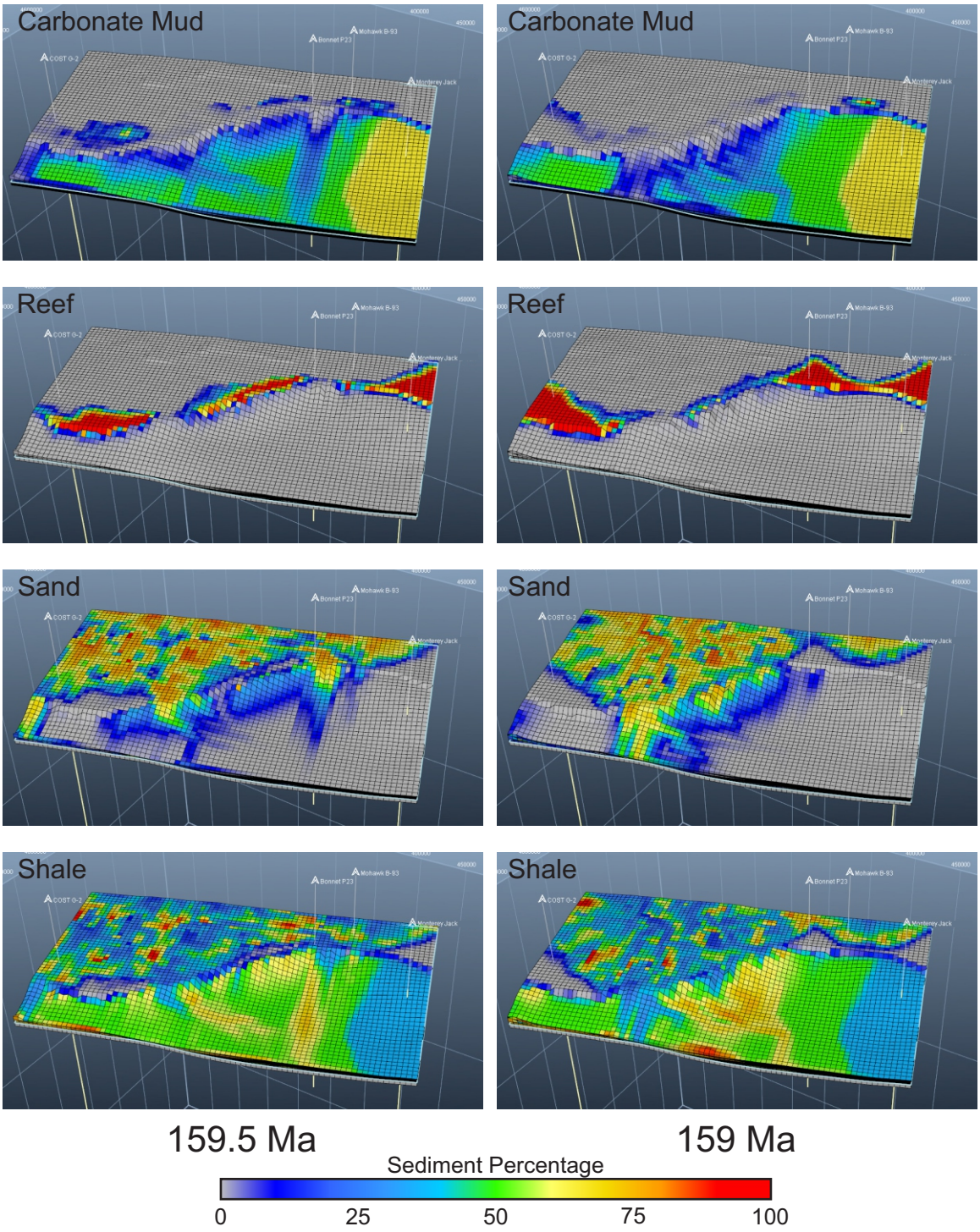

Figure 3.4: Sediment distribution maps. Vertical Exaggeration = 40x.

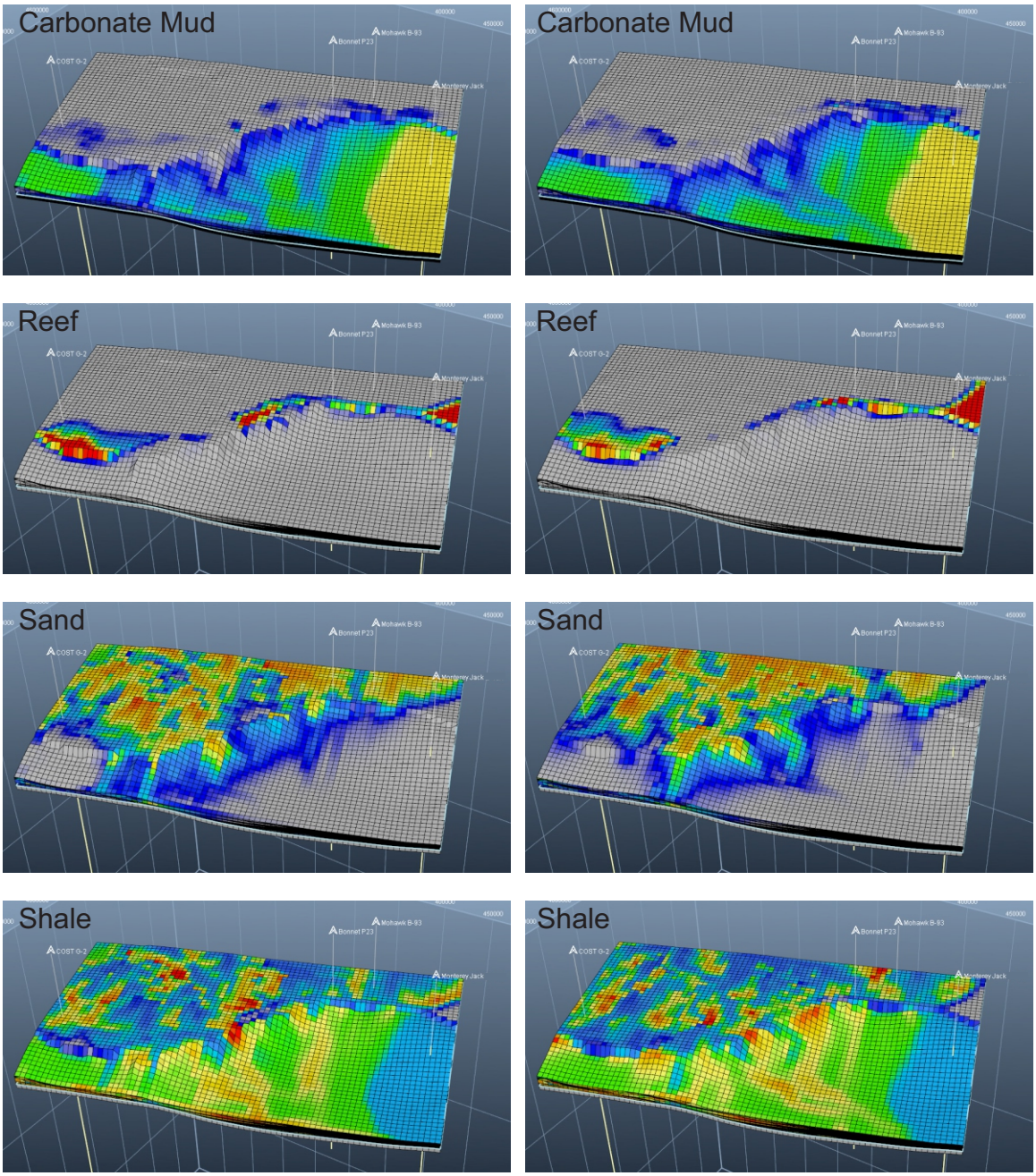

Figure 3.5: Sediment distribution maps. Vertical Exaggeration = 40x.

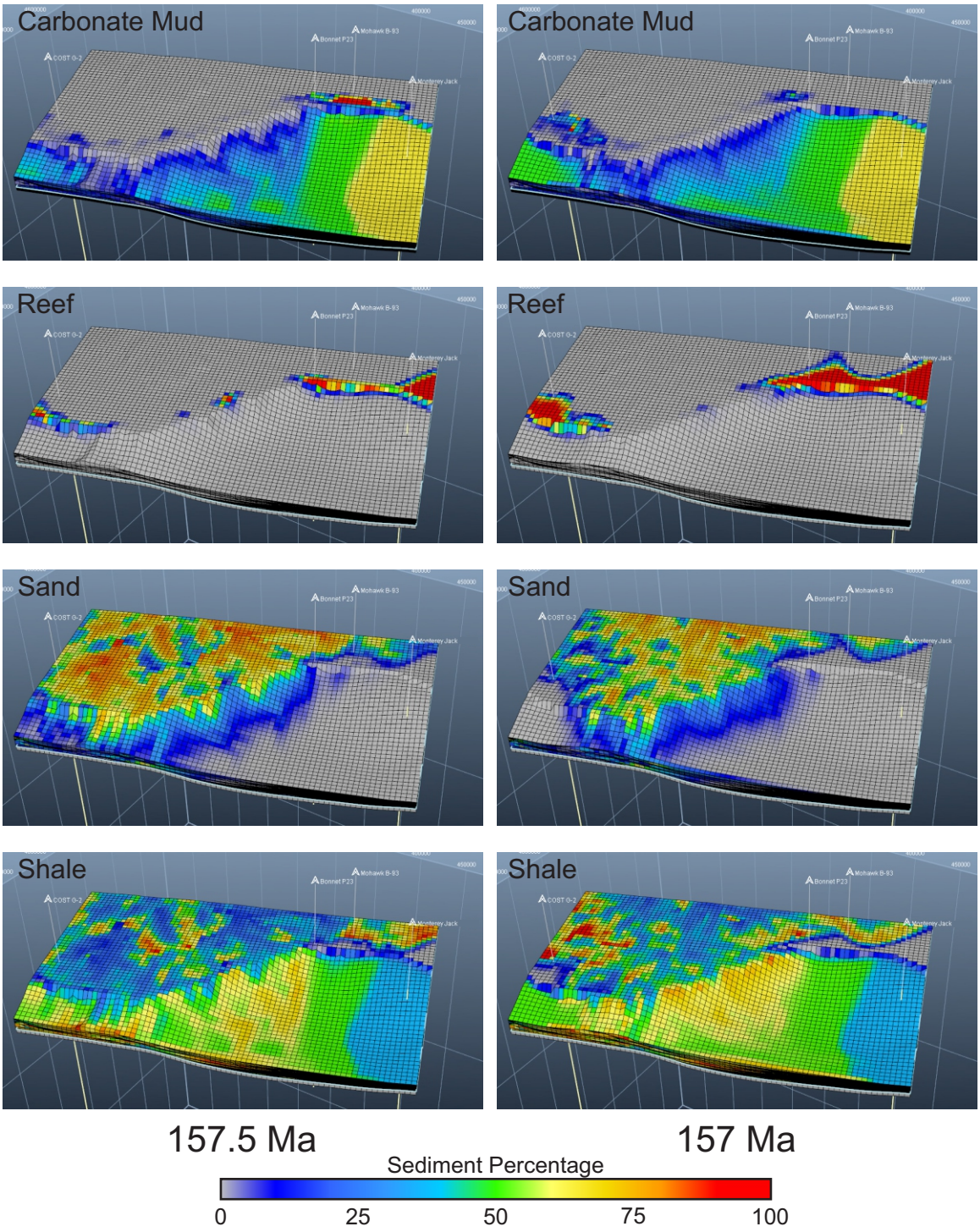

Figure 3.6: Sediment distribution maps. Vertical Exaggeration = 40x.

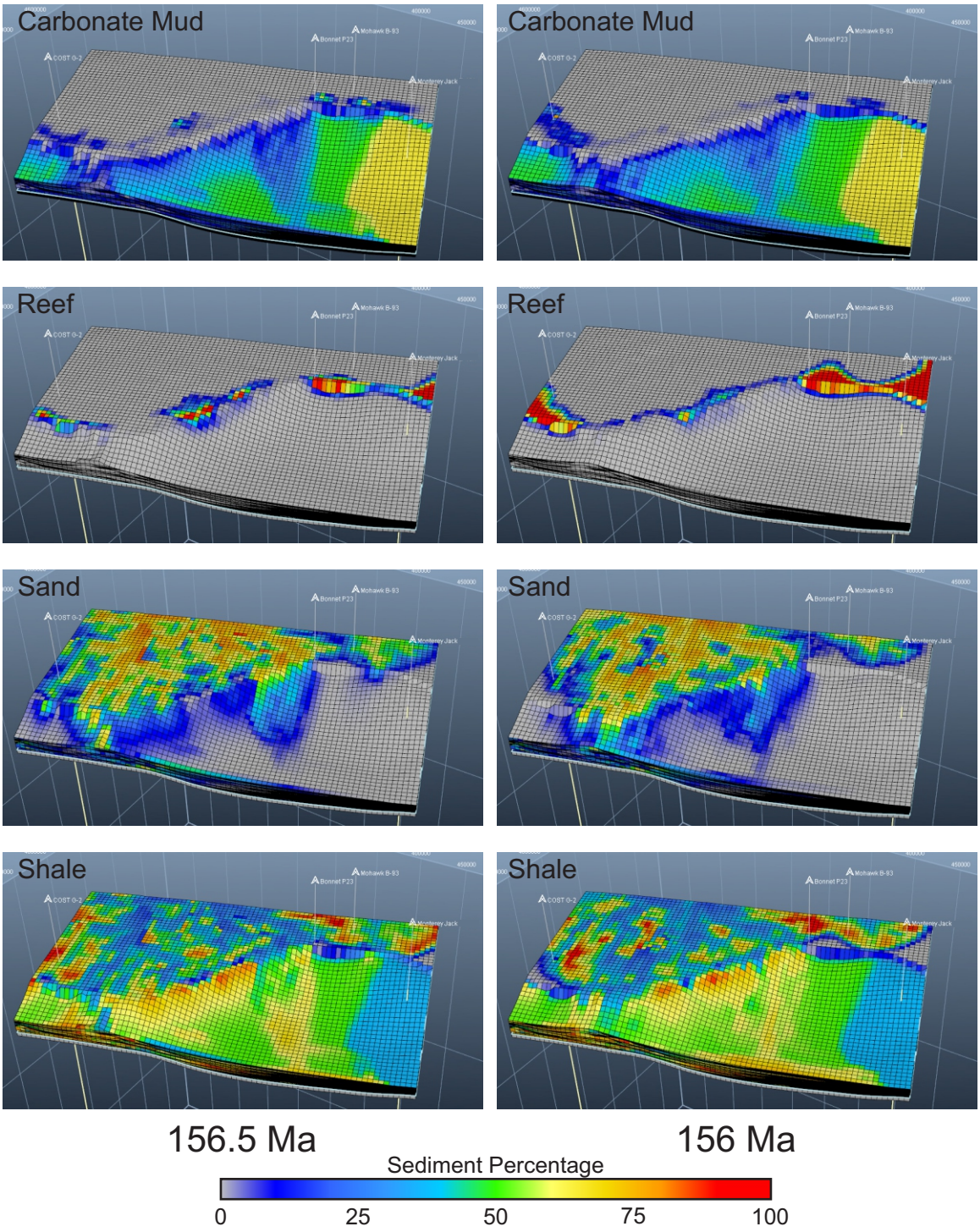

Figure 3.7: Sediment distribution maps. Vertical Exaggeration = 40x.

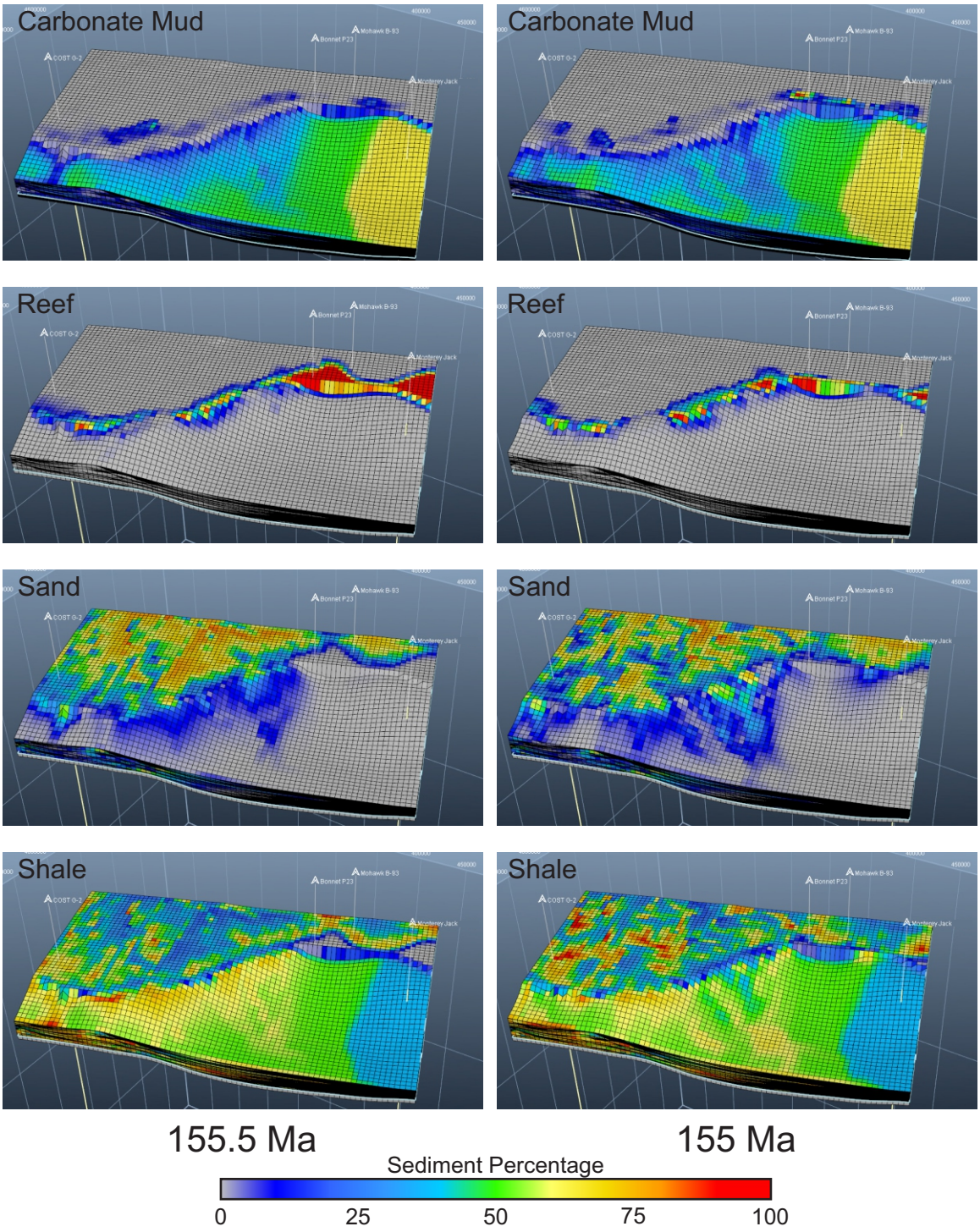

Figure 3.8: Sediment distribution maps. Vertical Exaggeration = 40x.

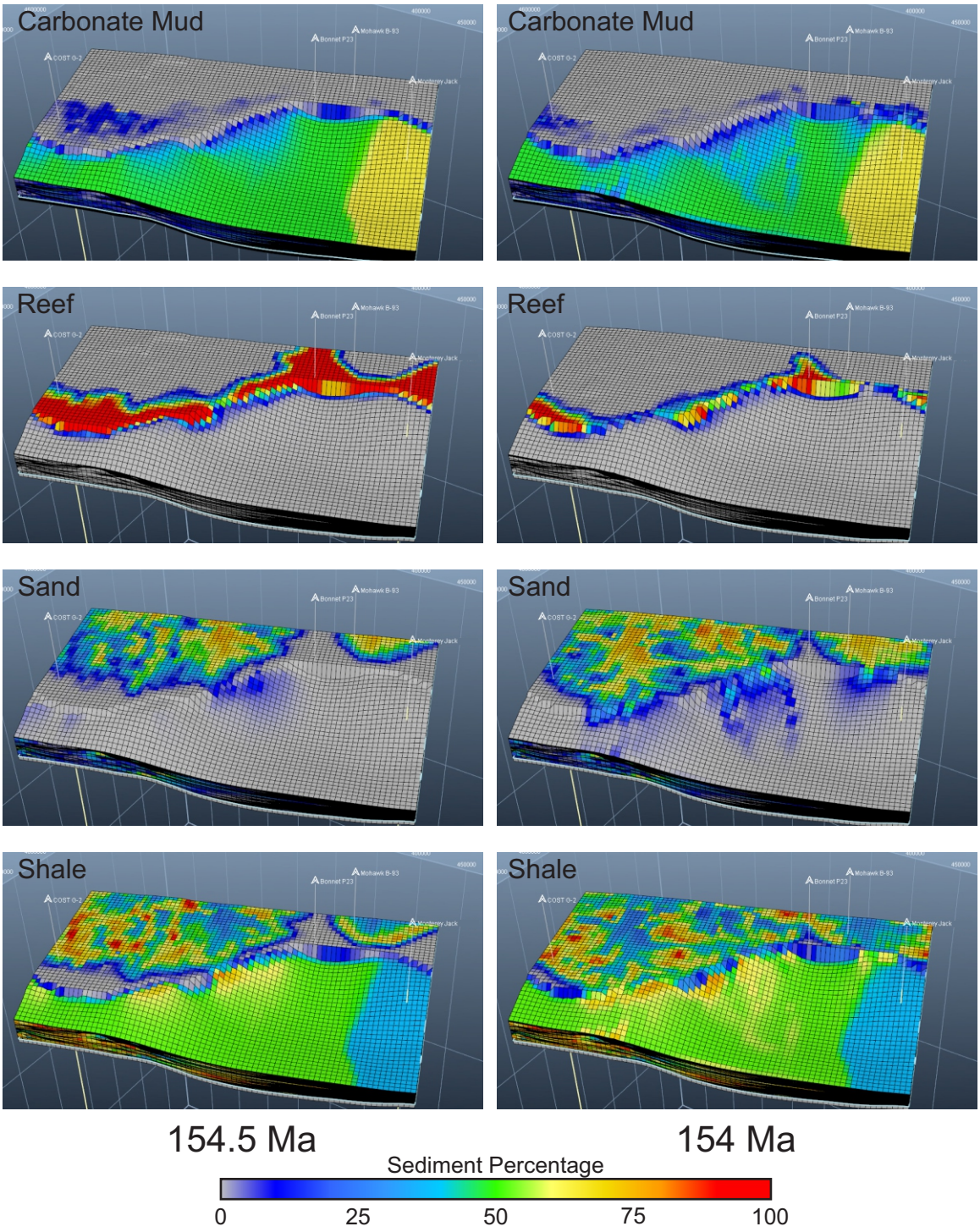

Figure 3.9: Sediment distribution maps. Vertical Exaggeration = 40x.

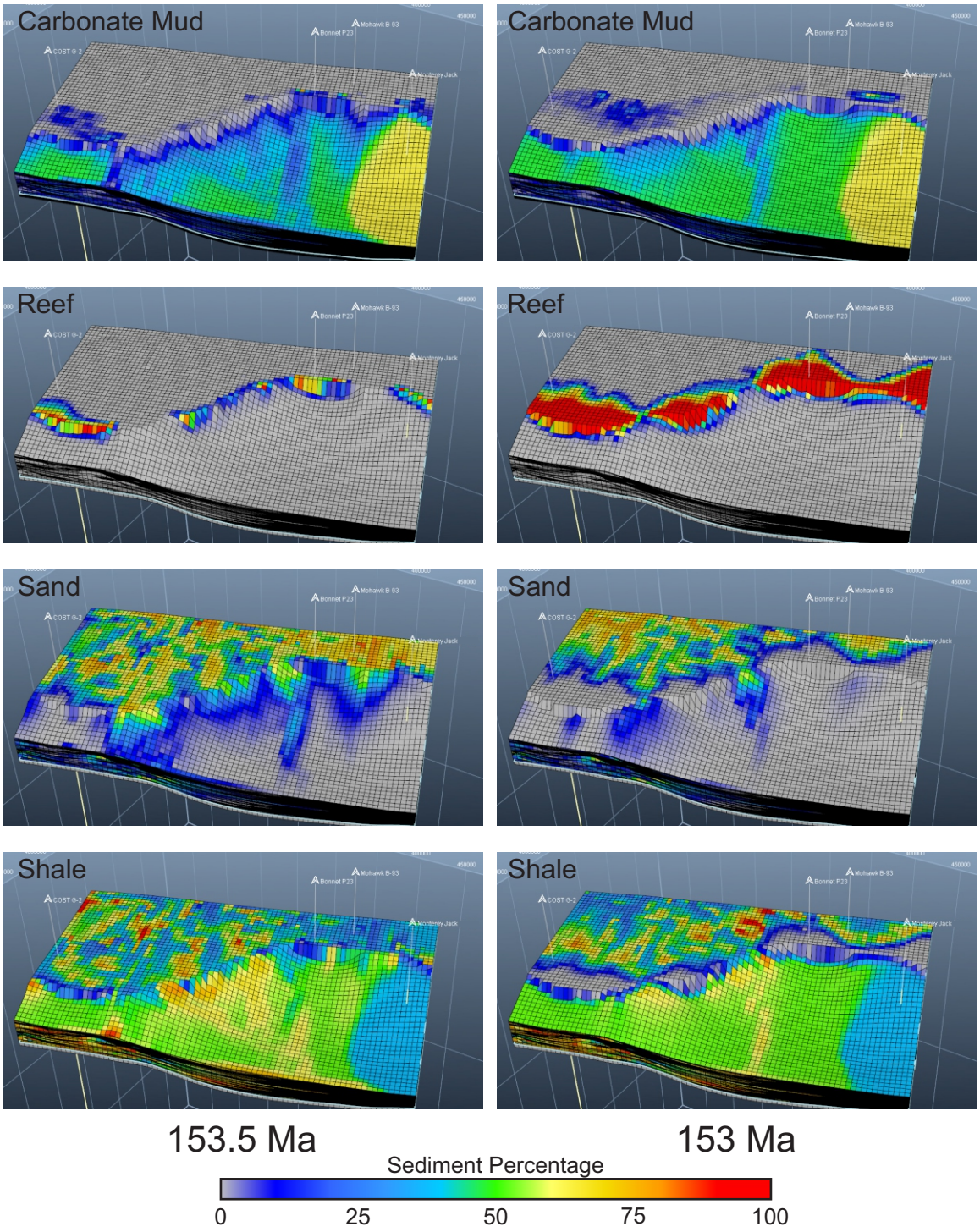

Figure 3.10: Sediment distribution maps. Vertical Exaggeration = 40x.

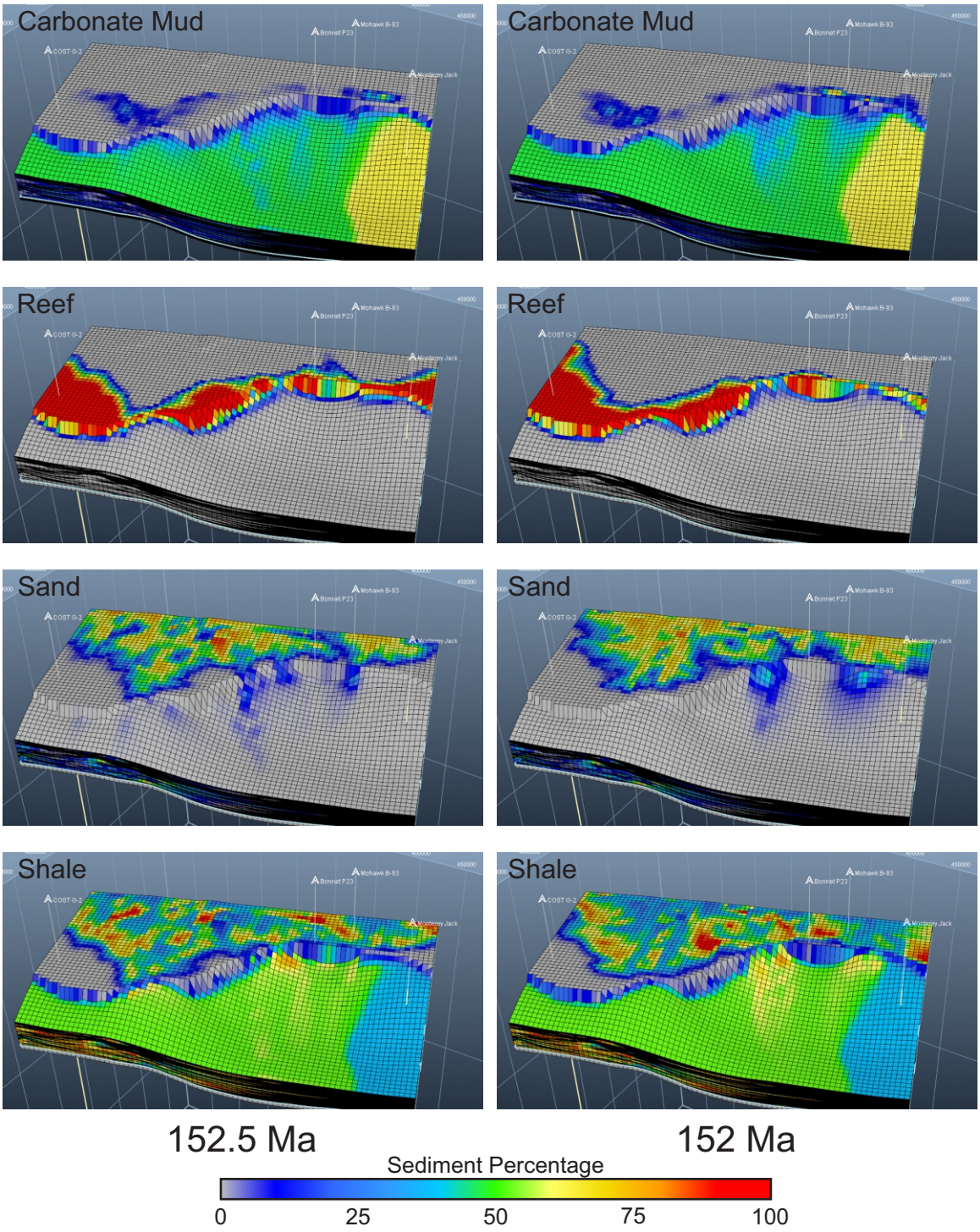

Figure 3.11: Sediment distribution maps. Vertical Exaggeration = 40x.

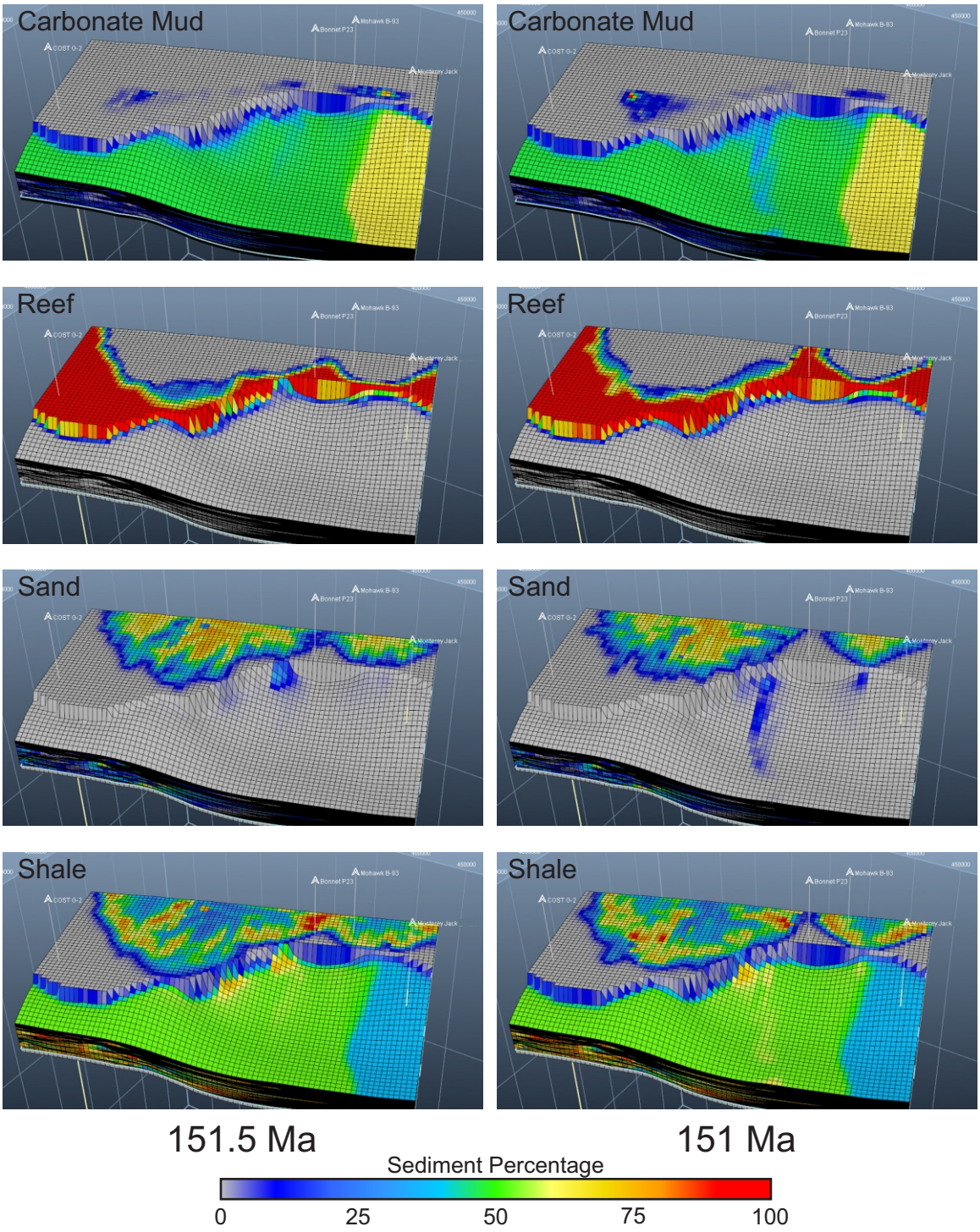

Figure 3.12: Sediment distribution maps. Vertical Exaggeration = 40x.

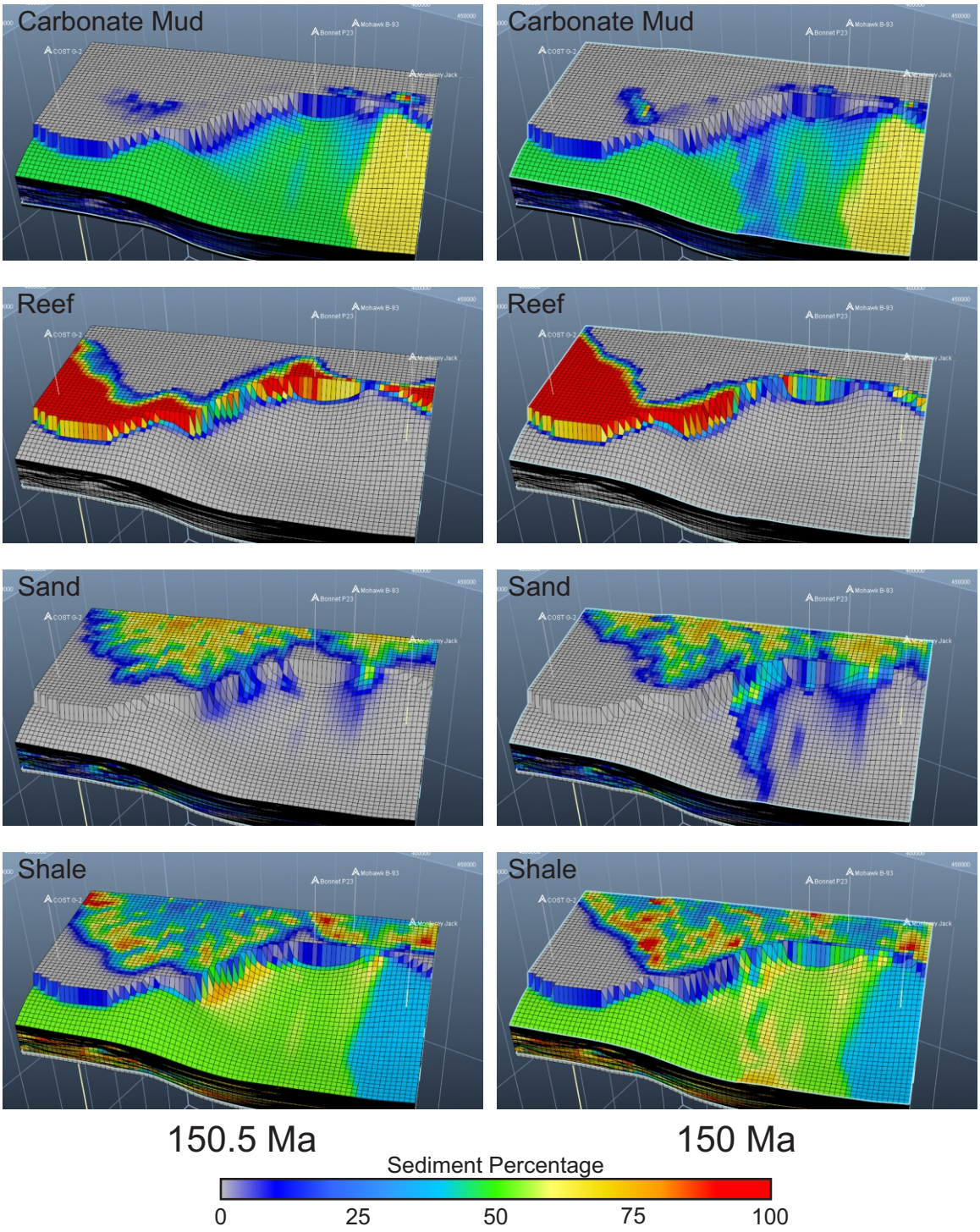

Figure 3.13: Sediment distribution maps. Vertical Exaggeration = 40x.

Facies and sedimentation rate maps

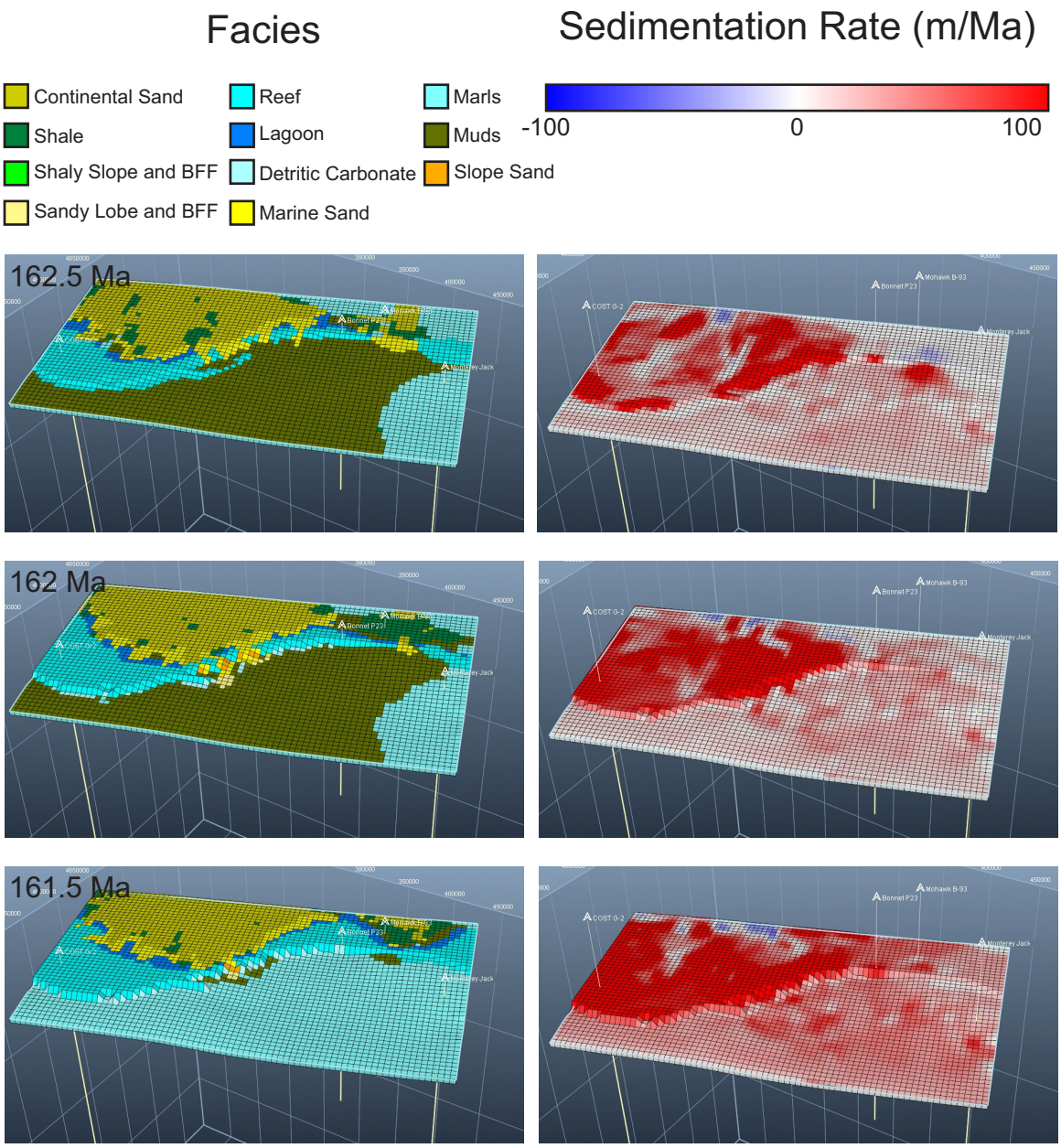

Figure 3.14: Facies distribution maps and sedimentation rates. Vertical exaggeration = 40x.

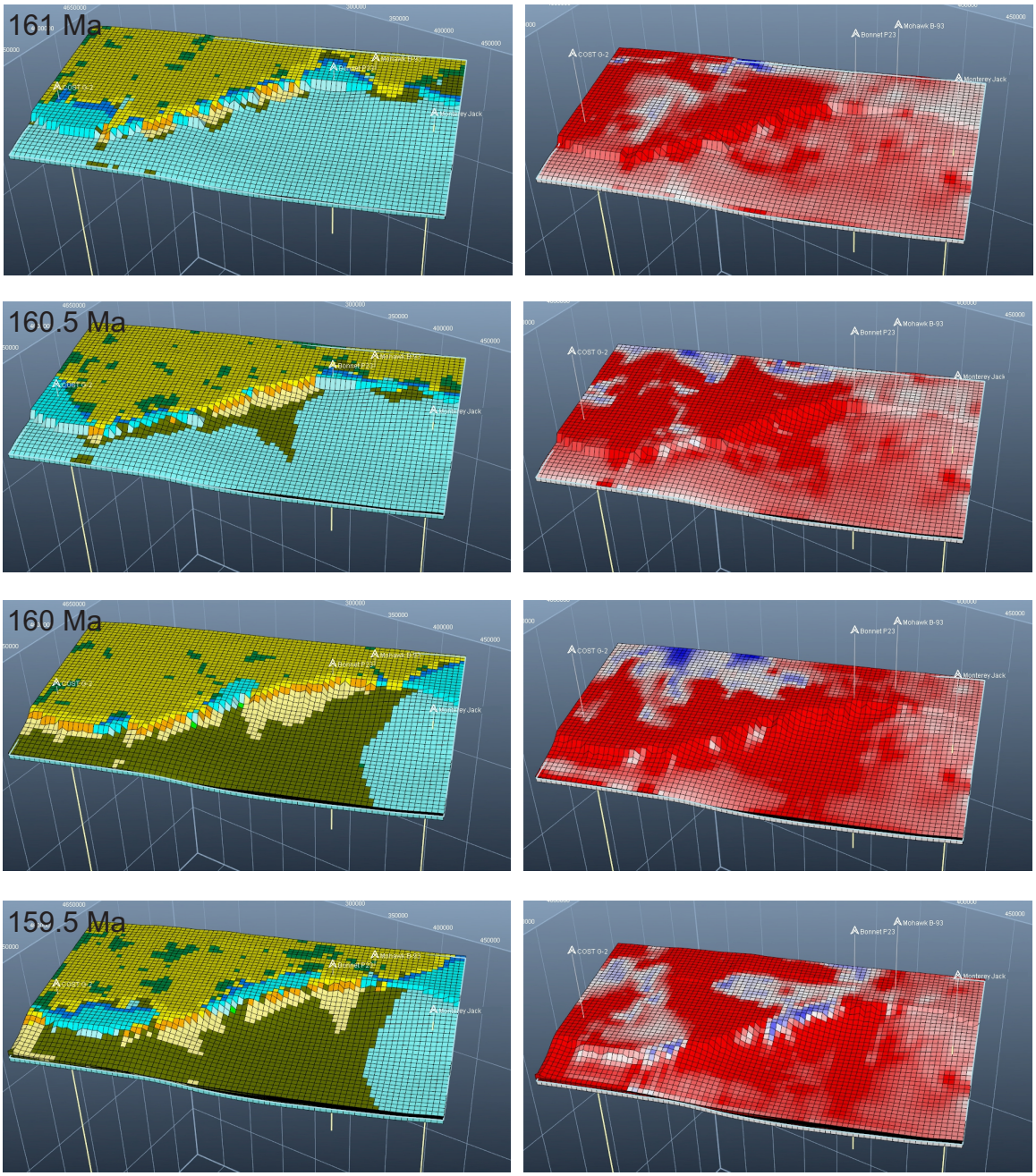

Figure 3.15: Facies distribution maps and sedimentation rates. Vertical exaggeration = 40x.

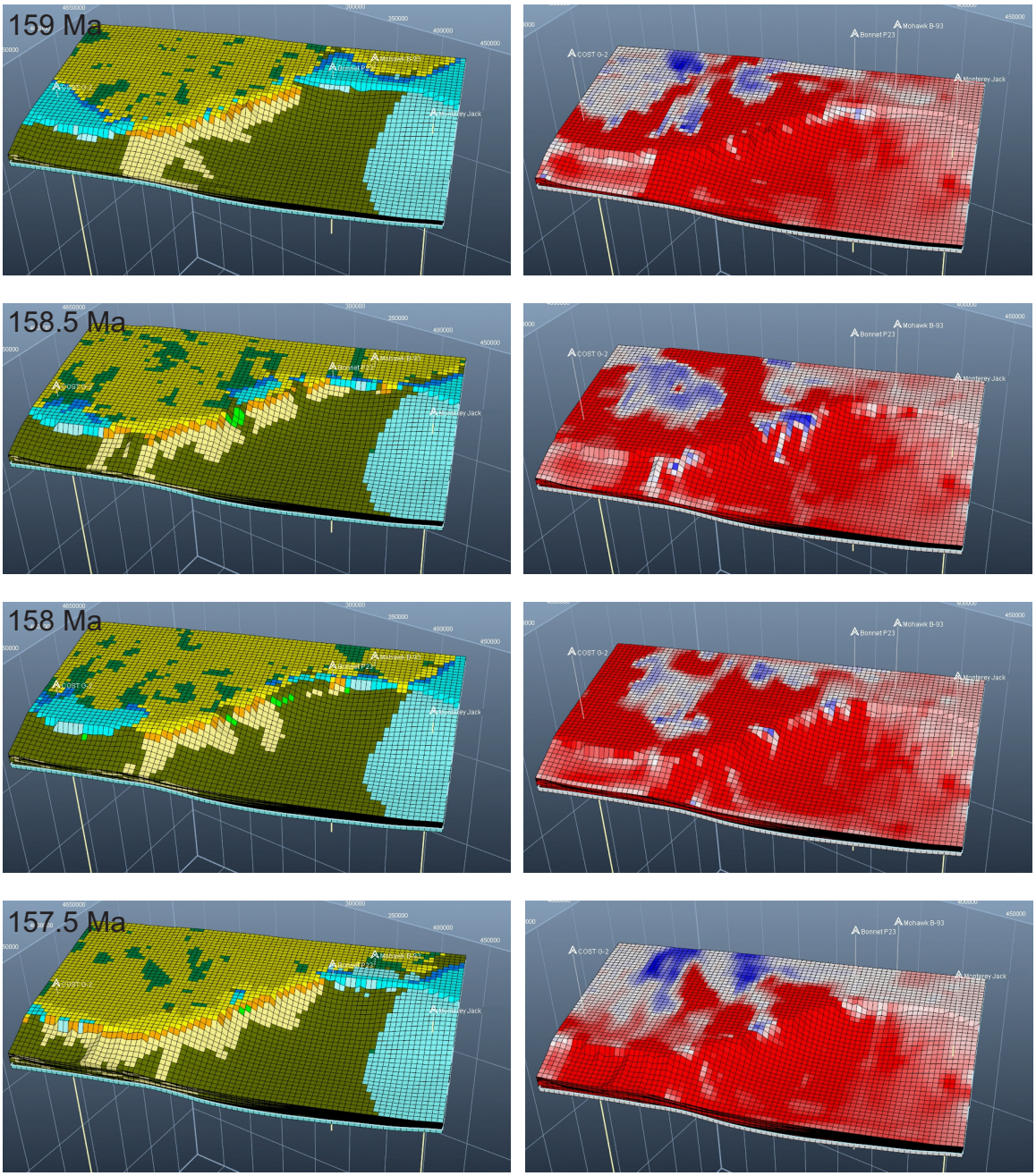

Figure 3.16: Facies distribution maps and sedimentation rates. Vertical exaggeration = 40x.

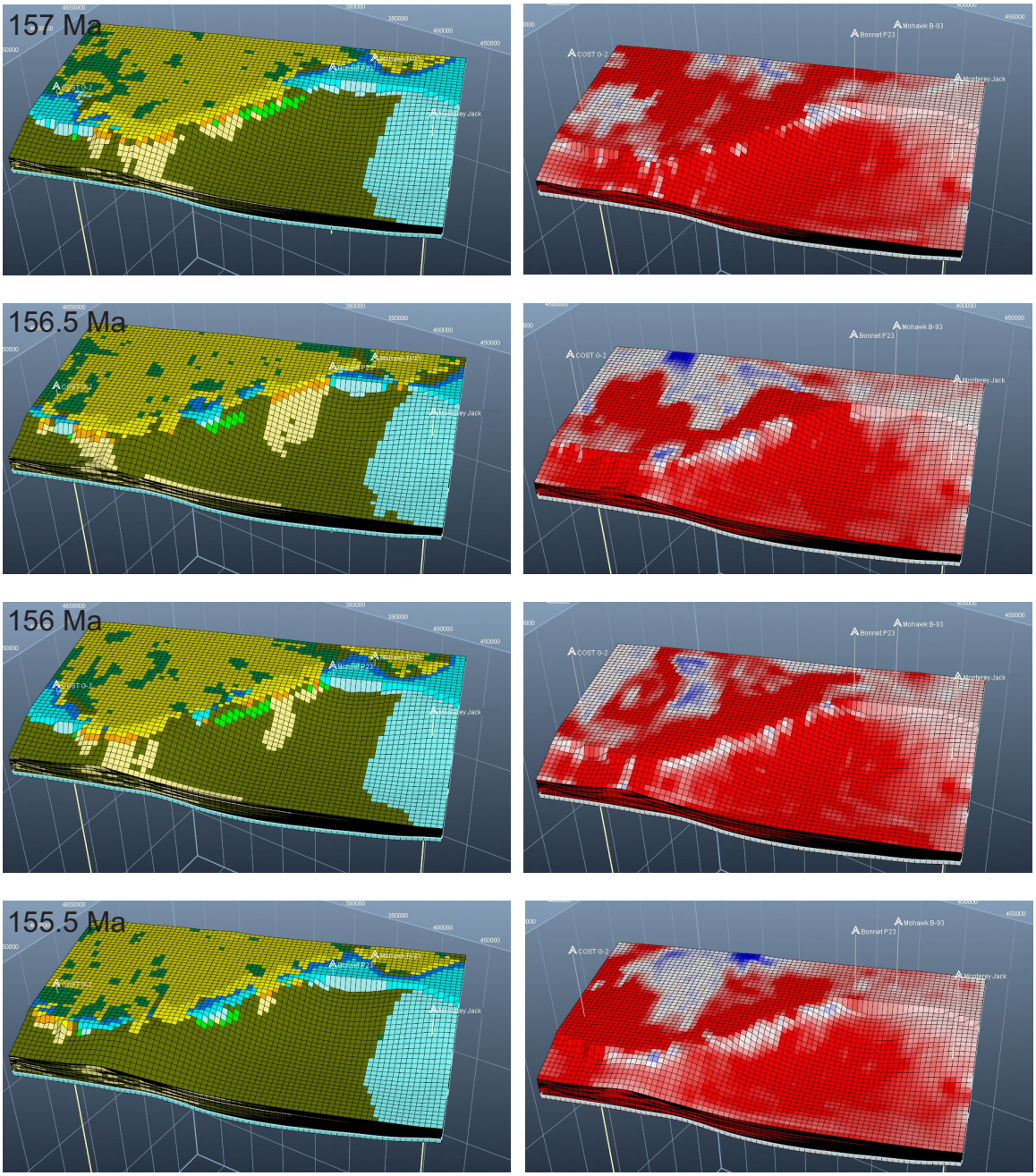

Figure 3.17: Facies distribution maps and sedimentation rates. Vertical exaggeration = 40x.

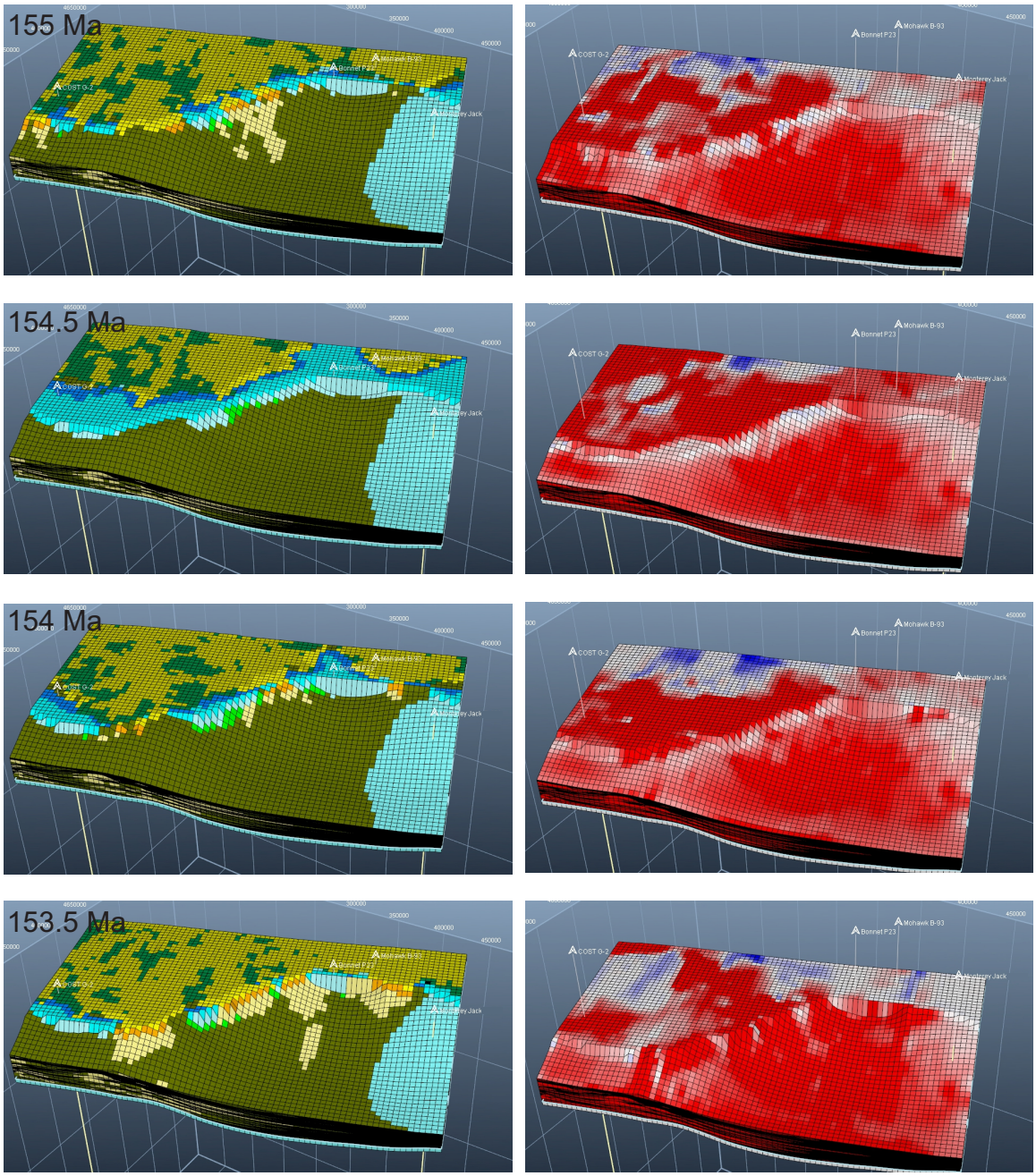

Figure 3.18: Facies distribution maps and sedimentation rates. Vertical exaggeration = 40x.

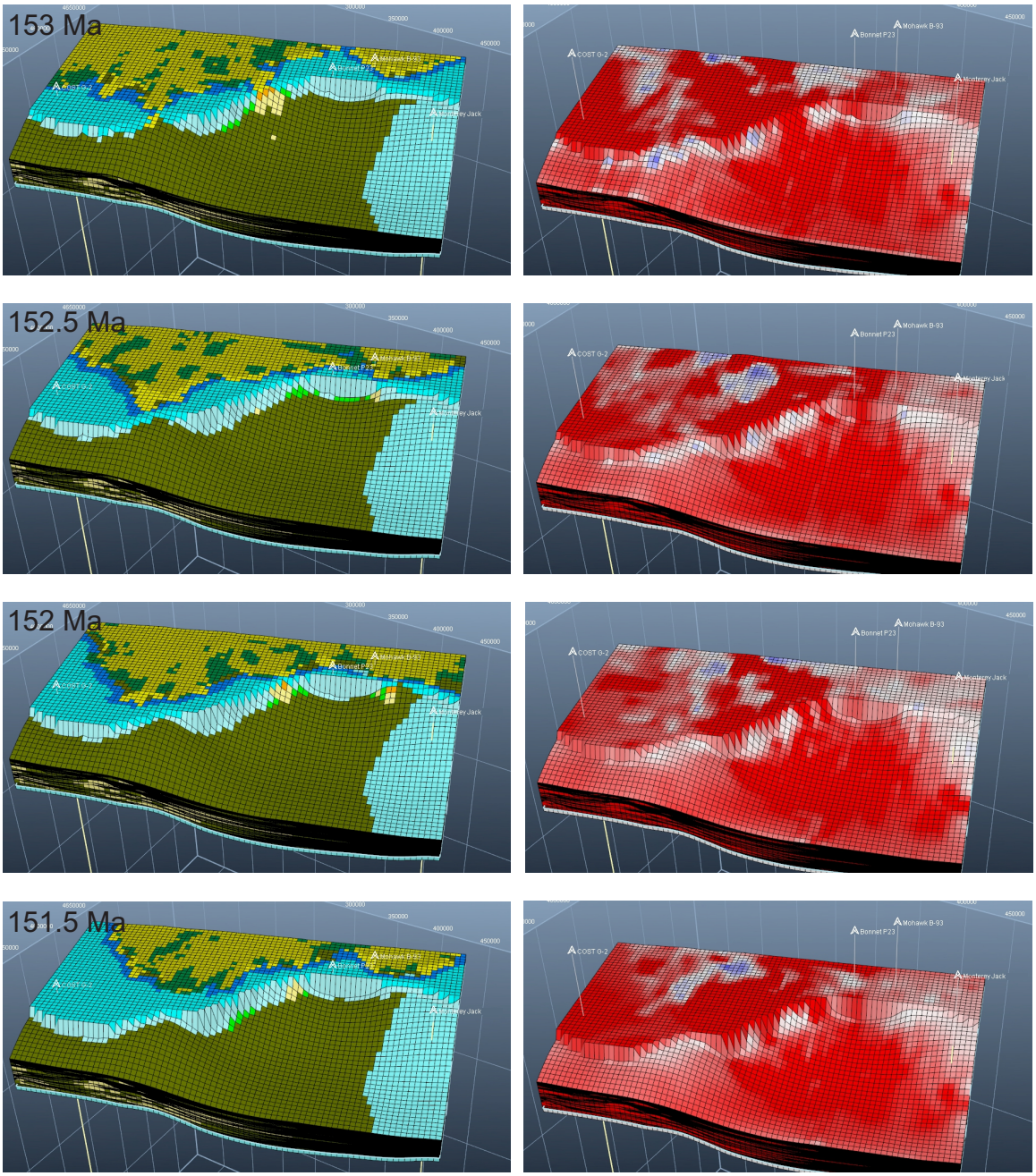

Figure 3.19: Facies distribution maps and sedimentation rates. Vertical exaggeration = 40x.

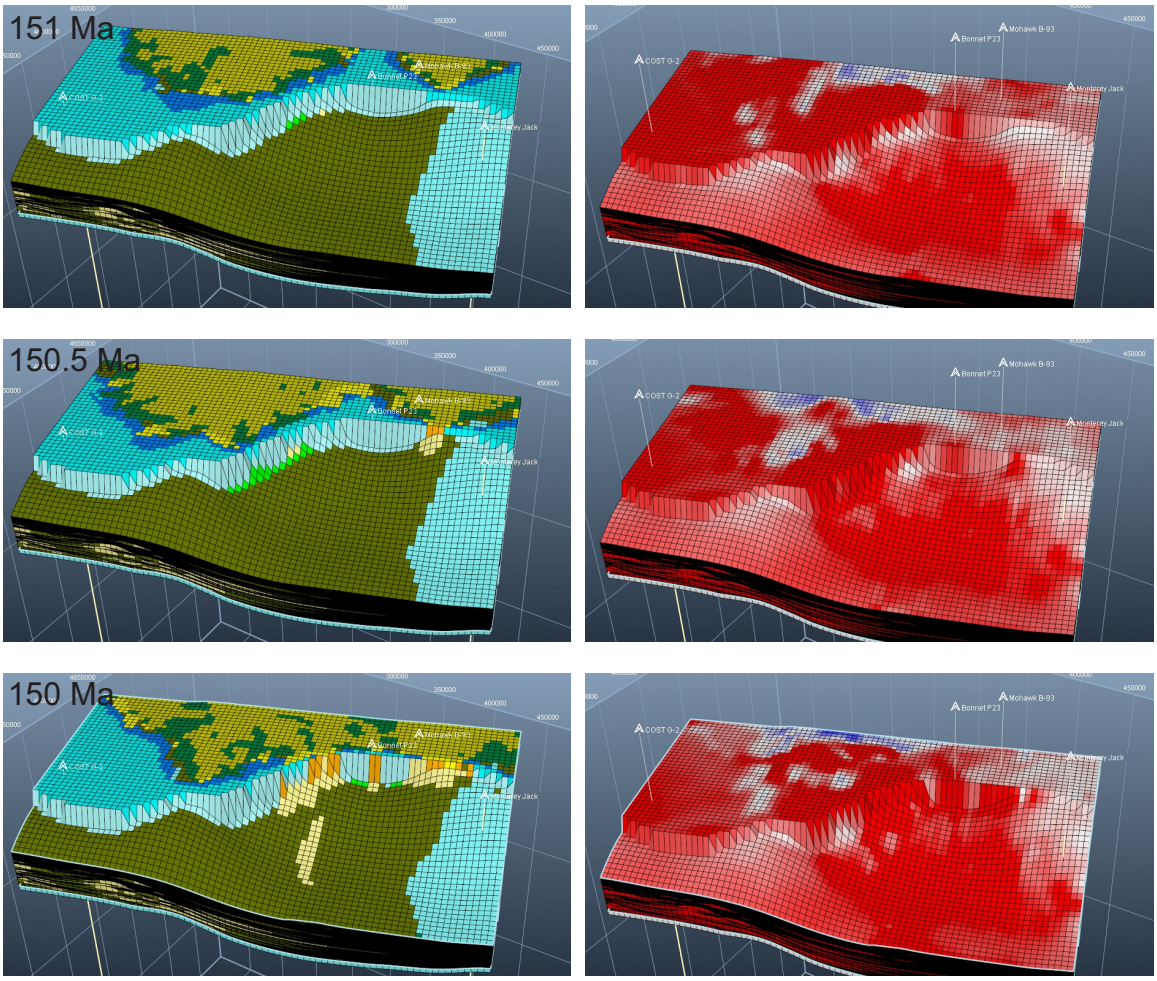

Figure 3.20: Facies distribution maps and sedimentation rates. Vertical exaggeration = 40x.

Appendix 4: Chapter 4 Supplementary Appendices

Supplementary Table S1: Lithofacies Classification Scheme used in the Models.

Facies	Slope Min	Slope Max	Carbonate Mud Min	Carbonate Mud Max	Bathymetry Min	Bathymetry Max	Water Discharge Min	Water Discharge Max	Sand Min	Sand Max	Reef Min	Reef Max	Shale Min	Shale Max
Continental Sand					-1000	0			40	100				
Detrital Carbonate					100	4500					15	100		
Lagoon					0	10			0	30	1	50		
Marine Sandstones					0	250			30	100				
Marls			35	100	0	4500							0	48
Muds			0	51.9	0	4500							35	100
Reef					-100	200					30	100		
Sand Lobe and BFF	0	50			140	4500			20	100				
Shale					-1000	4500							30	100
Shaly Slope and BFF	20	1000			100	4500	0	200					50	100
Slope Sands	10	1000			50	4500			27	100				

Supplementary Table S2: Estimated Water Discharge and Sediment Load Values for the River Systems from Figure 4.

Source River	Source Area	Area (km^2)	Uplift (km)	Water Discharge (m^3/s)			Sediment Load (km^3/Ma)
				Max	Min	Avg.	
Bay of Fundy Area	Appalachians + Maritimes Basin	151100	1?	3900	225	2062.5	1070
Maine	Appalachians	97650	1.3	2872	183	1527.5	1353
	Coastal Maine	17410	0.5?	1127	65	596	284
	White Mountains	3200	3	361	11	186	2348
Meguma Terrane	Inner Shelf and Onshore Nova Scotia and shear zones	55200	0.25	2000	145	1072.5	417

Supplementary Table S3: Uncertain Parameters used for CougarFlow Analysis.

Uncertain Parameters	Minimum Value	Maximum Value
Initial Bathymetry	32%	-
Bay of Fundy Water Discharge	-20%	50%
Maine Water Discharge	-20%	50%
Meguma Water Discharge	-20%	50%
Bay of Fundy Source Location	-30km	+30km
Maine Source Location	-30km	+30km
Meguma Source Location	-30km	+30km
Bay of Fundy Sediment Proportion	-20%	20%
Maine Sediment Proportion	-20%	20%
Meguma Sediment Proportion	-20%	20%
Production vs Time	-20%	20%
Sand Kcontinental	20	2000
Sand Kmarine	0.05	5
HEST/LELT ratio	1.6	10
Eustasy Curve	-20%	20%

Supplementary Table S4: Calibration Indicator Percent for the Three Bathymetric Models.

Calibrated Models	COST G-2		Bonnet P-23		Mohawk B-93		Monterey Jack E-43A		Total Well Thickness	Total Facies	Total Well (thickness + facies)	Thickness Map
	Thickness	Facies	Thickness	Facies	Thickness	Facies	Thickness	Facies				
Shallow Ramp (Ref)	99.34	67.26	99.02	82.18	95.22	74.88	99.4	87.47	98.87	76.23	87.55	97.67
Model B	99.37	70	99.84	88.24	96.16	75.48	99.3	87.46	99.28	79.8	89.54	97.78
Model C	99.39	68.6	99.28	88.24	96.22	75.24	89.66	87.41	97.94	79.21	88.58	98

Supplementary Table S5: Sediment Supply values for the reference case model.

Source		Phase 1 (163-161 Ma)					Phase 2 (161-153.1 Ma)											Phase 3 (153.1-150 Ma)				
Age (Ma)		**163**	**162**	**161.5**	**161.4**	**161.3**	**161**	**160**	**159**	**158**	**157.8**	**157**	**156.5**	**156**	**155**	**154**	**153.3**	**153.1**	**153**	**152**	**151**	**150**
Maine	Supply (km^3/Ma)	900	700	1100	1100	1400	2400	3100	2300	2600	2300	2600	2300	2300	2500	2300	2350	1800	1000	350	350	150
	Fluvial Discharge (m^3/s)	1300	1300	2000	1600	1900	3300	4400	4400	4800	4800	5300	4400	4400	3500	3000	3100	2500	1500	400	400	400
	Sand (%)	56.8	58.89	58	58.54	58.48	57.78	55.17	51.2	49.8	49.7	49.52	49.38	49.24	40	40	45.67	45.44	45.32	44.57	41.19	40.17
	Shale (%)	43.2	41.11	42	41.46	41.52	42.22	44.83	48.8	50.2	50.3	50.48	50.62	50.76	60	60	54.33	54.56	54.68	55.43	58.81	59.83
Bay of Fundy	Supply (km^3/Ma)	500	1500	1000	950	800	1500	3500	2500	2500	2000	2000	1600	1700	800	500	1250	1400	1500	1500	1800	2000
	Fluvial Discharge (m^3/s)	1500	2500	2000	1900	2000	3000	4000	3000	3500	2950	2500	2300	2500	2100	1500	2000	2400	2500	2500	2000	2800
	Sand (%)	56.8	58.89	58	58.54	58.48	57.78	55.17	51.2	49.8	49.7	49.52	49.38	49.24	48.89	46.48	45.67	45.44	45.32	44.57	41.19	40.17
	Shale (%)	43.2	41.11	42	41.46	41.52	42.22	44.83	48.8	50.2	50.3	50.48	50.62	50.76	51.11	53.52	54.33	54.56	54.68	55.43	58.81	59.83
Meguma	Supply (km^3/Ma)	50	200	250	200	200	250	250	200	200	50	100	150	150	200	300	300	260	250	200	300	350
	Fluvial Discharge (m^3/s)	200	400	400	250	500	300	500	400	500	300	550	300	200	400	400	475	490	500	600	500	550
	Sand (%)	30	20	30	35	40	57.78	55.17	51.2	49.8	40	40	40	45	48.89	46.48	45.67	45.44	45.32	44.57	41.19	40.17
	Shale (%)	70	80	70	65	60	42.22	44.83	48.8	50.2	60	60	60	55	51.11	53.52	54.33	54.56	54.68	55.43	58.81	59.83

Supplementary Table S6: Carbonate Production and Hemipelagic sedimentation rates for the reference case model.

Age (Ma)	**163**	**162.5**	**162**	**161.7**	**161.5**	**161.3**	**160.9**	**160**	**150**	**0**
Carbonate Mud (m/Ma)	0	10	10	30	35	40	45	35	40	18
Reef (m/Ma)	0	250	250	250	250	250	250	250	250	180
Hemipelagic Shale (m/Ma)	10	10	10	10	10	10	10	35	45	10

Supplementary Appendix S7: Well calibration for the three models

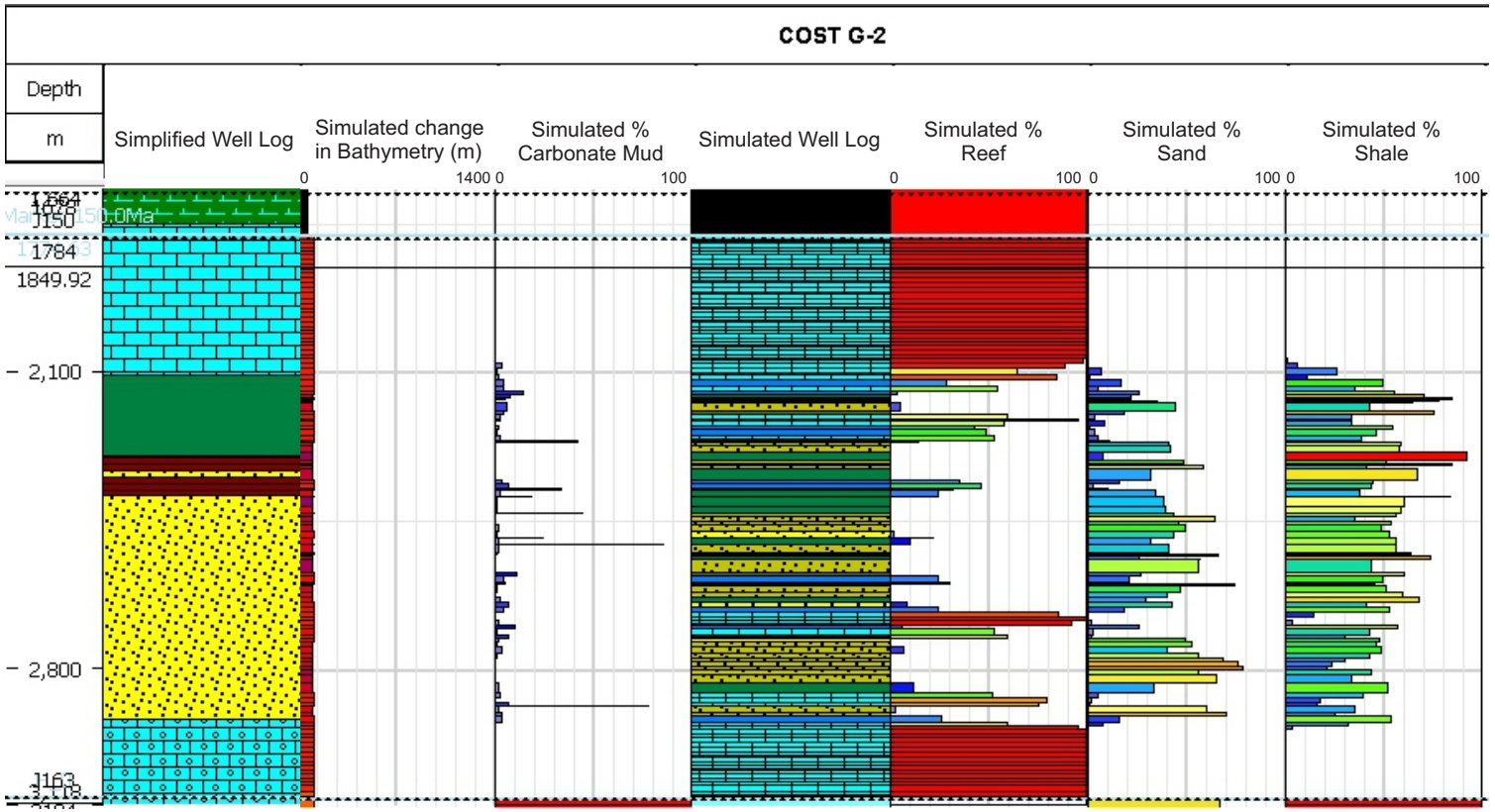

Figure S7.1: Shallow ramp reference case well calibration.

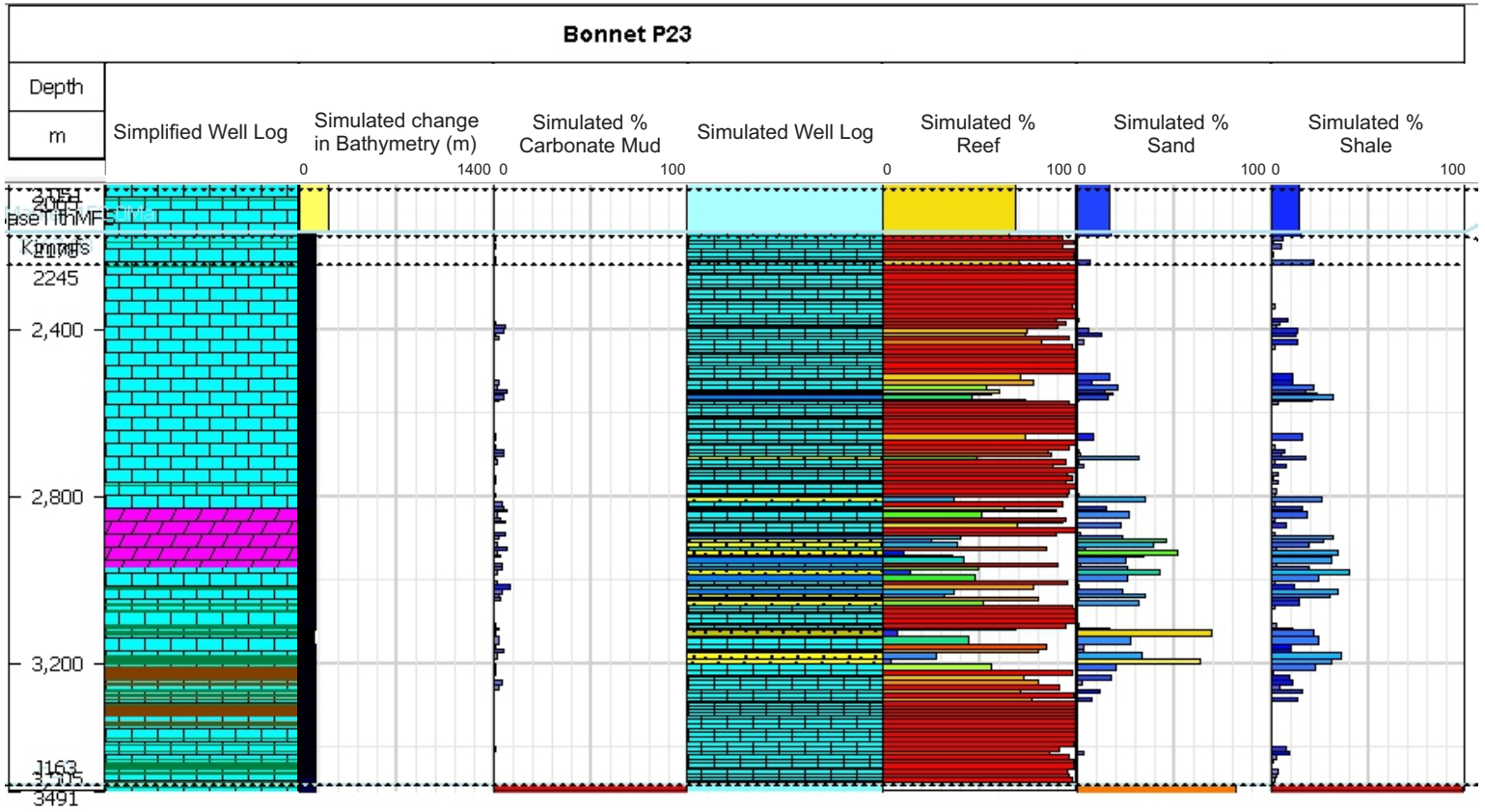

Figure S7.2: Shallow ramp reference case well calibration.

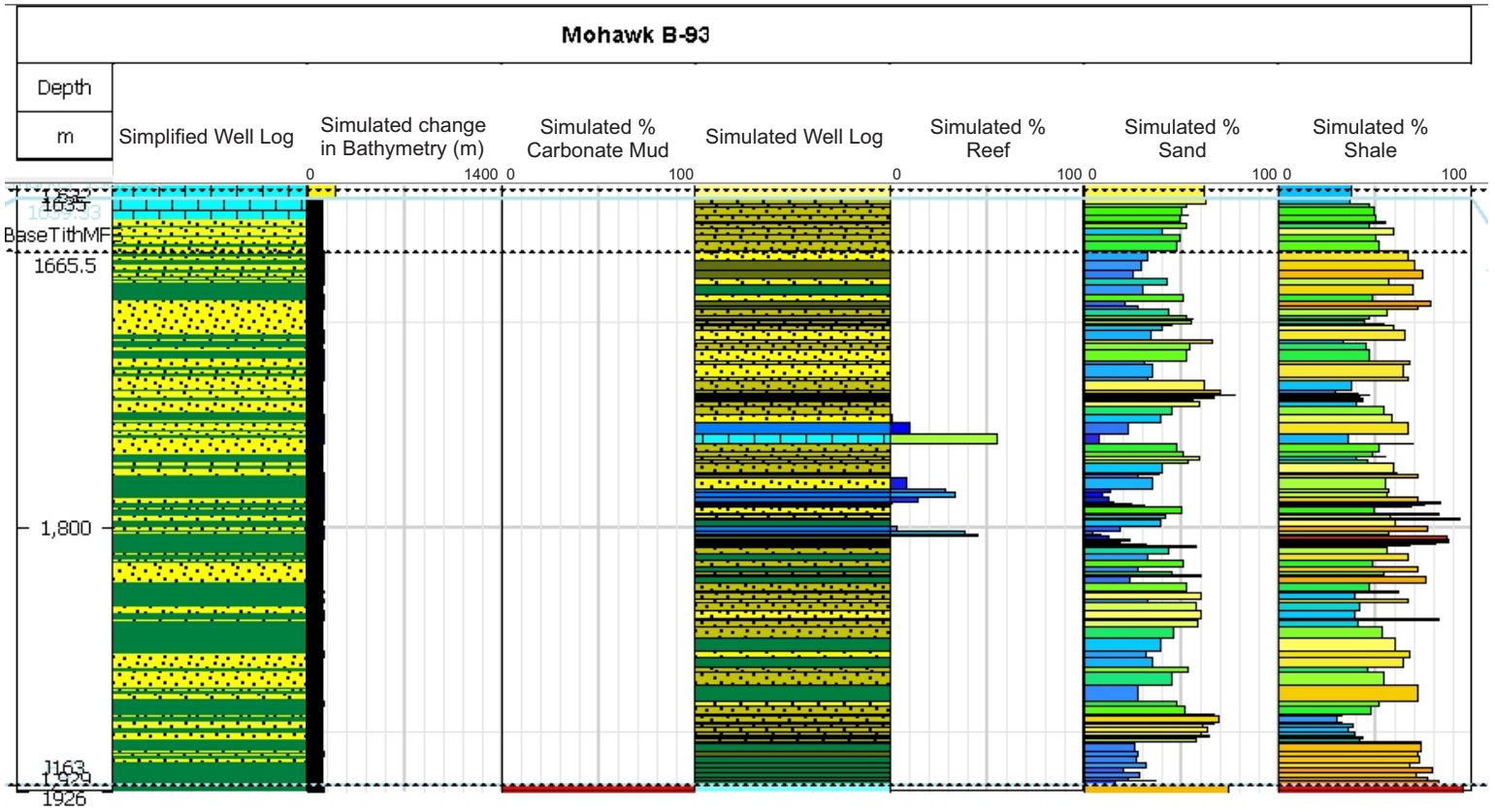

Figure S7.3: Shallow ramp reference case well calibration.

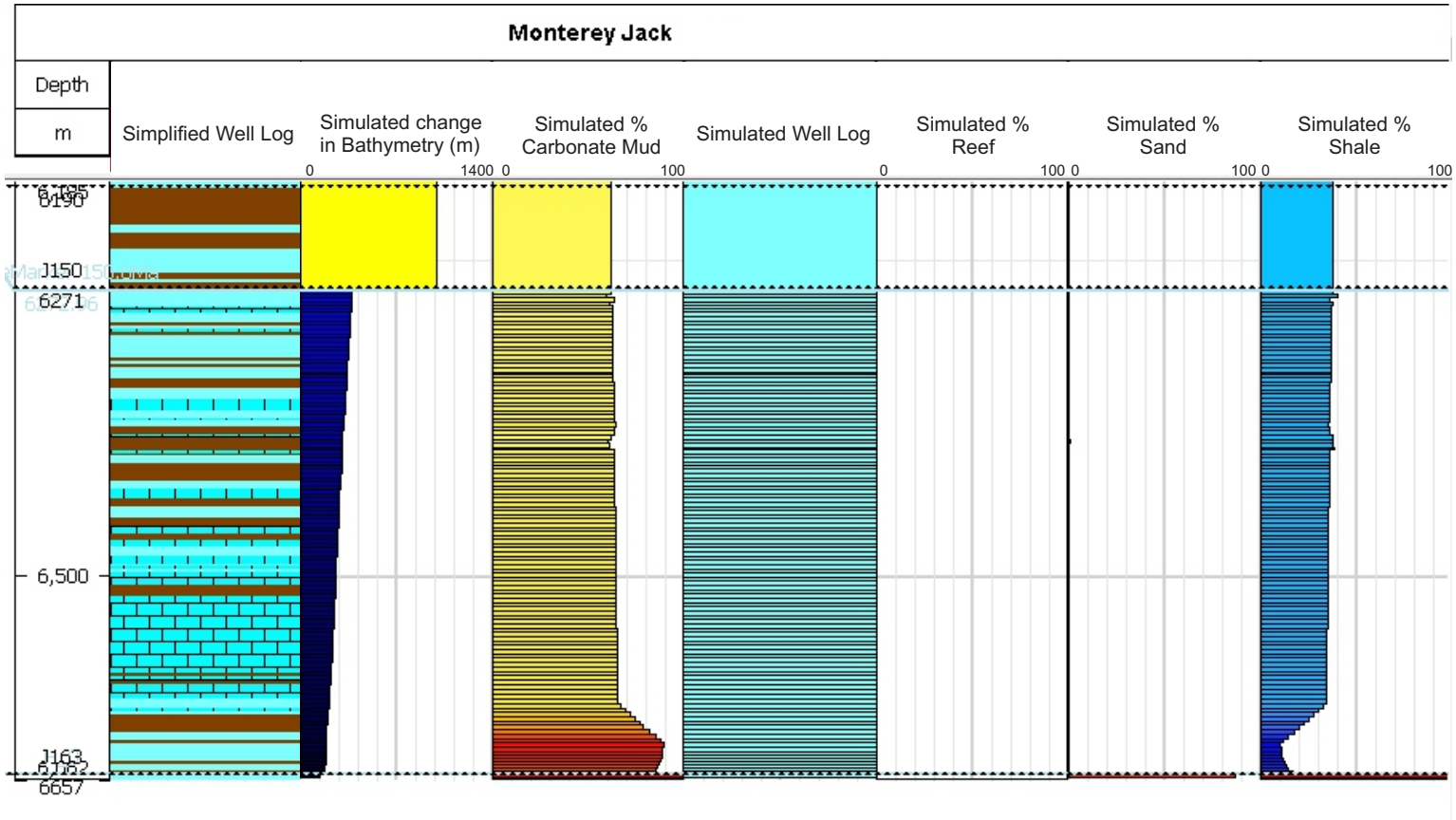

Figure S7.4: Shallow ramp reference case well calibration.

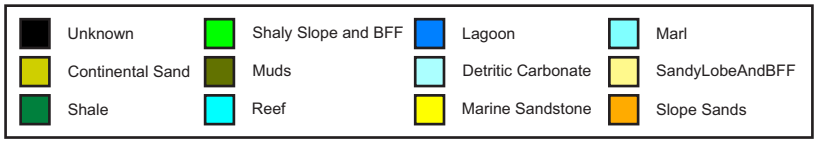

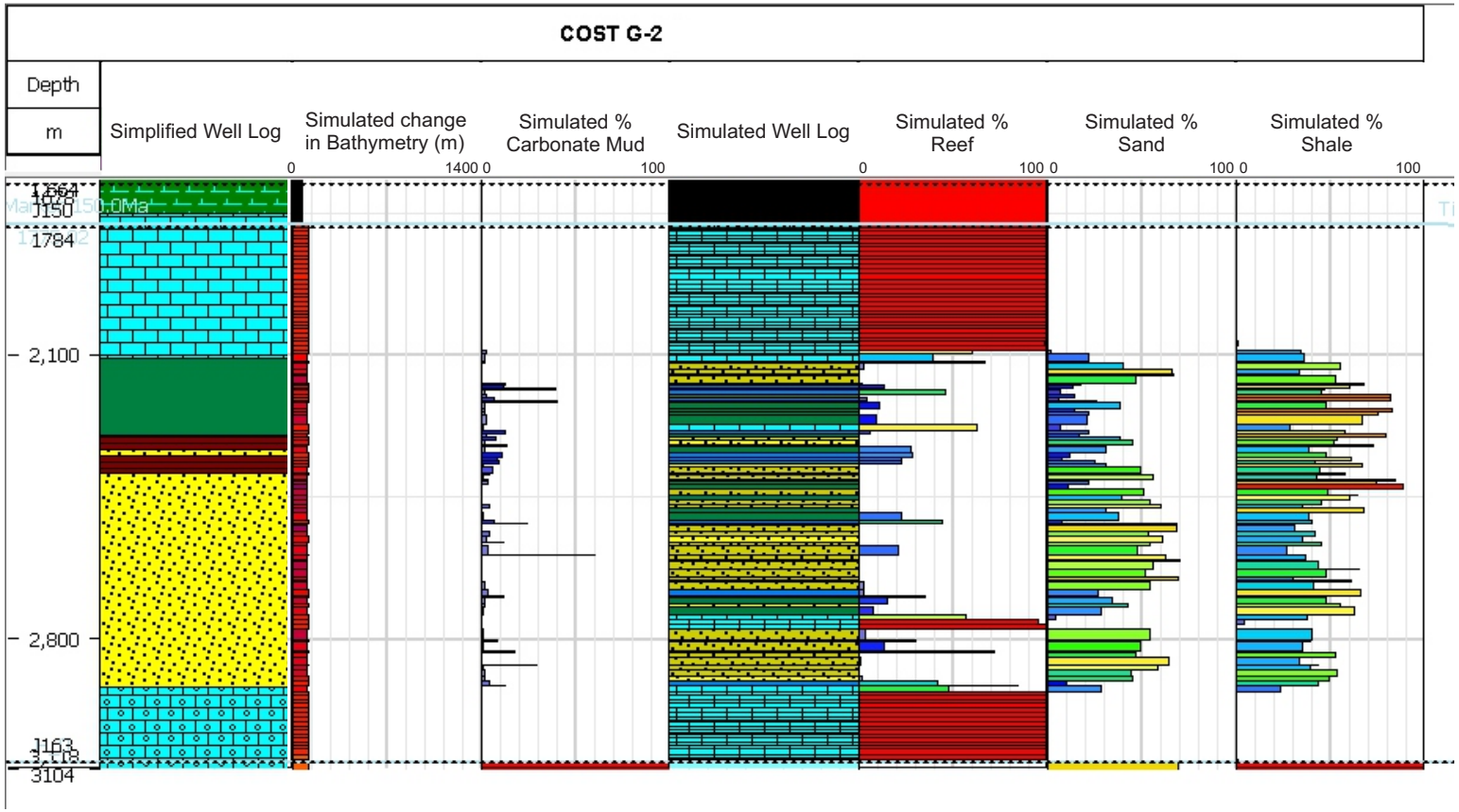

Figure S7.5: Model B (persistent reef) reference case well calibration.

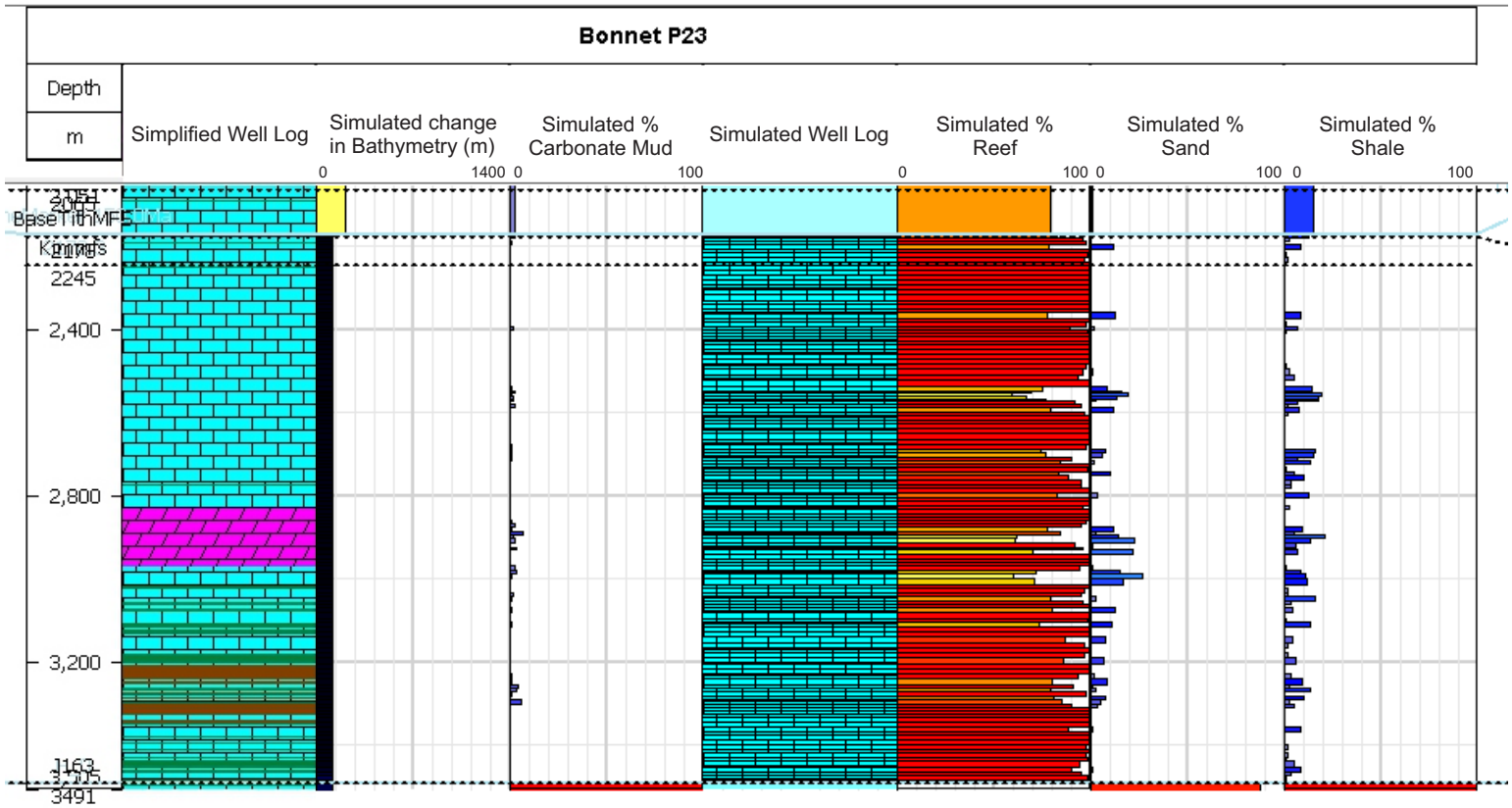

Figure S7.6: Model B (persistent reef) reference case well calibration.

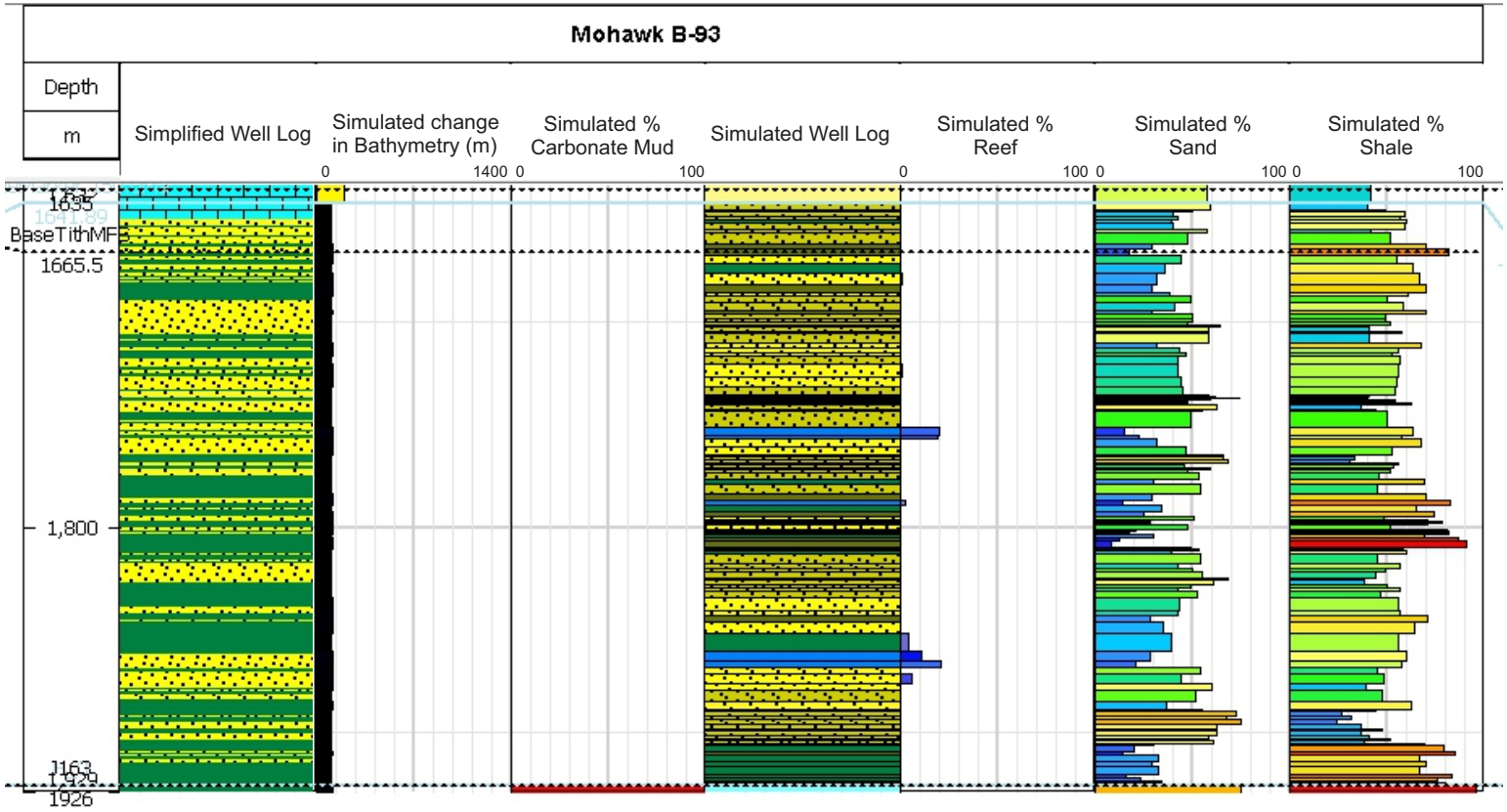

Figure S7.7: Model B (persistent reef) reference case well calibration.

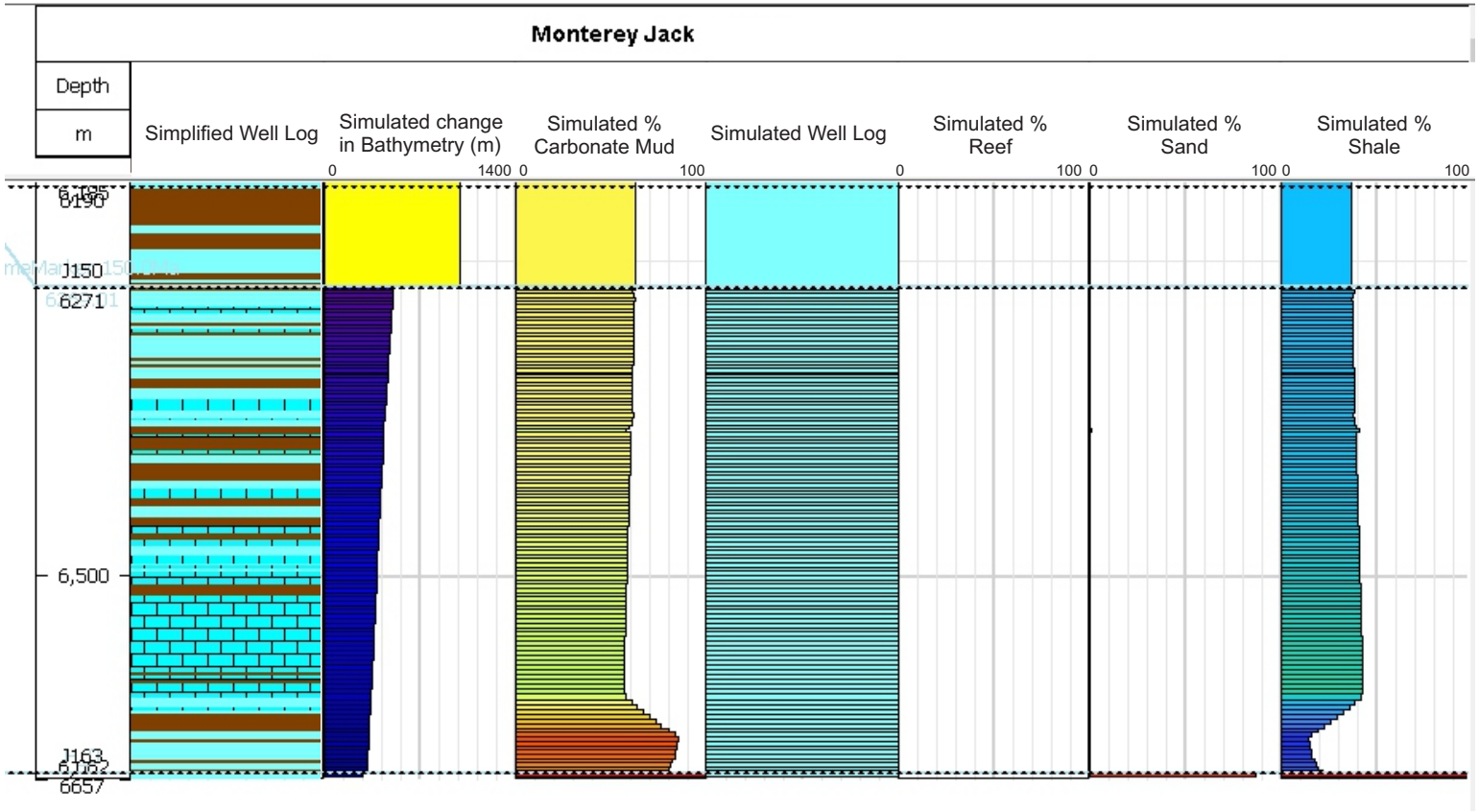

Figure S7.8: Model B (persistent reef) reference case well calibration.

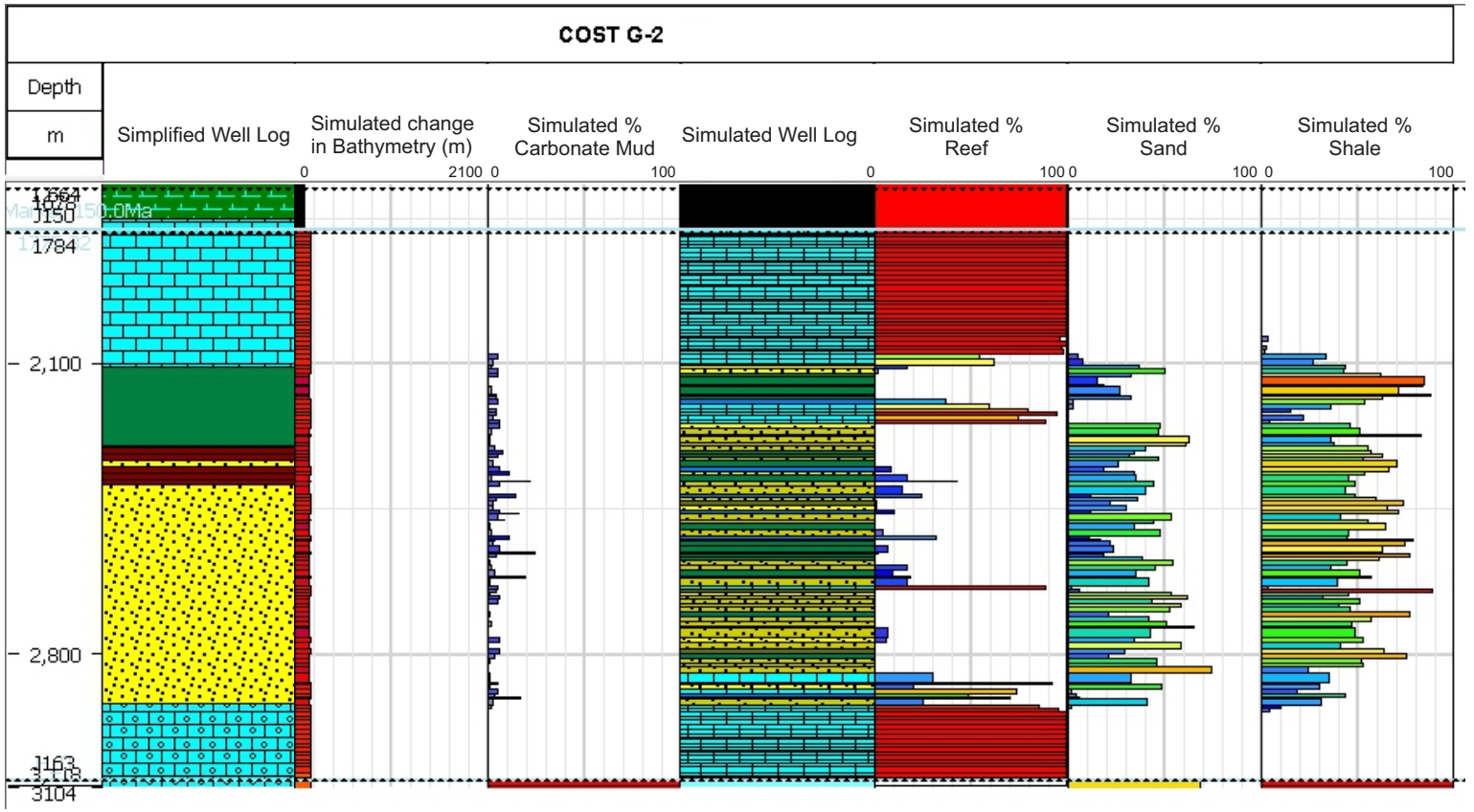

Figure S7.9: Model C (deep basin) reference case well calibration.

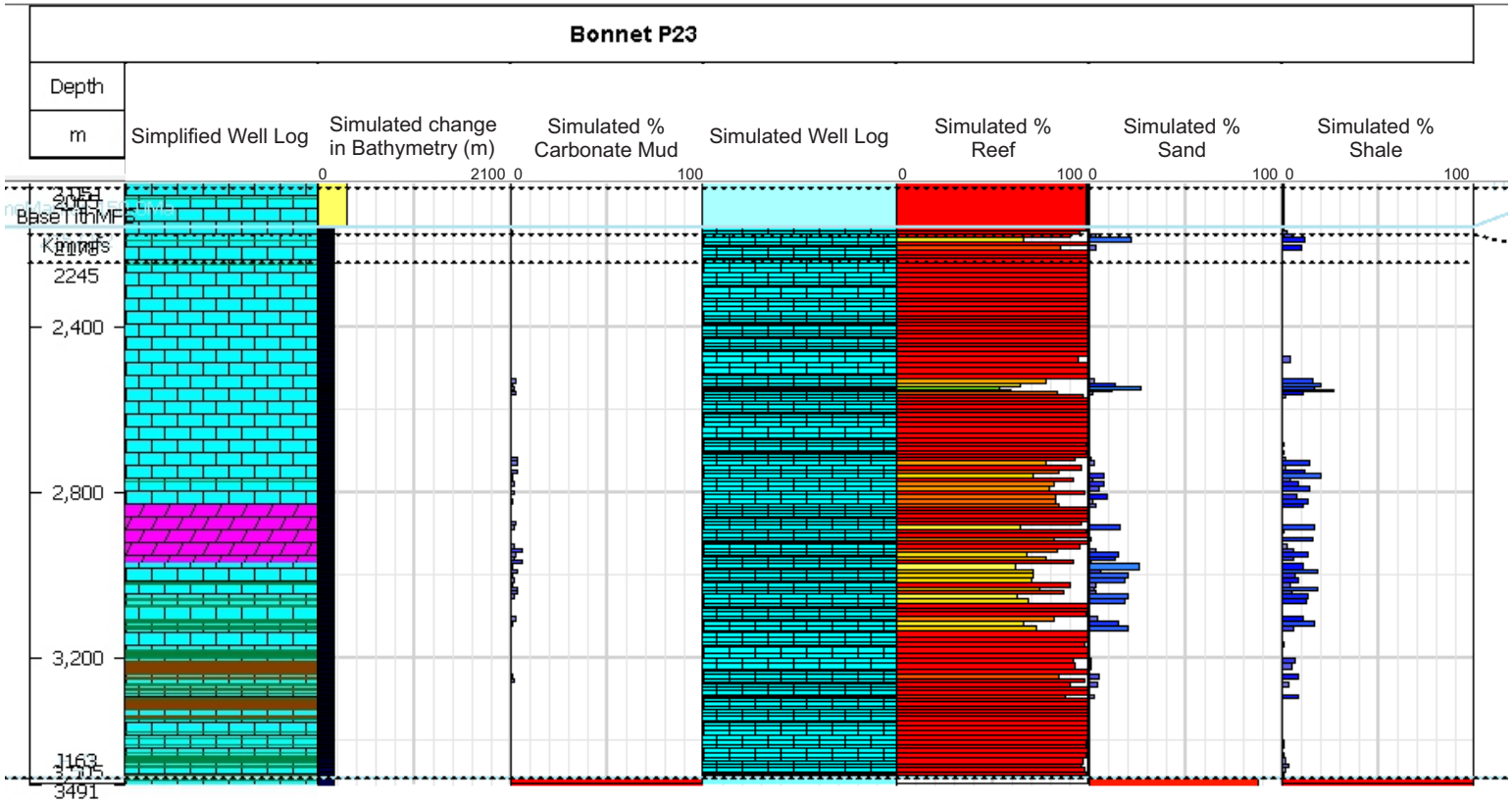

Figure S7.10: Model C (deep basin) reference case well calibration.

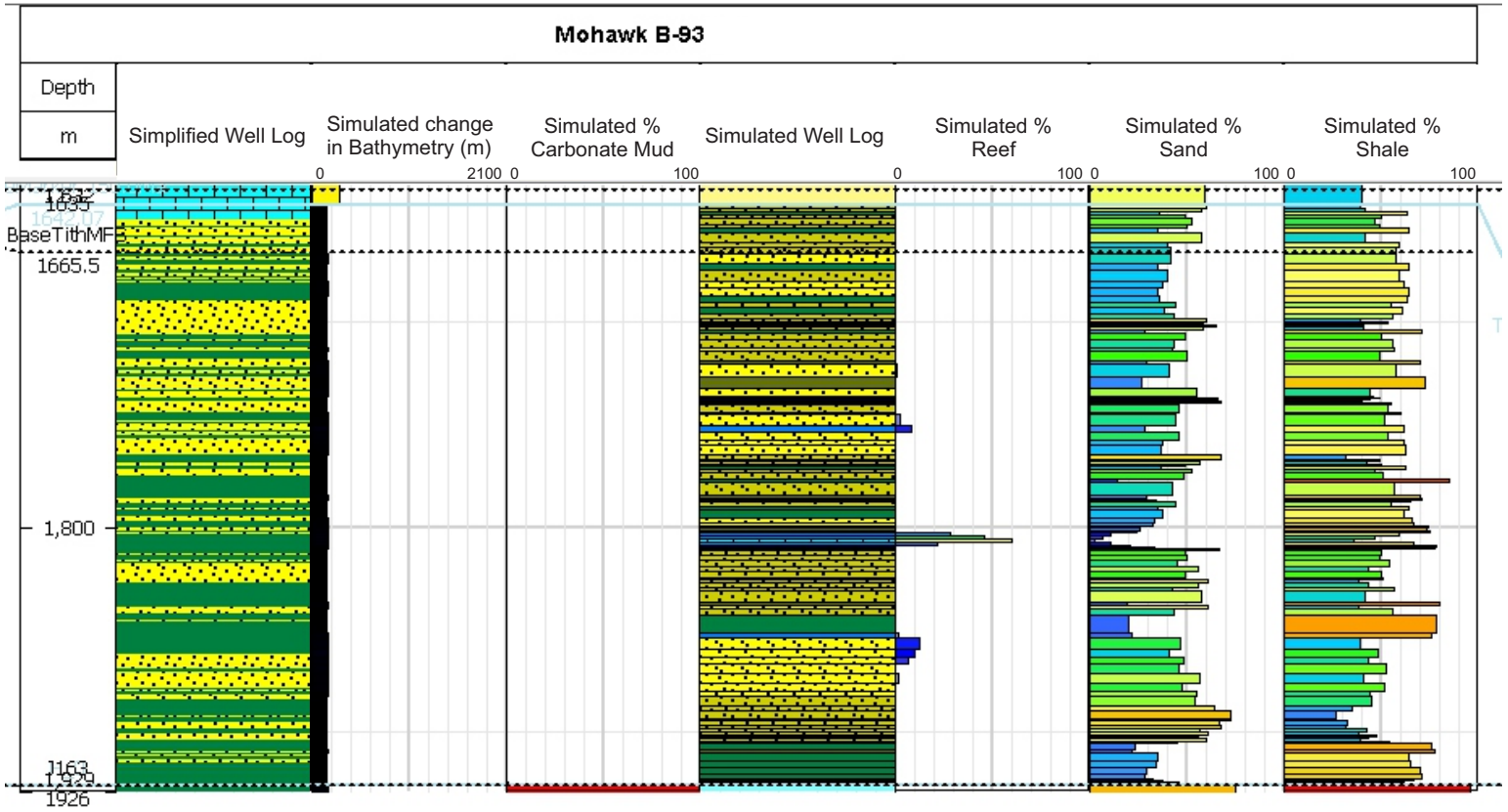

Figure S7.11: Model C (deep basin) reference case well calibration.

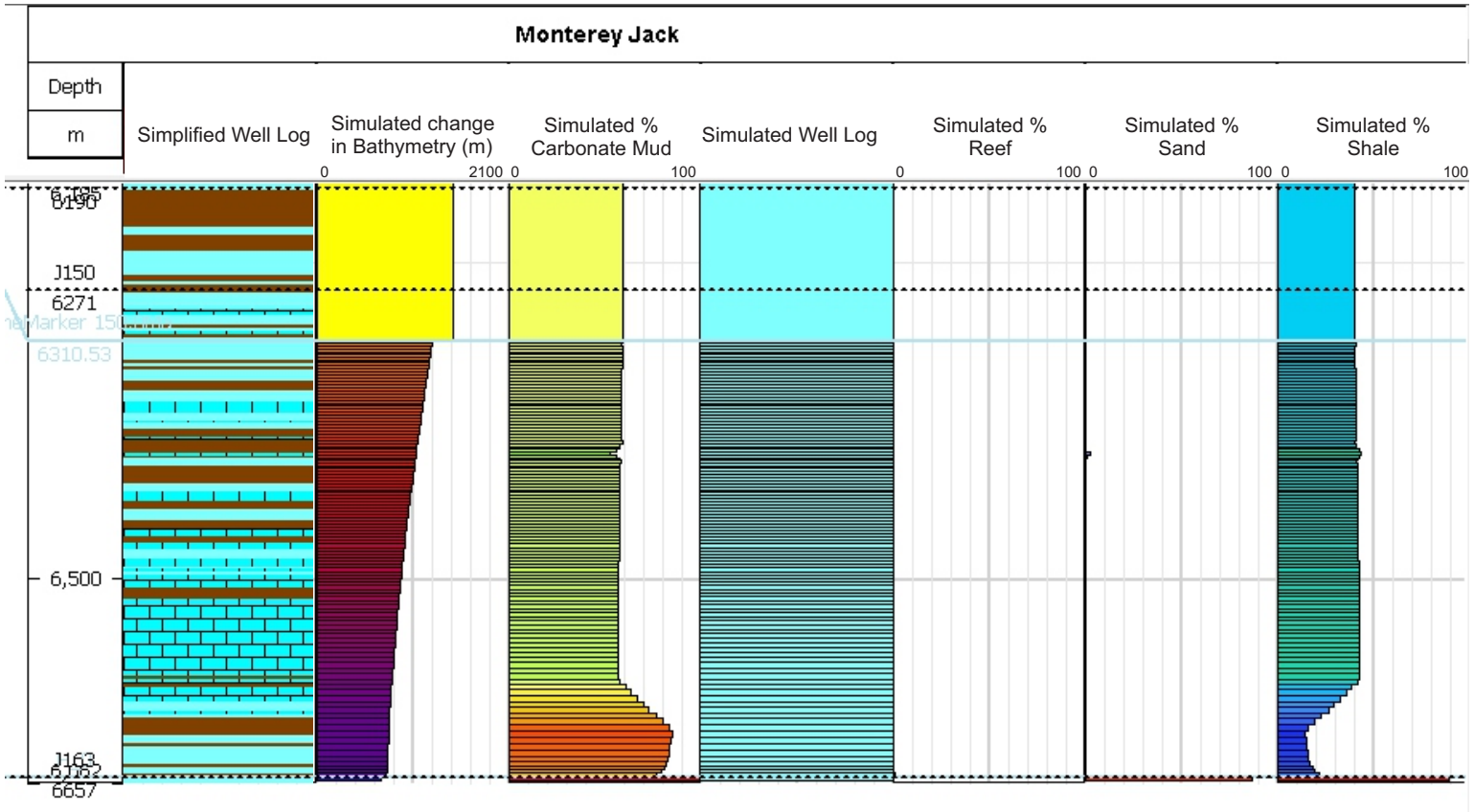

Figure S7.12: Model C (deep basin) reference case well calibration.

Appendix 5: Chapter 5 Supplementary Appendices

Supplementary Appendix 1: Sediment supply values for the reference case model and the no information on sources model

Reference Case Model

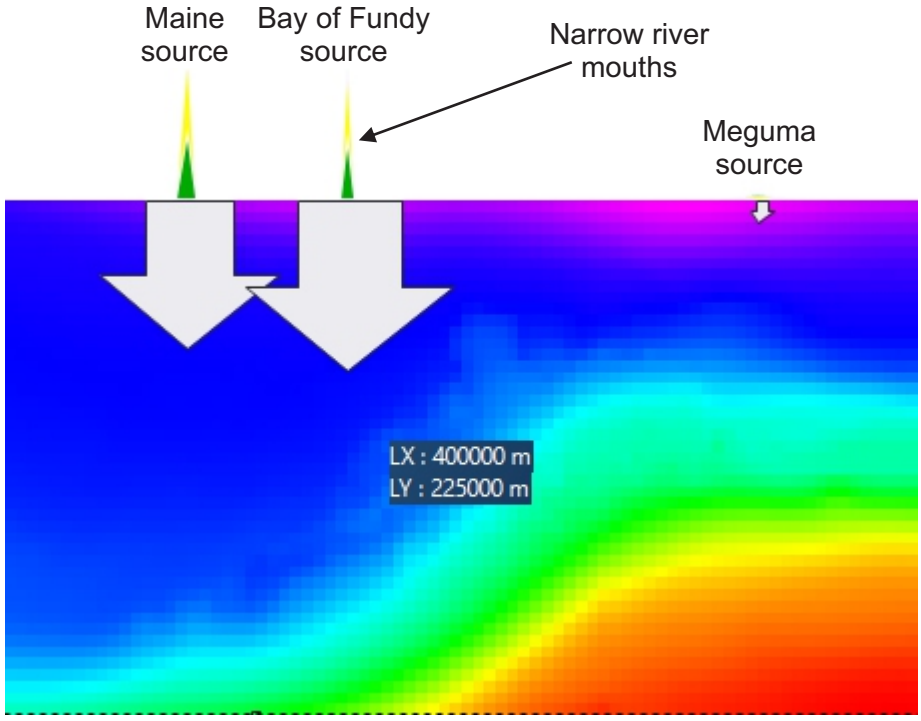

No Information on Sources Model

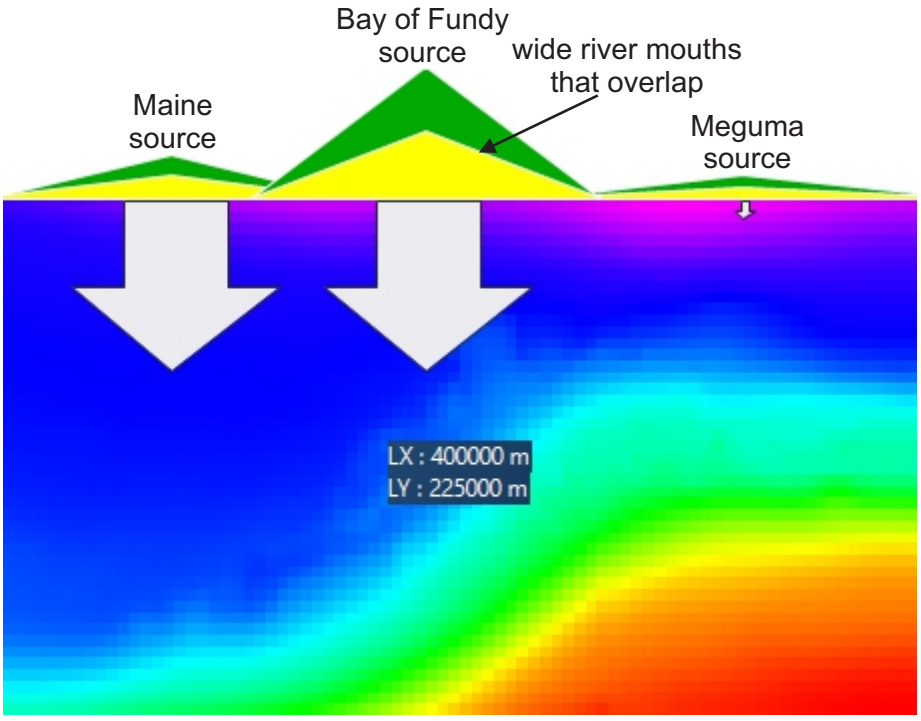

Table S1: Sediment supply values for the reference case model and the no information on sources model.

Reference Case Model

Source			Phase 1 (163-161 Ma)					Phase 2 (161-153.1 Ma)											Phase 3 (153.1-150 Ma)				
Age (Ma)		Width (m)	**163**	**162**	**161.5**	**161.4**	**161.3**	**161**	**160**	**159**	**158**	**157.8**	**157**	**156.5**	**156**	**155**	**154**	**153.3**	**153.1**	**153**	**152**	**151**	**150**
Maine	Supply (km^3/Ma)	5000	900	700	1100	1100	1400	2400	3100	2300	2600	2300	2600	2300	2300	2500	2300	2350	1800	1000	350	350	150
	Fluvial Discharge (m^3/s)		1300	1300	2000	1600	1900	3300	4400	4400	4800	4800	5300	4400	4400	3500	3000	3100	2500	1500	400	400	400
	Sand (%)		56.8	58.89	58	58.54	58.48	57.78	55.17	51.2	49.8	49.7	49.52	49.38	49.24	40	40	45.67	45.44	45.32	44.57	41.19	40.17
	Shale (%)		43.2	41.11	42	41.46	41.52	42.22	44.83	48.8	50.2	50.3	50.48	50.62	50.76	60	60	54.33	54.56	54.68	55.43	58.81	59.83
Bay of Fundy	Supply (km^3/Ma)	5000	500	1500	1000	950	800	1500	3500	2500	2500	2000	2000	1600	1700	800	500	1250	1400	1500	1500	1800	2000
	Fluvial Discharge (m^3/s)		1500	2500	2000	1900	2000	3000	4000	3000	3500	2950	2500	2300	2500	2100	1500	2000	2400	2500	2500	2000	2800
	Sand (%)		56.8	58.89	58	58.54	58.48	57.78	55.17	51.2	49.8	49.7	49.52	49.38	49.24	48.89	46.48	45.67	45.44	45.32	44.57	41.19	40.17
	Shale (%)		43.2	41.11	42	41.46	41.52	42.22	44.83	48.8	50.2	50.3	50.48	50.62	50.76	51.11	53.52	54.33	54.56	54.68	55.43	58.81	59.83
Meguma	Supply (km^3/Ma)	5000	50	200	250	200	200	250	250	200	200	50	100	150	150	200	300	300	260	250	200	300	350
	Fluvial Discharge (m^3/s)		200	400	400	250	500	300	500	400	500	300	550	300	200	400	400	475	490	500	600	500	550
	Sand (%)		30	20	30	35	40	57.78	55.17	51.2	49.8	40	40	40	45	48.89	46.48	45.67	45.44	45.32	44.57	41.19	40.17
	Shale (%)		70	80	70	65	60	42.22	44.83	48.8	50.2	60	60	60	55	51.11	53.52	54.33	54.56	54.68	55.43	58.81	59.83

No Information on Sources Model

Source								
Age (Ma)		Width (m)	**162**	**161**	**156.5**	**155**	**153.5**	**150**
Maine	Supply (km^3/Ma)	150000	500	3500	3500	3000	500	500
	Fluvial Discharge (m^3/s)		1000	3500	3500	1000	1000	1000
	Sand (%)		50	50	50	50	50	50
	Shale (%)		50	50	50	50	50	50
Bay of Fundy	Supply (km^3/Ma)	150000	1500	1500	1500	1500	1500	1500
	Fluvial Discharge (m^3/s)		1000	1000	1000	1000	1000	1000
	Sand (%)		50	50	50	50	50	50
	Shale (%)		50	50	50	50	50	50
Meguma	Supply (km^3/Ma)	170000	300	300	300	300	300	200
	Fluvial Discharge (m^3/s)		100	50	75	200	300	400
	Sand (%)		45	45	45	45	45	45
	Shale (%)		55	55	55	55	55	55

Supplementary Appendix 2: Workflow process

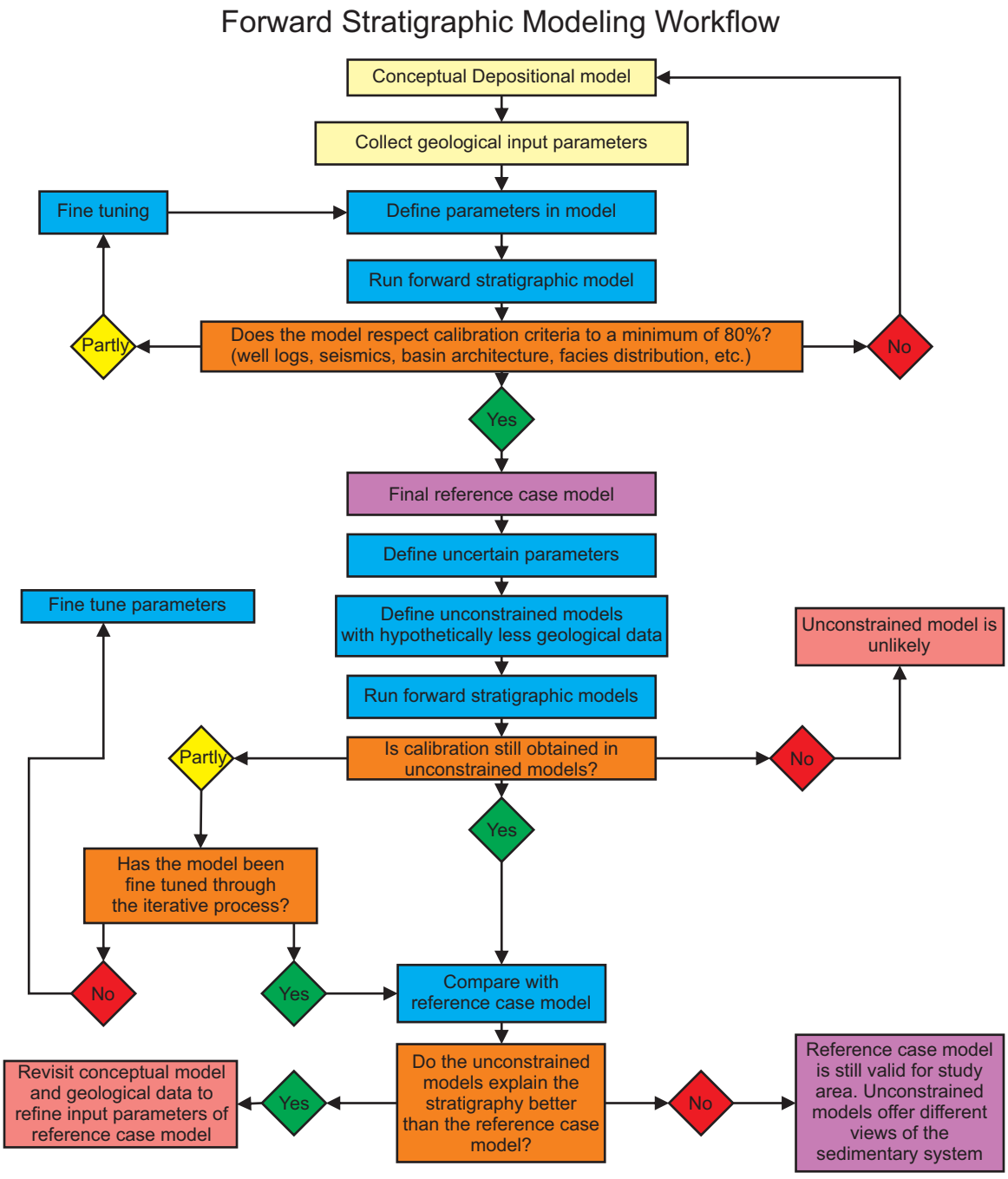
Forward Stratigraphic Modeling Workflow
Conceptual Depositional model
Collect geological input parameters
Fine tuning
Define parameters in model
Run forward stratigraphic model
Partly
Does the model respect calibration criteria to a minimum of 80%? (well logs, seismics, basin architecture, facies distribution, etc.)
No
Yes
Final reference case model
Define uncertain parameters
Fine tune parameters
Define unconstrained models with hypothetically less geological data
Unconstrained model is unlikely
Run forward stratigraphic models
Partly
Is calibration still obtained in unconstrained models?
No
Yes
Has the model been fine tuned through the iterative process?
No
Yes
Compare with reference case model
Revisit conceptual model and geological data to refine input parameters of reference case model
Yes
Do the unconstrained models explain the stratigraphy better than the reference case model?
No
Reference case model is still valid for study area. Unconstrained models offer different views of the sedimentary system